Spring 5-15-2019

Spatio-temporal Principles of Infra-slow Brain Activity

Anish Mitra
Washington University in St. Louis

WASHINGTON UNIVERSITY IN ST. LOUIS

Division of Biology and Biomedical Sciences
Neurosciences

Dissertation Examination Committee:
Marcus Raichle, Chair
Beau Ances
Timothy Holy
Jin-Moo Lee
Abraham Snyder
Lawrence Snyder

Spatio-temporal Principles of Infra-slow Brain Activity

by
Anish Mitra

A dissertation presented to
The Graduate School
of Washington University in
partial fulfillment of the
requirements for the degree
of Doctor of Philosophy

May 2019
St. Louis, Missouri

Table of Contents

List of Figures

List of Tables

Acknowledgments

Perhaps we should each write a private “acknowledgements” section every month, because in reflecting over the amazing community of support I have here in Saint Louis, I am filled with gratitude. Theobald Smith, one of America’s first prominent physician scientists (and discoverer of Salmonella!), wrote that “the joy of science must be in the doing, for any other harvest is uncertain.” By his standards, the past five years have been a bumper crop.

First, and foremost, I must thank my advisor Marc Raichle, who is most responsible for giving me such a remarkable graduate school experience. People often ask me what it is like to be a student in Marc’s lab, and I tell them “it’s like being in an intellectual playground”. I could never have imagined such an incredible environment, where every idea, no matter how fanciful, is fostered and entertained. Work, in Marc’s lab, is truly play. And although we are often persuaded to back off from some of our crazier ideas, Marc’s belief in the existence of answers to questions that matter, and persistent search of a greater, more elegant truth, is a model for all scientists. The point is never the next paper, but rather the pursuit of a deep and intuitive understanding of the universe we inhabit. Even more important are the values Marc espouses in his conduct: he is endlessly generous with his time and deeply invested in his students. Although my PhD is coming to an end, I look forward to working on our book, and on sailing Barnacle to destinations unknown.

I would also like to thank the other members of my thesis committee. Beau Ances has been an integral source of advice on how to navigate the practical ins and outs of the MSTP program. Tim Holy has provided valuable neurophysiological insight, especially over the past year as we pushed the boundaries of our experimental experience. I want to thank Ilya Monosov for generously stepping in at the last possible moment to provide a physiology point of view at the defense. Lawrence Snyder, Joseph Culver, and Jin-Moo Lee have also been incredible assets in helping to frame the work we have done, as well as in providing sometimes contrarian input that is worth its weight in gold. Most importantly, Larry, Joe, and Jin-Moo played pivotal roles in helping to craft the final chapter of this thesis, which represents a remarkable collaboration between their labs and ours. Patrick Wright, Ben Acland, and Andrew Kraft have also been indispensable partners in our collaborative mouse studies over the past year. I especially want to thank Andrew; his indefatigable worth ethic and relentless creativity is something to behold.

There are also several people without whom the work contained in this document could never have been done. Foremost among them is Avi Snyder. Avi is one of the most brilliant and dedicated scientists I have ever met, and an indispensable pillar of the Neuroimaging Laboratories. I shudder to think of the state of neuroimaging research without his profound influence. To me, Avi is also effectively a co-mentor along with Marc. No matter how busy he is, Avi has always taken the time (surely thousands of late night hours by now) to help me understand in detail whatever matter I may have brought

to his attention. Avi's generosity of spirit and encyclopedic knowledge of neuroscience is a model for all of us.

Next is Manu Goyal, who was a post-doc in the lab when I joined. Manu's early advice to me played a large role in shaping my approach to graduate school, and his broad reading and expansive understanding of all things neuroscience, medicine, and beyond (like scotch!) is an inspiration to me.

My fellow graduate students in Marc's lab, Tyler Blazey and Ryan Raut, have also influenced me deeply. I have learned a lot from Tyler's rigorous approach to science, and his company through good and difficult moments has been a pleasure. Ryan joined our lab recently, but his fresh perspective and hard work has already reframed how I understand the work I have done, not to mention my new appreciation of peanuts. I have no doubts that both of them will be far more successful than I!

I have also enjoyed meeting all the other hard-working and fun people around the Neuroimaging Laboratories, especially Darlene Dwyer and Russ Hornbeck. Without Darlene's hard work and amazing spirit, I'm fairly certain the electricity bills would go unpaid (as it were), and all of us would have far less fun. Russ is just a tremendous presence, directs me to all the latest Saint Louis culinary destinations, and critically lent me his backpacking gear without which I surely would not have survived to this day.

I would also like to thank all of the amazing people in the MSTP office, who make life so easy for us, including Wayne Yokoyama, the director of the MSTP program, Brian Sullivan, Christy Durbin, Liz Bayer, and Linda Perniciaro,. I also want to give a huge thank you to Shirley McTigue, without whom I would surely have never received NIH funding.

I must also express my gratitude for all the incredible MSTP students with whom I have been fortunate enough to overlap. Jonathan Power, Tim Laumann, Matthew Brier, Carl Hacker, Joshua Siegel, and Andrew Kraft have been indispensable colleagues and friends.

Finally, I want to thank my parents, Sharmila and Amitava Mitra. I do not say it enough, but they have both sacrificed significantly to help give me every possible opportunity. Without their help, I very much doubt I could have applied to Washington University to begin with. If I ever accomplish anything of note, it will be entirely due to their efforts.

Funding: This work was supported by NIMH F30 grant MN106253.

Anish Mitra

Washington University in St. Louis

May 2019

ABSTRACT OF THE DISSERTATION

Spatio-temporal Principles of Infra-slow Brain Activity

by

Anish Mitra

Doctor of Philosophy in Biology and Biomedical Sciences

Neurosciences

Washington University in St. Louis, 2019

Professor Marcus Raichle, Chairperson

In the study of systems where basic laws have eluded us, as is largely the case in neuroscience, the simplest approach to progress might be to ask: what are the biggest, most noticeable things the system does when left alone? Without any perturbations or fine dissections, can regularities be found in the basic operations of the system as a whole? In the case of the brain, it turns out that there is an amazing amount of activity even in the absence of explicit environmental inputs or outputs. We call this spontaneous, or resting state, brain activity. Prior work has shown that spontaneous brain activity is dominated by very low frequencies: the biggest changes in brain activity happen relatively slowly, over 10's-100's of seconds. Moreover, this very slow activity of the brain is quite metabolically expensive. The brain accounts for 2% of body mass in an adult, but requires 20% of basal metabolic expenditure. Remarkably, the energy required to sustain brain function is nearly constant whether one is engaged in a demanding mental task or simply out to lunch. Furthermore, work over the past three

decades has established that the spontaneous activities of the brain are not random, but instead organized into specific patterns, most often characterized by correlations within large brain systems. Yet, how do these correlations arise, and does spontaneous activity support slow signaling within and between neural systems? In this thesis, we approach these questions by providing a comprehensive analysis of the temporal structure of very low frequency spontaneous activity. Specifically, we focus on the direction of travel in low frequency activity, measured using resting state fMRI in humans, but also using electrophysiological techniques in humans and mice, and optical calcium imaging in mice. Our temporal analyses reveal heretofore unknown regularities in the way slow signals move through the brain. We further find that very low frequency activity behaves differently than faster frequencies, that it travels through distinct layers of the cortex, and that its travel patterns give rise to correlations within networks. We also demonstrate that the travel patterns of very low frequency activity are highly dependent on the state of the brain, especially the difference between wake and sleep states. Taken together, the findings in this thesis offer a glimpse into the principles that govern brain activity.

Chapter 1: Introduction

Contemporary neuroscience is rife with remarkable tools for exploring the brain in ever greater detail. As of this writing, we have access to experimental methodologies that allow us to delineate the wide diversity of individual cells in the brain with unprecedented fidelity (Tasic et al. 2016), to turn on or off individual ion channels in cell types of interest (Urban and Roth 2015; Yizhar et al. 2011), to manipulate single genes in living brains (Swiech et al. 2015), to map the connectivity structure of individual neurites (Lichtman et al. 2008), and even to record neural activity at nanosecond resolution from thousands of *in vivo* individual neurons (Stevenson and Kording 2011). In combination, these techniques may indeed make it possible, as articulated by President Obama's BRAIN Initiative executive committee, "to produce dynamic pictures of the brain that show how individual brain cells (…) interact at the speed of thought." Yet rather than capitalizing on modern developments to study fast interactions among small brain elements, the present thesis aims to understand very slow activity across the whole brain. Why?

The best defense I can muster is that although the reductionist approach of mainstream neuroscience may very well yield insights, there are reasons to believe that a full understanding of the brain will not emerge from reductionism alone. Consider, for example, our physical understanding of the universe. A reductionist approach to physics could reasonably posit that a complete understanding of electron pairs (although there are, of course, even smaller elements to consider!) is necessary to understand the bulk behavior of matter. While this approach might yield significant insight on quantum mechanical principles and the electrostatic force, in a two-electron system, one would

never notice gravity, a force 10^{42} times weaker than the electrostatic force. Of course, the fact that gravity emerges as a noticeable influence only in enormous collections of matter does not diminish its importance in shaping our universe, and to this day, there still does not exist a reductionist quantum theory of gravity. Indeed, historically, failure to grasp quantum mechanics did not hinder Johannes Kepler from describing planetary motion or Isaac Newton from finding the law of gravitation. Evidently, there are limits to reductionist understandings of complex systems, and as Philip Anderson observed, "more is different".

How does this relate to neuroscience and the present thesis? The answer is that there is mounting evidence, aided by the advent of large-scale neuroimaging tools, that there are functional brain properties that are best observed and understood at the whole-brain scale. In particular, very low frequency brain activity exhibits a remarkable long-distance organization in both space and time in the absence of any explicit input or output (Fox and Raichle 2007; Hiltunen et al. 2014). The spatio-temporal patterns discovered in very low frequency spontaneous (or "resting state") brain activity were not presaged by previous studies of circuit-level neural activity, and although these findings were initially dismissed as "noise", artifact, or epi-phenomena, recent work has linked these low frequency resting state patterns to several aspects of human brain function in health and disease (Biswal et al. 2010; Buckner et al. 2008; Emerson et al. 2017; Smith et al. 2015; Snyder and Raichle 2012). These findings have established the existence and practical utility of organized low frequency activity in the brain. Yet, we still lack answers to fundamental questions of how spontaneous patterns arise in very low frequency brain activity, the rules that govern their organization, and their relationship to

higher frequency brain activity. The temporal properties of low frequency resting state activity are especially unclear, as the predominant strategy for quantifying the organization of low frequencies has been zero-lag correlations, which by definition preclude any understanding of directed signaling (Mitra and Raichle 2016). Thus, the focus of this thesis is to explore the principles underlying the whole-brain spatio-temporal organization of infra-slow (<0.1 Hz) frequency brain activity specifically from a temporal perspective, including an examination of directed signaling in infra-slow frequencies. We will then leverage our understanding of the temporal structure of infra-slow activity to understand how the spontaneous organization in these frequencies varies over state and interacts with higher frequencies, as well as how specific cortical layers contribute to the organization of systems-wide activity.

To frame the relevance of this work, it is necessary to appreciate in greater detail how low frequency activity has shaped our understanding of the brain to date. Work involving spontaneous very low frequency activity in the brain can be traced to two strains in the extant literature. First, and more recent, are findings attributable to the advent of neuroimaging. Positron Emission Tomography (PET) imaging represented a breakthrough in functional neuroimaging, as it allowed the first truly reliable, whole-brain *in vivo* view of brain function in humans (Snyder and Raichle 2012). Unlike previous modalities such as the electroencephalogram (EEG) (Berger 1929), which measured electrophysiogical brain activity, early PET studies measured brain metabolism or “cost” (Raichle and Mintun 2006). Using ingenious “subtraction paradigms”, researchers measured brain metabolism during an experimental condition, and then subtracted out brain metabolism measurement in a corresponding control (Raichle 2015). The resulting

difference yields remarkably beautiful pictures of the spatial topographies of large-scale brain systems involved in particular tasks, such as language generation (Petersen et al. 1988; Raichle 2015). In addition to providing *in vivo* pictures of known brain networks, the subtraction paradigm in PET imaging also led to the discovery of new brain networks that were previously unknown to neuroscience, including the default mode network (Raichle et al. 2001). In retrospect, it is difficult to imagine neuron-by-neuron investigations ever revealing this large brain-wide system.

The ability to visualize *in vivo* activity in specific brain networks during tasks in many ways stole the show with respect to the scientific content of PET. Yet lurking in the PET subtraction paradigm was another powerful finding: brain networks identified through the subtraction paradigm represented minuscule changes in brain cost. For example, metabolism in the language network during verb-generation only increases by 1% or less (Raichle 2015), a finding that is concordant with a previous mental arithmetic study conducted by Sokoloff at the whole-brain level which showed no appreciable increase in metabolism during task (Sokoloff et al. 1955). Ongoing basal brain metabolism, on the other hand, is quite expensive. In a resting adult, although the brain is 2% of the body's mass, it comprises 20% of the body's metabolic activity (Raichle and Mintun 2006). These findings bring to the fore an important principle: although the brain is tremendously active from a metabolic perspective, task-induced changes in brain metabolism are negligible. Most of the brain's metabolism is instead attributable to spontaneous (or task-independent) activities (Raichle 2011).

This statement raises an obvious question: if not task-linked neural activity, then what is responsible for the brain's enormous cost? One answer is the energy required to

maintain electrochemical hyperpolarization in neurons, primarily established by Na^+-K^+ transport pumps, which is a necessary precondition for neuronal cells to undergo action potentials (although surprisingly energy-dependent ion transport only accounts for ~40% of brain metabolism (Astrup et al. 1981)). Putting aside the 40% detail for a moment (perhaps Astrup neglected to poison a heavy tail of energetically costly ion pumps), we can compose a simple portrait: the brain expends tremendous energy maintaining a stable, quiescent baseline (electrochemical hyperpolarization) from which neurons are briefly released (in the form of action potentials) to send high frequency electrical signals. Task-based neural activity appears “cheap” because the cost is paid up front by establishing the hyperpolarized baseline.

The only difficulty with this explanation is that it does not align with experimental fact. The “quiescent baseline” model suggests a reflexive brain that is intrinsically silent in the absence of explicit input or output. Instead, even prior to imaging, recordings of brain activity ranging from *in vivo* EEG to slice preparations revealed that the brain is spontaneously active (Berger 1929). However, these spontaneous activities of the brain were often dismissed as artifact, noise in the neural system, or simply neural activity attributable to uncontrolled variables. In retrospect, several findings laid the groundwork for challenging this perspective, but a critical breakthrough came in work conducted using voltage sensitive dye imaging by Grinvald and colleagues (Kenet et al. 2003). Grinvald imaged brain activity in the anesthetized cat visual area 18, where most cells were known to be sensitive to stimulus orientation, and first produced a standard orientation map of the cortex using measured evoked activity to full-field gratings of vertical orientation. Then comes the clever part: Grinvald also recorded the

spontaneous activity in visual area 18 of anesthetized cats in a dark room with no visual input. He then computed a map of the correlation structure of spontaneous visual activity in the absence of any visual input, and surprisingly, the correlation structure of spontaneous (input-free) activity in the visual cortex precisely matched the evoked-patterns in response to vertical gratings. In other words, the spontaneous fluctuations were not merely noisy departures from the brain's attempt to hold a quiescent baseline. Instead, spontaneous fluctuations were exquisitely organized into correlated topographies in concordance with evoked topographies. However, there was a critical difference between the evoked and spontaneous activity: whereas the evoked maps were produced using neural activity within the first 100ms of grating presentation, that is activities of 10 Hz and faster, the fluctuations driving the correlation structure of the spontaneous activity were much slower, <1 Hz. Thus, while the correlation structure of spontaneous activity matched the evoked topography in visual area 18, spontaneous activity was far slower than evoked activity.

Shortly after the Grinvald study, Biswal and colleagues showed a similar correspondence between the correlation structure of spontaneous activity and task-evoked activity topography in primary motor cortex using fMRI (Biswal et al. 1995), where the frequency of the blood oxygen level dependent (BOLD) signal (<0.1 Hz infra-slow activity) is even lower than what Grinvald observed. Still, even in fMRI, the principle that evoked activities are faster than spontaneous fluctuations hold true: task-evoked fMRI activity generally describes at longest a 20 second period (0.05 Hz), whereas the correlation structure of fMRI activity is driven by cycles of 100 seconds or longer (0.01 Hz) (Biswal et al. 2010; Buckner and Vincent 2007; Damoiseaux et al.

2006). As an aside, although the fast-evoked versus slow-spontaneous principle is not explored in this thesis, Ken Harris has written about the mechanistic and possible functional consequences of this idea in elegant recent work (Sakata and Harris 2009).

The discovery that correlation patterns in spontaneous activity are organized into topographies that resemble task-evoked systems has led to thousands of papers exploring the details of spatial correlation networks and their relationships to a wide array of physiological and pathological neural functions in humans and animal models (Albert et al. 2009a; Albert et al. 2009b; Biswal et al. 2010; Buckner et al. 2008; Mantini et al. 2011; Smith et al. 2015; Stafford et al. 2014; Thomas Yeo et al. 2011; White et al. 2011). However, the question of how correlation patterns arise in spontaneous activity, especially those observed using resting state fMRI (rs-fMRI), and what these patterns might mean has received less attention. There is a perplexingly persistent dogma that BOLD signals, observed using fMRI or other techniques such as optical imaging, reflect a “sluggish” version of higher frequency activity (Friston et al. 1998). The idea is that neurons undergo action potentials, or neural networks oscillate at high frequencies (10-100 Hz), and that in response to this neural activity, there is a slow blood flow response, giving rise to BOLD measurements (de Zwart et al. 2005; Lindquist et al. 2009; Ma et al. 2016). The slow blood flow response is postulated to be a low-pass filter on high frequency neural activity, thus presenting a “smeared out” view of underlying neural activity (de Zwart et al. 2005; Kim and Kim 2011). Worse still, the parameters of the “vascular low-pass filter” are feared to vary across the brain, so much so that any timing differences in BOLD signals across the brain are reflexively attributed to properties of blood vessels as opposed to neural activity (Friston 2009; Handwerker et al. 2004).

Yet again, the difficulty with this model is that it is contradicted by experimental fact. First, simulations which model the correlation structure of rs-fMRI on the basis of high frequency resonance in structural networks explain only a modest portion of observed data (Honey et al. 2009). Second, direct recordings of brain electrophysiology and calcium fluctuations have demonstrated that spontaneous infra-slow fluctuations in BOLD signals are directly linked to spontaneous infra-slow fluctuations in neuronal physiology (He et al. 2008; Hiltunen et al. 2014; Leopold et al. 2003; Matsui et al. 2016; Pan et al. 2013). In other words, very low frequency brain activity is not the consequence of measuring through a "vascular low-pass filter". Instead, infra-slow activity is a bona fide feature of brain function, a fact that may have been obscured by the failure of many studies to record or analyze neural activity <0.1 Hz (Sirotin and Das 2009).

The understanding that infra-slow activity exists in the brain allows us to pose some interesting questions. For example, what is the purpose of infra-slow brain activity, and might infra-slow activity travel within the brain to give rise to its correlation structure? Here we arrive at the second strain of the extant literature. Although neuroimaging may have popularized low frequency brain activity in recent times, robust investigations into very low frequency neural activity were conducted in the 1950's and 60's. Indeed, to the best of my knowledge, the Soviet scientist Nina Aleksanda Aladjalova was the first to use the term "infra-slow" with reference to neural activity in her 1954 letter to *Nature* (Aladjalova 1954), where she reported spontaneous very slow fluctuations (periods of 10 seconds or greater) in local field potential activity in the rabbit visual and motor cortex (*in vivo)*, recorded using a direct-current coupled amplifier of her

own design. Aladjalova also made several further contributions to the understanding of infra-slow activity in the brain (Aladjalova 1962): (1) She noted that unlike the sinusoidal characterization of higher frequency rhythms, infra-slow activity is arrhythmic, in accordance with our present understanding of scale-free spectral content in brain activity, (2) She found that very brief visual stimulations did not elicit infra-slow activity changes, but that longer, seconds long stimuli did, and (3) She found that although there was no simple relationship between infra-slow activity and action potentials, action potentials were far more likely in certain phases of the infra-slow fluctuation, leading her to believe that infra-slow activity represented changes in cortical excitability. In each of these discoveries, Aladjalova was remarkably prescient.

On the final point, that infra-slow activity may represent changes in cortical excitability, Aladjalova cited work conducted by Benjamin Libet in the 1940's that studied propagation of very low frequency neural activity in cortical slices (Libet and Kahn 1947). Libet found that he could document reproducible patterns of propagated spontaneous infra-slow frequency activity (although he did no call it that) in the frog cortex, and that these patterns were remarkably robust to even transection of the frog cortex. That is, the waves Libet was observing could move across cuts in the cortex, leading him to theorize that "the whole [cortical] sheet would behave like the polarized membrane of a nerve fiber. A local depolarization, resulting from the discharge of one cell or a few adjacent ones, would permit neighboring cells to discharge through the "leak" current and so initiate a spreading wave of depolarization." The idea that spontaneous activity can spread, relatively slowly, across the cortex as if the cortical sheet were itself a medium has also been advanced in contemporary studies using

calcium and voltage sensitive dye imaging in mice (Chan et al. 2015; Matsui et al. 2016; Mohajerani et al. 2010; Stroh et al. 2013).

The purpose of presenting this history, which is by no means complete (see also: (Bishop 1932; O'Leary and Goldring 1964; Steriade et al. 1993)) is to emphasize that the central ideas in this thesis, while out of the mainstream fashion of neuroscience, are not without precedent. As is evident, decades of prior work has already suggested that infra-slow neural activity is a genuine phenomenon of biological interest, that there are reproducible patterns in the way infra-slow activity travels through the brain, and that these infra-slow activity patterns appear to be an emergent phenomenon of large groups of neurons (and possibly glia and other brain cell types (Poskanzer and Yuste 2011)).

The ensuing chapters of this thesis will build upon these ideas in the following steps:

- First, we will demonstrate that there is a consistent set of lead-lag relationships (that is, apparent propagation) in resting state fMRI data collected in humans. These lead-lag relationships in infra-slow BOLD signals are roughly on the order of 1 second, that is, below the temporal sampling density of most fMRI data. Nonetheless, I will show that we can compute these temporal delays by applying parabolic interpolation to empirically computed cross-correlation curves. Moreover, we will showcase the first evidence that the temporal structure of rs-fMRI can be altered as a function of state.
- Second, we will explore the dimensionality of the temporal structure of rs-fMRI, as a means of estimating the number of temporal sequences or “lag threads” found in the data. Decomposing the general delay structure of rs-fMRI into a set

of temporal sequence factors allows us to explore two issues. First, if the dimensionality of the temporal structure is greater than 1, then by definition, no single factor (set of delays) can explain the entirety of rs-fMRI temporal structure. In particular, it means that even if one set of delays is attributable purely to differences in vasculature across the brain, the other temporal sequences must be attributable to other presumably neural processes. Second, we are able to leverage the extracted temporal sequences to demonstrate that the correlation structure of rs-fMRI is the consequence of specific properties in its temporal structure. The reverse is not true: the correlation structure of rs-fMRI does not constrain its temporal structure.

- Third, we will explore how the temporal structure of rs-MRI is altered in as a function of arousal state, specifically in wakefulness versus slow wave sleep. The difference between these states has been previously studied using functional connectivity analysis on rs-fMRI, and although differences have been found, the effect sizes are quite small. We demonstrate dramatic reversals in the direction of rs-fMRI activity travel across arousal states.
- Fourth, we continue our exploration of the role of spontaneous infra-slow rs-fMRI activity during sleep by specifically studying cortical-hippocampal temporal structure in wakefulness and slow wave sleep. In addition to rs-fMRI, we also study infra-slow electrophysiology, acquired in humans, in wake and sleep. On this basis, we demonstrate that the direction of infra-slow signals between cortex and hippocampus reverses across wake and sleep, in both rs-fMRI and electrocorticography, establishing an electrophysiological correlate of rs-fMRI

directionality. We further find that higher frequency delta band (1-4Hz) activity travels in the opposite direction as infra-slow activity, during both wakefulness and sleep, implying that infra-slow propagation may serve as a very low frequency feedback signal which moves in the opposite direction as higher frequency feed forward activity.

- Fifth, we move from the human to the mouse. Using whole-cortex calcium/hemoglobin imaging and laminar electrophysiology in mice, we show that infra-slow activity in each of these modalities travels through the cortex along stereotyped trajectories that are distinct from trajectories in delta (1-4Hz) activity. Moreover, there is directionality reversal in both infra-slow and delta activity trajectories across wakefulness and anesthesia. Finally, we find that infra-slow travels through distinct cortical layers as compared to both delta activity and higher frequencies. These findings expand our understanding of resting state BOLD signal relationships and illustrate the unique physiology of long-distance organization in spontaneous infra-slow brain activity.

The specific arguments contained in these chapters are sometimes rather technical, but the final argument advanced in this thesis is quite simple: spontaneous infra-slow brain activity has a distinct, lawful, state-dependent temporal structure as it moves through specific layers of the cerebral cortex.

References

Aladjalova NA. Infra-slow rhythmic oscillations of the steady potential of the cerebral cortex. *Nature* 179: 957-959, 1954.

Aladjalova NA. *Slow electrical processes in the brain*. New York, New York: Elsevier, 1962.

Albert NB, Robertson EM, Mehta P, and Miall RC. Resting state networks and memory consolidation. *Commun Integr Biol* 2: 530-532, 2009a.

Albert NB, Robertson EM, and Miall RC. The resting human brain and motor learning. *Curr Biol* 19: 1023-1027, 2009b.

Astrup J, Sorensen PM, and Sorensen HR. Oxygen and glucose consumption related to Na+-K+ transport in canine brain. *Stroke; a journal of cerebral circulation* 12: 726-730, 1981.

Berger H. Über das elektrenkephalogramm des menschen. *European Archives of Psychiatry and Clinical Neuroscience* 87: 527-570, 1929.

Bishop GH. Cyclic changes in excitability of the optic pathway of the rabbit. *American Journal of Physiology--Legacy Content* 103: 213-224, 1932.

Biswal B, Yetkin FZ, Haughton VM, and Hyde JS. Functional connectivity in the motor cortex of resting human brain using echo-planar MRI. *Magn Reson Med* 34: 537-541, 1995.

Biswal BB, Mennes M, Zuo XN, Gohel S, Kelly C, Smith SM, Beckmann CF, Adelstein JS, Buckner RL, Colcombe S, Dogonowski AM, Ernst M, Fair D, Hampson M, Hoptman MJ, Hyde JS, Kiviniemi VJ, Kotter R, Li SJ, Lin CP, Lowe MJ, Mackay C, Madden DJ, Madsen KH, Margulies DS, Mayberg HS, McMahon K,

Monk CS, Mostofsky SH, Nagel BJ, Pekar JJ, Peltier SJ, Petersen SE, Riedl V, Rombouts SA, Rypma B, Schlaggar BL, Schmidt S, Seidler RD, Siegle GJ, Sorg C, Teng GJ, Veijola J, Villringer A, Walter M, Wang L, Weng XC, Whitfield-Gabrieli S, Williamson P, Windischberger C, Zang YF, Zhang HY, Castellanos FX, and Milham MP. Toward discovery science of human brain function. *Proc Natl Acad Sci U S A* 107: 4734-4739, 2010.

Buckner RL, Andrews-Hanna JR, and Schacter DL. The brain's default network: anatomy, function, and relevance to disease. *Ann N Y Acad Sci* 1124: 1-38, 2008.

Buckner RL, and Vincent JL. Unrest at rest: default activity and spontaneous network correlations. *Neuroimage* 37: 1091-1096; discussion 1097-1099, 2007.

Chan AW, Mohajerani MH, LeDue JM, Wang YT, and Murphy TH. Mesoscale infraslow spontaneous membrane potential fluctuations recapitulate high-frequency activity cortical motifs. *Nature communications* 6: 7738, 2015.

Damoiseaux JS, Rombouts SA, Barkhof F, Scheltens P, Stam CJ, Smith SM, and Beckmann CF. Consistent resting-state networks across healthy subjects. *Proc Natl Acad Sci U S A* 103: 13848-13853, 2006.

de Zwart JA, Silva AC, van Gelderen P, Kellman P, Fukunaga M, Chu R, Koretsky AP, Frank JA, and Duyn JH. Temporal dynamics of the BOLD fMRI impulse response. *Neuroimage* 24: 667-677, 2005.

Emerson RW, Adams C, Nishino T, Hazlett HC, Wolff JJ, Zwaigenbaum L, Constantino JN, Shen MD, Swanson MR, Elison JT, Kandala S, Estes AM, Botteron KN, Collins L, Dager SR, Evans AC, Gerig G, Gu H, McKinstry RC, Paterson S, Schultz RT, Styner M, Network I, Schlaggar BL, Pruett JR, Jr., and

Piven J. Functional neuroimaging of high-risk 6-month-old infants predicts a diagnosis of autism at 24 months of age. *Science translational medicine* 9: 2017.

Fox MD, and Raichle ME. Spontaneous fluctuations in brain activity observed with functional magnetic resonance imaging. *Nat Rev Neurosci* 8: 700-711, 2007.

Friston K. Causal modelling and brain connectivity in functional magnetic resonance imaging. *PLoS Biol* 7: e33, 2009.

Friston KJ, Fletcher P, Josephs O, Holmes A, Rugg MD, and Turner R. Event-related fMRI: characterizing differential responses. *Neuroimage* 7: 30-40, 1998.

Handwerker DA, Ollinger JM, and D'Esposito M. Variation of BOLD hemodynamic responses across subjects and brain regions and their effects on statistical analyses. *Neuroimage* 21: 1639-1651, 2004.

He BJ, Snyder AZ, Zempel JM, Smyth MD, and Raichle ME. Electrophysiological correlates of the brain's intrinsic large-scale functional architecture. *Proc Natl Acad Sci U S A* 105: 16039-16044, 2008.

Hiltunen T, Kantola J, Abou Elseoud A, Lepola P, Suominen K, Starck T, Nikkinen J, Remes J, Tervonen O, Palva S, Kiviniemi V, and Palva JM. Infra-slow EEG fluctuations are correlated with resting-state network dynamics in fMRI. *J Neurosci* 34: 356-362, 2014.

Honey CJ, Sporns O, Cammoun L, Gigandet X, Thiran JP, Meuli R, and Hagmann P. Predicting human resting-state functional connectivity from structural connectivity. *Proc Natl Acad Sci U S A* 106: 2035-2040, 2009.

Kenet T, Bibitchkov D, Tsodyks M, Grinvald A, and Arieli A. Spontaneously emerging cortical representations of visual attributes. *Nature* 425: 954-956, 2003.

Kim T, and Kim SG. Temporal dynamics and spatial specificity of arterial and venous blood volume changes during visual stimulation: implication for BOLD quantification. *J Cereb Blood Flow Metab* 31: 1211-1222, 2011.

Leopold DA, Murayama Y, and Logothetis NK. Very slow activity fluctuations in monkey visual cortex: implications for functional brain imaging. *Cereb Cortex* 13: 422-433, 2003.

Libet B, and Kahn JB, Jr. Steady potentials and neurone activity in mammals. *Federation proceedings* 6: 152, 1947.

Lichtman JW, Livet J, and Sanes JR. A technicolour approach to the connectome. *Nat Rev Neurosci* 9: 417-422, 2008.

Lindquist MA, Meng Loh J, Atlas LY, and Wager TD. Modeling the hemodynamic response function in fMRI: efficiency, bias and mis-modeling. *Neuroimage* 45: S187-198, 2009.

Ma Y, Shaik MA, Kozberg MG, Kim SH, Portes JP, Timerman D, and Hillman EM. Resting-state hemodynamics are spatiotemporally coupled to synchronized and symmetric neural activity in excitatory neurons. *Proc Natl Acad Sci U S A* 113: E8463-E8471, 2016.

Mantini D, Gerits A, Nelissen K, Durand JB, Joly O, Simone L, Sawamura H, Wardak C, Orban GA, Buckner RL, and Vanduffel W. Default mode of brain function in monkeys. *J Neurosci* 31: 12954-12962, 2011.

Matsui T, Murakami T, and Ohki K. Transient neuronal coactivations embedded in globally propagating waves underlie resting-state functional connectivity. *Proc Natl Acad Sci U S A* 113: 6556-6561, 2016.

Mitra A, and Raichle ME. How networks communicate: propagation patterns in spontaneous brain activity. *Philos Trans R Soc Lond B Biol Sci* 371: 2016.

Mohajerani MH, McVea DA, Fingas M, and Murphy TH. Mirrored bilateral slow-wave cortical activity within local circuits revealed by fast bihemispheric voltage-sensitive dye imaging in anesthetized and awake mice. *J Neurosci* 30: 3745-3751, 2010.

O'Leary JL, and Goldring S. D-C Potentials of the Brain. *Physiol Rev* 44: 91-125, 1964.

Pan WJ, Thompson GJ, Magnuson ME, Jaeger D, and Keilholz S. Infraslow LFP correlates to resting-state fMRI BOLD signals. *Neuroimage* 74: 288-297, 2013.

Petersen SE, Fox PT, Posner MI, Mintun M, and Raichle ME. Positron emission tomographic studies of the cortical anatomy of single-word processing. *Nature* 331: 585-589, 1988.

Poskanzer KE, and Yuste R. Astrocytic regulation of cortical UP states. *Proc Natl Acad Sci U S A* 108: 18453-18458, 2011.

Raichle ME. The restless brain. *Brain Connect* 1: 3-12, 2011.

Raichle ME. The restless brain: how intrinsic activity organizes brain function. *Philos Trans R Soc Lond B Biol Sci* 370: 2015.

Raichle ME, MacLeod AM, Snyder AZ, Powers WJ, Gusnard DA, and Shulman GL. A default mode of brain function. *Proc Natl Acad Sci U S A* 98: 676-682, 2001.

Raichle ME, and Mintun MA. Brain work and brain imaging. *Annu Rev Neurosci* 29: 449-476, 2006.

Sakata S, and Harris KD. Laminar structure of spontaneous and sensory-evoked population activity in auditory cortex. *Neuron* 64: 404-418, 2009.

Sirotin YB, and Das A. Anticipatory haemodynamic signals in sensory cortex not predicted by local neuronal activity. *Nature* 457: 475-479, 2009.

Smith SM, Nichols TE, Vidaurre D, Winkler AM, Behrens TE, Glasser MF, Ugurbil K, Barch DM, Van Essen DC, and Miller KL. A positive-negative mode of population covariation links brain connectivity, demographics and behavior. *Nat Neurosci* 18: 1565-1567, 2015.

Snyder AZ, and Raichle ME. A brief history of the resting state: the Washington University perspective. *Neuroimage* 62: 902-910, 2012.

Sokoloff L, Mangold R, Wechsler RL, Kenney C, and Kety SS. The effect of mental arithmetic on cerebral circulation and metabolism. *J Clin Invest* 34: 1101-1108, 1955.

Stafford JM, Jarrett BR, Miranda-Dominguez O, Mills BD, Cain N, Mihalas S, Lahvis GP, Lattal KM, Mitchell SH, David SV, Fryer JD, Nigg JT, and Fair DA. Large-scale topology and the default mode network in the mouse connectome. *Proc Natl Acad Sci U S A* 111: 18745-18750, 2014.

Steriade M, Contreras D, Curro Dossi R, and Nunez A. The slow (< 1 Hz) oscillation in reticular thalamic and thalamocortical neurons: scenario of sleep rhythm generation in interacting thalamic and neocortical networks. *J Neurosci* 13: 3284-3299, 1993.

Stevenson IH, and Kording KP. How advances in neural recording affect data analysis. *Nat Neurosci* 14: 139-142, 2011.

Stroh A, Adelsberger H, Groh A, Ruhlmann C, Fischer S, Schierloh A, Deisseroth K, and Konnerth A. Making waves: initiation and propagation of corticothalamic Ca2+ waves in vivo. *Neuron* 77: 1136-1150, 2013.

Swiech L, Heidenreich M, Banerjee A, Habib N, Li Y, Trombetta J, Sur M, and Zhang F. In vivo interrogation of gene function in the mammalian brain using CRISPR-Cas9. *Nature biotechnology* 33: 102-106, 2015.

Tasic B, Menon V, Nguyen TN, Kim TK, Jarsky T, Yao Z, Levi B, Gray LT, Sorensen SA, Dolbeare T, Bertagnolli D, Goldy J, Shapovalova N, Parry S, Lee C, Smith K, Bernard A, Madisen L, Sunkin SM, Hawrylycz M, Koch C, and Zeng H. Adult mouse cortical cell taxonomy revealed by single cell transcriptomics. *Nat Neurosci* 19: 335-346, 2016.

Thomas Yeo BT, Krienen FM, Sepulcre J, Sabuncu MR, Lashkari D, Hollinshead M, Roffman JL, Smoller JW, Zollei L, Polimeni JR, Fischl B, Liu H, and Buckner RL. The organization of the human cerebral cortex estimated by intrinsic functional connectivity. *Journal of neurophysiology* 106: 1125-1165, 2011.

Urban DJ, and Roth BL. DREADDs (designer receptors exclusively activated by designer drugs): chemogenetic tools with therapeutic utility. *Annual review of pharmacology and toxicology* 55: 399-417, 2015.

White BR, Bauer AQ, Snyder AZ, Schlaggar BL, Lee JM, and Culver JP. Imaging of functional connectivity in the mouse brain. *PLoS One* 6: e16322, 2011.

Yizhar O, Fenno LE, Davidson TJ, Mogri M, and Deisseroth K. Optogenetics in neural systems. *Neuron* 71: 9-34, 2011.

Chapter 2: Computing temporal delays in resting state fMRI

This chapter has been published as a journal article. The citation is:

Mitra A, Snyder A, Hacker C, Raichle M. (2014). Lag structure in resting state fMRI. J. Neurophysiol. doi:10.1152/jn.00804.2013.

Marc Raichle, Abraham Snyder and I conceived the project and research approach. I designed and implemented the methods and performed the data analysis. Carl Hacker helped with figure construction. Marc Raichle, Abraham Snyder and I wrote the paper.

2.1 Preface

At the time this paper was published in 2014, the idea that temporal lags in resting state fMRI data might be meaningful had never been articulated in print. Two points of common wisdom precluded consideration of BOLD signal temporal lags. First, conventional fMRI sequences provide one image of the human brain every 2-3 seconds. The fMRI community believed that such slow sampling of bran activity meant that meaningful temporal delays could not be computed from the data. Second, even if temporal delays were found, it was widely held that these delays were likely due to vascular factors. Indeed, the only papers that had considered temporal lags in fMRI to date were solely focused on long vascular delays in stroke tissue.

In this paper, we demonstrated that parabolic interpolation can be applied to cross-correlation/covariance curves derived from fMRI data to compute temporal delays on the order of ~0.5 seconds, and that the temporal structure derived from these computations is extremely stable in a group of ~700 subjects. We further argued that computed temporal delays are not attributable to purely vascular factors by demonstrating focal differences in temporal delays across conditions and providing a rough estimate of the dimensionality of temporal structure in resting state fMRI (more on this in Chapter 3). Finally, this work revealed one of the first yet enduring principles of the organization of resting state fMRI signals: in normal, awake adults, there is no net temporal sequence to activity among networks. That is, we do not consistently observe, for example, the visual network as a whole sending signals to the motor network. Instead, we find bi-directional signal flow between networks.

2.2 Abstract

The discovery that spontaneous fluctuations in BOLD (blood oxygen level dependent) signals contain information about the functional organization of the brain has caused a paradigm shift in neuroimaging. It is now well established that intrinsic brain activity is organized into spatially segregated resting state networks (RSNs). Less is known regarding how spatially segregated networks are integrated by the propagation of intrinsic activity over time. To explore this question, we examined the latency structure of spontaneous fluctuations in the fMRI BOLD signal. Our data reveal that intrinsic activity propagates through and across networks on a timescale of approximately one second. Variations in the latency structure of this activity resulting from sensory state manipulation (eyes open versus closed), antecedent motor task (button press) performance, and time of day (morning vs. evening) suggest that BOLD signal lags reflect neuronal processes rather than hemodynamic delay. Our results emphasize the importance of the temporal structure of the brain's spontaneous activity.

2.3 Introduction

It has been recognized since the inception of fMRI that the blood oxygen level dependent (BOLD) signal exhibits spontaneous fluctuations (Purdon and Weisskoff 1998). Although this phenomenon was initially regarded as noise, Biswal and colleagues showed that spontaneous fluctuations of the BOLD signal are temporally synchronous within the somatomotor system (Biswal et al. 1995). This basic result has since been extended to multiple functional systems spanning the entire brain (Buckner et al. 2011a; Choi et al. 2012; Power et al. 2011; Thomas Yeo et al. 2011). Synchronicity of intrinsic activity is widely referred to as functional connectivity; the

associated topographies are known as resting state networks (RSNs; equivalently, intrinsic connectivity networks (Fox and Raichle 2007)). The importance of understanding intrinsic activity is underscored by the fact that RSNs recapitulate the topographies of fMRI responses to a wide variety of sensory, motor and cognitive task paradigms (Cordes et al. 2000; Smith et al. 2009) providing a powerful means of delineating brain functional organization without the need for subjects to perform tasks. RSNs also provide an important window on the pathophysiology of various diseases (Fox and Greicius 2010; Zhang and Raichle 2010). These results establish that intrinsic brain activity is spatially structured, linked to the representation of function, and clinically relevant.

Almost all prior fMRI studies of intrinsic brain activity have used either seed-based correlation mapping (Biswal et al. 2010) or spatial independent components analysis (sICA) (Beckmann et al. 2005). Critically, both of these computational strategies incorporate the assumption that activity within RSNs is exactly synchronous. However, resting state fMRI studies in rat and man suggest that intrinsic activity is spatiotemporally structured (Majeed et al. 2011; Majeed et al. 2009). Ample evidence of temporally structured intrinsic activity has been observed in the mouse using voltage sensitive dye imaging (Ferezou et al. 2007; Han et al. 2008; Huang et al. 2010; Mohajerani et al. 2013; Mohajerani et al. 2010; Sato et al. 2012). In humans, Garg and colleagues (Garg et al. 2011) performed vector autoregressive (VAR) modeling of intrinsic activity followed by dimensionality reduction and identified two main spatiotemporal streams propagating through the brain. More recently, Smith and

colleagues (Smith et al. 2012) used temporal independent component analysis (tICA) to isolate multiple “temporal functional modes” in human resting state fMRI data. Implicit in this analysis is the notion that intrinsic brain activity can be decomposed into spatiotemporal components. However, the temporal features of these components were not explicitly explored.

Here, we specifically focus on the temporal features of intrinsic brain activity as expressed in its latency structure. We demonstrate that lags in intrinsic activity, as reflected in the BOLD signal, are highly reproducible across several large cohorts of young healthy adults. Moreover, this structure is modified, with appropriate focality, by the state of the eyes (open or closed), recent motor task performance, and time of day (i.e., morning vs. evening). When represented in 3D image format, iso-lag contours superficially resemble resting state networks (RSNs). However, closer analysis shows that lag topography actually is orthogonal to RSNs. Thus, each RSN encompasses a range of early and late regions and no RSN leads or follows any other. Rather, a temporal structure emerges which provides a framework for the functional integration of more conventionally defined RSNs.

2.4 Methods

Theory

Conventional seed-based correlation analysis involves computation of the Pearson correlation, r, between the time series extracted from a seed region, e.g., $x_1(t)$, and a second time series, $x_2(t)$, extracted from other loci (either single voxels or another region of interest). Thus,

$$r_{x_1x_2} = \frac{1}{\sigma_{x_1}\sigma_{x_2}}\frac{1}{T}\int x_1(t)\cdot x_2(t)dt, \quad (1)$$

where σ_{x_1} and σ_{x_2} are the temporal standard deviations of signals x_1 and x_2, and T is the interval of integration. Here, we generalize the assumption of exact temporal synchrony and compute lagged cross-covariance functions. Thus,

$$C_{x_1x_2}(\tau) = \frac{1}{T}\int x_1(t+\tau)\cdot x_2(t)dt, \quad (2)$$

where τ is the lag (in units of time). The value of τ at which $C_{x_1x_2}(\tau)$ exhibits an extremum defines the temporal lag (equivalently, delay) between signals x_1 and x_2 (Konig 1994). (Alternative strategies for latency analysis are discussed in the Appendix.) Clearly, *Eqs. 1* and *2* are related. Thus, $C_{x_1x_2}(0) = \sigma_{x_1}\sigma_{x_2}r_{x_1x_2}$. In other words, the Pearson correlation is equal to the cross-covariance at zero lag, normalized by the signal standard deviations. Because cross-covariance functions are not normalized, they retain sensitivity to signal magnitudes, which is critical in the present analyses. Although cross-covariance functions can exhibit multiple extrema in the analysis of periodic signals, BOLD time series are aperiodic (He et al. 2010; Maxim et al. 2005), and almost always give rise to lagged cross-covariance functions with a single, well defined extremum, typically in the range $\pm$0.5 sec. We determined the extremum abscissa and ordinate using parabolic interpolation (Figure 1).

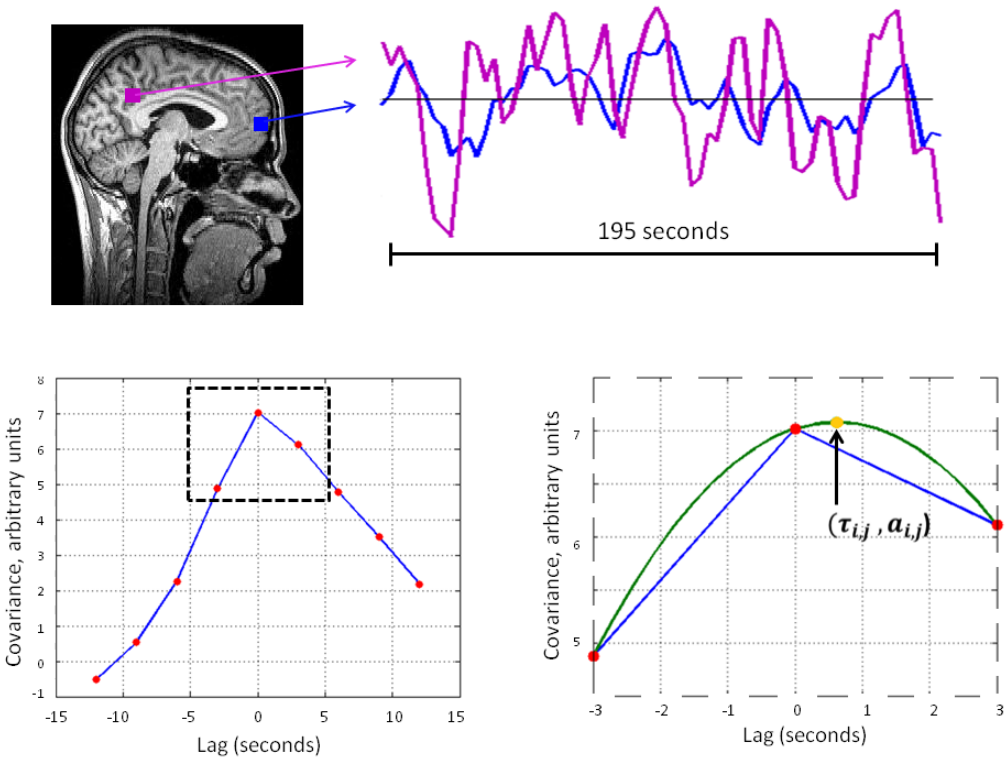

Figure 2-1: Calculation of pair-wise timeseries lag using cross-covariance and parabolic interpolation. The top right panel shows 195 s of two sampled time series extracted from two loci in the brain. The corresponding lagged cross-covariance function, computed over a full run (~300 s), is shown in the lower left panel (*Eq. 2*). The lagged cross-covariance is defined over the range ±L, where L is the run duration. The range of the plotted values is restricted to ±12 s, which is equivalent to ±4 frames (red markers) when the repetition time is 3s. The lag between the timeseries is the value at which the [absolute value of the] cross-covariance function is maximal. This extremum can be determined at a resolution finer than the temporal sampling density (one frame every 3 seconds) by performing parabolic interpolation (green line, lower right panel) through the computed values (red markers). This extremum (arrow, yellow marker) defines both the lag between time series i and j ($\tau_{i,j}$; *Eq. 4*) and the corresponding amplitude ($a_{i,j}$; *Eq. 5*).

Given a set of n time series, $\{x_1(t), x_2(t), \cdots, x_n(t)\}$, extracted from n regions of interest (ROIs), a lagged cross-covariance function can be computed between every pair of time series. Thus,

$$C_{x_i x_j}(\tau) = \frac{1}{T}\int x_i(t+\tau)\cdot x_j(t)dt \qquad i,j \in 1,2,\ldots,n. \tag{3}$$

$C_{xx}(\tau)$ is an $n \times n$ matrix that describes the covariance structure of the signal system parametric in lag. Finding all $\tau_{i,j}$ corresponding to the extrema, $a_{i,j}$, of $C_{x_i x_j}(\tau)$ yields the anti-symmetric matrix, T:

$$T = \begin{bmatrix} \tau_{1,1} & \cdots & \tau_{1,n} \\ \vdots & \ddots & \vdots \\ -\tau_{1,n} & \cdots & \tau_{n,n} \end{bmatrix}. \quad (4)$$

The diagonal entries of T are necessarily zero, as any time series has zero lag with itself. Moreover, $\tau_{i,j} = -\tau_{j,i}$, since time series $x_i(t)$ preceding $x_j(t)$ implies that $x_j(t)$ follows $x_i(t)$ by the same interval. T is widely known as a time-delay (TD) matrix, and represents all lag information contained in $\{x_1(t), x_2(t), \cdots, x_n(t)\}$.

The TD matrix does not contain any information regarding signal magnitudes. Therefore, the relative contribution of each signal pair to the entire spatiotemporal process is lost. To recover signal magnitude information, we define a second anti-symmetric matrix, A:

$$A = \begin{bmatrix} \tau_{1,1} \cdot a_{1,1} & \cdots & \tau_{1,n} \cdot a_{1,n} \\ \vdots & \ddots & \vdots \\ -\tau_{1,n} \cdot a_{1,n} & \cdots & \tau_{n,n} \cdot a_{n,n} \end{bmatrix}. \quad (5)$$

A is anti-symmetric for the same reasons as is T. In A, the time delays, $\tau_{i,j}$, are weighted by the magnitude of the signals at the extremum of $C_{x_i x_j}(\tau)$. We refer to A as an amplitude-weighted time-delay (AWTD) matrix.

We projected the multivariate data represented in the TD and AWTD matrices onto one-dimensional maps using the technique described by Nikolic and colleagues (Nikolic 2007; Schneider et al. 2006). We refer to these one-dimensional maps as latency projections. Operationally, the projection is done by taking the mean across the columns of T (*Eq. 4*) and A (*Eq. 5*), that is,

$$T_p = \left[\sum_{j=1}^{n} \tau_{1,j} \ \ldots \ \sum_{j=1}^{n} \tau_{n,j}\right], \qquad (6)$$

and

$$A_p = \left[\sum_{j=1}^{n} \tau_{1,j}.a_{1,j} \ \ldots \ \sum_{j=1}^{n} \tau_{n,j}.a_{n,j}\right], \qquad (7)$$

where T_p and A_p are $1 \times n$ latency projections of the TD and AWTD matrices, respectively. Thus T_p and A_p are row vectors whose elements represent latency and amplitude-weighted latency at each ROI. These projections can be represented in 3D image format (e.g., Figure 2). Critically, the projection technique is valid only if the TD and AWTD matrices are significantly transitive. Transitivity refers to the existence of consistent lag relations. Perfect transitivity means that the sum of lags over all closed loops is exactly zero. Given measurement error, perfect transitivity is never observed in

real neural data. A test for significant transitivity can be implemented by considering all time series triples (Nikolic 2007). Partial transitivity is defined as the fraction of all possible triples in a TD matrix that exhibit transitivity. A TD matrix is said to be significantly transitive if the fraction of all possible triples that exhibit transitivity significantly exceeds the number expected by chance alone ($p < .05$). All TD and AWTD matrices presented here satisfy this condition. Additional details regarding the projection technique are given in (Schneider et al. 2006).

Latency projections represent spatiotemporal processes in the brain. An estimate of the regional amplitude (in units of BOLD percent change) of each such process can be computed as the quotient of A_p divided by T_p. Thus,

$$Amp = A_p./T_p, \tag{8}$$

where the division is performed element-wise. Amp is a $1 \times n$ row vector, which we refer to as the latency process amplitude (LPA) image, that estimates the contribution of the spatiotemporal process to the total BOLD time series at each ROI. To compute this estimate, we first apply principal component analysis (PCA) to the complete set of BOLD time series. PCA assigns a percentage of the variance in the BOLD time series to each PC. Amp is projected onto each PC to find a weight w_i:

$$w_i^{Amp} = Proj\left(Amp, PC_i^{BOLD}\right),\ i = 1 \ldots n. \tag{9}$$

These weights are used to compute a weighted sum of PC variances.

$$Var_{LP}^{BOLD} = \sum_i w_i^{Amp} \cdot Var_{PC_i^{BOLD}}, i = 1 \ldots n. \quad (10)$$

Thus, each latency projection accounts for a computable fraction, Var_{LP}, of BOLD time series variance. Analogously, the TD matrix is subjected to PCA, and latency projections (in units of seconds) are projected onto the TD matrix eigenvectors.

$$w_i^{LP} = Proj(LP, PC_i^{TD}),\ i = 1 \ldots n. \quad (11)$$

These weights are used to compute the variance of the TD matrix accounted for by the latency projection.

$$Var_{LP}^{TD} = \sum_i w_i^{LP} \cdot Var_{PC_i^{TD}}, i = 1 \ldots n. \quad (12)$$

Imaging methods

Participants

Four extant, independent data sets were analyzed in this study. A large data set (N = 692) was obtained from the Harvard-MGH Brain Genomics Superstruct Project (Yeo et al. 2011b) (dataset 1, Table 1). The 692 subjects in dataset 1 were randomly divided into 7 cohorts of approximately 99 subjects each to test the reproducibility of our analyses. Three additional data sets (Fox et al. 2005b; Fox et al. 2007; Shannon et al. 2013) were previously acquired at the Neuroimaging Laboratories of the Mallinckrodt Institute of Radiology at the Washington University School of Medicine (datasets 2-4, see Table 1). All patients were young adults screened to exclude neurological impairment and psychotropic medications. Demographic information and acquisition parameters are given in Table 1.

Dataset	1	2	3	4
Number of subjects	692 (305 M + 387 F)	10 (4 M + 6 F)	17 (8 M + 9 F)	24 (15 M + 9 F)
Age in years	21.4 ± 2.4 (S.D.)	23.3 ± 3 (S.D.)	23.1 ± 2.4 (S.D.)	25.9 ± 2.3 (S.D.)
Scanner	Siemens Tim Trio	Siemens Allegra	Siemens Allegra	Siemens Tim Trio
Acquisition voxel size	$(3mm)^3$	$(4mm)^3$	$(4mm)^3$	$(4mm)^3$
Flip Angle	85°	90°	90°	90°
Repetition Time (s)	3.00	3.03	2.16	2.08
Number of frames	124 X 2 runs	110 X 6 runs	194 X 2 runs	194 X 2 runs
Citation	(Yeo et al., 2011)	(Fox et al., 2005)	(Fox, Snyder et al. 2007)	(Shannon et al., 2012)
Experimental Question	Replicability	Eyes open vs. Eyes closed	Before vs. After motor task	Morning vs. Evening

Table 2-1: Characteristics of analyzed datasets.

MRI acquisition

Imaging was performed with a 3T Siemens Allegra (Washington University) or a 3T Siemens Tim Trio (Harvard-MGH) scanner. Functional images were acquired using a BOLD contrast sensitive gradient echo echo-planar sequence [parameters listed in Table 1]. In dataset 1, all participants were simply instructed to keep their eyes open, remain still, and not fall asleep. Two fMRI runs were acquired per subject. In dataset 2, three runs were acquired in the eyes open visual fixation condition and 3 runs were acquired with eyes closed (Fox et al. 2005b). In dataset 3, we contrasted 2 resting state runs separately acquired before and after an intervening run during which subjects performed an attention demanding button press task (Fox et al. 2007). During the button press task, subjects were instructed to press a button in response to a visual cue (dimming of the fixation cross-hair). In dataset 4, we contrasted 2 resting state runs acquired in the morning (~1 hour after each subject's usual wake time) and evening (~2 hours before usual bed time). In all datasets, anatomical imaging included one sagittal T1-weighted magnetization prepared rapid gradient echo (MP–RAGE) scan (T1W) and one T2-weighted scan (T2W). The MP-RAGE sequence in dataset 1 was multi-echo.

fMRI preprocessing

Initial fMRI preprocessing followed conventional practice (Shulman et al. 2010). Briefly, this included compensation for slice-dependent time shifts, elimination of systematic odd-even slice intensity differences due to interleaved acquisition, and rigid body correction of head movement within and across runs. Atlas transformation was achieved by composition of affine transforms connecting the fMRI volumes with the T2W and

T1W structural images. Head movement correction was included with the atlas transformation in a single resampling that generated volumetric timeseries in $(3mm)^3$ atlas space. Additional preprocessing in preparation for latency analysis included spatial smoothing (6 mm full width at half maximum (FWHM) Gaussian blur in each direction), voxel-wise removal of linear trends over each fMRI run, temporal low-pass filtering retaining frequencies below 0.1 Hz, and zero-meaning each voxel time series. Spurious variance was reduced by regression of nuisance waveforms derived from head motion correction and timeseries extracted from regions (of "non-interest") in white matter and CSF. Nuisance regressors included also the BOLD timeseries averaged over the brain (Fox et al. 2005b). Additionally, we employed frame-censoring with a threshold of 0.5% root mean square frame-to-frame intensity change (Power et al. 2012). Frame-censoring excluded 3.8 ± 1.1% of all magnetization steady-state frames from the correlation mapping computations.

Gray matter segmentation and ROI definition

All present analyses were restricted to gray matter. A gray matter mask was constructed on the basis of a group averaged ^{18}F-flurodeoxyglucose positron emission tomography (FDG-PET) image. Group level gray matter masks conventionally are constructed by segmenting structural scans, e.g., using FreeSurfer (Fischl 2012). Here we achieved the same objective by thresholding a group average metabolic image, exploiting the fact that gray matter has approximately uniform FDG uptake. This strategy generates smoother gray matter partitions than structural segmentation. The source FDG-PET image, in $(3mm)^3$ atlas space, was generated in a separate

experiment (Vaishnavi et al. 2010), and was thresholded to exclude white matter, large vessels, and cerebrospinal fluid (CSF) spaces. To reduce the dimensionality of the latency analyses (number of ROIs), the gray matter mask was divided into $(6mm)^3$ cubic ROIs, discounting any cubes containing fewer than 50% gray matter voxels.

2.5 Results

Resting state latency projections

Latency projection results obtained in dataset 1 are displayed in Figure 2. The latency projection result (Figure 2A,C) spans approximately one second between the earliest and latest areas of the brain. The principle features of this map are: (i) a high degree of bilateral symmetry, and (ii) spatially distinct early and late regions. The earliest and latest brain regions are the posterior cingulate cortex/precuneus (PCC) and the cerebellum, respectively. The amplitude-weighted latency projection (Figure 2B) and the un-weighted TD latency projection (Figure 2A) exhibit similar topographies. Figure 2D illustrates the across sub-group spatial correlogram corresponding to the 7 sub-groups comprising dataset 1. This correlogram quantitatively demonstrates the spatial similarity between time delay (TD) and amplitude-weighted time delay (AWTD) latency projections (off diagonal blocks) as well as reproducibility across sub-groups (diagonal blocks).

The latency process amplitude (LPA) image (Figure 3A,B; see Eq. 8 for derivation) has high values in brain areas that strongly contribute to the brain's latency structure. As is true of the results shown in Figure 2, the LPA maps are highly similar across sub-

groups of dataset 1 (Figure 3C). High amplitude values appear in the default mode network (Raichle et al. 2001), as well as some other areas, most notably the visual cortex. The cerebellum, as a whole, contributes relatively little to the brain's latency structure except in parts that belong to the DMN (Crus II and the inferior vermis). We note that the topographies of lag (Figure 2A,C) and latency process amplitude (Figure 3A,B) are distinct.

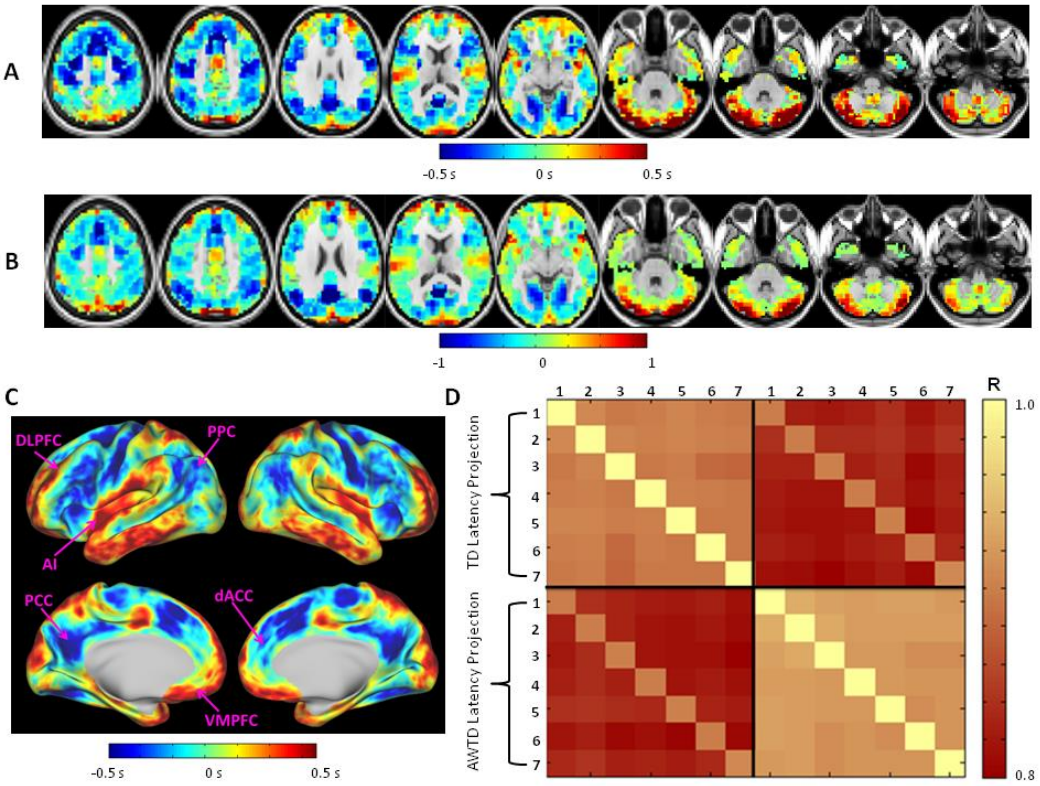

Figure 2-2: Results obtained in dataset 1. The 692 subjects were randomly divided into 7 equally sized subgroups of approximately 99 subjects each. (A) Latency projection of the time delay (TD) result obtained in the first sub-group illustrated in voxel-space. Lag is measured in seconds. (B) Latency projection of the amplitude-weighted time delay (AWTD) result corresponding to the TD result shown in (A). Because the BOLD signal magnitude depends on multiple fMRI sequence parameters, the unit of amplitude-weighted lag is arbitrary. (C) Surface representation of the volumetric result shown in (A). Arrows point to specific regions mentioned in the Discussion: posterior precuneus cortex (PCC), ventromedial prefrontal cortex (VMPFC), dorsal anterior cingulate cortex (dACC), anterior insula (AI), posterior parietal cortex (PPC), dorsolateral prefrontal cortex (DLPFC). (D) Spatial correlation between all TD (first 7 rows/columns) and AWTD (last 7 rows/columns) latency projections calculated in the 7 sub-groups.

The amplitude map can be used to estimate the relative contribution of the corresponding latency projection to the total variance of the BOLD signal within gray matter. This accounting is analogous to fractionating variance using principal component analysis. In our data, on average, 20.1% (+/- 0.7%) of the total variance in the whole brain BOLD signal time series is explained by the latency projection (*Eq. 10*). Moreover, 71.5% (+/- 1.4%) of the TD matrix variance is attributable to the latency projection (*Eq. 12*). Therefore, the latency process we have identified is a significant driver of sequential BOLD activity in the resting state, but it represents only a first component.

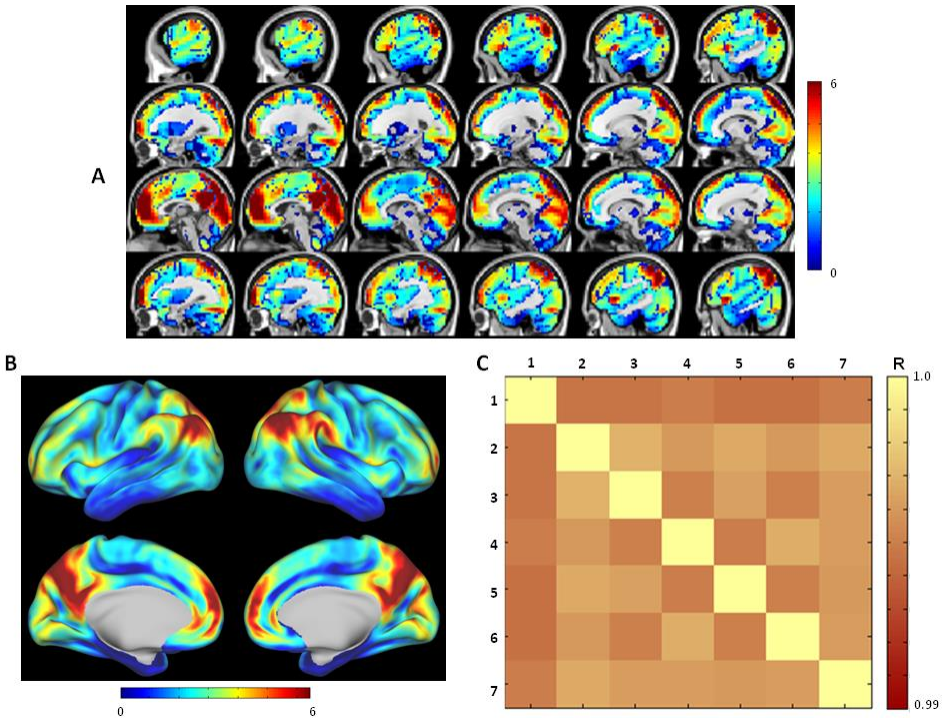

Figure 2-3: (A) Latency process amplitude (LPA) map illustrated in voxel-space obtained in the first sub-group of dataset 1 (same data as in Figure 2A-C). The scale is in units of BOLD amplitude. See *Eq. 8* for derivation. (B) Surface representation of the volumetric result shown in (A). (C) Spatial correlation between all amplitude maps calculated in the 7 subgroups of dataset 1.

State contrasts

The effect of state contrast on the latency structure of intrinsic activity was studied in three experiments. We first compared the eyes open versus the eyes closed (EO-EC) condition (dataset 2, Table 1). In the eyes open state, subjects were instructed to maintain visual fixation on a small crosshair. This state contrast is known to modulate the amplitude of intrinsic BOLD activity in visual cortex (Marx et al. 2004; McAvoy et al. 2008). The latency projection correlates of this experiment are shown in Figure 4. The most prominent change in latency was a shift toward later values in the dorsal visual stream with eyes open as compared with eyes closed. Similar changes were observed in the ventral visual stream, curiously omitting V1. The latency projection amplitude (LPA) also showed a large shift toward higher values in the dorsal visual stream with eyes closed as compared with eyes open. This result is consistent with numerous previous reports documenting reduced amplitude of BOLD fluctuations in the eyes open state (Bianciardi et al. 2009; Marx et al. 2004; McAvoy et al. 2008). This set of observations is significant in the light of potential relations between latency and perfusion (see below).

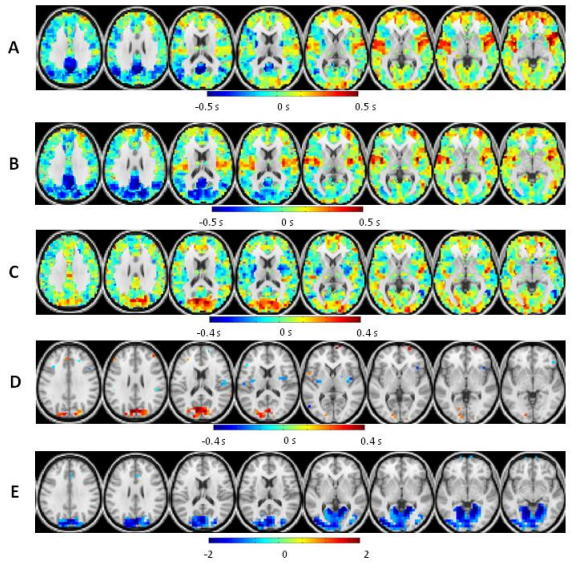

Figure 2-4: Latency results obtained in dataset 2. (A) Eyes Open (EO). (B) Eyes Closed (EC). (C) Eyes Open minus Eyes Closed. (D) Voxels with a statistically significant EO versus EC latency effect. (E) EO minus EC latency process amplitude (LPA) difference image. Color indicates statistically significant voxels.

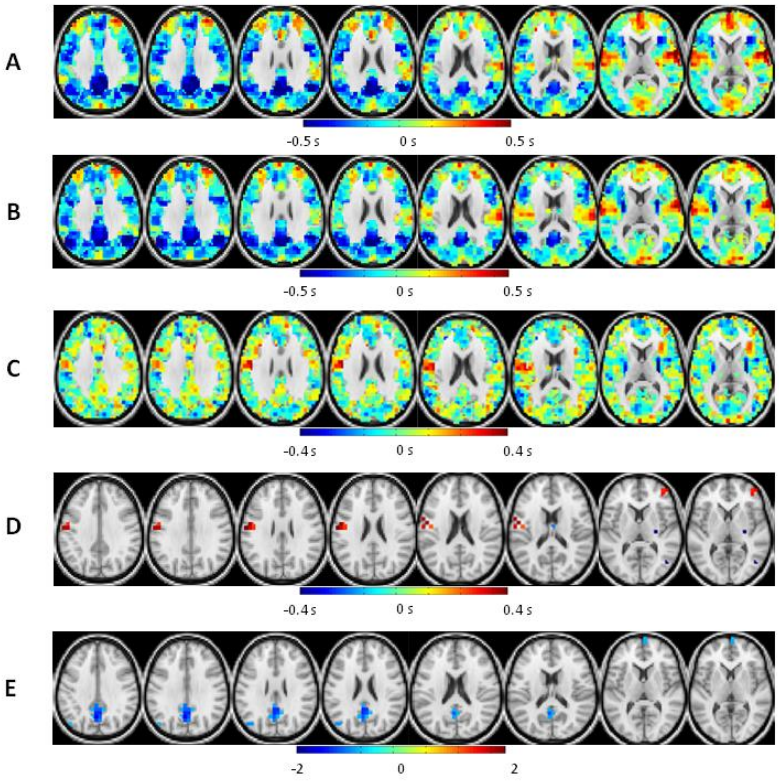

Figure 2-5: Latency results obtained in dataset 3. (A) Before button-press task. (B) After button-press task. (C) After minus Before. (D) Voxels with a statistically significant recent task performance latency effect. (E) After minus Before latency process amplitude (LPA) difference image. Color indicates statistically significant voxels.

In the second experiment, we compared the resting state after versus before performance of a cued right hand button push task (Fox et al. 2007; Fox et al. 2006). During the task fMRI run, subjects were instructed to press a button in response to a visual cue (dimming of the fixation cross-hair). The most prominent latency change was a shift toward later latency values in left ventral motor cortex following task performance (Figure 5). A shift toward earlier latency values was observed in bilateral striatum, although this effect was significant in only a small cluster of voxels in the right putamen (Figure 5D). As opposed to the EO-EC experiment, this contrast was computed over two identical resting state conditions (i.e., before and after task performance) rather than concurrent state contrast (i.e., eyes open at rest versus eyes closed at rest). Consequently, the change in latency structure seen following the button press task is a

function of antecedent task performance. The latency projection amplitude (LPA) showed a large reduction in the PCC (Figure 5E). No LPA change was observed in the voxels showing significant latency shifts. Thus, the LPA and latency effects were spatially dissociated in the button-push paradigm, whereas in the EO-EC experiment the effects were spatially overlapping.

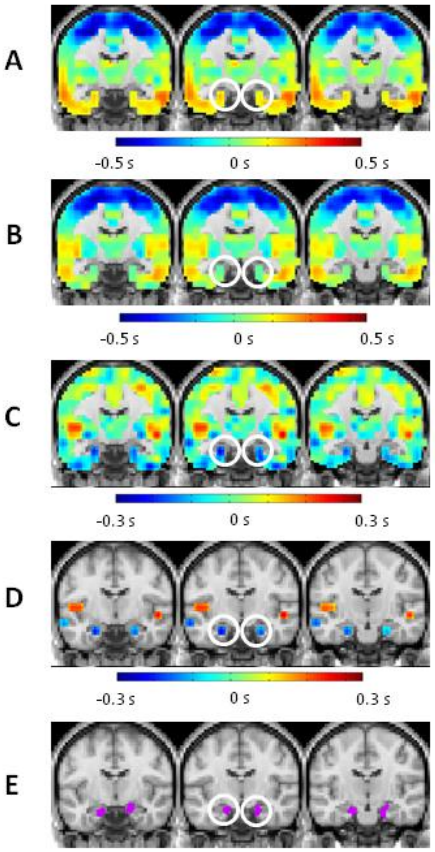

Figure 2-6: Latency results obtained in dataset 4. (A) Morning latency map. (B) Evening latency map. (C) Evening minus morning change in latency. Warm hues indicate increased lateness in the evening. Cool hues indicate increased earliness in the evening. (D) Statistically significant latency differences are seen in entorhinal and insular cortex. (E) Previously reported (Shannon et al. 2013) diurnal change in functional connectivity. Magenta indicates the two regions of interest, right and left entorhinal cortex, exhibiting the greatest diurnal change in functional connectivity with the rest of the brain (circled in central slices in panels A-E). Presently reported diurnal changes in latency (panels A-D) correspond to previously published functional connectivity changes in entorhinal cortex (panel E).

Finally, we contrasted resting state latency in data acquired shortly after waking in the morning and just prior to retiring in the evening (Shannon et al. 2013). This contrast was chosen specifically because it revealed significant diurnal changes in functional connectivity bilaterally in entorhinal cortex (magenta region in Figure 6E). In the morning, entorhinal cortices were functionally connected prominently to anterior insula.

In the evening, entorhinal cortices exhibited strong functional connectivity with cortical areas involved in memory retrieval as well as a significant reduction in functional connectivity with anterior insula. The present results, shown in Figure 6A-D, demonstrate significant latency changes in the entorhinal cortices from late in the morning (Figure 6A) to relatively early in the evening (Figure 6B). In contrast, latency shifted in the opposite direction in insular cortex (i.e., later in the evening as compared to morning). There were no statistically significant changes in LPA in the morning vs. evening contrast, again demonstrating that latency and amplitude effects can be dissociated.

Latency in relation to RSNs

Inspection of Figure 2A suggests a similarity in spatial scale between RSNs (Figure 7) and latency maps. This observation raises the question of the relation between RSNs and latency maps. To address this question, we computed the mean latency within each RSN. The obtained result was remarkably close to zero in every RSN (root mean squared latency value averaged over RSNs = 0.03 s). This outcome is not imposed by our analytic strategy. We generated surrogate RSNs matched in spatial frequency and scale to true RSNs to test whether the orthogonal relationship between RSNs and latency structure could be attributed to chance (Figure 7, See Appendix for more details). This analysis indicated that the likelihood of observing a root mean square value of 0.03 s is less than 1% (Figure 8), suggesting that the observed latency-RSN relationship is not attributable to chance alone. The implication of this result is that no RSN is either early or late. Instead, activity propagates both through and across RSNs.

Figure 9 shows the TD matrix corresponding to the results shown in Figure 2. Critically, the ROIs have been ordered first by RSN membership (Hacker et al. 2013) (see Figure 7), and, within RSN, by temporal order using latency projections by RSN block. Figure 9 also includes voxels assigned to the cerebrospinal fluid (CSF) category. The diagonal blocks in the TD matrix represent latency within RSNs (e.g., within DMN latencies, outlined in white); the off diagonal blocks represent latencies across RSNs.

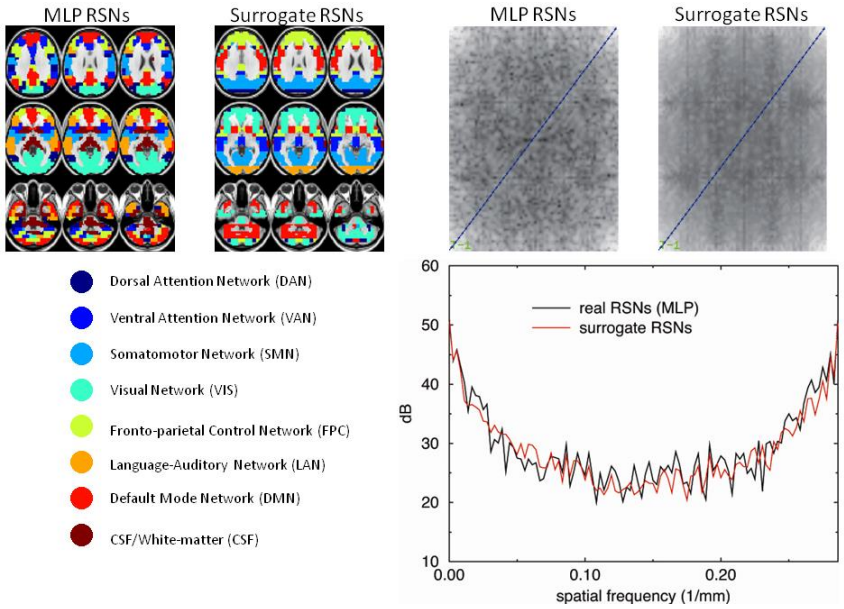

Figure 2-7: Real and surrogate RSNs. RSN labels and color-codes are presented in lower left. To test the statistical significance of the latency-RSN relationship, we created surrogate RSNs matched in spatial frequency to real RSNs. The real RSNs were defined as the group level winner-take-all result in Hacker et. al. 2013 (referred to here as "MLP RSNs"). Surrogate RSNs (N = 1000) were generated by applying symmetric group operations to the real RSNs (see Appendix). One typical example of surrogate RSNs is illustrated adjacent to the real RSNs. Spatial frequency domain representations (3D Fourier transforms of RSNs and surrogate RSNs) are on the upper right. The spatial frequency domain results are averaged over all real RSNs and over all surrogate RSNs, respectively, omitting the CSF component. Only the f_z=0 planes of the 3D spatial frequency domain representations are shown. The graph (lower right) shows relative spectral power (in dB) read out along the diagonal blue traces in the frequency domain representations. The plots are symmetric about the Nyquist folding frequency = $\frac{0.5}{3mm}$, which reflects the spatial sampling density (3mm cubic voxels). Critically, the spatial frequency content of the surrogate RSNs is well matched to the real RSNs.

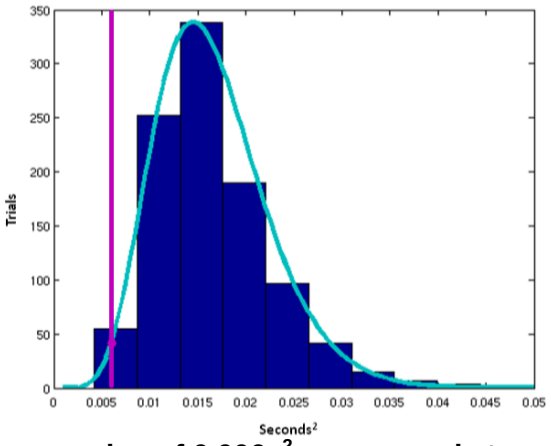

Figure 2-8: Histogram of summed squared mean latency values in surrogate RSNs. 1000 surrogate RSN partitions (e.g., Figure 7) were generated. The latency mean was evaluated for each surrogate RSN. On the assumption that mean RSN latencies are normally distributed about zero, the sum of squares of these values theoretically is distributed as $\chi^2(7)$. The light blue trace represents the theoretical gamma probability density function fit to the simulations (blue histogram). The vertical pink line represents the summed squared latency values in the real RSNs ($0.006s^2$). A squared sum value of $0.006s^2$ corresponds to a root mean square value of 0.03s, as reported in the main text. The surrogate data indicate the probability of this outcome occurring by chance is $p < 0.0096$.

Figure 9 includes some features that are algebraically constrained. In particular, the TD matrix is anti-symmetric. Therefore, each diagonal block is anti-symmetric as well. However, the algebra does not impose any relation between latency and RSN membership. Therefore, the structure evident in Figure 9 is informative. The diagonal blocks show a wide range and well-ordered distribution of latencies. Thus, activity propagation is present within each RSN. The CSF block is much less well ordered even though it was analyzed identically to the true RSNs. This distinction demonstrates that the observed intra-RSN latency structure reflects brain organization at the systems level and is not an algebraic artifact.

The off-diagonal blocks represent activity propagation across networks. Each block contains well-ordered early, middle, and late components much like the diagonal blocks. Again, this is not algebraically imposed. To obtain a numerical measure of latency spread within blocks, we computed the latency standard deviation. The mean value of this measure across the diagonal blocks was 0.15s. The same result (0.15s) was

obtained in off-diagonal blocks. The existence of latency ordering within off-diagonal blocks suggests organized lag relations between constituent parts of RSNs. As an example, consider the off-diagonal block corresponding to the DMN paired with the dorsal attention network (DAN), outlined in white in Figure 9. A well-ordered progression from early (blue) to late (red) is evident, indicating that parts of the DMN lead the DAN and vice versa. Again, a comparison with the CSF blocks is informative. Very little structure is evident in the DAN:CSF block (outlined in white), reflecting the absence of organized reciprocal latency.

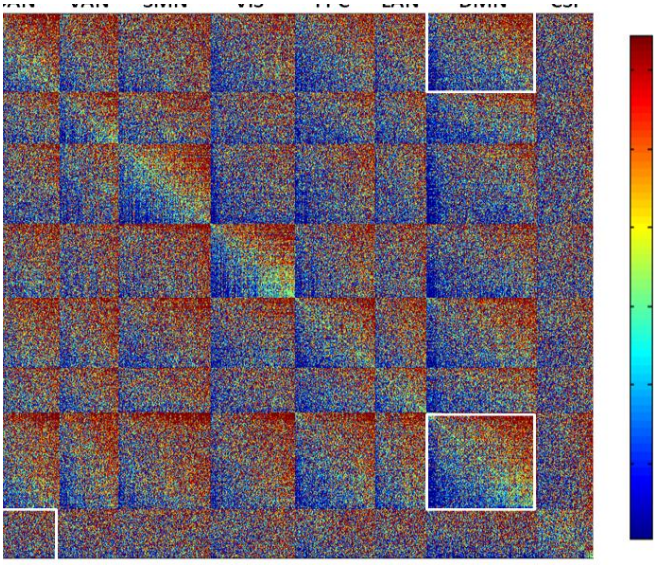

Figure 2-9: Relationship of latency to RSNs. The figure shows a TD matrix with ROIs ordered by RSN membership (see Figure 7 for abbreviations). Within each RSN, the ROIs are further ordered by latency. Note wide range of latencies within RSNs (diagonal blocks, each necessarily anti-symmetric) and anti-symmetric features across RSNs (off-diagonal blocks). Note also absence of organization in CSF blocks. Blocks referred to in the Main Text are outlined in white. The diagonal blocks in the TD matrix illustrate that each network has early, middle, and late components. Moreover, the off diagonal blocks have early, middle, and late components. Therefore, no network leads or follows any other network. Rather, lags are equivalently distributed within and across RSNs.

To examine the possibility that the latency process is present with more power within certain RSNs or RSN pairs, we computed the amplitude-weighted time-delay matrix (Figure 10), in which ROIs are ordered as in Figure 9. Since the lag values are weighted by amplitude, ROI interactions with little power have values closer to zero (green hues in Figure 10). As above, we computed a measure of spread within blocks as the amplitude-weighted latency standard deviation. Among the RSNs, the DMN and

VIS exhibited the greatest spread of amplitude weighted latencies. This feature appears in Figure 10 has a high level of blue/red saturation. In contrast, the CSF blocks are comprised primarily of values near zero (appear green). These results are in line with Figure 3. The critical feature in Figure 10 is that the diagonal and off-diagonal blocks are comparably saturated. In quantitative terms, the diagonal and off-diagonal blocks exhibit comparable mean standard deviations (0.35 and 0.33, respectively, in units of amplitude·seconds). Combining the results shown in Figures 9 and 10 implies that lag amplitudes are similarly distributed within and across RSNs.

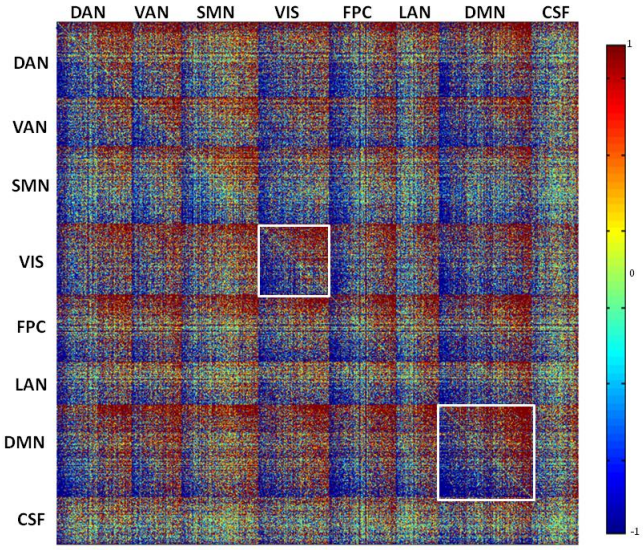

Figure 2-10: Amplitude-weighted time delay (AWTD) matrix corresponding to Figure 9. Blocks referred to in the Main Text are outlined in white.

Control analyses

We considered three non-neuronal explanations for the spatial patterns of BOLD latency projections (Figure 2). First, is there a relationship to vascular territories (anterior cerebral artery, middle cerebral artery, posterior cerebral artery)? Reference to standard vascular territory maps (Damasio 1983) shows no clear correspondence. In particular, Figure 2 shows latency contrast around the ventral central sulcus, whereas this part of the brain and widely surrounding areas are all middle cerebral artery territory.

Although different vascular territories see arterial blood at different latencies with respect to the aorta, there is no parsimonious mechanism by which this difference could translate to differential BOLD signal latencies. Second, better perfused tissue may be expected to show a more prompt response to neural activity. In fact, precisely this mechanism probably accounts for delayed BOLD signals in the vicinity of recent infarcts (Amemiya et al. 2013). Accordingly, we compared latency projections to a group average perfusion map constructed on the basis of PET data (Vaishnavi et al. 2010). A scatter plot of cerebral blood flow (CBF) versus latency was constructed (Figure 11). Inspection of this plot showed no clear evidence of a systematic relation between CBF and latency (Pearson r = -0.05). A negative correlation is in line with the theory that better perfused tissue shows more prompt BOLD response to neuronal activity. However, this effect is negligible, as it only explains 2.5% of latency variance.

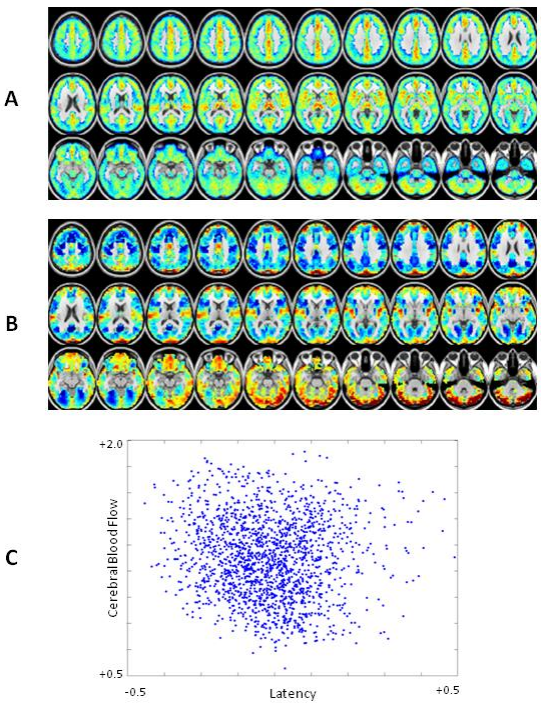

Figure 2-11: Comparison of cerebral blood flow versus time-delay (TD) latency projection. (A) Cerebral blood flow map obtained in a group of 33 normal young adults. (B) TD latency projection; same data as Figure 2A-C. (C) Scatter plot showing the relationship between cerebral blood flow and the latency projection. Each dot represents one ROI. To test whether the reproducibility of latency structure (Figure 2D) is attributable to CBF, we computed the mean cross-group correlation for the 7 cohorts in dataset 1, before and after regressing out the effects of CBF. The mean cross-group correlation was r = 0.898 in both cases. This result demonstrates that the effect of CBF on measured latency, if present, is negligible.

Finally, it is well known that the BOLD signal is strongly weighted toward the venous side of the circulation (Hall et al. 2002). Therefore, the BOLD signal in cerebral veins should appear at late latencies (Lee et al. 1995). To investigate this possibility, a group average "venogram" was constructed by computing the voxel-wise beta-map corresponding to the differentiated global signal (see Appendix for details). Thresholding this map to retain only negative values generated an image demarcating the major venous structures in the head (Figure 12). Reference to this map demonstrated that cerebral venous structures do account for some features of the latency map, in particular, lateness in the superior and sagittal sinuses. Most of the vascular spaces, however, were already excluded from our analysis by our gray matter mask (see Methods). Thus most of the features evident in Figure 2 do not correspond to the "venogram" and, therefore, are not attributable to cerebral venous outflow.

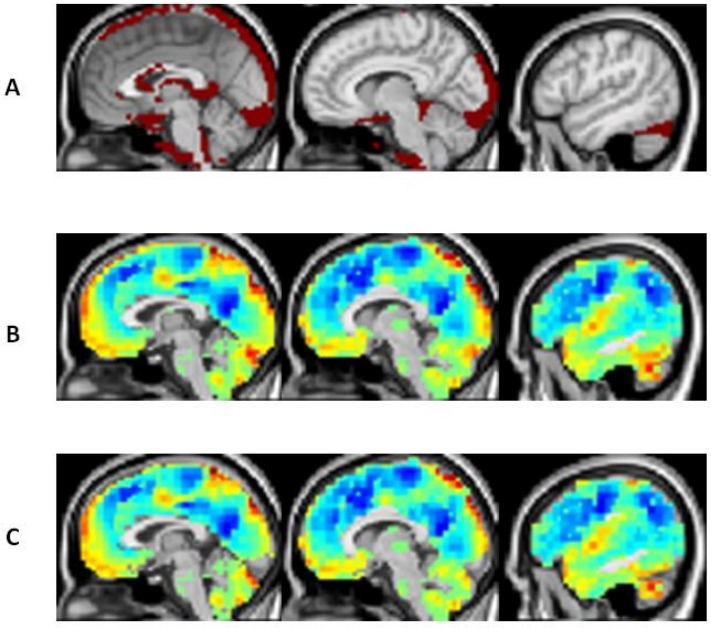

Figure 2-12: Venous contribution to latency structure. (A) Venogram. (B) TD latency projection for comparison. Our gray matter masking procedure (see Methods) excludes many of the voxels that correspond to venous structures, but some overlap is apparent. (C) TD latency projection with venous structures masked out.

2.6 Discussion

Summary of Present Findings

We used latency projections (Nikolic 2007) to study the lag structure of the resting state BOLD signal in healthy young adults. Substantial consistency was demonstrated over 7 large cohorts. The amplitude of lagged activity was highest in the default mode, control, and visual networks. Latency process amplitude (LPA) estimation indicated that the spatio-temporal process shown in Fig. 2A accounts for approximately 20% of the resting state BOLD signal. These results provide of means of studying integration within and across resting state networks, which so far have been defined primarily in terms of network segregation.

We studied the effects of three state contrasts (eyes open vs. eyes closed, before vs. after right handed button push in response to visual cue, morning vs. evening) to test whether latency structure depends on neuronal activity. Temporal structure was modified, with appropriate focality, in all three experiments, suggesting that the latency structure is indeed neuronally driven.

Time-delay matrices (Fig. 9) suggest functional integration within and across RSNs. Surprisingly, we found that the temporal structure of the BOLD signal is orthogonal to RSN topography. In other words, there is equivalent activity propagation both within and across RSNs. The well-ordered organization of activity propagation within and across RSNs contrasts with the highly disorganized activity evident in CSF, demonstrating that the observed propagation structure is not algebraically imposed. By

generating surrogate RSNs, we demonstrated that the orthogonal relationship between RSNs and latency is not attributable to chance (Figure 7, Appendix).

Finally, we investigated the effects of CBF and large vascular structures on latency structure.

CBF was found to have negligible explanatory power (Figure 11). The superior sagittal sinus contributed some late features in the latency map, but masking the latency image by an fMRI-derived "venogram" (see Appendix) demonstrated that most latency features are not attributable to large vascular structures (Figure 12).

Observed latency in relation to vascular physiology

The BOLD signal is governed by the local concentration of deoxyhemoglobin, which is paramagnetic and, therefore, an MRI contrast agent (Ogawa et al. 1990). Changes in the fMRI BOLD signal, either task-related or spontaneous, reflect changes in blood flow that are greater than changes in oxygen consumption. These changes have been physiologically linked to changes in local field potentials (Goense and Logothetis 2008; Logothetis 2008; Logothetis et al. 2001; Logothetis and Wandell 2004) and cellular metabolism (i.e., changes in cellular redox states (Mintun et al. 2004; Vern et al. 1997; 1998) and aerobic glycolysis (see (Raichle and Mintun 2006) for review)). Most recently, propagated activity in the mouse brain (see Neurophysiology of latency) has been visualized using voltage sensitive dye imaging (Mohajerani et al. 2013; Mohajerani et al. 2010), which entirely avoids the question of neurovascular coupling. Nevertheless, concern lingers that regional variations in the latency of neurovascular coupling could

largely account for observed delay structure (Friston 2009; 2011; Friston et al. 2013; Friston and Dolan 2010; Handwerker et al. 2004).

Hemodynamic and neuronal contributions to observed lag structure cannot be separated on the basis of the BOLD signal alone. However, we can adjudicate between a primarily neuronal vs. primarily hemodynamic explanation for observed lag structure by considering the plausibility of each of these explanations for our results.

First, we find changes in latency structure as a result of state contrasts (Figures 4-6). A vascular explanation for this result implies focal changes in the dynamics of neurovascular coupling. It might be argued that the latency differences in Figures 4 and 6 reflect changes in sympathetic tone (due to eye closure or time of day) leading to altered vascular dynamics. However, Figure 5 contrasts two resting states separated by a task run. It is highly plausible that task performance leaves a neural trace. In fact, such traces must underlie episodic memory and skill acquisition. It is much less plausible, although not inconceivable, that prior task performance leaves a trace manifesting as focally altered vascular hemodynamic coupling. Second, latency projections are orthogonal to RSNs (Figures 7 and 8) in a manner not attributable to chance. Thus, there exists a structured relationship between RSNs, which unquestionably reflect neuronal activity, and latency projections. A purely vascular explanation for this relationship is difficult to imagine, although we cannot exclude it. Conversely, a neuronal explanation for this relationship suggests that lagged activity plays a role in functional integration across segregated brain networks. Third, let us

suppose that regional differences in neurovascular coupling delays do exist. We further assume that neural processes are effectively simultaneous, that is, we neglect axonal conduction delays on the order of tens of msec (Vicente et al. 2008).Then, by hypothesis, some regions transduce neural activity into a BOLD signal before other regions. This time shift can be represented as a set of ordered relations, as illustrated in Figure 2. We show in the Appendix that such a structure gives rise to a lag matrix of dimensionality exactly one. However, Bayesian Information Criterion analysis (Minka 2001) indicates that the most likely dimensionality of the BOLD TD matrix (Figure 9) is 2 (Figure 13, See Appendix for details). This result implies the existence of two transitive systems of lags within the TD matrix. Regionally dependent latencies in neurovascular coupling mathematically can account for only one of these (see Appendix). Therefore, hemodynamic delays, even if they exist, cannot account for the entirety of the observed latency structure.

Although these considerations argue for a neuronal basis for latency structure, the present fMRI data provide only indirect evidence. Future direct tests combining other modalities (e.g., metabolic or electrophysiologic) with fMRI will be necessary to definitely assess the physiological basis of latency structure.

Neurophysiology of latency

Several features in our latency projection results are consistent with previous identification of sources and sinks of intrinsic activity obtained using vector auto-regressive (VAR) modeling. Sources and sinks correspond, respectively, to early and

late areas in the latency structure. Specifically, Garg and colleagues found that inferior parietal cortex and PCC are sources of propagated activity (Garg et al. 2011). This result matches our assignment of these regions as early in the latency projection (Figure 2). Similarly, Desphande and colleagues identified the DMN as a major locus of propagated intrinsic brain activity, in agreement with our amplitude map result (Figure 3) (Deshpande et al. 2011). Moreover, the anterior prefrontal cortex was reported to be a sink of propagated activity, which matches our assignment of this region as late in the latency projection (Figure 2). Many of the above discussed features were also obtained by Majeed and colleagues using a novel iterative technique based on computing lagged correlation functions (Majeed et al. 2011).

Propagated activity is well documented in the electrophysiology literature. Recent work in the mouse using voltage sensitive dye (VSD) imaging has documented wave-like propagation of both evoked and spontaneous activity (Ferezou et al. 2007; Han et al. 2008; Huang et al. 2010; Mohajerani et al. 2013; Mohajerani et al. 2010; Sato et al. 2012). Although VSD is capable of millisecond temporal resolution, the observed spontaneous activity motifs in the mouse cortex play out over approximately 0.5s (Mohajerani et al. 2013; Mohajerani et al. 2010), in close agreement with our results (Figure 2A). The speed of spontaneous activity propagation in the mouse has been estimated as approximately 0.2 m/s (Han et al. 2008; Mohajerani et al. 2010). In our data, we take as typical a latency difference of 0.5 s over 10 cm, which yields a propagation speed of 0.2 m/s, in agreement with the mouse estimate. Slow wave propagation has also been documented during slow wave sleep (SWS). The speed of

slow wave propagation in SWS has been estimated as 0.4 to 6.3 m/s (Massimini et al. 2004; Murphy et al. 2009b). This speed of propagation estimate is reasonably comparable to the estimate from our data (0.2m/s, see above), given that the SWS figure was obtained on the basis of scalp electroencephalography (EEG) and inverse source modeling (Murphy et al. 2009b). Interestingly, Murphy and colleagues report that the DMN is preferentially involved in slow wave propagation during SWS (Murphy et al. 2009b), which is concordant with our finding that the DMN is represented with high amplitude in the latency projection (Figure 3). Although SWS and waking quiet rest are distinct states, intrinsic activity exhibits many similarities across levels of arousal (Larson-Prior et al. 2009; Vincent et al. 2007). RSNs are present, albeit with arousal-dependent features, in both wakefulness and SWS (Samann et al. 2011). Substantial evidence indicates that the slow waves in SWS represent UP and DOWN state oscillations (Huber et al. 2004; Massimini et al. 2004; Murphy et al. 2009b; Yuste 1997). It has been reported that UP and DOWN states persist during wakefulness, although they are intermixed with other activity and are much less periodic (Vyazovskiy et al. 2011). If so, the same mechanism may drive slow activity in waking and SWS. Thus, there exists a plausible electrophysiological mechanism underlying slow propagated BOLD activity.

Murphy and colleagues find that sources and sinks of spontaneous activity in the mouse recapitulate patterns of activity observed in task responses (Mohajerani et al. 2013). In other words, primary areas (such as primary somatosensory cortex) tend to be sources in task-evoked and spontaneous activity, while higher order areas such as the parietal

lobule are sinks during task-evoked and spontaneous activity. Our results show partial correspondence with this principle. In particular, primary motor cortex is early and superior parietal lobule is late (Figure 2C), in agreement with task-evoked studies in mice (Mohajerani et al. 2013). Additionally, lateral prefrontal cortex exhibits very delayed response to item recognition trials (Schacter et al. 1997), which is in agreement with our spontaneous activity lag results (Figure 2A,C). However, primary sensory and auditory cortices are late in our data (Figure 2C), in contrast with the Murphy results. These divergences could be attributable to differences in species or technique, but we believe that the more likely explanation lies in a fundamental distinction between spontaneous and task-evoked activity. Task-evoked BOLD responses in humans exhibit a wide variety of waveforms and variable mixtures of sustained and transient components, depending on locus and task paradigm (Fox et al. 2005a; Gonzalez-Castillo et al. 2012). Moreover, these responses play out on a time scale on the order of several seconds. In contrast, our lag results are generally confined to a range of ±0.5 seconds. Thus, although there may be some shared motifs between lagged spontaneous and task-evoked activity, the two phenomena most likely represent different processes with different temporal structures (see (Raichle 2011) for further discussion).

Functional significance of latency

It is striking that the resting state BOLD signal, which has been used to identify spatially segregated functional networks (Power et al. 2011; Yeo et al. 2011a), also carries a signature of functional integration within and across RSNs. Critically, resting state

activity propagation is directed, as reflected in a latency map (Figure 2). Thus, there is a stereotyped pattern of activity propagation in the human brain, such that, on average, certain brain loci initiate propagated activity (early regions) while other loci are destinations (late regions). While it is widely believed that cross-network communication underlies brain function (Bressler and Menon 2010), discussion of this point largely derives from task based experiments. Our analyses reveal loci corresponding to sources and sinks of propagated intrinsic activity. Remarkably, many of the same loci have been independently identified, on the basis of task-based fMRI, as key cortical nodes regulating behavior (Bressler and Menon 2010; Nelson et al. 2010). Specifically, these loci (Figure 2C) are: posterior precuneus cortex (PCC, early), ventromedial prefrontal cortex (VMPFC, late), dorsal anterior cingulate cortex (dACC, early), anterior insula (AI, late), posterior parietal cortex (PPC, early), dorsolateral prefrontal cortex (DLPFC, late). These areas represent three pairs of regions belonging to the default mode, salience, and fronto-parietal control networks, respectively. It is probably not coincidental that, within each network pair, one region is early while the other is late. Indeed, the orthogonality of RSN and latency topography suggests that propagated activity in the resting state may serve as a framework for RSN integration. Thus, analyzing latency structure might be a useful method to increase our understanding of cognitive processes, whether they are physiologic or pathologic in nature.

One feature of our results that deserves further comment is that the cerebellum as a whole is late in the latency map (Figure 2A). The cerebellum is widely regarded as

responsible for reflexive adjustments during active behavior (Buckner et al. 2011b; Leiner et al. 1991; Strick et al. 2009), for example, adjusting motor programs in response to unanticipated changes in environmental parameters (e.g., load). In the resting state, the role of the cerebellum appears to be minor, as reflected by the low amplitude of intrinsic cerebellar BOLD fluctuations (Li et al. 2012; Logothetis and Wandell 2004). Our data suggest that, at least in the resting state, the primary direction of information flow appears to be from prosencephalon to cerebellum. This observation is consistent with the current understanding of the cerebellum as primarily a receiver of multimodal information from the cerebral cortex (Leiner et al. 1991). Nonetheless, we cannot exclude the possibility that the vascular response to neural demand is generally late in the cerebellum. However, this explanation would be specific to the cerebellum as opposed to the posterior circulation, because visual and infero-temporal cortices are mostly early.

State Contrasts in Latency

The original motivation for examining state contrasts was to present evidence that neuronal phenomenology drives latency structure. However, the observed effects of state contrast on latency are potentially of physiologic interest. In the eyes open condition, propagated signals appear to flow from primary to higher order visual cortex (Figure 4A), in accordance with known direction information flow in visual processing (Van Essen et al. 1992). In the eyes closed condition, the direction of signal propagation appears to reverse (Figure 4B). Speculatively, this reversal may reflect may reflect top-down influences supporting mental imagery (Stokes et al. 2009). In the button push

contrast, we theorize that changes in latency after performance of a motor task reflect physiologic processes related to learning. Although the task is simple (pushing a button in response to cross-hair dimming), it is attention demanding, and subjects do show an improvement in reaction time (data not shown). Enhanced signaling from putamen to the left motor region (Figure 5D) may underlie this improvement. This result is consistent for the known role of the putamen in motor learning (Grafton et al. 1995).

The presently observed latency differences between morning and evening (Figure 6C,D) spatially correspond to previously reported functional connectivity changes in medial temporal lobe and insula (Figure 6E) (Shannon et al. 2013). The previous findings point to changes in signal correlation; the present results point to diurnal changes in directed signaling. Specifically, the entorhinal cortex is late in the morning and early in the evening. Entorhinal cortex is the main interface between hippocampus and neocortex (Lavenex and Amaral 2000). It is believed that the hippocampus accumulates encoded experiences during the day, and that this form of memory is labile (Axmacher et al. 2009). Memory consolidation is thought to require transfer of information from hippocampus to neocortex, which takes place later in the day and during sleep (Axmacher et al. 2009). Accordingly, entorhinal cortex may be late in the morning because it is acting as an information accumulator. Conversely, entorhinal cortex is early in the evening because it is transferring information to cortex, thereby facilitating formation of hippocampal independent memories. The insula is relatively early in the morning and late in the evening. Interpreting this effect will require further investigation.

Limitations

There are 3 principle limitations of this work. First, our method for estimating latencies (parabolic interpolation of pair-wise cross-covariance estimates) undoubtedly includes some imprecision, in part because the temporal sampling density is relatively low (see Repetition Times in Table 1). However, our conclusions are based on results obtained at the group level. These group level latency estimates are reproducible across 7 large cohorts (Figure 2D).

Second, our findings are based on resting state fMRI data pre-processed using global signal regression (GSR). GSR is a controversial processing step (Fox et al. 2009; Murphy et al. 2009a); however, in preliminary analyses, it was determined that omission of GSR greatly reduces the range of observed latencies. This is easily understandable as a consequence of retaining large quantities of instantaneously correlated shared variance. It is likely that some fraction of the global signal is neuronally derived (Scholvinck et al. 2010); however, it is certain that a large fraction is non-neuronal artifact attributable to head motion (Power et al. 2012; Power et al. 2013; Yan et al. 2013) and variable pCO_2 (Birn et al. 2006). Moreover, the artifactual component of the global signal exhibits substantial cross subject variability (He and Liu 2012; Power et al. 2013). Therefore, GSR is a necessary noise-reduction technique in the present analysis.

Finally, to estimate the statistical significance of the orthogonality of latency structure with respect to RSNs, we developed a method to generate surrogate RSNs with the aim of matching the spatial characteristics of real RSNs (see Appendix). While the topology of true RSN structure was preserved in the surrogates, the spatial frequency distribution was only approximately matched (Figure 7). Nevertheless, we are persuaded that the orthogonality relationship is statistically significant.

2.7 Acknowledgements

We thank Manu Goyal, Ben Palanca, and Benjamin Shannon for helpful discussion. This work was supported by the National Institute of Health (NS080675 to Drs. Raichle and Snyder and P30NS048056 to Dr. Snyder). Dataset 1 was obtained, with assistance from Dr. Randy Buckner, from The Brain Genomics Superstruct Project, funded by the Simons Foundation Autism Research Initiative.

2.8 Appendix

Alternative Strategies for Computing and Analyzing Latencies

We directly computed lags between time series on the basis of lagged cross-covariance functions. Parabolic interpolation was used to determine the lag of maximal covariance at a temporal resolution finer than the sampling density. An alternative method based on iterating lagged correlation functions has been described (Majeed et al. 2011; Majeed et al. 2009), but it applies to whole images as opposed to ROI pairs. Additionally, the iterative method provides no basis for calculating what percentage of variance attributable to latency components. The major alternative strategy for estimating lags is the phase-slope method, in which lag is computed as the derivative

with respect to frequency of complex coherence phase (Jenkins and Watts 1968). Although the phase slope method has been used to analyze fMRI data (Hinkley et al. 2013; Sun et al. 2005), we chose a time domain method because the frequency domain method requires differentiation, which yields noisy and unstable estimates. Moreover, the phase-slope method requires evaluating slope over some interval under the assumption that the slope is constant, which is not necessarily true.

Having obtained a time delay matrix by any method, alternatives for extracting latency components include the present (projection) method (Nikolic 2007; Schneider et al. 2006) and eigenvector decomposition. We tested both approaches and found that the principal eigenvector generally is very similar to the result obtained by the projection method. However, the projection method yielded much more reproducible results in cross-subgroup analysis shown in Main Text Figure 2.

A substantial body of previous work has applied vector autoregressive (VAR) methods to the study of directed influences in fMRI data (Deshpande et al. 2011; Friston et al. 2003; Garg et al. 2011; Goebel et al. 2003; Smith et al. 2012). All of these methods require the computation of $k \times k \times \tau$ matricies, where k is the number of ROIs, and τ is the order of the model. Even if model order is limited to 1 (Garg et al. 2011; Smith et al. 2012), VAR does not directly return lag, which is the present quantity of interest. Dynamic causal modeling (dcm) is a VAR based method for estimating the most likely topology of directed graphs. However, in practice, dcm is limited to a handful of ROIs, and therefore, is unsuited to the present investigation. Granger causality (Deshpande

et al. 2011; Goebel et al. 2003) is theoretically less combinatorically demanding than dcm, but like dcm, is essentially an information-theoretic analysis. The scope of our analysis is much more restricted and does not rely on models. Our results carry implications regarding the existence of propagated disturbances and directed influences in intrinsic brain activity, but we here avoid information theoretic approaches in favor of a more concrete and interpretable analysis based on lags.

Generation of surrogate RSNs

We generated surrogate RSNs topologically matched to real RSNs and approximately matched in spatial frequency distribution (Figure 7). Surrogate RSNs were generated by treating the left hemisphere of the real RSN brain as an element of a high dimensional symmetric group that respects the topology of the true RSNs. We then applied randomly generated full-rank permutations on the uni-hemispheric RSN brain partition. In greater detail, the 3D MLP RSN partition was converted to a 1D vector and the ends were connected to form a ring. The ring, then, was randomly rotated and the 3D to 1D transform inverted. In principle, other group operations could have been applied, but rotation theoretically preserves spatial scale. The resulting 3D map was reflected across the mid-sagittal line to generate hemispherically symmetric surrogate RSNs. Equivalence of spatial scale was verified by 3D-Fourier analysis (Figure 7).

Generation of "venograms"

Regression frequently is used to compute the topography within the brain of reference signals, e.g., estimated response waveforms in task fMRI. Similarly, the topography of

a time shifted reference signal can be computed by regressing the derivative of the time signal (Friston et al. 1998). This technique is easily understood as an application of a Taylor Expansion: $f(t + \Delta t) = f(t) + \Delta t \cdot \frac{df}{dt}$. In the present work, $f(t)$ is the global signal, which has already been removed by regression during pre-processing. Thus, regression of the differentiated global signal yields the topography of the delayed global signal, i.e., large venous structures.

Estimation of TD matrix dimensionality

Experimentally observed lag structures include measurement errors. Hence, the dimensionality of our TD matrices must be estimated. To perform this estimation, we ran the procedure created by T. P. Minka, which compares the eigenspectrum of the actual data to the eigenspectrum of a random matrix and expresses the result in terms of likelihood (Minka 2001). The Minka algorithm requires a positive definite matrix. As the TD matrix is not positive definite, the algorithm was run on the square of the TD matrix, which is mathematically required to have the same dimensionality of the TD matrix itself (Allison et al. 2010). The most likely dimensionality of the lag structure illustrated in Figure 9 is 2 (Figure 13).

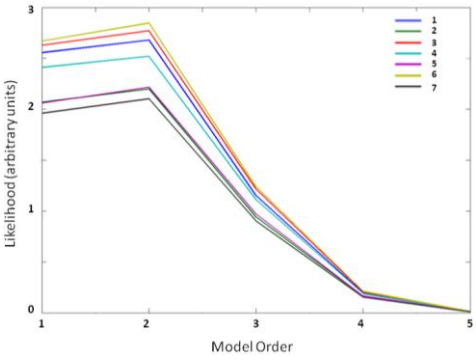

Figure 2-13: Estimation of time-delay (TD) matrix model order. The TD matrix intrinsic dimensionality likelihood was calculated (Minka 2001) using Bayesian Information Criterion (BIC) in the 7 groups corresponding to Figure 2. In each group, the dimensionality of highest likelihood is 2. This result implies the existence of two transitive systems of lags within the TD matrix. Regionally dependent neurovascular coupling can explain only one of these transitive systems of lags. Therefore, hemodynamic delays, even if they are substantial, cannot account for the entirety of latency structure.

Dimensionality of a TD matrix representing a single set of fixed delays

We prove that a fixed set of regionally distinct neurovascular coupling delays explains only one component of a TD matrix. The proof depends on showing that a TD matrix representing a single set of lagged relationships has only a single eigenvector.

Let the fixed set of regional delays be represented as the column vector, $\begin{pmatrix} d_1 \\ d_2 \\ d_3 \\ \vdots \\ d_n \end{pmatrix}$, where n is the number of regions. Suppose that T is the anti-symmetric matrix generated by this set of delays. Thus,

$$T = \begin{bmatrix} 0 & \cdots & \tau_{1,n} \\ \vdots & \ddots & \vdots \\ -\tau_{1,n} & \cdots & 0 \end{bmatrix} = \begin{bmatrix} 0 & \cdots & d_n - d_1 \\ \vdots & \ddots & \vdots \\ d_1 - d_n & \cdots & 0 \end{bmatrix}. \qquad (A1)$$

Previous work has shown that, for a nonzero anti-symmetric matrix $A \in \mathbb{R}^{n\times n}, rank(A) \leq 2k$ if and only if there exists $\boldsymbol{x}_1, \ldots, \boldsymbol{x}_k, \boldsymbol{y}_1, \ldots \boldsymbol{y}_1 \in \mathbb{R}^n$ such that $A = \sum_{i=1}^{k}(\boldsymbol{x}_i\boldsymbol{y}_i^T - \boldsymbol{y}_i\boldsymbol{x}_i^T)$ (Allison et al. 2010). Hence, if we construct $\boldsymbol{x}, \boldsymbol{y}$ such that $T = \boldsymbol{x}\boldsymbol{y}^T - \boldsymbol{y}\boldsymbol{x}^T$, then $k = 1$, and $rank(T) \leq 2$. Since the rank of any anti-symmetric matrix over $\mathbb{R}$ must be even (Allison et al. 2010), $rank(T) = 2$, as T is nonzero. The eigenvalues of a real, anti-symmetric matrix come in conjugate imaginary pairs (Allison et al. 2010). Therefore, T has only 2 conjugate imaginary eigenvalues, $\pm ci$, corresponding to a single eigenvector, $\pm v$, except for sign. Notice that the dimensionality of T is 1 even though its rank is 2. This is because for all real, anti-symmetric matrices, the rank is 2 times the dimensionality, as eigenvalues come in conjugate imaginary pairs (see above). Thus, once we construct $\boldsymbol{x}, \boldsymbol{y}$ such that $T =$

$\boldsymbol{xy}^T - \boldsymbol{yx}^T$, we have proven that a TD matrix representing a single set of lagged relationships has only a single eigenvector.

Now, it remains to construct $\boldsymbol{x}, \boldsymbol{y}$ such that $T = \boldsymbol{xy}^T - \boldsymbol{yx}^T$. Let $\boldsymbol{x} \in \mathbb{R}^n$ such that $x_i = 1$ for all i and $y_j = d_j$ for $j = 1, \ldots, n$. Then,

$$\boldsymbol{xy}^T - \boldsymbol{yx}^T = \begin{pmatrix} 1 \\ 1 \\ 1 \\ . \\ . \\ . \\ 1 \end{pmatrix} (d_1\ d_2 \ldots d_n) - \begin{pmatrix} d_1 \\ d_2 \\ d_3 \\ . \\ . \\ . \\ d_n \end{pmatrix} (1\ 1\ 1 \ldots 1) = \begin{bmatrix} d_1\ d_2 & \ldots & d_n \\ d_1\ d_2 & \ldots & d_n \\ & . & \\ & . & \\ & . & \\ d_1\ d_2 & \ldots & d_n \end{bmatrix} - \begin{bmatrix} d_1\ d_1 & \ldots & d_1 \\ d_2\ d_2 & \ldots & d_2 \\ & . & \\ & . & \\ & . & \\ d_n\ d_n & \ldots & d_n \end{bmatrix}$$

$$= \begin{bmatrix} 0 & \cdots & d_n - d_1 \\ \vdots & \ddots & \vdots \\ d_1 - d_n & \cdots & 0 \end{bmatrix}$$

$$= T, \qquad (A2)$$

completing the construction required for the proof.

An alternative formulation applies the principle that the eigenvalues of a linear system satisfy the characteristic equation of its matrix. We illustrate this principle in a simple case of a 3 × 3 time delay matrix. Let $\begin{pmatrix} d_1 \\ d_2 \\ d_3 \end{pmatrix}$ be the onset times for the system. Then:

$$T = \begin{bmatrix} 0 & d_1 - d_2 & d_3 - d_1 \\ d_2 - d_1 & 0 & d_2 - d_3 \\ d_3 - d_1 & d_3 - d_2 & 0 \end{bmatrix}. \qquad (A3)$$

The characteristic equation is:

$$det \begin{bmatrix} -\lambda & d_1 - d_2 & d_1 - d_3 \\ d_2 - d_1 & -\lambda & d_2 - d_3 \\ d_3 - d_1 & d_3 - d_2 & -\lambda \end{bmatrix}$$

$$= -\lambda \cdot det\begin{bmatrix} -\lambda & d_2 - d_3 \\ d_3 - d_2 & -\lambda \end{bmatrix} - (d_1 - d_2) det\begin{bmatrix} d_2 - d_1 & d_2 - d_3 \\ d_3 - d_1 & -\lambda \end{bmatrix}$$

$$+ (d_1 - d_3) det\begin{bmatrix} d_2 - d_1 & -\lambda \\ d_3 - d_1 & d_3 - d_2 \end{bmatrix}$$

$$= -\lambda\big(\lambda^2 - (d_2 - d_3)(d_3 - d_2)\big) - (d_1 - d_2)\big(-\lambda(d_2 - d_1) - (d_2 - d_3)(d_3 - d_1)\big)$$

$$+ (d_1 - d_3)\big(\lambda(d_3 - d_1) - (d_2 - d_1)(d_3 - d_2)\big)$$

$$= [-\lambda^3 - \lambda(d_2 - d_3)^2] + [-\lambda(d_2 - d_1)^2 + (d_1 - d_2)(d_2 - d_3)(d_3 - d_1)]$$

$$+ [-(d_1 - d_2)(d_2 - d_3)(d_3 - d_1) - \lambda((d_3 - d_1)^2]$$

$$= -\lambda^3 - \lambda \sum_{j \neq k} \big(d_j - d_k\big)^2 = 0$$

$$\Leftrightarrow \lambda^2 + \sum_{j \neq k} \big(d_j - d_k\big)^2$$

$$= 0. \qquad (A4)$$

Since $\sum_{j \neq k} \big(d_j - d_k\big)^2$ is a sum of squares, it must be positive. Therefore $(A4)$ has two conjugate imaginary solutions corresponding to a single eigenvector, as claimed.

2.9 References

Allison M, Bodine E, DeAlba LM, Debnath J, DeLoss L, Garnett C, Grout J, Hogben L, Im B, Kim H, Nair R, Pryporova O, Savage K, Shader B, Wehe AW, and Rank I-IRGM. Minimum rank of skew-symmetric matrices described by a graph. *Linear Algebra Appl* 432: 2457-2472, 2010.

Amemiya S, Kunimatsu A, Saito N, and Ohtomo K. Cerebral Hemodynamic Impairment: Assessment with Resting-State Functional MR Imaging. *Radiology* 2013.

Axmacher N, Draguhn A, Elger CE, and Fell J. Memory processes during sleep: beyond the standard consolidation theory. *Cell Mol Life Sci* 66: 2285-2297, 2009.

Beckmann CF, DeLuca M, Devlin JT, and Smith SM. Investigations into resting-state connectivity using independent component analysis. *Philos Trans R Soc Lond B Biol Sci* 360: 1001-1013, 2005.

Bianciardi M, Fukunaga M, van Gelderen P, Horovitz SG, de Zwart JA, and Duyn JH. Modulation of spontaneous fMRI activity in human visual cortex by behavioral state. *Neuroimage* 45: 160-168, 2009.

Birn RM, Diamond JB, Smith MA, and Bandettini PA. Separating respiratory-variation-related fluctuations from neuronal-activity-related fluctuations in fMRI. *Neuroimage* 31: 1536-1548, 2006.

Biswal B, Yetkin FZ, Haughton VM, and Hyde JS. Functional connectivity in the motor cortex of resting human brain using echo-planar MRI. *Magn Reson Med* 34: 537-541, 1995.

Biswal BB, Mennes M, Zuo XN, Gohel S, Kelly C, Smith SM, Beckmann CF, Adelstein JS, Buckner RL, Colcombe S, Dogonowski AM, Ernst M, Fair D, Hampson M, Hoptman MJ, Hyde JS, Kiviniemi VJ, Kotter R, Li SJ, Lin CP, Lowe MJ, Mackay C, Madden DJ, Madsen KH, Margulies DS, Mayberg HS, McMahon K, Monk CS, Mostofsky SH, Nagel BJ, Pekar JJ, Peltier SJ, Petersen SE, Riedl V, Rombouts SA, Rypma B, Schlaggar BL, Schmidt S, Seidler RD, Siegle GJ, Sorg C, Teng GJ, Veijola J, Villringer A, Walter M, Wang L, Weng XC, Whitfield-Gabrieli S, Williamson P, Windischberger C, Zang YF, Zhang HY, Castellanos FX, and Milham MP. Toward discovery science of human brain function. *Proceedings of the National Academy of Sciences of the United States of America* 107: 4734-4739, 2010.

Bressler SL, and Menon V. Large-scale brain networks in cognition: emerging methods and principles. *Trends Cogn Sci* 14: 277-290, 2010.

Buckner RL, Krienen FM, Castellanos A, Diaz JC, and Yeo BT. The organization of the human cerebellum estimated by intrinsic functional connectivity. *J Neurophysiol* 106: 2322-2345, 2011a.

Buckner RL, Krienen FM, Castellanos A, Diaz JC, and Yeo BT. The organization of the human cerebellum estimated by intrinsic functional connectivity. *J Neurophysiol* 106: 2322-2345, 2011b.

Choi EY, Yeo BT, and Buckner RL. The organization of the human striatum estimated by intrinsic functional connectivity. *Journal of neurophysiology* 108: 2242-2263, 2012.

Cordes D, Haughton VM, Arfanakis K, Wendt GJ, Turski PA, Moritz CH, Quigley MA, and Meyerand ME. Mapping functionally related regions of brain with functional connectivity MR imaging. *AJNR Am J Neuroradiol* 21: 1636-1644, 2000.

Damasio H. A computed tomographic guide to the identification of cerebral vascular territories. *Arch Neurol* 40: 138-142, 1983.

Deshpande G, Santhanam P, and Hu X. Instantaneous and causal connectivity in resting state brain networks derived from functional MRI data. *Neuroimage* 54: 1043-1052, 2011.

Ferezou I, Haiss F, Gentet LJ, Aronoff R, Weber B, and Petersen CC. Spatiotemporal dynamics of cortical sensorimotor integration in behaving mice. *Neuron* 56: 907-923, 2007.

Fischl B. FreeSurfer. *Neuroimage* 62: 774-781, 2012.

Fox MD, and Greicius M. Clinical applications of resting state functional connectivity. *Front Syst Neurosci* 4: 19, 2010.

Fox MD, and Raichle ME. Spontaneous fluctuations in brain activity observed with functional magnetic resonance imaging. *Nat Rev Neurosci* 8: 700-711, 2007.

Fox MD, Snyder AZ, Barch DM, Gusnard DA, and Raichle ME. Transient BOLD responses at block transitions. *Neuroimage* 28: 956-966, 2005a.

Fox MD, Snyder AZ, Vincent JL, Corbetta M, Van Essen DC, and Raichle ME. The human brain is intrinsically organized into dynamic, anticorrelated functional networks. *Proc Natl Acad Sci U S A* 102: 9673-9678, 2005b.

Fox MD, Snyder AZ, Vincent JL, and Raichle ME. Intrinsic fluctuations within cortical systems account for intertrial variability in human behavior. *Neuron* 56: 171-184, 2007.

Fox MD, Snyder AZ, Zacks JM, and Raichle ME. Coherent spontaneous activity accounts for trial-to-trial variability in human evoked brain responses. *Nat Neurosci* 9: 23-25, 2006.

Fox MD, Zhang D, Snyder AZ, and Raichle ME. The global signal and observed anticorrelated resting state brain networks. *J Neurophysiol* 101: 3270-3283, 2009.

Friston K. Causal modelling and brain connectivity in functional magnetic resonance imaging. *PLoS Biol* 7: e33, 2009.

Friston K. Dynamic causal modeling and Granger causality Comments on: the identification of interacting networks in the brain using fMRI: model selection, causality and deconvolution. *Neuroimage* 58: 303-305; author reply 310-301, 2011.

Friston K, Moran R, and Seth AK. Analysing connectivity with Granger causality and dynamic causal modelling. *Curr Opin Neurobiol* 23: 172-178, 2013.

Friston KJ, and Dolan RJ. Computational and dynamic models in neuroimaging. *Neuroimage* 52: 752-765, 2010.

Friston KJ, Fletcher P, Josephs O, Holmes A, Rugg MD, and Turner R. Event-related fMRI: characterizing differential responses. *Neuroimage* 7: 30-40, 1998.

Friston KJ, Harrison L, and Penny W. Dynamic causal modelling. *NeuroImage* 19: 1273-1302, 2003.

Garg R, Cecchi GA, and Rao AR. Full-brain auto-regressive modeling (FARM) using fMRI. *Neuroimage* 58: 416-441, 2011.

Goebel R, Roebroeck A, Kim DS, and Formisano E. Investigating directed cortical interactions in time-resolved fMRI data using vector autoregressive modeling and Granger causality mapping. *Magnetic resonance imaging* 21: 1251-1261, 2003.

Goense JB, and Logothetis NK. Neurophysiology of the BOLD fMRI signal in awake monkeys. *Curr Biol* 18: 631-640, 2008.

Gonzalez-Castillo J, Saad ZS, Handwerker DA, Inati SJ, Brenowitz N, and Bandettini PA. Whole-brain, time-locked activation with simple tasks revealed using massive averaging and model-free analysis. *Proc Natl Acad Sci U S A* 109: 5487-5492, 2012.

Grafton ST, Hazeltine E, and Ivry R. Functional mapping of sequence learning in normal humans. *J Cogn Neurosci* 7: 497-510, 1995.

Hacker CD, Laumann TO, Szrama NP, Baldassarre A, Snyder AZ, Leuthardt EC, and Corbetta M. Resting state network estimation in individual subjects. *Neuroimage* 82C: 616-633, 2013.

Hall DA, Goncalves MS, Smith S, Jezzard P, Haggard MP, and Kornak J. A method for determining venous contribution to BOLD contrast sensory activation. *Magn Reson Imaging* 20: 695-706, 2002.

Han F, Caporale N, and Dan Y. Reverberation of recent visual experience in spontaneous cortical waves. *Neuron* 60: 321-327, 2008.

Handwerker DA, Ollinger JM, and D'Esposito M. Variation of BOLD hemodynamic responses across subjects and brain regions and their effects on statistical analyses. *Neuroimage* 21: 1639-1651, 2004.

He BJ, Zempel JM, Snyder AZ, and Raichle ME. The temporal structures and functional significance of scale-free brain activity. *Neuron* 66: 353-369, 2010.

He H, and Liu TT. A geometric view of global signal confounds in resting-state functional MRI. *Neuroimage* 59: 2339-2348, 2012.

Hinkley LBN, Sekihara K, Owen JP, Westlake KP, Byl NN, and Nagarajan SS. Complex-value coherence mapping reveals novel abnormal resting-state functional connectivity networks in task-specific focal hand dystonia. *Frontiers in Neurology* 2013.

Huang X, Xu W, Liang J, Takagaki K, Gao X, and Wu JY. Spiral wave dynamics in neocortex. *Neuron* 68: 978-990, 2010.

Huber R, Ghilardi MF, Massimini M, and Tononi G. Local sleep and learning. *Nature* 430: 78-81, 2004.

Jenkins GM, and Watts DG. *Spectral Analysis and its Applications*. San Francisco: Holden-Day, 1968.

Konig P. A method for the quantification of synchrony and oscillatory properties of neuronal activity. *J Neurosci Methods* 54: 31-37, 1994.

Larson-Prior LJ, Zempel JM, Nolan TS, Prior FW, Snyder AZ, and Raichle ME. Cortical network functional connectivity in the descent to sleep. *Proc Natl Acad Sci U S A* 106: 4489-4494, 2009.

Lavenex P, and Amaral DG. Hippocampal-neocortical interaction: a hierarchy of associativity. *Hippocampus* 10: 420-430, 2000.

Lee AT, Glover GH, and Meyer CH. Discrimination of large venous vessels in time-course spiral blood-oxygen-level-dependent magnetic-resonance functional neuroimaging. *Magn Reson Med* 33: 745-754, 1995.

Leiner HC, Leiner AL, and Dow RS. The human cerebro-cerebellar system: its computing, cognitive, and language skills. *Behav Brain Res* 44: 113-128, 1991.

Li Z, Zhu Y, Childress AR, Detre JA, and Wang Z. Relations between BOLD fMRI-derived resting brain activity and cerebral blood flow. *PLoS One* 7: e44556, 2012.

Logothetis NK. What we can do and what we cannot do with fMRI. *Nature* 453: 869-878, 2008.

Logothetis NK, Pauls J, Augath M, Trinath T, and Oeltermann A. Neurophysiological investigation of the basis of the fMRI signal. *Nature* 412: 150-157, 2001.

Logothetis NK, and Wandell BA. Interpreting the BOLD signal. *Annu Rev Physiol* 66: 735-769, 2004.

Majeed W, Magnuson M, Hasenkamp W, Schwarb H, Schumacher EH, Barsalou L, and Keilholz SD. Spatiotemporal dynamics of low frequency BOLD fluctuations in rats and humans. *Neuroimage* 54: 1140-1150, 2011.

Majeed W, Magnuson M, and Keilholz SD. Spatiotemporal dynamics of low frequency fluctuations in BOLD fMRI of the rat. *J Magn Reson Imaging* 30: 384-393, 2009.

Marx E, Deutschlander A, Stephan T, Dieterich M, Wiesmann M, and Brandt T. Eyes open and eyes closed as rest conditions: impact on brain activation patterns. *Neuroimage* 21: 1818-1824, 2004.

Massimini M, Huber R, Ferrarelli F, Hill S, and Tononi G. The sleep slow oscillation as a traveling wave. *J Neurosci* 24: 6862-6870, 2004.

Maxim V, Sendur L, Fadili J, Suckling J, Gould R, Howard R, and Bullmore E. Fractional Gaussian noise, functional MRI and Alzheimer's disease. *Neuroimage* 25: 141-158, 2005.

McAvoy M, Larson-Prior L, Nolan TS, Vaishnavi SN, Raichle ME, and d'Avossa G. Resting states affect spontaneous BOLD oscillations in sensory and paralimbic cortex. *J Neurophysiol* 100: 922-931, 2008.

Minka TP. Automatic choice of dimensionality for PCA. In: *Advances in Neural Information Processing Systems 13*. Cambridge, MA: MIT Press, 2001, p. 598-604.

Mintun MA, Vlassenko AG, Rundle MM, and Raichle ME. Increased lactate/pyruvate ratio augments blood flow in physiologically activated human brain. *Proc Natl Acad Sci U S A* 101: 659-664, 2004.

Mohajerani MH, Chan AW, Mohsenvand M, Ledue J, Liu R, McVea DA, Boyd JD, Wang YT, Reimers M, and Murphy TH. Spontaneous cortical activity alternates between motifs defined by regional axonal projections. *Nat Neurosci* 16: 1426-1435, 2013.

Mohajerani MH, McVea DA, Fingas M, and Murphy TH. Mirrored bilateral slow-wave cortical activity within local circuits revealed by fast bihemispheric voltage-sensitive dye imaging in anesthetized and awake mice. *J Neurosci* 30: 3745-3751, 2010.

Murphy K, Birn RM, Handwerker DA, Jones TB, and Bandettini PA. The impact of global signal regression on resting state correlations: are anti-correlated networks introduced? *Neuroimage* 44: 893-905, 2009a.

Murphy M, Riedner BA, Huber R, Massimini M, Ferrarelli F, and Tononi G. Source modeling sleep slow waves. *Proc Natl Acad Sci U S A* 106: 1608-1613, 2009b.

Nelson SM, Dosenbach NU, Cohen AL, Wheeler ME, Schlaggar BL, and Petersen SE. Role of the anterior insula in task-level control and focal attention. *Brain Struct Funct* 214: 669-680, 2010.

Nikolic D. Non-parametric detection of temporal order across pairwise measurements of time delays. *J Comput Neurosci* 22: 5-19, 2007.

Ogawa S, Lee TM, Kay AR, and Tank DW. Brain magnetic resonance imaging with contrast dependent on blood oxygenation. *Proc Natl Acad Sci U S A* 87: 9868-9872, 1990.

Power JD, Barnes KA, Snyder AZ, Schlaggar BL, and Petersen SE. Spurious but systematic correlations in functional connectivity MRI networks arise from subject motion. *Neuroimage* 59: 2142-2154, 2012.

Power JD, Cohen AL, Nelson SM, Wig GS, Barnes KA, Church JA, Vogel AC, Laumann TO, Miezin FM, Schlaggar BL, and Petersen SE. Functional network organization of the human brain. *Neuron* 72: 665-678, 2011.

Power JD, Mitra A, Laumann TO, Snyder AZ, Schlaggar BL, and Petersen SE. Methods to detect, characterize, and remove motion artifact in resting state fMRI. *Neuroimage* 84C: 320-341, 2013.

Purdon PL, and Weisskoff RM. Effect of temporal autocorrelation due to physiological noise and stimulus paradigm on voxel-level false-positive rates in fMRI. *Hum Brain Mapp* 6: 239-249, 1998.

Raichle ME. The restless brain. *Brain Connect* 1: 3-12, 2011.

Raichle ME, MacLeod AM, Snyder AZ, Powers WJ, Gusnard DA, and Shulman GL. A default mode of brain function. *Proc Natl Acad Sci U S A* 98: 676-682, 2001.

Raichle ME, and Mintun MA. Brain work and brain imaging. *Annu Rev Neurosci* 29: 449-476, 2006.

Samann PG, Wehrle R, Hoehn D, Spoormaker VI, Peters H, Tully C, Holsboer F, and Czisch M. Development of the brain's default mode network from wakefulness to slow wave sleep. *Cereb Cortex* 21: 2082-2093, 2011.

Sato TK, Nauhaus I, and Carandini M. Traveling waves in visual cortex. *Neuron* 75: 218-229, 2012.

Schacter DL, Buckner RL, Koutstaal W, Dale AM, and Rosen BR. Late onset of anterior prefrontal activity during true and false recognition: an event-related fMRI study. *Neuroimage* 6: 259-269, 1997.

Schneider G, Havenith MN, and Nikolic D. Spatiotemporal structure in large neuronal networks detected from cross-correlation. *Neural Comput* 18: 2387-2413, 2006.

Scholvinck ML, Maier A, Ye FQ, Duyn JH, and Leopold DA. Neural basis of global resting-state fMRI activity. *Proc Natl Acad Sci U S A* 107: 10238-10243, 2010.

Shannon BJ, Dosenbach RA, Su Y, Vlassenko AG, Larson-Prior LJ, Nolan TS, Snyder AZ, and Raichle ME. Morning-evening variation in human brain metabolism and memory circuits. *J Neurophysiol* 109: 1444-1456, 2013.

Shulman GL, Pope DL, Astafiev SV, McAvoy MP, Snyder AZ, and Corbetta M. Right hemisphere dominance during spatial selective attention and target detection occurs outside the dorsal frontoparietal network. *J Neurosci* 30: 3640-3651, 2010.

Smith SM, Fox PT, Miller KL, Glahn DC, Fox PM, Mackay CE, Filippini N, Watkins KE, Toro R, Laird AR, and Beckmann CF. Correspondence of the brain's functional architecture during activation and rest. *Proc Natl Acad Sci U S A* 106: 13040-13045, 2009.

Smith SM, Miller KL, Moeller S, Xu J, Auerbach EJ, Woolrich MW, Beckmann CF, Jenkinson M, Andersson J, Glasser MF, Van Essen DC, Feinberg DA, Yacoub ES, and Ugurbil K. Temporally-independent functional modes of spontaneous brain activity. *Proc Natl Acad Sci U S A* 109: 3131-3136, 2012.

Stokes M, Thompson R, Cusack R, and Duncan J. Top-down activation of shape-specific population codes in visual cortex during mental imagery. *J Neurosci* 29: 1565-1572, 2009.

Strick PL, Dum RP, and Fiez JA. Cerebellum and nonmotor function. *Annu Rev Neurosci* 32: 413-434, 2009.

Sun FT, Miller LM, and D'Esposito M. Measuring temporal dynamics of functional networks using phase spectrum of fMRI data. *Neuroimage* 28: 227-237, 2005.

Thomas Yeo BT, Krienen FM, Sepulcre J, Sabuncu MR, Lashkari D, Hollinshead M, Roffman JL, Smoller JW, Zollei L, Polimeni JR, Fischl B, Liu H, and Buckner RL. The organization of the human cerebral cortex estimated by intrinsic functional connectivity. *Journal of neurophysiology* 106: 1125-1165, 2011.

Vaishnavi SN, Vlassenko AG, Rundle MM, Snyder AZ, Mintun MA, and Raichle ME. Regional aerobic glycolysis in the human brain. *Proc Natl Acad Sci U S A* 107: 17757-17762, 2010.

Van Essen DC, Anderson CH, and Felleman DJ. Information processing in the primate visual system: an integrated systems perspective. *Science* 255: 419-423, 1992.

Vern BA, Leheta BJ, Juel VC, LaGuardia J, Graupe P, and Schuette WH. Interhemispheric synchrony of slow oscillations of cortical blood volume and cytochrome aa3 redox state in unanesthetized rabbits. *Brain Res* 775: 233-239, 1997.

Vern BA, Leheta BJ, Juel VC, LaGuardia J, Graupe P, and Schuette WH. Slow oscillations of cytochrome oxidase redox state and blood volume in unanesthetized cat and rabbit cortex. Interhemispheric synchrony. *Adv Exp Med Biol* 454: 561-570, 1998.

Vicente R, Gollo LL, Mirasso CR, Fischer I, and Pipa G. Dynamical relaying can yield zero time lag neuronal synchrony despite long conduction delays. *Proc Natl Acad Sci U S A* 105: 17157-17162, 2008.

Vincent JL, Patel GH, Fox MD, Snyder AZ, Baker JT, Van Essen DC, Zempel JM, Snyder LH, Corbetta M, and Raichle ME. Intrinsic functional architecture in the anaesthetized monkey brain. *Nature* 447: 83-86, 2007.

Vyazovskiy VV, Olcese U, Hanlon EC, Nir Y, Cirelli C, and Tononi G. Local sleep in awake rats. *Nature* 472: 443-447, 2011.

Yan CG, Cheung B, Kelly C, Colcombe S, Craddock RC, Di Martino A, Li Q, Zuo XN, Castellanos FX, and Milham MP. A comprehensive assessment of regional variation in the impact of head micromovements on functional connectomics. *Neuroimage* 76: 183-201, 2013.

Yeo BT, Krienen FM, Sepulcre J, Sabuncu MR, Lashkari D, Hollinshead M, Roffman JL, Smoller JW, Zollei L, Polimeni JR, Fischl B, Liu H, and Buckner RL. The organization of the human cerebral cortex estimated by intrinsic functional connectivity. *J Neurophysiol* 106: 1125-1165, 2011a.

Yeo BT, Krienen FM, Sepulcre J, Sabuncu MR, Lashkari D, Hollinshead M, Roffman JL, Smoller JW, Zollei L, Polimeni JR, Fischl B, Liu H, and Buckner RL. The organization of the human cerebral cortex estimated by intrinsic functional connectivity. *J Neurophysiol* 106: 1125-1165, 2011b.

Yuste R. Introduction: spontaneous activity in the developing central nervous system. *Semin Cell Dev Biol* 8: 1-4, 1997.

Zhang D, and Raichle ME. Disease and the brain's dark energy. *Nat Rev Neurol* 6: 15-28, 2010.

Chapter 3: Spontaneous temporal sequences give rise to human resting state networks

This chapter has been published as a journal article. The citation is:

Mitra A, Snyder A, Blazey T, Raichle M. (2015). Lag threads organize the brain's intrinsic activity. Proceedings of the National Academy of Sciences. doi: 10.1073/pnas.1503960112.

I conceived the project and research approach. I designed and implemented the methods and performed the data analysis. Tyler Blazey helped with figure construction. Marc Raichle, Abraham Snyder and I wrote the paper.

3.1 Preface

In Chapter 2, we demonstrated that reproducible temporal lags on the order of ~0.5 seconds can be computed in resting state fMRI data. Furthermore, we showed that resting state fMRI temporal structure cannot be attributed purely to vascular factors. Finally, we demonstrated interesting connections between the temporal and correlation structure of resting state fMRI.

These findings raise an important question: what is the fundamental relationship between correlation-based resting state networks and the temporal structure of resting state fMRI? Some relation is expected, as the two measures are derived from precisely the same time series. Chapter 3 tackles this question by demonstrating that the correlation structure of resting state fMRI emerges as a consequence of its temporal structure. In detail, we present an improved dimensionality estimation strategy for the temporal structure of resting state fMRI. Using this strategy, we factor resting state fMRI temporal structure into multiple temporal sequences, which we call “lag threads”. We find a striking regularity among lag threads: in each temporal sequence, the direction of activity through canonical resting state networks is a preserved unidirectional sequence. We demonstrate through simulation that this property, along with temporal delays that are short relative to the frequency of fluctuation, is sufficient to produce correlations within the unidirectional routes. Finally, we show that we can recover, to a fair approximation, the correlation structure of resting state fMRI starting only from its temporal structure. The reverse cannot be done, as there is degeneracy in the mapping between correlation structure to temporal structure.

As a practical matter, the supplemental materials for this paper are not included in this thesis. The reason for this is that the supplemental materials are 60 pages of dense technical matter with nearly 30 figures. Readers interested in this material can find it online with the published manuscript; the supplemental references in this text correspond exactly the published supplement.

3.2 Abstract

It has been widely reported that intrinsic brain activity, in a variety of animals including humans, is spatiotemporally structured. Specifically, propagated slow activity has been repeatedly demonstrated in animals. In human resting state fMRI, spontaneous activity has been understood predominantly in terms of zero-lag temporal synchrony within widely distributed functional systems (resting state networks). Here, we use resting state fMRI from 1376 normal, young adults to demonstrate that multiple, highly reproducible, temporal sequences of propagated activity, which we term “lag threads”, are present in the brain. Moreover, this propagated activity is largely unidirectional within conventionally understood resting state networks. Modeling experiments show that resting state networks naturally emerge as a consequence of shared patterns of propagation. An implication of these results is that common physiologic mechanisms may underlie spontaneous activity as imaged with fMRI in humans and slowly propagated activity as studied in animals.

3.3 Introduction

Spontaneous (intrinsic) neural activity is ubiquitously present in the mammalian brain as first noted by Hans Berger (Berger 1969). Spontaneous activity persists in all

physiological states, although the statistical properties of this activity are modified by level of arousal and ongoing behavior (Buzsaki and Draguhn 2004; Cossart et al. 2003; Grinvald et al. 2003; Gusnard et al. 2001; Ikegaya et al. 2004; Luczak et al. 2007; Ringach 2009). Invasive studies in animals using diverse techniques, e.g., local field potentials (Ferezou et al. 2007; Hahn et al. 2006; Logothetis et al. 2001), voltage sensitive dyes (Grinvald and Hildesheim 2004; Kenet et al. 2003; Mohajerani et al. 2013; Petersen et al. 2003), and calcium imaging (Ikegaya et al. 2004; Miller et al. 2014; Stroh et al. 2013), have demonstrated richly organized intrinsic activity at multiple temporal and spatial scales. The most utilized technique for studying whole brain intrinsic activity in humans is resting state functional magnetic resonance imaging (rs-fMRI). Biswal and colleagues first reported that slow (<0.1 Hz) spontaneous fluctuations of the blood oxygen level dependent (BOLD) signal are temporally synchronous within the somatomotor system (Biswal et al. 1995). This basic result has since been extended to multiple functional systems spanning the entire brain (Buckner et al. 2011; Choi et al. 2012; Power et al. 2011; Thomas Yeo et al. 2011). Synchrony of intrinsic activity is widely referred to as functional connectivity; the associated topographies are known as resting state networks (RSNs (Fox and Raichle 2007); equivalently, intrinsic connectivity networks (Seeley et al. 2007)).

Almost all prior rs-fMRI studies have used either seed-based correlation mapping (Biswal et al. 2010) or spatial independent components analysis (sICA) (Beckmann et al. 2005). Critically, neither or these techniques provide for the possibility that activity within RSNs may exhibit temporal lags on a time scale finer than the temporal sampling

density. However, we recently demonstrated highly reproducible lags on the order of ~1 sec by application of parabolic interpolation to resting state fMRI data acquired at a rate of one volume every 3 sec (Fig. S1; (Mitra et al. 2014)). Moreover, this lag structure can be modified, with appropriate focality, by a variety of task paradigms (Mitra et al. 2014).

Investigations of rs-fMRI lag structure previously have been limited by the concern that observed lags may reflect regional differences in the kinetics of neurovascular coupling rather than primary neural processes (Friston and Dolan 2010; Handwerker et al. 2004). However, our previous dimensionality analysis demonstrated that there are at least two independent lag processes within the brain (Mitra et al. 2014). The neurovascular model can account for only one of these. Hence, there must be at least one lag process that is genuinely of neural origin. We have since made significant methodological improvements (Theory; Fig. 1) that enable a more detailed characterization of lag structure in BOLD rs-fMRI data. We report our results in two parts.

In **Part I**, we present an expanded view of the lag structure within the normal adult human brain culled from BOLD rs-fMRI data in 1376 individuals. Specifically, we show that at least eight orthogonal lag processes can be reproducibly demonstrated. We refer to these processes as "threads" by way of analogy with modern computer programming practice in which single applications contain multiple, independent thread sequences.

In **Part II**, we investigate the relation between lag threads and zero-lag temporal correlations, that is, conventional, resting-state functional connectivity. We find that,

although there is no simple relation between lag and zero-lag temporal correlation over all pairs of voxels, apparent propagation is largely unidirectional within RSNs. We also show that zero-lag temporal correlation structure of rs-fMRI arises as a consequence of lags, whereas the reverse is not true. These results suggest that lag threads account for observed patterns of zero-lag temporal synchrony, and that RSNs are an emergent property of lag structure.

3.4 Methods

Theory

We define the lag between two fMRI timeseries by computing the cross-covariance function at intervals of one frame and identifying the local extremum using parabolic interpolation (Fig.S1). This analysis assumes the existence of a single temporal lag between regions. The validity of this assumption depends on the fact that BOLD fMRI timeseries are aperiodic (He et al. 2010; Maxim et al. 2005) (see “lagged cross-covariance curves exhibit a single peak” in SI for additional discussion of this point). Measured lags at the group level (i.e., averaged over individuals) typically assume values in the range ± 1 sec. Apparent propagation is inferred on the basis of observed lag between two timeseries. This formulation makes no assumptions regarding the path over which the activity "propagates" between regions. Thus, "propagation," as defined here, entails lags on the order of ~1 sec in activity over spatial scales on the order of centimeters.

As an aid to understanding the methodology, we describe our approach to characterizing lag structure using a simple illustrative model containing three orthogonal lag processes (threads) propagating through six nodes (Fig. 1). Apparent propagation, as defined here, is shown using synthetic timeseries with “1/f” spectral content duplicated from real BOLD rs-fMRI data ((He et al. 2010); see “simulating synthetic BOLD fMRI timeseries” in SI for further detail) propagating through six nodes (Fig. 1A). The superposition of the three thread processes is shown in Fig. 1B. Analysis of the superposed timeseries observed at the six nodes (using the procedure illustrated in Fig. S1) yields the time delay matrix shown in Fig. 1C; we call this matrix TD. Having computed TD, we can compute a mean for each column, using the previously described projection strategy for computing BOLD rs-fMRI lag topographies (Mitra et al. 2014). In the case of a single lag process, the projection strategy is sufficient to recover the ordering (see Figs. S2, S3). However, as shown in the Fig. 1D, in the case of multiple superposed lag processes, the column-wise projection generates an over-simplified approximation of the dynamic system.

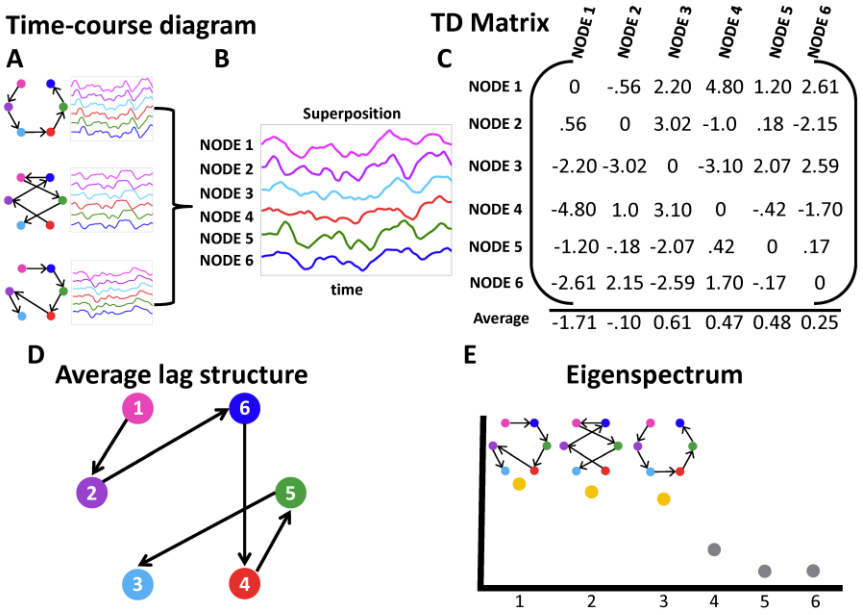

Figure 3-1: Illustration of lag threads. Panel A shows three patterns of propagation (lag threads) through 6 nodes. The objective is to demonstrate the mapping between lag structure and principal components analysis (PCA). The illustration is not intended as a model of propagation in neural tissue. Each lag thread is also shown as a multi-dimensional timeseries with spectral content duplicated from real BOLD rs-fMRI data. Panel B shows the superposition of the three lag threads. Panel C shows the time-delay matrix (TD) recovered by analysis of the superposed timeseries in (B), using the technique illustrated in SI Appendix, Fig. S1. The bottom row of panel C shows the latency projection of TD, computed as the average over each column. Panel D illustrates the latency projection as a node diagram. This projection represents nodes that are, on average, early or late. Critically, the projection fails to capture the full lag structure. Panel E illustrates eigendecomposition of the covariance structure of TD_z, derived from TD by removing the mean of each column (see SI Appendix, equations [S4] - [S8]). There are 3 significant eigenvalues, indicating the presence of 3 lag threads. In an ideal case, eigenvalues 4-6 would be zero; in this example, imperfect superposition leads to a small fourth non-zero eigenvalue. The eigenvectors corresponding to the first three eigenvalues are the thread topographies (shown above the eigenvalues). The lag thread sequences defined in (A) were accurately recovered purely by eigen-analysis of TD_z. It should be noted that the lag threads in this illustration were *a priori* constructed to be mutually orthogonal (see SI Appendix, equation [S7]). Hence, they were neatly recovered intact by eigendecomposition of TD_z. Also, although the nodes in this illustration are represented as foci, the algebra applies equally well to voxels, regions of interest, or extended, possibly disjoint, topographies.

In the present work, to recover lag processes in multidimensional timeseries, we use principal components analysis (PCA). PCA assumes linear superposition of components. The validity of this assumption is discussed in SI (see "validity of applying PCA to recover lag thread topographies"). In each column, $i \in \{1,2,\ldots 6\}$, of the time delay matrix TD, the vector corresponding to column i is a lag map of the system with

reference to timeseries i. That is, the first column of TD is a lag map of the system with respect to the first timeseries, and so on. Now, consider the matrix, TD_z, constructed by subtracting the mean of each column from TD. The columns of TD_z are zero-centered lag maps. Application of PCA to TD_z, recovers the eigenspectrum representing the number of lag threads present in the system. Fig. 1E shows that precisely three non-zero eigenvalues are found in this illustrative case. The eigenvectors corresponding to these non-zero eigenvalues can be used to recover the topography of the lag threads; the node diagrams above the non-zeros eigenvalues in the lower right panel of Fig. 1 illustrate the recovered lag processes. In the case of no delays (Fig. S2), or only a single set of delays (Fig. S3), PCA finds 0 or 1 non-zero eigenvalue. Thus, TD analysis is sufficient to assess the number of lag threads in the system. Although Fig. 1 illustrates TD and TD_z as square matrices (i.e., the number of voxels in each lag map is equal to the number of lag maps), lag thread computation is algebraically well defined also when the number of voxels greatly exceeds the number of lag maps.

To increase the signal to noise ratio in real BOLD rs-fMRI data, we produced 6 mm^3 voxel resolution lag maps from timeseries extracted from 330 15 mm^3 cubic ROIs, uniformly distributed throughout gray matter (see SI for further detail).

Imaging data

A large data set (*n* = 1376) was obtained from the Harvard-MGH Brain Genomics Superstruct Project ((Buckner et al. 2012); Table 1). The 1376 subjects were randomly divided into 2 groups of 688 subjects to test the reproducibility of our analyses. Please see SI (or methods in Chapter 2) for further detail regarding preprocessing and computational methods.

Group	1	2
Number of subjects	688 (402 F)	688 (383 F)
Age in years	21.5 ± 3.1 (S.D.)	21.3 ± 2.7 (S.D.)
Scanner	Siemens Tim Trio	
Acquisition voxel size	$(3mm)^3$	
Flip Angle	85°	
Repetition Time (s)	3.00	
Number of frames	124 X 2 runs	
Citation	Buckner et al. 2012	

Table 3-1: Subjects analyzed in the present study.

3.5 Results

Part I

Existence and reproducibility of lag threads

Fig. 2 shows the topography of four lag threads derived from real BOLD rs-fMRI data acquired in the first group of 688 subjects. Blue hues indicate regions that are early, i.e., "sources" of propagated BOLD activity; red hues indicate regions that are late, i.e., "destinations" of propagated BOLD activity. The range of lag values in each thread is ~2 seconds. The threads exhibit a high degree of bilateral symmetry. Interestingly, although specific anatomical structures are often prominent sources or destinations within threads, these topographies do not respect RSN boundaries (Fig. 2; Movies 1-4). BOLD rs-fMRI signals propagate in lag threads both within and across resting state networks. We have previously reported this principle in relation to the distribution of lag values over pairs of nodes in the brain (Mitra et al. 2014).

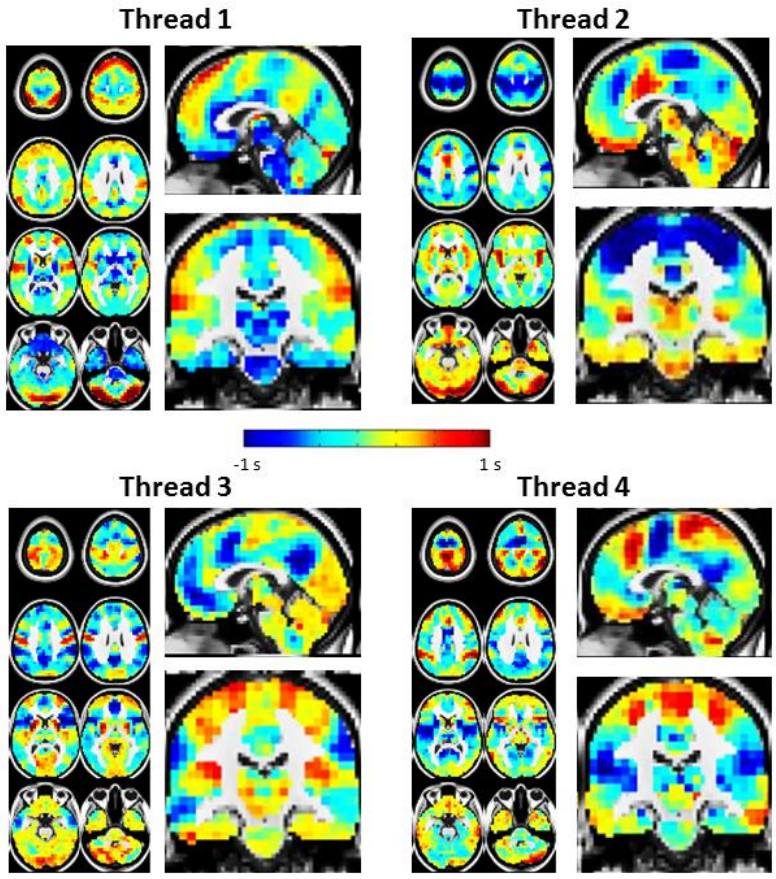

Figure 3-2: Four lag threads computed from real BOLD rs-fMRI data in the first group of 688 subjects. Blue and red hues represent, respectively, voxels that are early or late relative to the thread mean. Each map is in units of seconds. Note that brainstem and subcortical regions are early in Thread 1, whereas higher order cortical regions such as frontopolar cortex (seen in transverse slices) are late. The significance of these observations is considered in the Discussion.

Fig. 3A shows the first 20 eigenvalues derived by spatial PCA of the lag threads derived from the first 688-subject group (the first 4 threads of which are illustrated in Fig. 2). In Fig. 1E, only non-zero eigenvalues correspond to lag threads, making it easy to infer the dimensionality of the system. In real data, the presence of noise means that all eigenvalues are non-zero; hence, dimensionality must be estimated (Minka 2001). Using an information criterion, we estimated the dimensionality in Fig. 3A to be 8 (see SI for further detail). To explore the reproducibility of our results, we applied the same calculations to a second, separate group of 688 subjects and obtained eigenspectrum and dimensionality estimates indistinguishable from the results shown in Figure 3A. Reproducibility of lag thread topographies across the two groups of *688 subjects* is

illustrated in Figure 3B. It is evident that lag threads are highly reproducible across groups. The full topographies of the first 8 lag threads are reported in SI (Figs. S7-S14).

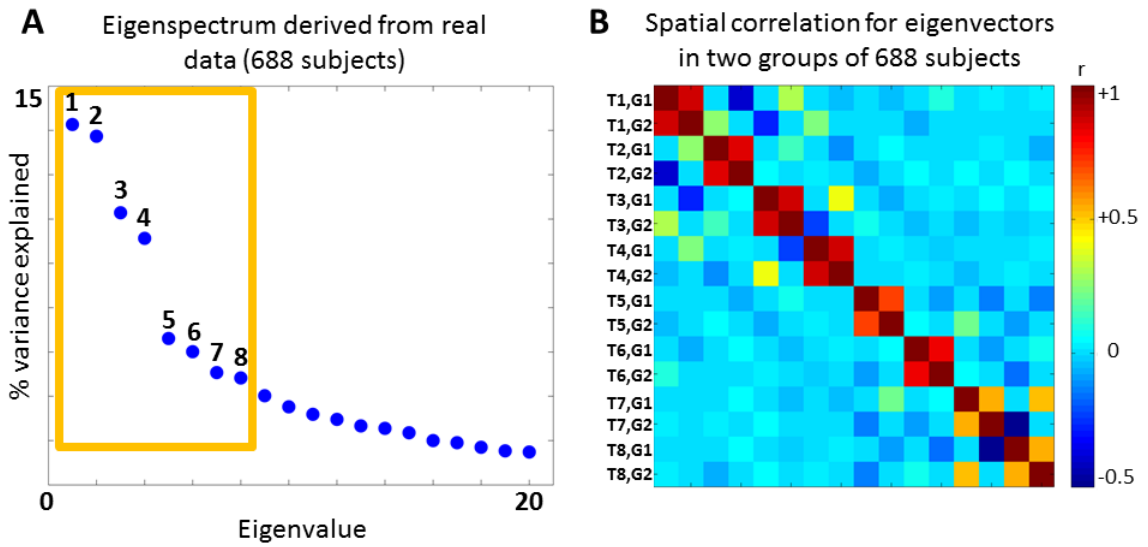

Figure 3-3: Dimensionality and reproducibility of lag threads. Panel A displays the first 20 eigenvalues derived from the BOLD rs-fMRI lag structure computed in the first group of 688 subjects; the maximum likelihood dimensionality estimate is 8 (see SI equation [S7]). The orange box encloses the first 8 eigenvalues. Panel B shows the spatial correlation matrix (Pearson r) representing the first 8 lag thread maps in the first and second groups of 688 subjects. The rows and columns are ordered by thread map (T1, T2, …) and group (G1, G2). The 2 × 2 blocks of high correlation along the diagonal demonstrate that lag thread topographies are highly reproducible across the two groups.

Multiple lag threads in a small number of regions

The high dimensionality of the lag system shown in Fig. 3 theoretically could reflect our specific choices of ROIs and lag map resolution (see SI; Fig. S5). To test this possibility, we constructed 17 regions of interest by thresholding the eight thread maps to define prominent sources and destinations. These ROIs are shown in Fig. 4A. Many of these regions have been previously identified as critical nodes that organize the brain's ongoing activity (van den Heuvel et al. 2012). The corresponding 17 × 17 time delay matrices in the two groups of 688 subjects each are shown in Fig. 4B. Excellent reproducibility is evident (Fig. 4C). Moreover, the maximum likelihood dimensionality

estimate in both groups is 8 (Fig. 4D), precisely the same result shown in Fig. 3A. Fig. 4 demonstrates that high dimensional lag structure can emerge from a relatively small set of ROIs as long as key regions of the brain are represented. Seed-based lag maps of these ROIs are shown in Figs. S15-S24.

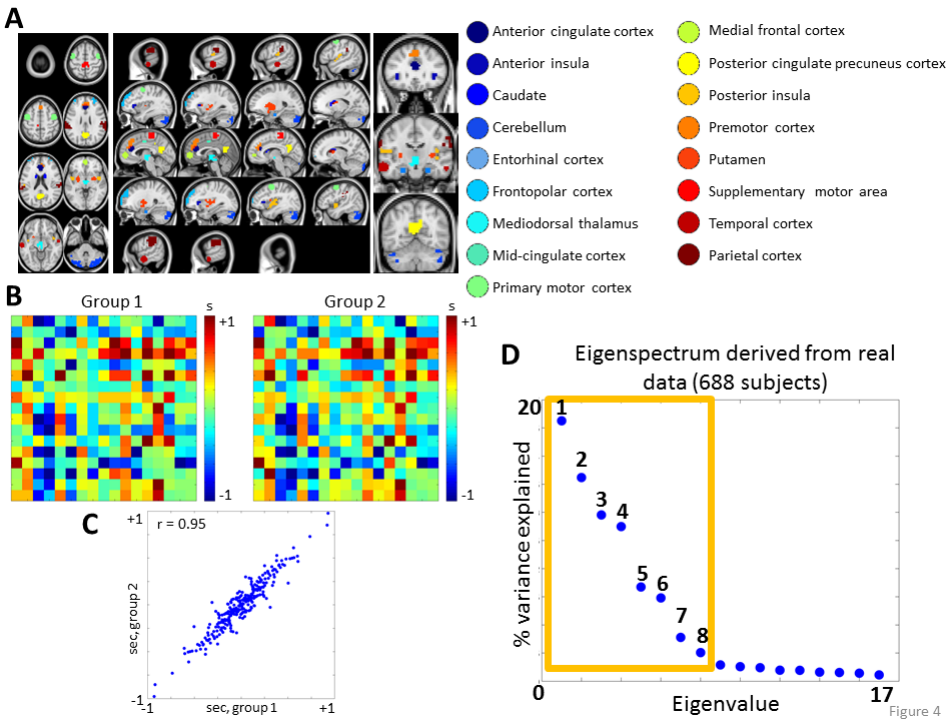

Figure 3-4: High dimensionality lag structure derived from selected regions of interest (ROIs). Panel A shows 17 ROIs obtained by thresholding the first 8 lag thread maps derived in the first group of 688 subjects (Fig. 2; Figs. S7-S14). These ROIs represent maximally early and late nodes over several lag threads. The color code in (A) identifies ROIs without relation to latency. Panel B shows the 17 × 17 time delay matrix (TD) corresponding to these ROIs in both groups of 688 subjects. These matrices are exactly skew-symmetric (Mitra et al. 2014). Panel C shows a scatter plot of group 2 vs. group 1 unique (upper triangle) TD values; excellent reproducibility is evident. Panel D shows the 17 eigenvalues of TD_z in the first group of 688 subjects. The second group of 688 subjects yielded a nearly identical eigenspectrum (not shown in panel D as the plotted points overlap). In both groups, the estimated dimensionality is 8, in agreement with Fig. 3.

Part II

Lag threads in relation to zero-lag temporal correlation

Having demonstrated the existence and reproducibility of multiple lag threads in human rs-fMRI data, we next investigated the relation of lag threads to zero-lag temporal correlation structure. To this end, we examined shared patterns of propagation across lag threads. We did this by defining a matrix $\tilde{L}$, whose columns represent the topographies of the first 8 lag threads (in units of sec, as in Fig. 2). We include 8 lag threads on the basis of the dimensionality estimate of lag structure (Fig. 3). $\tilde{L}$ is a 6528

$\times$ 8 (voxels $\times$ threads) matrix, where each voxel has 8 latency values (in units of sec), one for each thread. To find common patterns of propagation across lag threads, we computed, across all voxel pairs, correlations in latency values across lag threads ($(1/k)\tilde{L}\Lambda_k^{-1}\tilde{L}^T$; see Eq. [S9] in SI). The corresponding 6526 $\times$ 6526 (voxels $\times$ voxels) correlation matrix (Fig. 5A) reveals commonalities in signal propagation across lag threads (see SI for additional discussion). Critically, the voxel-wise correlation structure across lag threads (Fig. 5A) resembles the conventional zero-lag temporal correlation structure of BOLD rs-fMRI (Fig. 5B; RSN membership as in (Hacker et al. 2013)). We quantitatively confirmed the similarity between the correlation structures in Figs. 5A and 5B by computing the Pearson r correlation between the unique values in each matrix (r = 0.41). Thus, there is a correspondence between common patterns of propagation across lag threads (Fig. 5A) and the zero-lag temporal structure of rs-fMRI.

The similarity between the matrices shown in Figs. 5A and 5B raises the question of whether, across pairs of voxels, lag is directly related to zero-lag temporal correlation. Hypothetically, voxel pairs exhibiting shorter temporal lags could be exhibit higher temporal correlation at zero-lag. However, a 2-dimensional histogram of zero-lag Pearson r vs. lag for all voxel pairs (Fig. 5C) demonstrates no *systematic* relation. A second possibility is that regions belonging to the same resting state network are iso-latent (i.e., exhibit the same lag value) in each lag thread. For example, the entire default mode network could be early in one thread but late in another. However, the topographies shown in Fig. 2 show that this is not the case. Additionally, we have previously shown that resting state networks are not iso-latent. Rather, the range of

intra- and inter-RSN lag values is the same and no RSN is either early or late as a whole (see Fig. 9 in (Mitra et al. 2014)). Therefore, the similarity between the cross-thread correlations (Fig. 5A) and zero-lag BOLD rs-fMRI temporal correlations (Fig. 5B) requires a more subtle explanation. To provide the basis for this explanation, we introduce the concept of “lag thread motifs”.

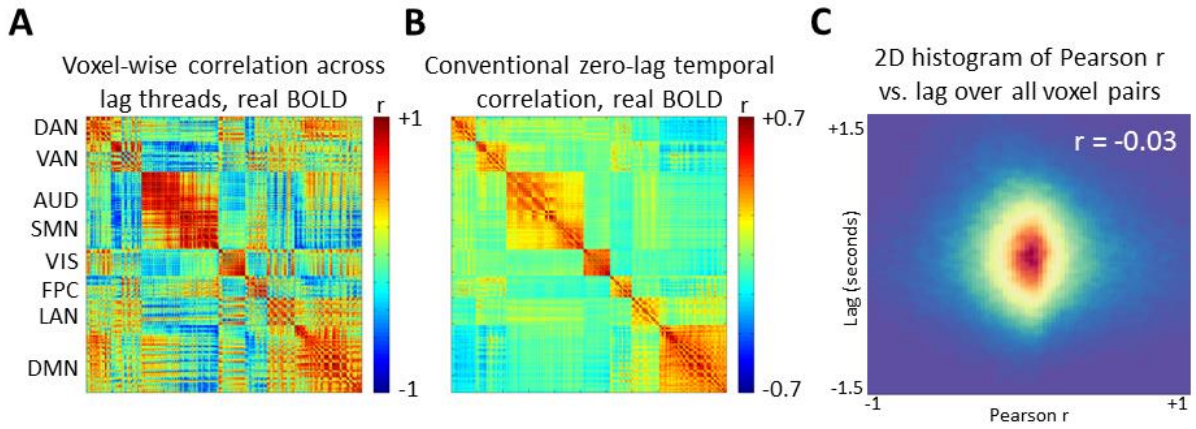

Figure 3-5: Voxel:voxel correlation structure of two different measures derived from the first group 688 subjects. Panel A shows the voxel-wise correlation matrix computed over latency values in the 8 lag threads (Eq. [S9] in SI). These correlations represent the extent to which voxel pairs exhibit similar latency values across all 8 lag threads. Panel B shows the corresponding zero-lag temporal correlation matrix. Note similarity of block structure in panels A and B (Pearson r = 0.41; $p < 10^{-5}$). As there are 6526 (6 mm)^3 voxels in each map, the full correlation matrices are 6526 $\times$ 6526. The matrices displayed in (A) and (B) have been masked to include only voxels with a ≥90% chance of belonging to one of 8 resting state networks (RSNs) (Hacker et al. 2013) (Fig. S5). Thus, the displayed matrices are 1065 $\times$ 1065. The rows and columns are ordered by RSN: dorsal attention network (DAN), ventral attention network (VAN), auditory network (AUD), primary sensorimotor network (SMN), visual network (VIS), frontoparietal network (FPC), language network (LAN), default mode network (DMN). Panel C displays a 2D histogram, compiled over voxel pairs, of lag vs. temporal correlation. All 6526 $\times$ 6526 voxel pairs are represented, excluding those within 1 cm of each other (to reduce the influence of local correlations). Note no systematic relation, over voxel pairs, of lag vs. zero-lag temporal correlation (r = -0.03). The same result is found using only the voxels shown in panels A and B (r = -0.02).

Lag thread motifs

We illustrate the concept of a lag thread motif using a 4 voxel model system with 2 lag threads (Fig. 6). The overall pattern of propagation between the 4 voxels is different in

the two threads (Fig. 6A). However, the sequence of propagation through voxels 1 and 2 is identical. Voxels 1 and 2, therefore, constitute a “lag thread motif”: a set of regions in which the sequence of propagation is the same across lag threads. There are no other motifs in Fig. 6. The patterns of propagation shown in Fig. 6A are realized in Fig. 6B using synthetic timeseries with “1/f” spectral content duplicating that of real BOLD rs-fMRI data ((He et al. 2010); see “simulating synthetic BOLD fMRI timeseries” in SI for further detail). Again, although the overall pattern of propagation differs between threads, the sequence of propagation between the first two voxels is preserved (dotted arrows in the dark red boxes).

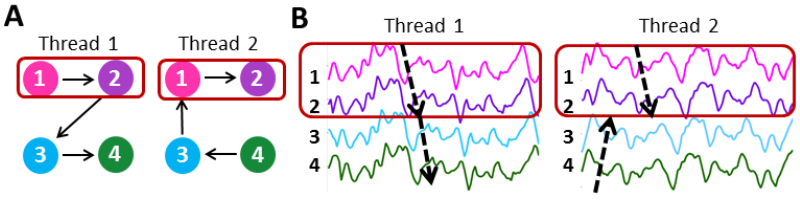

Figure 3-6: Simple illustration of lag thread motifs. Panel A illustrates 2 lag threads propagating through 4 nodes The overall pattern of propagation differs in the two threads but the sequences through nodes 1 and 2 are the same (red box). Thus, nodes 1 and 2 represent a lag thread motif. Panel B illustrates simulated timeseries realized with spectral content duplicated from real BOLD rs-fMRI data (see SI for further details). The sequences of propagation (dotted arrows) are as in (A). Red boxes indicate the preserved sequence (thread motif). True lag threads are mutually orthogonal; here, this constraint is ignored to illustrate the idea of a thread motif using a minimal number of nodes. As in Fig. 1, nodes can represent voxels or regions of interest.

We asked whether the thread motif model can explain the findings in Fig. 5, specifically the similarity between the cross-thread correlations (Fig. 5A) and zero-lag temporal correlations (Fig. 5B); and the absence of a *systematic* relation between zero-lag Pearson r vs. lag for all voxel pairs (Fig. 5C). We explore this question in Fig. 7, which presents a simulation experiment based on the model presented in Fig. 6, but scaled up to include 30 voxels, 8 orthogonal lag threads and 2 thread motifs (see SI for details concerning generation of orthogonal model lag threads. Fig. S6 shows an explicit description of the model). Motif 1 propagates through voxels 1-5; motif 2 propagates

through voxels 6-10. Fig. 7A shows the voxel-wise correlation across simulated lag threads (paralleling Fig. 5A). Voxels sharing a thread motif necessarily exhibit perfectly correlated lag sequences (diagonal blocks labeled "1" and "2"). Fig. 7B shows the 30 × 30 zero-lag temporal correlation matrix (paralleling Fig. 5B) computed on the basis of the synthetic "1/f" time series representing the lag threads (see SI for additional details). Thus, thread motifs are sufficient to induce lag thread correlation structure, as in real rs-fMRI data (Fig. 5A). Moreover, the matrices shown in Figs. 7A and 7B (synthetic data) exhibit the same similarity as the matrices shown in Figs. 5A and 5B (real data). This similarity suggests that the existence of shared lag thread motifs is sufficient to explain zero-lag temporal correlations. We note that this model depends on the “1/f” spectral content of BOLD rs-fMRI time series. The existence of an association between lag structure and temporal correlation requires that the underlying time series exhibit some degree of autocorrelation; lag structure would be dissociated from correlation structure in a system in which the signals were comprised of infinitely narrow impulses or white noise. Finally, Fig. 5C indicates that there is no *systematic* relationship in real BOLD rs-fMRI data across voxel pairs between conventional zero-lag Pearson r and lag. This feature is present also in our simulation (Fig. 7C). The low correlation between conventional zero-lag Pearson r and lag in the synthetic data (r = -.04) confirms that thread motifs need not introduce a systematic relation between these quantities. Therefore, the results of Fig. 7 (simulation) suggest that the results shown in Fig. 5 (real data) can be explained if thread motifs correspond to conventional resting state networks, in other words, if intra-RSN sequences of propagation are preserved across threads.

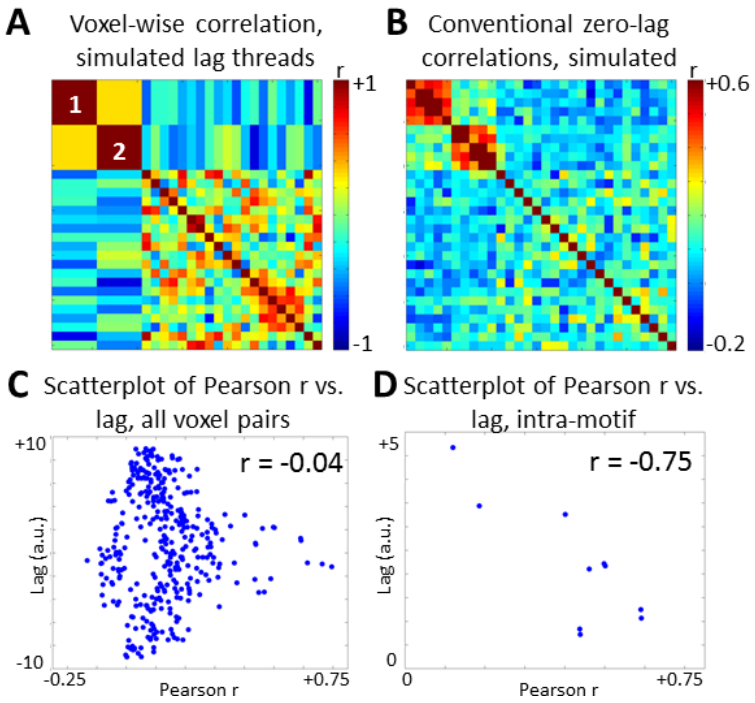

Figure 3-7: Scaled up illustration of lag thread motifs. This simulation includes 30 voxels (equivalently, 30 ROIs), 8 orthogonal lag threads, and 2 thread motifs. The 2 thread motifs consist of voxels 1-5 and voxels 6-10, respectively. Panel A displays the voxel:voxel correlation matrix across latency values in the 8 simulated lag threads (as in Fig. 5A; Eq. [S9] in SI). Voxels belonging to a thread motif are perfectly correlated (diagonal blocks labeled "1" and "2"). Panel B illustrates a zero-lag temporal correlation matrix (as in Fig. 5B), computed from timeseries reconstructed on the basis of thread structure (as in Fig. 6B). Voxels belonging to a thread motif exhibit high zero-lag temporal correlation. Panel C displays a scatter plot of the pairwise lag vs. pairwise zero-lag temporal correlation, as in Fig. 5C. Note no systematic relation, for pairs of voxels, between lag and zero-lag temporal correlation. Thus, thread motifs do not impose a systematic relation between these quantities. Panel D shows a scatter plot as in panel C, but limited to voxels within the first thread motif (similar results are obtained with the second motif). For voxel pairs within a motif, lag and zero-lag temporal correlation are negatively correlated.

RSNs correspond to lag thread motifs

The simulation in Fig. 7 suggests a model in which conventionally defined RSNs correspond to thread motifs, and implies two testable predictions. First, if the sequence of propagation is preserved within thread motifs, it follows that the dimensionality of intra-RSN lag structure should be one (see Fig. S3 for further explanation). Second, though the simulation in Fig. 7 contains no systematic relation, over all voxel pairs, between lag and zero-lag temporal correlation (Fig. 7C), if we examine the relationship between zero-lag Pearson r and lag considering only voxels within a motif, a substantial negative correlation emerges (r = -0.75; Fig. 7D). The basis for this relation is that, within a single thread motif, more nearly synchronous time series must be more

correlated. However, in general, threads propagate in multiple directions outside of motifs (e.g., as in Fig. 6). Consequently, relations of the type shown in Fig. 7D are obscured in Figs. 5C and 7C, because the fraction of intra-motif voxel pairs is a small fraction of all voxel pairs. Therefore, if RSNs correspond to lag thread motifs, voxel-pairs within a RSN should exhibit a substantial negative correlation between zero-lag Pearson r and lag (Fig. 7D).

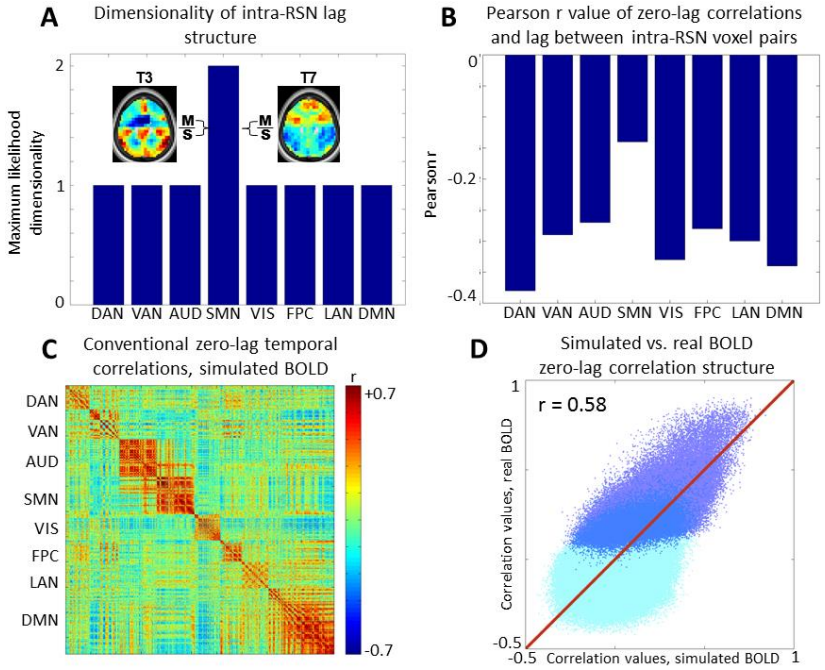

Figure 3-8: Thread motifs in real BOLD rs-fMRI data. Panel A shows the maximum likelihood dimensionality of lag structure computed within resting state networks as defined in Fig. 5. With the exception of the SMN, intra-RSN lag structure has dimensionality 1. SMN is an exception because the ordering of primary motor (M) and primary sensory (S) cortices is not fixed. M is earlier than S in some threads, e.g., Thread 3 (T3), whereas the reverse is true in other threads, e.g., Thread 7 (T7). Panel B shows the correlation, over pairs of voxels within RSNs, between lag and zero-lag temporal correlation. With the exception of the SMN, there is a substantial negative correlation between these quantities in each RSN. Panel C shows a zero-lag temporal correlation matrix for BOLD rs-fMRI timeseries reconstructed on the basis of 8 lag threads derived from real data (Fig. 2). Note similarity of the matrices shown in panel C and Fig. 5B (both 1065 × 1065). Panel D shows a scatter plot of the unique (upper triangle) values in the simulated (panel C) vs. real (Fig. 5B) zero-lag temporal correlation matrices. Dark blue dots represent intra-RSN relations, whereas light blue dots represent inter-RSN relations; the dark blue dots are semi-transparent to make all the data visible. The line of identity is indicated in red. The scatter plot demonstrates substantial agreement between the reconstructed and real data (r = 0.58 over all data; r = 0.62 for intra-RSN relations, r = 0.24 for inter-RSN relations).

We test these predictions in Fig. 8A-B. Fig. 8A shows the maximum likelihood dimensionality for the temporal lag structure calculated within resting state networks as

defined in (Hacker et al. 2013). As predicted by the thread motif model, the maximum likelihood dimensionality is 1 for all RSNs except the sensorimotor network (SMN). Fig. 8B shows the Pearson correlation derived from a scatter plot of zero-lag temporal correlation vs. lag over all intra-network voxels (as in Figs. 5C and 7C). Again, as predicted by the thread motif model, there is a substantial negative correlation in every RSN except the SMN. Therefore, although lag threads represent various patterns of propagation with generally reciprocal signaling across regions, within each RSN, BOLD rs-fMRI signal propagation is largely unidirectional.

The apparently anomalous dimensionality result obtained with respect to the sensorimotor network (SMN; Fig. 8A,B) highlights an interesting point concerning the correspondence between RSNs and thread motifs. Conventional BOLD rs-fMRI analyses generally agglomerate primary somatomotor and somatosensory areas into a single RSN (Esposito et al. 2013; Thomas Yeo et al. 2011) (see also Fig. 5B). Separation of motor and sensory areas into distinct parcels has only recently been achieved using a boundary mapping technique (Gordon et al. 2014). In contrast, lag threads sharply distinguish primary sensory vs. primary motor cortices (see Fig. 8A). Primary motor cortex is earlier than primary sensory cortex in most threads (Fig. 2; threads 3 and 4), but the ordering is reversed in other threads (Figs. S11, S12). This feature is also illustrated in Fig. 8A. Consequently, the observed dimensionality of lag structure in the SMN (as conventionally defined) is 2 (Fig. 8A). We verified that the dimensionality of lag structure in the separated motor and sensory components of the SMN is 1 in both cases (results not shown).

Zero lag temporal synchrony emerges from lag structure

The previous results suggest that RSNs correspond to lag thread motifs, that is, that the sequence of propagation within RSNs is largely preserved across lag threads. This finding raises the possibility that zero-lag temporal synchrony (i.e., conventional functional connectivity) within RSNs emerges from lag structure. To test this hypothesis, we converted each of the first eight lag threads extracted from real data (Fig. 2) into time series with the same spectral content as BOLD rs-fMRI (as in Fig. 6B; see "Simulating lag threads" in SI for further details). We then superposed these time series, weighted in proportion to their respective eigenvalues (see Fig. 4A and equation [S9]), to reconstruct synthetic BOLD rs-fMRI data with appropriate spectral content and imposed structure derived only from lag threads. The zero-lag temporal correlation matrix computed from the reconstructed time series is shown in Fig. 8C. This matrix is strikingly similar to the zero-lag temporal correlation matrix computed from real BOLD rs-fMRI data (Fig. 5B). Figure 8D shows a scatterplot of the real (Fig. 5B) vs. reconstructed (Fig. 8C) zero-lag temporal correlation values. Light blue and dark blue dots in Fig. 8D represent inter-RSN and intra-RSN correspondence, respectively. The scatterplot quantitatively demonstrates substantial agreement between the zero-lag temporal correlation structure of real and reconstructed data ($r = 0.58$). The model better predicts intra-RSN correlation structure ($r = 0.62$) vs. inter-RSN correlation structure ($r = 0.24$); the implication of this difference is at present not understood. Nevertheless, Figs. 8C and 8D suggest that intra-RSN synchrony RSNs is an emergent property of lag structure.

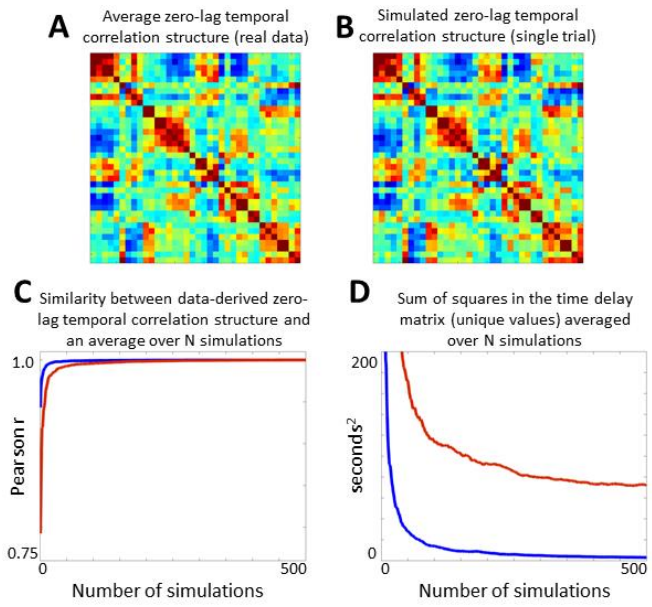

Figure 3-9: Simulated timeseries with the same zero-lag temporal correlation structure as rs-fMRI does not contain a consistent lag structure. In this simulation, we produced 12 minute epochs of synthetic BOLD timeseries for a set of 36 previously defined ROIs (Brier et al. 2012) such that spectral content and zero-lag temporal correlation structure of each simulation was matched to real data (see SI for further detail). A single 12 minute simulation closely approximates the true zero-lag temporal correlation structure of rs-fMRI, as shown by the close agreement between the group average structure of real data (A) and a single simulation (B). The zero-lag temporal correlation matrix and time delay matrix (TD; as in Fig. 4B) were computed for each simulation. The blue line in panel C plots the correlation between the upper triangle values in the zero-lag correlation matrix of real group average data vs. simulated data as a function of the number of simulations. The red line plots the same quantity as a function of number of real data sets. Panel C demonstrates that the zero-lag temporal correlation structure of real and simulated data both rapidly converge to the same mean. Panel D plots the sum of the upper triangle of the time delay matrix as a function of the quantity of included data. The blue line (simulated data) rapidly converges to zero; thus, the average time delay structure of simulated data converges to the all zeros matrix. In contrast, the red line (real data) converges to a non-zero value. Panel D demonstrates that a consistent, non-trivial lag structure is present in real but not simulated rs-fMRI timeseries.

Fig. 8 demonstrates that zero-lag temporal correlation can arise from patterns in lag. Fig. 9 demonstrates that lag structure is not uniquely determined by zero-lag temporal correlation structure. To illustrate this point, we generated synthetic, multi-dimensional timeseries with spectral content and second order statistics (i.e., zero-lag correlation structure) matched to that of the real BOLD rs-fMRI data (Figs. 9A,B; see “zero-lag temporal correlation need not specify lag structure” in SI for details). Fig. 9C shows that the average zero-lag temporal correlation matrix, in both synthetic (blue) and real (red) data, converges to the average structure derived from real data. Fig. 9D concerns lag and demonstrates a very different result. In particular, the average time delay matrix

computed over synthetic data rapidly converges to the all zeros matrix (blue line in Fig. 9D), whereas the TD matrix computed over real data converges to a consistent, non-zero delay structure (red line in Fig. 9D). Fig. 8C demonstrates that lag structure can be used to reconstruct zero-lag temporal correlations, whereas Fig. 9 shows that the reverse does not hold. The implication of these results is that lag structure represents the more fundamental level of organization in rs-fMRI.

3.6 **Discussion**

Summary of findings

The structure of human intrinsic brain activity, as imaged with resting state BOLD fMRI, has been understood predominantly in terms of zero-lag, temporal synchrony within widely distributed functional systems (RSNs). We previously demonstrated that inter-regional lags are reproducibly present in BOLD rs-fMRI data and that these lags are not attributable to hemodynamic factors (Mitra et al. 2014). We have substantially expanded on our previous findings here. In Part I, we demonstrated that lag threads in human rs-fMRI exhibit multiple, highly reproducible patterns of propagated activity (lag threads) in BOLD rs-fMRI data (Figs. 2-4). We also showed that there are most likely 8 lag threads in our current analysis, and that 8 lag threads can emerge from a small set of key ROIs (Figs. 3-4).

In Part II, we investigated the relation between lag threads and zero-lag temporal correlations in BOLD rs-fMRI. To this end, we examined common patterns of propagation across lag threads by computing voxel-wise correlations across 8 lag

threads (Fig. 5A). We found that voxel-wise lag-thread correlations and BOLD rs-fMRI zero-lag temporal correlations exhibit similar structure (Fig. 5). To explain this similarity, we hypothesize the existence of lag thread motifs, that is, sequences of propagation through subsets of regions that are shared across multiple threads (Fig. 6). Simulation experiments showed that zero-lag temporal synchrony within RSNs naturally emerges as a consequence of lag thread motifs (Fig. 7). We also demonstrated that conventionally defined zero-lag RSNs very likely correspond to lag thread motifs (Figs. 8A, 8B). Finally, we reproduced, to a fair approximation, the zero-lag temporal correlation structure of BOLD rs-fMRI using synthetic time series with imposed structure derived only from lag threads (Figs. 8C, 8D). The reverse relation does not hold, that is, zero-lag temporal correlation structure does not determine a unique lag structure (Fig. 9). Hence, temporal synchrony can be understood as a consequence of BOLD rs-fMRI lag structure.

It is important to note that, although the thread motif model provides a basis for understanding how synchrony arises from patterns in lag, this model is in no way imposed in the reconstruction in Fig. 8C; BOLD time series were reconstructed purely on the basis of lag threads calculated from real data. We conclude that lag threads represent a fundamental organizing property of the brain's intrinsic activity.

Physiology of propagated activity

A prominent concern regarding lags in human rs-fMRI has been that all observed phenomenology could be attributable to regional variations in the kinetics of

neurovascular coupling (Friston 2009; 2011; Friston et al. 2013; Friston and Dolan 2010; Handwerker et al. 2004) Such regional differences can be represented as an ordered sequence, as illustrated in Figure 1. Importantly, this set of temporal shifts can account for only a single lag thread (Mitra et al. 2014). Delayed signals in large venous structures most likely contribute to the topography of lag Thread 5 (Fig. S11). However, the existence of at least 8 lag threads demonstrates that regional differences in neurovascular coupling account for a minor component of BOLD rs-fMRI lag structure.

Our results raise the question of what physiological mechanisms might underlie propagation of slow spontaneous activity over the whole brain. Propagation of low frequency (<1Hz) spontaneous activity has been extensively described in the rodent brain using various modalities, including whole cell recordings (Hahn et al. 2006), local field potentials (Luczak et al. 2007; Sheroziya and Timofeev 2014; Sirota et al. 2003), voltage sensitive dyes (Ferezou et al. 2007; Mohajerani et al. 2013; Mohajerani et al. 2010), and calcium imaging (Stroh et al. 2013). We have previously shown that spontaneous BOLD signal fluctuations correspond to low frequency (<1Hz) local field potentials, also known as slow cortical potentials (SCPs), which represent slow endogenous changes in excitability (He et al. 2008; Pan et al. 2013). Thus, we speculate that propagation of activity in the BOLD signal is likely to represent propagation of slow changes in neuronal excitability.

Propagated changes in neuronal excitability have been previously described in terms of UP/DOWN states (UDS). UDS are slow (<1Hz), spontaneous, subthreshold changes in

neuronal membrane potential. These membrane potential fluctuations are effectively synchronous at a sub-millimeter spatial scale (Petersen et al. 2003; Steriade et al. 1993a; Steriade et al. 1993b), but exhibit multiple, complex patterns of propagation over larger spatial scales (Cossart et al. 2003; Fucke et al. 2011; Hahn et al. 2006; Ikegaya et al. 2004; Nir et al. 2011; Petersen et al. 2003; Sheroziya and Timofeev 2014), spanning thalamus (Sheroziya and Timofeev 2014), striatum (Plenz and Kitai 1998), and cortex (Sheroziya and Timofeev 2014). Although UDS were initially associated with anesthesia and slow wave sleep, it is now known that UDS persist and propagate during quiet wakefulness (Ferezou et al. 2007; Hahn et al. 2006; Petersen et al. 2003). The lags we found (on the order of ~1sec over the whole brain) in human spontaneous activity are comparable to UDS propagation delays in rodents (Amzica and Steriade 1995; Ferezou et al. 2007; Hahn et al. 2006; Mohajerani et al. 2013; Mohajerani et al. 2010; Petersen et al. 2003; Sheroziya and Timofeev 2014). There also are intriguing correspondences between the directionality of lags in the BOLD signal and lags in UDS in rodents. Reports by Hahn and colleagues (Hahn et al. 2006) and Sirota and colleagues (Sirota et al. 2003) both document that slow fluctuations in somatosensory neocortical areas lead activity in hippocampus by less than a second. These findings agree with lags between hippocampus and somatosensory cortex in a seed-based lag map derived from entorhinal cortex (Fig. S17).

Thus, UDS might underlie BOLD rs-fMRI signal fluctuations (He et al. 2008; Poskanzer and Yuste 2011; Ringach 2009). However, some features of these two phenomena are discrepant. In particular, UDS are generally periodic with frequency content in the range

0.5-0.8Hz (Hahn et al. 2006; Petersen et al. 2003; Steriade et al. 1993a), whereas the resting state BOLD fMRI signal is aperiodic and dominated by frequencies ≤ 0.1Hz (He et al. 2010). Whether or not UDS are responsible for the present results, we note that there is no consensus regarding the mechanisms underlying slowly propagated activity. Proposed explanations include shifts in excitatory-inhibitory balance (Amzica and Steriade 1995), thalamo-cortical interactions (Sheroziya and Timofeev 2014), astrocytic gliotransmission (Araque et al. 2014; Poskanzer and Yuste 2011), and metabolic neuromodulators such as adenosine (Amzica and Steriade 1995; Fellin et al. 2009). Future work is required to definitively elucidate the physiologic mechanisms underlying propagation in the BOLD rs-fMRI signal.

Topography of lag threads

Each lag thread (Fig. 2; Movies 1-4; Fig. S7-S14) exhibits a unique, highly reproducible (Fig. 3B) topography. It is evident that these topographies generally are bilaterally symmetric, as are most functional systems and resting state networks. Although fragments of functional systems can be observed in the lag threads (e.g., frontopolar cortex components of the frontoparietal control network in Thread 1), the contours of the thread maps do not correspond to the topographies of RSNs. This point relates to our previous demonstration that RSNs as a whole are not iso-latent; rather, each RSN contains a wide range of latency values and includes both early and late nodes (Mitra et al. 2014).

Several topographic features of the lag threads suggest functional properties. Since these points are speculative, we consider only the first two lag threads. In Thread 1, the earliest regions are brainstem, thalamus, hippocampus, and putamen; late areas include frontopolar cortex and central insula. This sequence suggests a "bottom-up" process in which activity begins subcortically and propagates to progressively higher order areas of the cerebral cortex (Fig. 2; Movie 1). Another striking finding is that the putamen is early while the caudate is late. See Movie 1 to visualize activity propagation from posterior putamen to the head of the caudate. As far as we are aware, this finding has not been previously described. In Thread 2, thalamus, hippocampus, and brainstem are late with respect to cerebral cortex, i.e., opposite to their temporal position in Thread 1. This sequence suggests a "top-down" process in which activity propagates from higher to lower centers (Fig. 2; Movie 2). However, other features, e.g., late cerebellum, early putamen, and late caudate, are common to Threads 1 and 2. The functional significance of specific lag thread topographies is unknown and requires further study.

The role of lag threads in integration vs. segregation

Activity in the brain, at various spatial scales, has been discussed in terms of two fundamental concepts: synchrony (Buzsaki and Draguhn 2004; Kenet et al. 2003; Lachaux et al. 1999) and lagged propagation (Cossart et al. 2003; Ikegaya et al. 2004; Massimini et al. 2004; Nikolic 2007; Sheroziya and Timofeev 2014). Taken to their logical extremes, synchrony and lag are opposed in a simple system: a perfectly synchronous system contains no lags, and a system with a single set of lags is not synchronous ((Tognoli and Kelso 2014); Fig. S3). The fact that the brain’s spontaneous

activity exhibits both of these properties may be a manifestation of the dual functions of neuronal segregation and integration (Mitra et al. 2014; Raichle 2011). Conventional zero-lag resting state functional connectivity analysis has provided a powerful tool for utilizing synchronicity to map spatially distinct functional areas (Buckner et al. 2011; Choi et al. 2012; Fox and Raichle 2007; Gordon et al. 2014; Power et al. 2011; Thomas Yeo et al. 2011). However, functional parcellations do not explain how spatially segregated modules in the brain become integrated (Raichle 2011). Lag threads demonstrate that spontaneous activity exhibits apparent propagation both within and between spatially segregated resting state networks. Therefore, lag threads may explain how spatially segregated networks can be integrated over a time scale of seconds.

Conversely, lag threads pose their own problem: if spontaneous activity is characterized by a lag structure, how does synchrony arise? Our results suggest that lag thread motifs provide an answer. Preservation of lag sequencing within certain regions of the brain (i.e., resting state networks) across multiple threads gives rise to zero-lag synchrony within these systems (Fig. 8C and 8D). Thus, the lag thread motif model unifies the coexistence of synchrony (spatial segregation) and lags (temporal integration) in the brain's spontaneous activity.

The physiological functions served by lag threads remain unknown, but previous work sheds some light on this matter. We have shown that the lag structure of rs-fMRI is focally modulated, in humans, following the performance of a motor task (Mitra et al. 2014), suggesting that the lag structure of intrinsic activity may be involved in learning

and memory. Indeed, the spatiotemporal structure of UDS (discussed above), a potential correlate of lags in the BOLD rs-fMRI signal, has been linked to consolidation and plasticity mechanisms (Hahn et al. 2006; Petersen et al. 2003; Sheroziya and Timofeev 2014; Steriade and Timofeev 2003). Additional support for this perspective comes from studies of neurodevelopment showing that precise patterns of propagated intrinsic activity are essential for fine-tuning synaptic connections (Adelsberger et al. 2005; Goodman and Shatz 1993; Katz and Shatz 1996). It is believed that persistence of this principle into adulthood supports the brain's capacity for lifelong plasticity (Hensch 2005; Katz and Shatz 1996; Penn and Shatz 1999; Spitzer 2006). A second hypothesis is that the cortex, like the spinal cord, acts as a central pattern generator (Yuste 1997; Yuste et al. 2005), and that patterns of propagated intrinsic activity represent neuronal programs that are recruited to perform tasks (Hall et al. 2014; Ikegaya et al. 2004; Luczak et al. 2007). Thus, lag threads may form the basis for activity sequences that naturally play out in responses to events.

Lag threads are a robust and reproducible organizational feature of spontaneous slow activity, here demonstrated in two groups of 688 young normal adults (Figs. 3 and 4). Regardless of their specific functions, the consistency of lag thread phenomenology suggests that this organizational feature is essential to normal brain physiology and function. We hypothesize that perturbed lag thread structure may underlie some neuropathological conditions. If so, these conditions may not manifest as altered conventional functional connectivity, since changes in lag thread structure (for instance, altered thread hierarchy in Fig. 3A) may not change zero-lag temporal correlations.

Hence, an understanding of the physiologic functions of lag threads may lead to better understanding of the brain in health and disease.

Limitations and future directions

The signal to noise ratio (SNR) of BOLD rs-fMRI is limited. Accordingly, extensive averaging over very large subject groups was required to obtain stable lag estimates at $(6\ mm)^3$ voxel resolution using $(15\ mm)^3$ reference ROIs. We are optimistic that future improvements in BOLD fMRI (Feinberg and Yacoub 2012), for instance, increased temporal resolution, will allow detection of lag threads in smaller populations, provided that voxelwise SNR remains adequate and preprocessing strategies effectively remove artifact. Alternative approaches to studying rs-fMRI lags, at coarser resolution, but with less sensitivity to SNR limitations, include deriving lag structure from selected ROIs, as in Figure 4, and computing lag projections, as in (Mitra et al. 2014).

A second caveat is that the presently reported correspondence between lag thread motifs and RSNs (Figs. 8A,8B) reflects a specific RSN parcellation (see Fig. S5; (Hacker et al. 2013)), although the inferences derived from this result most likely depend only minimally on the details on any particular parcellation scheme (Power et al. 2011; Thomas Yeo et al. 2011). We note that the correlation-based results (Figs. 5A, 5B, 8C, 8D) are parcellation independent.

Third, as lag threads are simply principal components of lag structure, they formally constitute only a basis set for lagged activity. Consequently, the sign of the lag threads

are, by definition, undetermined by a factor of ± 1. Moreover, the assumption of linear superposition in PCA implies that topologically complex or non-linear temporal sequence topographies cannot be recovered. However, we did find that kernel PCA, a non-linear technique, recovers lag thread topographies (Fig. S28) quite similar to those shown in Fig. 2. Additionally, the sign and topographies of seed-based lag maps (Fig. S15-S24) are uniquely determined. We used these maps to demonstrate that lag thread topographies reasonably separate seed-based lag maps into common clusters, and that the sign of each lag thread has most likely been correctly assigned (see “Validity of applying PCA to recover lag thread topographies” in SI).

Fourth, there is an ambiguity concerning voxels with lag values near zero in each lag thread. One possibility is that these voxels are in the middle of the temporal sequence represented by the lag thread. Alternatively, the voxel may not participate in the temporal sequence. At present, we cannot distinguish between these possibilities.

Finally, Fig. 8C shows a temporal correlation matrix computed on the basis of reconstructed BOLD rs-fMRI timeseries. This result reproduces many features of real data (Fig. 5B), but the correspondence obviously is imperfect (Pearson r = 0.58; Fig. 8D). Importantly, we assumed that the spectral content of BOLD rs-fMRI is uniform over gray matter and that lag threads superpose linearly. These assumptions represents an approximation (Salvador et al. 2008), although the extent to which spectral shapes are regionally dependent at frequencies below 0.1 Hz is uncertain (He et al. 2010). We also restricted our reconstruction to only the first 8 lag threads deemed significant by

maximum likelihood dimensionality analysis. Although the remaining lag threads contribute less individual variance, they may collectively play an important role in shaping correlation structure. In view of these approximations, a more complete model may be expected to provide a closer match between a reconstructed and true correlation structure of BOLD rs-fMRI timeseries. As our reconstruction relies only on lag threads, we have also excluded other phenomena which may contribute to the coordination of zero-lag correlation structure.

3.7 Acknowledgements

We thank John McCarthy, Manu Goyal, and Carl Hacker for helpful discussion and Dr. Randy Buckner for assistance in obtaining the MRI data. This work was supported by the National Institute of Health (NS080675 to MER and AZS; P30NS048056 to AZS; F30MH106253 to AM). The Brain Genomics Superstruct Project is funded by the Simons Foundation Autism Research Initiative.

3.8 References

Adelsberger H, Garaschuk O, and Konnerth A. Cortical calcium waves in resting newborn mice. *Nat Neurosci* 8: 988-990, 2005.

Amzica F, and Steriade M. Short- and long-range neuronal synchronization of the slow (< 1 Hz) cortical oscillation. *J Neurophysiol* 73: 20-38, 1995.

Araque A, Carmignoto G, Haydon PG, Oliet SH, Robitaille R, and Volterra A. Gliotransmitters travel in time and space. *Neuron* 81: 728-739, 2014.

Beckmann CF, DeLuca M, Devlin JT, and Smith SM. Investigations into resting-state connectivity using independent component analysis. *Philosophical transactions of the Royal Society of London Series B, Biological sciences* 360: 1001-1013, 2005.

Berger H. On the electroencephalogram of man. Second report. *Electroencephalogr Clin Neurophysiol* Suppl 28:75+, 1969.

Biswal B, Yetkin FZ, Haughton VM, and Hyde JS. Functional connectivity in the motor cortex of resting human brain using echo-planar MRI. *Magn Reson Med* 34: 537-541, 1995.

Biswal BB, Mennes M, Zuo XN, Gohel S, Kelly C, Smith SM, Beckmann CF, Adelstein JS, Buckner RL, Colcombe S, Dogonowski AM, Ernst M, Fair D, Hampson M, Hoptman MJ, Hyde JS, Kiviniemi VJ, Kotter R, Li SJ, Lin CP, Lowe MJ, Mackay C, Madden DJ, Madsen KH, Margulies DS, Mayberg HS, McMahon K, Monk CS, Mostofsky SH, Nagel BJ, Pekar JJ, Peltier SJ, Petersen SE, Riedl V, Rombouts SA, Rypma B, Schlaggar BL, Schmidt S, Seidler RD, Siegle GJ, Sorg C, Teng GJ, Veijola J, Villringer A, Walter M, Wang L, Weng XC, Whitfield-Gabrieli S, Williamson P, Windischberger C, Zang YF, Zhang HY, Castellanos FX, and Milham MP. Toward discovery science of human brain function. *Proceedings of the National Academy of Sciences of the United States of America* 107: 4734-4739, 2010.

Brier MR, Thomas JB, Snyder AZ, Benzinger TL, Zhang D, Raichle ME, Holtzman DM, Morris JC, and Ances BM. Loss of intranetwork and internetwork resting state functional connections with Alzheimer's disease progression. *J Neurosci* 32: 8890-8899, 2012.

Buckner R, Hollinshead M, Holmes A, Brohawn D, Fagerness J, O'Keefe T, Petrov V, Fariello G, Bakst L, and Rubenstein S. The Brain Genomics Superstruct Project. 2012.

Buckner RL, Krienen FM, Castellanos A, Diaz JC, and Yeo BT. The organization of the human cerebellum estimated by intrinsic functional connectivity. *Journal of neurophysiology* 106: 2322-2345, 2011.

Buzsaki G, and Draguhn A. Neuronal oscillations in cortical networks. *Science* 304: 1926-1929, 2004.

Choi EY, Yeo BT, and Buckner RL. The organization of the human striatum estimated by intrinsic functional connectivity. *Journal of neurophysiology* 108: 2242-2263, 2012.

Cossart R, Aronov D, and Yuste R. Attractor dynamics of network UP states in the neocortex. *Nature* 423: 283-288, 2003.

Esposito F, Tessitore A, Giordano A, De Micco R, Paccone A, Conforti R, Pignataro G, Annunziato L, and Tedeschi G. Rhythm-specific modulation of the sensorimotor network in drug-naive patients with Parkinson's disease by levodopa. *Brain* 136: 710-725, 2013.

Feinberg DA, and Yacoub E. The rapid development of high speed, resolution and precision in fMRI. *Neuroimage* 62: 720-725, 2012.

Fellin T, Halassa MM, Terunuma M, Succol F, Takano H, Frank M, Moss SJ, and Haydon PG. Endogenous nonneuronal modulators of synaptic transmission control cortical slow oscillations in vivo. *Proc Natl Acad Sci U S A* 106: 15037-15042, 2009.

Ferezou I, Haiss F, Gentet LJ, Aronoff R, Weber B, and Petersen CC. Spatiotemporal dynamics of cortical sensorimotor integration in behaving mice. *Neuron* 56: 907-923, 2007.

Fox MD, and Raichle ME. Spontaneous fluctuations in brain activity observed with functional magnetic resonance imaging. *Nat Rev Neurosci* 8: 700-711, 2007.

Friston K. Causal modelling and brain connectivity in functional magnetic resonance imaging. *PLoS Biol* 7: e33, 2009.

Friston K. Dynamic causal modeling and Granger causality Comments on: the identification of interacting networks in the brain using fMRI: model selection, causality and deconvolution. *Neuroimage* 58: 303-305; author reply 310-301, 2011.

Friston K, Moran R, and Seth AK. Analysing connectivity with Granger causality and dynamic causal modelling. *Curr Opin Neurobiol* 23: 172-178, 2013.

Friston KJ, and Dolan RJ. Computational and dynamic models in neuroimaging. *Neuroimage* 52: 752-765, 2010.

Fucke T, Suchanek D, Nawrot MP, Seamari Y, Heck DH, Aertsen A, and Boucsein C. Stereotypical spatiotemporal activity patterns during slow-wave activity in the neocortex. *J Neurophysiol* 106: 3035-3044, 2011.

Goodman CS, and Shatz CJ. Developmental mechanisms that generate precise patterns of neuronal connectivity. *Cell* 72 Suppl: 77-98, 1993.

Gordon EM, Laumann TO, Adeyemo B, Huckins JF, Kelley WM, and Petersen SE. Generation and Evaluation of a Cortical Area Parcellation from Resting-State Correlations. *Cereb Cortex* 2014.

Grinvald A, Arieli A, Tsodyks M, and Kenet T. Neuronal assemblies: single cortical neurons are obedient members of a huge orchestra. *Biopolymers* 68: 422-436, 2003.

Grinvald A, and Hildesheim R. VSDI: a new era in functional imaging of cortical dynamics. *Nat Rev Neurosci* 5: 874-885, 2004.

Gusnard DA, Raichle ME, and Raichle ME. Searching for a baseline: functional imaging and the resting human brain. *Nat Rev Neurosci* 2: 685-694, 2001.

Hacker CD, Laumann TO, Szrama NP, Baldassarre A, Snyder AZ, Leuthardt EC, and Corbetta M. Resting state network estimation in individual subjects. *Neuroimage* 82C: 616-633, 2013.

Hahn TT, Sakmann B, and Mehta MR. Phase-locking of hippocampal interneurons' membrane potential to neocortical up-down states. *Nat Neurosci* 9: 1359-1361, 2006.

Hall TM, de Carvalho F, and Jackson A. A common structure underlies low-frequency cortical dynamics in movement, sleep, and sedation. *Neuron* 83: 1185-1199, 2014.

Handwerker DA, Ollinger JM, and D'Esposito M. Variation of BOLD hemodynamic responses across subjects and brain regions and their effects on statistical analyses. *Neuroimage* 21: 1639-1651, 2004.

He BJ, Snyder AZ, Zempel JM, Smyth MD, and Raichle ME. Electrophysiological correlates of the brain's intrinsic large-scale functional architecture. *Proc Natl Acad Sci U S A* 105: 16039-16044, 2008.

He BJ, Zempel JM, Snyder AZ, and Raichle ME. The temporal structures and functional significance of scale-free brain activity. *Neuron* 66: 353-369, 2010.

Hensch TK. Critical period plasticity in local cortical circuits. *Nat Rev Neurosci* 6: 877-888, 2005.

Ikegaya Y, Aaron G, Cossart R, Aronov D, Lampl I, Ferster D, and Yuste R. Synfire chains and cortical songs: temporal modules of cortical activity. *Science* 304: 559-564, 2004.

Katz LC, and Shatz CJ. Synaptic activity and the construction of cortical circuits. *Science* 274: 1133-1138, 1996.

Kenet T, Bibitchkov D, Tsodyks M, Grinvald A, and Arieli A. Spontaneously emerging cortical representations of visual attributes. *Nature* 425: 954-956, 2003.

Lachaux JP, Rodriguez E, Martinerie J, and Varela FJ. Measuring phase synchrony in brain signals. *Hum Brain Mapp* 8: 194-208, 1999.

Logothetis NK, Pauls J, Augath M, Trinath T, and Oeltermann A. Neurophysiological investigation of the basis of the fMRI signal. *Nature* 412: 150-157, 2001.

Luczak A, Bartho P, Marguet SL, Buzsaki G, and Harris KD. Sequential structure of neocortical spontaneous activity in vivo. *Proc Natl Acad Sci U S A* 104: 347-352, 2007.

Massimini M, Huber R, Ferrarelli F, Hill S, and Tononi G. The sleep slow oscillation as a traveling wave. *J Neurosci* 24: 6862-6870, 2004.

Maxim V, Sendur L, Fadili J, Suckling J, Gould R, Howard R, and Bullmore E. Fractional Gaussian noise, functional MRI and Alzheimer's disease. *Neuroimage* 25: 141-158, 2005.

Miller JE, Ayzenshtat I, Carrillo-Reid L, and Yuste R. Visual stimuli recruit intrinsically generated cortical ensembles. *Proc Natl Acad Sci U S A* 111: E4053-4061, 2014.

Minka TP. Automatic choice of dimensionality for PCA. In: *Advances in Neural Information Processing Systems 13*. Cambridge, MA: MIT Press, 2001, p. 598-604.

Mitra A, Snyder AZ, Hacker CD, and Raichle ME. Lag structure in resting state fMRI. *J Neurophysiol* 2014.

Mohajerani MH, Chan AW, Mohsenvand M, Ledue J, Liu R, McVea DA, Boyd JD, Wang YT, Reimers M, and Murphy TH. Spontaneous cortical activity alternates

between motifs defined by regional axonal projections. *Nat Neurosci* 16: 1426-1435, 2013.

Mohajerani MH, McVea DA, Fingas M, and Murphy TH. Mirrored bilateral slow-wave cortical activity within local circuits revealed by fast bihemispheric voltage-sensitive dye imaging in anesthetized and awake mice. *J Neurosci* 30: 3745-3751, 2010.

Nikolic D. Non-parametric detection of temporal order across pairwise measurements of time delays. *J Comput Neurosci* 22: 5-19, 2007.

Nir Y, Staba RJ, Andrillon T, Vyazovskiy VV, Cirelli C, Fried I, and Tononi G. Regional slow waves and spindles in human sleep. *Neuron* 70: 153-169, 2011.

Pan WJ, Thompson GJ, Magnuson ME, Jaeger D, and Keilholz S. Infraslow LFP correlates to resting-state fMRI BOLD signals. *Neuroimage* 74: 288-297, 2013.

Penn AA, and Shatz CJ. Brain waves and brain wiring: the role of endogenous and sensory-driven neural activity in development. *Pediatr Res* 45: 447-458, 1999.

Petersen CC, Hahn TT, Mehta M, Grinvald A, and Sakmann B. Interaction of sensory responses with spontaneous depolarization in layer 2/3 barrel cortex. *Proc Natl Acad Sci U S A* 100: 13638-13643, 2003.

Plenz D, and Kitai ST. Up and down states in striatal medium spiny neurons simultaneously recorded with spontaneous activity in fast-spiking interneurons studied in cortex-striatum-substantia nigra organotypic cultures. *J Neurosci* 18: 266-283, 1998.

Poskanzer KE, and Yuste R. Astrocytic regulation of cortical UP states. *Proc Natl Acad Sci U S A* 108: 18453-18458, 2011.

Power JD, Cohen AL, Nelson SM, Wig GS, Barnes KA, Church JA, Vogel AC, Laumann TO, Miezin FM, Schlaggar BL, and Petersen SE. Functional network organization of the human brain. *Neuron* 72: 665-678, 2011.

Raichle ME. The restless brain. *Brain Connect* 1: 3-12, 2011.

Ringach DL. Spontaneous and driven cortical activity: implications for computation. *Curr Opin Neurobiol* 19: 439-444, 2009.

Salvador R, Martinez A, Pomarol-Clotet E, Gomar J, Vila F, Sarro S, Capdevila A, and Bullmore E. A simple view of the brain through a frequency-specific functional connectivity measure. *Neuroimage* 39: 279-289, 2008.

Seeley WW, Menon V, Schatzberg AF, Keller J, Glover GH, Kenna H, Reiss AL, and Greicius MD. Dissociable intrinsic connectivity networks for salience processing and executive control. *The Journal of neuroscience : the official journal of the Society for Neuroscience* 27: 2349-2356, 2007.

Sheroziya M, and Timofeev I. Global intracellular slow-wave dynamics of the thalamocortical system. *J Neurosci* 34: 8875-8893, 2014.

Sirota A, Csicsvari J, Buhl D, and Buzsaki G. Communication between neocortex and hippocampus during sleep in rodents. *Proc Natl Acad Sci U S A* 100: 2065-2069, 2003.

Spitzer NC. Electrical activity in early neuronal development. *Nature* 444: 707-712, 2006.

Steriade M, Contreras D, Curro Dossi R, and Nunez A. The slow (< 1 Hz) oscillation in reticular thalamic and thalamocortical neurons: scenario of sleep rhythm generation in interacting thalamic and neocortical networks. *J Neurosci* 13: 3284-3299, 1993a.

Steriade M, Nunez A, and Amzica F. A novel slow (< 1 Hz) oscillation of neocortical neurons in vivo: depolarizing and hyperpolarizing components. *J Neurosci* 13: 3252-3265, 1993b.

Steriade M, and Timofeev I. Neuronal plasticity in thalamocortical networks during sleep and waking oscillations. *Neuron* 37: 563-576, 2003.

Stroh A, Adelsberger H, Groh A, Ruhlmann C, Fischer S, Schierloh A, Deisseroth K, and Konnerth A. Making waves: initiation and propagation of corticothalamic Ca2+ waves in vivo. *Neuron* 77: 1136-1150, 2013.

Thomas Yeo BT, Krienen FM, Sepulcre J, Sabuncu MR, Lashkari D, Hollinshead M, Roffman JL, Smoller JW, Zollei L, Polimeni JR, Fischl B, Liu H, and Buckner RL. The organization of the human cerebral cortex estimated by intrinsic functional connectivity. *Journal of neurophysiology* 106: 1125-1165, 2011.

Tognoli E, and Kelso JA. Enlarging the scope: grasping brain complexity. *Front Syst Neurosci* 8: 122, 2014.

van den Heuvel MP, Kahn RS, Goni J, and Sporns O. High-cost, high-capacity backbone for global brain communication. *Proc Natl Acad Sci U S A* 109: 11372-11377, 2012.

Yuste R. Introduction: spontaneous activity in the developing central nervous system. *Semin Cell Dev Biol* 8: 1-4, 1997.

Yuste R, MacLean JN, Smith J, and Lansner A. The cortex as a central pattern generator. *Nat Rev Neurosci* 6: 477-483, 2005.

Chapter 4: Propagated infra-slow resting state fMRI activity in humans reorganizes across wake and slow wave sleep

This chapter has been published as a journal article. The citation is:

Mitra A, Snyder A, Tagliazucchi E, Laufs, H, Raichle M. (2015). Propagated infra-slow activity is reorganized across wake and slow wave sleep. eLife. doi:10.7554/eLife.10781.

Marc Raichle and I conceived the project and research approach. I designed and implemented the methods and performed the data analysis. Abraham Snyder and I processed the data, which was provided by Helmut Laufs and Enzo Tagliazucchi. I wrote the paper; Abraham Snyder, Enzo Tagliazucchi, Helmut Laufs, and Marc Raichle edited it.

4.1 Preface

The previous chapters have established that a reproducible temporal structure exists in resting state fMRI, and that there is a rule for explaining how resting state correlation structure emerges from temporal structure. However, simply knowing the existence of a phenomenon does not provide any explanation of its possible functions.

Chapter 4 explores the temporal structure of resting state fMRI in human wakefulness versus slow wave sleep. We find that whereas the correlation structure is only modestly altered across arousal states, the temporal structure changes drastically. In particular, we demonstrate that the cross-network temporal structure is dramatically altered across arousal states, whereas the within-network temporal structure is largely preserved. The major implications of this chapter are (1) The temporal structure of resting state fMRI is labile, and highly sensitive to state of arousal, and (2) That the cross-network temporal structure of resting state fMRI may play a role in conscious awareness. The latter conclusion is reached on the basis of findings that show spontaneous cross-network temporal structure to be highly ordered in wakeful, but not slow wave sleep, conditions.

4.2 Abstract

Propagation of slow intrinsic brain activity has been widely observed in electrophysiogical studies of slow wave sleep (SWS). However, in human resting state fMRI (rs-fMRI), intrinsic activity has been understood predominantly in terms of zero-lag temporal synchrony (functional connectivity) within systems known as resting state networks (RSNs). Prior rs-fMRI studies have found that RSNs are generally preserved

across wake and sleep. Here, we use a recently developed analysis technique to study propagation of infra-slow intrinsic blood oxygen level dependent (BOLD) signals in normal adults during wake and SWS. This analysis reveals marked changes in propagation patterns in SWS vs. wake. Broadly, ordered propagation is preserved within traditionally defined RSNs but lost between RSNs. Additionally, propagation between cerebral cortex and subcortical structures reverses directions, and intra-cortical propagation becomes reorganized, especially in visual and sensorimotor cortices. These findings show that propagated rs-fMRI activity informs theoretical accounts of the neural functions of sleep.

4.3 Introduction

Sleep is a state during which interactions with the environment are greatly attenuated. The behavioral consequences of this state, namely, immobility and reduced responsiveness, carry obvious costs, such as compromised avoidance of predators. Nevertheless, nearly all animals sleep, suggesting that sleep is essential to normal physiology (Cirelli and Tononi 2008). In most mammals, including humans, prolonged sleep deprivation leads to impaired performance, psychosis, and eventually death (Brown et al. 2012; Everson et al. 1989; Rechtschaffen 1998). Sleep is attended by changes in gene expression (Abel et al. 2013; Cirelli and Tononi 2000), neuromodulator levels (Brown et al. 2012), metabolism (Boyle et al. 1994; Braun et al. 1997), and markedly altered patterns of neural activity (Dang-Vu 2012; Loomis et al. 1935a; b; McCormick and Bal 1997). Yet, the fundamental functions of sleep remain elusive.

Sleep conventionally is divided into stages, the deepest of which is slow wave sleep (SWS; also known as N3 sleep) (Iber 2007; Rechtschaffen and Kales 1968). The electrophysiologic hallmark of SWS is the slow oscillation, which manifests as periodic alternations of membrane potential, also known as Up/Down states (UDSs), characteristically at frequencies in the range of 0.5 - 1.5 Hz (Achermann and Borbely 1997; Steriade et al. 1993). As observed with extracellular local field potential (LFP) recordings, slow oscillations are locally synchronous but exhibit apparent propagation over the whole brain on a time scale of 100's of milliseconds (Hahn et al. 2012; Nir et al. 2011; Riedner et al. 2007; Sheroziya and Timofeev 2014). Similar patterns of propagation have also been observed using electroencephalography (EEG), in which SWS manifests as a predominance of high amplitude, 1-4 Hz (delta) rhythms (Massimini et al. 2004).

The observation of propagated slow electrophysiological activity during SWS raises the question of whether similar phenomenology might be observed by other means, specifically, resting state functional magnetic resonance imaging (rs-fMRI). Infra-slow (<0.1 Hz) intrinsic (equivalently, spontaneous) activity recorded using rs-fMRI has been understood predominantly in terms of zero-lag temporal synchrony (functional connectivity) within systems known as resting state networks (RSNs) (Beckmann et al. 2005; Biswal et al. 2010). Prior rs-fMRI studies have found that RSNs are generally preserved across wake and SWS (Horovitz et al. 2009; Larson-Prior et al. 2009; Picchioni et al. 2013; Samann et al. 2011; Tagliazucchi et al. 2013a). Importantly,

conventional functional connectivity analyses assume temporal synchronicity and make no provision for the possibility that intrinsic activity may propagate between regions. We have recently described an alternative analysis technique which explicitly focuses on apparent propagation in rs-fMRI data (Mitra et al. 2015; Mitra et al. 2014; Yuste and Fairhall 2015). Our methodology applies parabolic interpolation to lagged cross-covariance curves to detect temporal lags at a resolution finer than the temporal sampling density of rs-fMRI (see Methods; Fig. 1). Using this technique, we previously demonstrated, in awake, normal humans, that the blood oxygen level dependent (BOLD) signal exhibits highly reproducible temporal lag patterns on a time scale of ~1 sec; some regions are systematically early with respect to the rest of brain, whereas other regions are systematically late (Mitra et al. 2015; Mitra et al. 2014). Moreover, temporal lags in BOLD signal activity are altered, with appropriate focality, by prior performance of motor tasks as well as by time of day (Mitra et al. 2014). We operationally infer apparent propagation on the basis of measured temporal lags, assuming nothing regarding the path or mechanism by which BOLD signals "propagate" between regions. In particular, the temporal scale of this phenomenology is much slower than axonal transmission via fiber tracts (Caminiti et al. 2009). With this understanding, we omit "apparent" in references to BOLD signal propagation.

Previous work has related propagated slow electrophysiological activity during SWS to several aspects of physiology. First, SWS is believed to represent an off-line state during which propagated slow activity plays a central role in the consolidation of memory (Born et al. 2006; Maquet 2001; Marshall et al. 2006; Stickgold 2005). In particular, propagation along the anterior-posterior axis of the brain has been linked to

consolidation of declarative memory (Marshall et al. 2006). Second, loss of environmental awareness during SWS is thought to be mediated by thalamic hyperpolarization, which is modulated by propagation of slow (< 1 Hz) activity from cortex to thalamus (Blethyn et al. 2006; Hughes et al. 2002). Evidence of such propagation has never been observed *in vivo*. Finally, it has been theorized that reduced subjective awareness ("unconsciousness") during SWS results from loss of integration across networks (Mashour 2005; Tononi 2004). Here, we report whole-brain patterns of propagated rs-fMRI activity in humans, contrasting eyes-closed wake vs. SWS. Our results lend support to each of the aforementioned perspectives.

4.4 Results

We characterize lag structure (e.g., apparent propagation) using three major approaches. First, we begin by computing lags for all pairs of voxels in gray matter in rs-fMRI data (Fig. 1; (Mitra et al. 2014)). These results are assembled into *time-delay (TD) matrices*, which have dimensions voxels × voxels and entries in units of seconds (Methods Eq. E3). TD matrices represent the lag between all pairs of voxels in gray matter. Second, computing the mean over all columns of the TD matrix yields a *lag projection map* (Methods Eq. E4; Fig. 1). Lag projection maps topographically represent the mean lag between each voxel and the rest of the brain. Third, computing lags over the whole brain with respect to a particular region yields a *seed-based lag map.* Seed-based lag maps topographically represent the degree to which each voxel is, on average, early vs. late with respect to the selected seed. The present results are reported in terms of lag projection maps (Figure 2), seed-based lag maps (Figures 3 and 4), and TD matrices (Figure 5). Additionally, it is possible to decompose lag

structure into multiple temporal sequences ("*lag threads*") by applying spatial principal components analysis (PCA) to the TD matrix (Mitra et al. 2015) (see Figure 7 caption for details). Lag thread results are presented in Figure 7.

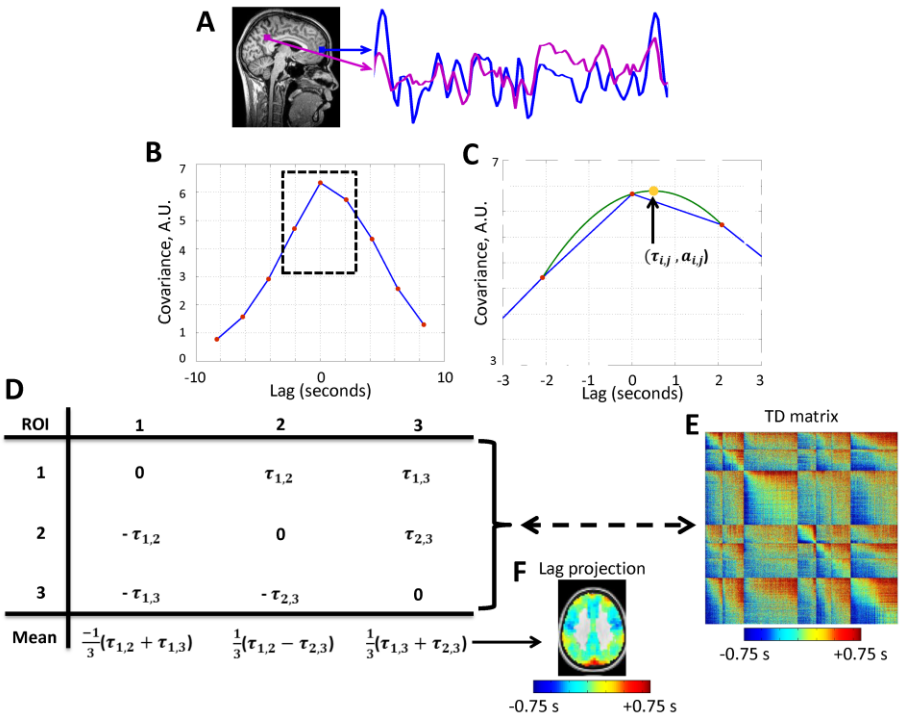

Figure 4-1: Calculation of lag structure using lagged cross-covariance functions and parabolic interpolation. Lags are defined by analysis of timeseries derived from two loci. (A): Two exemplar loci (both in the default mode network). The time series were extracted from the illustrated loci over ~200 s. (B): The corresponding lagged cross-covariance function (Methods equation E2). Although the lagged cross-covariance is defined over the range ± T, where T is the run duration, the range of the plotted values is restricted to ±8.32 s, which is equivalent to ±4 frames (red markers) as the repetition time was 2.08 s. The lag between the time series is the value at which the absolute value of the cross-covariance function is maximal. (C): This extremum can be determined at a resolution finer than the temporal sampling density by parabolic interpolation (green line) through the computed values (red markers). This extremum (arrow, yellow marker) defines both the lag between time series i and j ($\tau_{i,j}$) and the corresponding amplitude ($a_{i,j}$). (D): Toy case illustration of a time-delay (TD) matrix (Methods equation E3) representing 3 voxels. TD matrices encode the lag between every pair of analyzed voxels and are anti-symmetric by definition. The mean over each column of a TD matrix generates a lag projection map (Methods equation E4). A TD matrix obtained with real rs-fMRI data and the corresponding lag projection map are shown in panels (E) and (F), respectively. Panels A-D are adapted from (Mitra et al. 2014).

Figures 2A-B exhibit lag projection maps computed during wake and SWS. State-dependent shifts are evident in the lag projection maps, for example in occipital cortex and thalamus (Figs. 2A-B). Fig. 2C shows all statistically significant spatial clusters

($|Z| > 4.5, p < 0.05$ corrected; see Methods) in the wake vs. SWS comparison. These clusters include: thalamus, bilateral putamen, brainstem, visual cortex, medial prefrontal cortex (mPFC), and paracentral lobule (PCL) (Fig. 2C). Visual cortex was later (more positive lag values) during wake as compared to SWS, whereas the remaining clusters were earlier (more negative lag values).

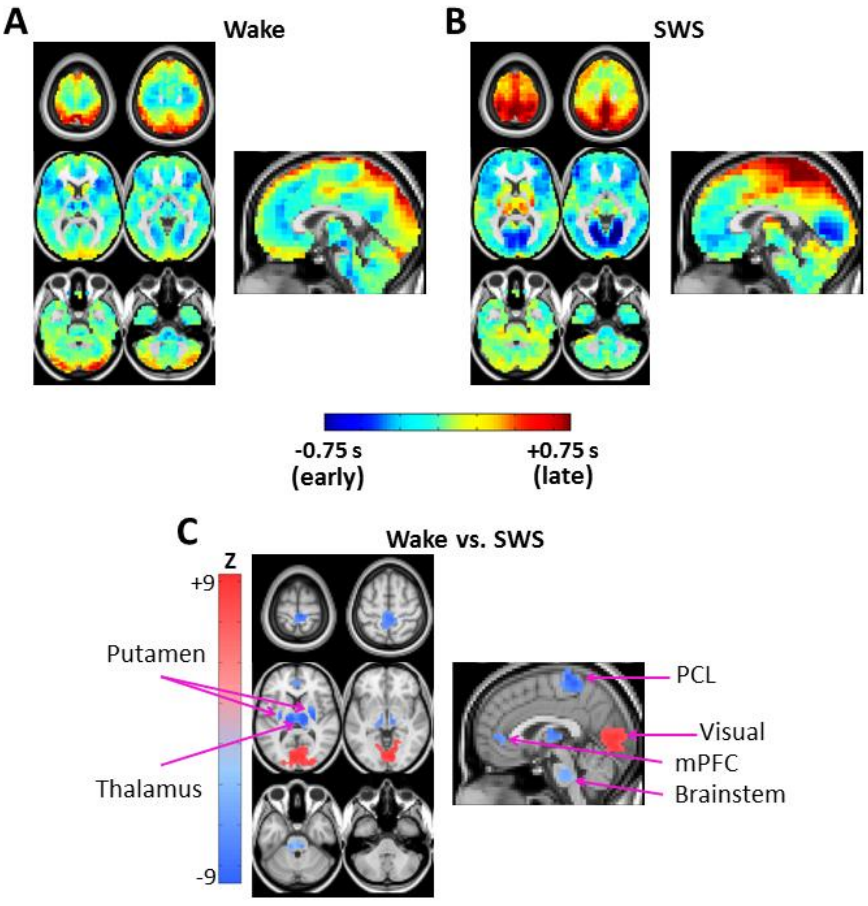

Figure 4-2: Lag projection maps in wake and slow wave sleep. Lag projection maps depict the mean lag between each voxel and the rest of the brain (Mitra et al. 2014; Nikolic 2007). Panels A-B display lag projection maps, in units of seconds, derived from wake (A) and SWS (B). These lag projection maps demonstrate changes in lag structure as a function of state. For example, thalamus is early (blue) during wake but late (red) during SWS; the opposite shift is evident in visual cortex. Panel C shows voxels exhibiting cluster-wise statistical significance in the wake vs. SWS comparison (|Z| > 4.5, p < 0.05 corrected). These clusters are centered on putamen bilaterally, thalamus, paracentral lobule (PCL), visual cortex, medial prefrontal cortex (mPFC), and brainstem. Axial slices: Z = +69, +57, +9, -3, -27, -39. Sagittal slice: X = +3.

Having found voxel clusters exhibiting statistically significant changes in lag structure in the whole-brain wake vs. SWS contrast, we next computed seed-based lag maps using the clusters shown in Fig. 2C as seeds (see Methods). Seed-based lag maps represent

temporal lags between each voxel and the average timecourse computed over the seed-region of interest.

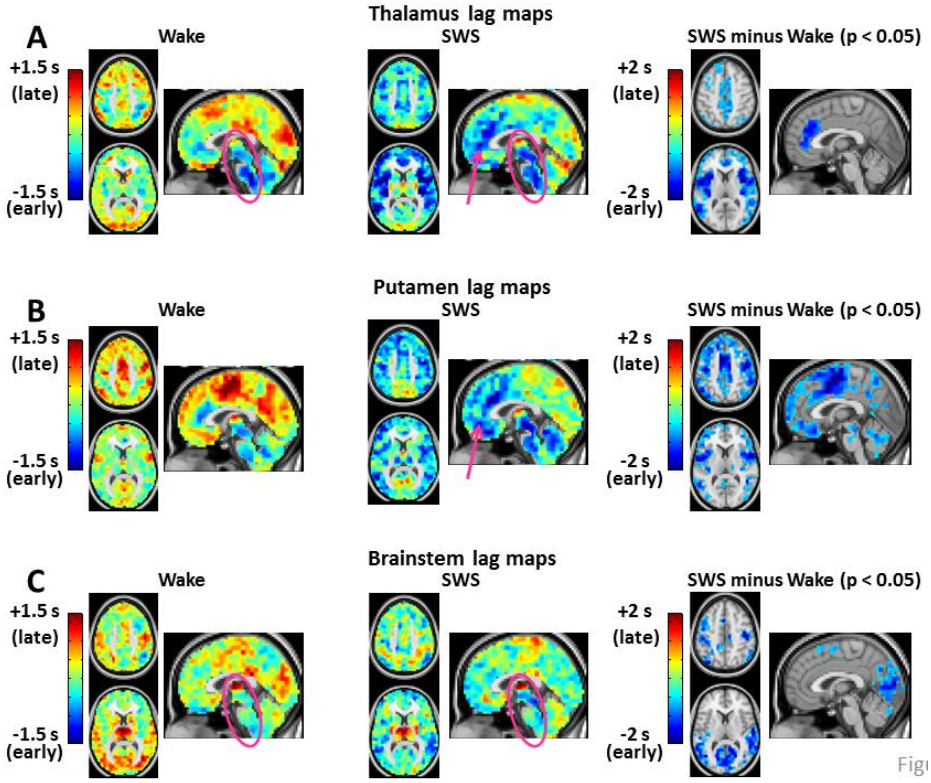

Figure 4-3: Seed-based lag maps in wake and SWS corresponding to the subcortical regions identified in Fig. 2C: thalamus (A), putamen (B), and brainstem (C). Also shown are lag difference maps (SWS minus wake) thresholded for cluster-wise statistical significance (|Z| > 4.5, p < 0.05 corrected; as in Fig. 2C). During wake, the cerebral cortex is generally late (yellow/red hues) with respect to subcortical regions. The cerebral cortex becomes early (blue/green hues) with respect to subcortical areas during SWS. All significant lag differences are negative (blue), and predominantly found in cortex. Pre-frontal cortex becomes markedly early with respect to the posterior parts of the brain (pink arrows in A and B). This feature suggests a "front-to-back" propagation of slow waves in SWS (Massimini et al. 2004). Lag structure in the brainstem and thalamus is relatively constant (pink ovals in A and C). Lag structure is present within the thalamus in panel A even though the whole thalamus was used as the reference seed. This effect is observed because voxels within large seed-regions, e.g., thalamus, can exhibit non-zero lags with the mean timecourse computed over the entire seed. Axial slices: Z = +45, +9. Sagittal slice: X = +3.

Seed-based lag maps obtained with the subcortical clusters, specifically, thalamus, putamen, and brainstem, are shown in Fig. 3, which illustrates altered lags during SWS compared to wake. Three principal findings are evident. First, whereas cortex is

generally late with respect to the subcortical seeds during wake, cortex becomes earlier than subcortical structures during SWS (see significant differences in Fig. 3). Second, a "front-to-back" propagation pattern appears in SWS; this phenomenon is best seen in the sagittal views of the thalamus and putamen lag maps (pink arrows, Figs. 3A-B). This pattern may correspond to previous reports of slow wave propagation along the anterior-posterior axis of the brain (Massimini et al. 2004; Murphy et al. 2009). Third, the lag structure within the thalamus and brainstem (Fig. 3A,C, pink ovals) remains largely constant across states. An early-to-late sequence extending from lower brainstem to rostral thalamus is evident in each of the seed-based lag maps shown in Fig. 3A,C (pink ovals). Hence, the general pattern of BOLD signal propagation between cortex and subcortical structures reverses during SWS, but propagation within the brainstem-thalamus axis is largely preserved across wake vs. SWS.

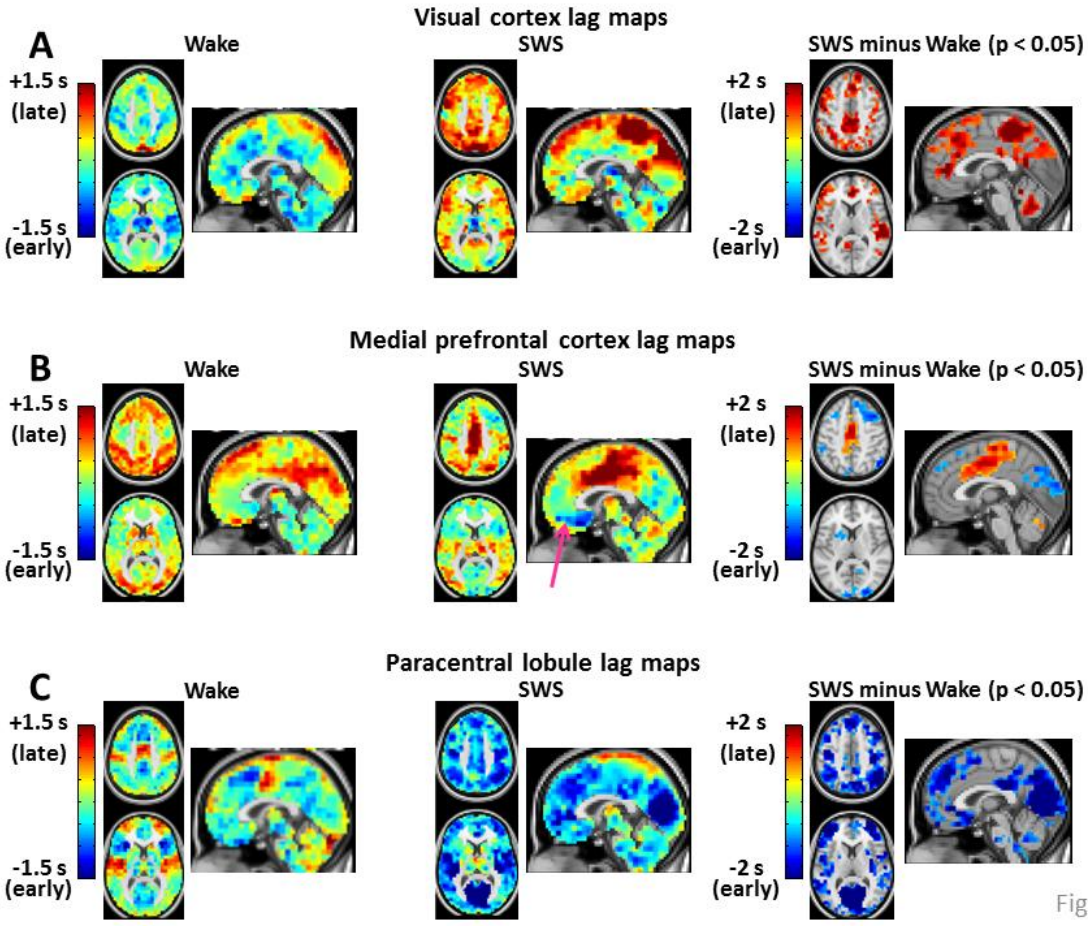

Figure 4-4: Seed-based lag maps in wake and SWS corresponding to the cortical regions identified in Fig. 2C: visual cortex (A), medial prefrontal cortex (B), and paracentral lobule (C). Also shown are lag difference maps (SWS minus wake), thresholded for statistical significance, as in Fig 2. Panel A shows that, whereas the visual seed is neither wholly late nor early in wake, nearly the entire cortex is late with respect to visual cortex during SWS. Panel B shows that medial prefrontal cortex (mPFC) exhibits both early and late lag shifts between wake and SWS. The mPFC lag map in SWS also exhibits the "front-to-back" propagation pattern highlighted in Figure 3 (pink arrow). Panel C shows that many of the lag relations of the paracentral lobule seed are reversed during SWS relative to wake. For example, in wake, the seed-region leads lateral sensory-motor cortex and posterior insula. These relations reverse in SWS and nearly the entire cerebral cortex becomes early with respect to the paracentral lobule. Slice coordinates identical to Fig. 3.

Figure 4 displays seed-based lag maps obtained with the cortical clusters shown in Fig. 2C. State-contrasts in lag structure differ by seed. Specifically, visual cortex (Fig. 4A) is neither wholly late nor early during wake, but nearly the entire cerebral cortex becomes late with respect to visual cortex during SWS. Two especially prominent foci of lateness

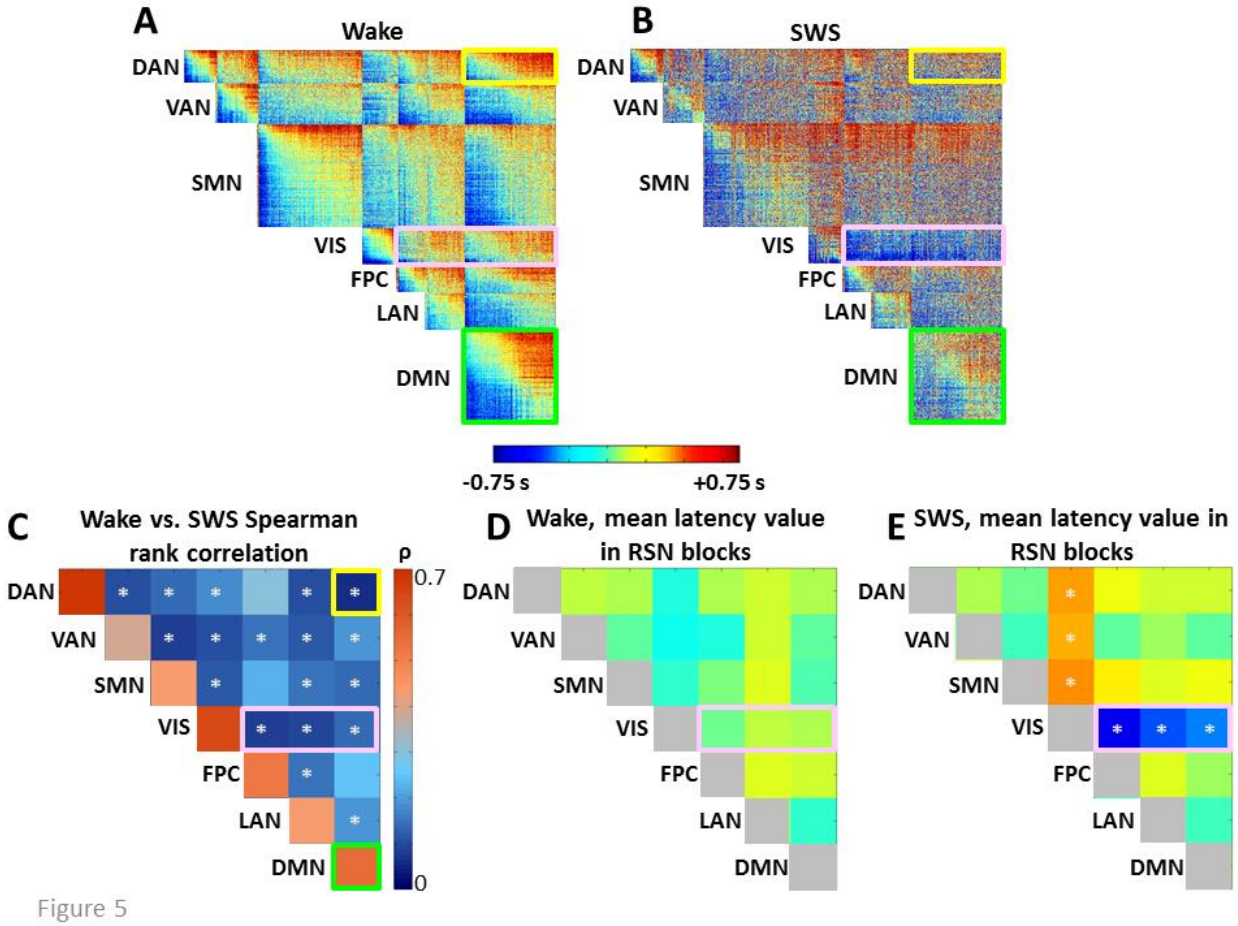

Figure 5

Figure 4-5: Time delay (TD) matrices. Panels A-B display TD matrices (in units of seconds) in wake and SWS, respectively. Each pixel represents the lag between two voxels. TD matrices are, by definition, anti-symmetric. Hence, all relevant information is contained in the displayed upper triangular values. The matrices displayed in (A-B) have been masked to include only cortical (6 mm)^3 voxels with a ≥90% chance of belonging to one of 7 resting state networks (RSNs: dorsal attention network (DAN), ventral attention network (VAN), sensory motor network (SMN), visual network (VIS), frontoparietal control network (FPC), language network (LAN), default mode network (DMN)) ((Hacker et al. 2013), see Fig. 5- figure supplement 2). The same RSN definitions are applied in wake and SWS. After sorting voxels by RSN membership, voxels were sorted from early to late within RSN in the wake state. The wake ordering was applied to the SWS TD matrix. Panel C shows the Spearman rank order correlation between wake and SWS lag values in each of the 28 intra- and inter- RSN blocks in panels (A-B). The diagonal blocks in panel C exhibit high correlation values, indicating that intra-RSN propagation is relatively preserved across wake and SWS. The correlation values in the off-diagonal blocks in panel C are low, demonstrating that inter-RSN propagation is strongly altered during SWS. White asterisks indicate significant ($p < 0.05$) effects computed by permutation resampling, including correction for multiple (N = 28) comparisons. Panel D plots the mean within-block values of the wake TD matrix shown in panel A. The values in panel D (in units of sec) are very near zero, implying that no RSN is entirely leads or follows other RSNs. Panel E plots the mean within-block values of the SWS TD matrix shown in panel B. Note significant visual network earliness with respect to other networks ($p < 0.05$ by permutation resampling, multiple comparisons corrected for 21 upper diagonal blocks). Owing to anti-symmetry, the horizontal blue and vertical orange blocks both represent visual earliness. Diagonal blocks in panels D and E are colored gray to symbolize that they are constrained to be zero-mean.

in SWS are dorsolateral prefrontal cortex and the paracentral lobule (Fig. 4A). A variety of lag shifts are evident in the results obtained with the medial prefrontal seed (Fig. 4B). For example, subgenual prefrontal cortex (red arrow) shifts from mid-latency (lag values near zero) during wake to very early during SWS, and the paracentral lobule shifts from mid-latency during wake to late during SWS. A “front-to-back” propagation pattern (also highlighted in Fig. 3) is clearly evident in the sagittal view in Fig. 4B during SWS. Fig. 4C illustrates dramatic changes in the lag relations of the paracentral lobule. In wake, paracentral lobule leads both lateral sensory-motor cortex and posterior insula. These relations are reversed in SWS, during which nearly the entire cortex becomes markedly early with respect to the paracentral lobule.

The results presented so far highlight topographic features of apparent propagation that change between wake and SWS. The next set of results considers pair-wise lag relations defined over pairs of 6mm^3 isotropic cortical gray matter voxels. The results are presented as time-delay (TD) matrices. Voxels in the TD matrices are ordered first by resting state network affiliation (see Fig. 5-figure supplement 2). Then, within RSNs, the voxels are ordered from earliest (most negative) to latest (most positive) according to mean latency determined in wake (Fig. 5A). The ordering computed during wake was applied to the SWS TD results (Fig. 5B). A key algebraic feature of TD matrices is that they are exactly anti-symmetric ($\tau_{i,j} = -\tau_{j,i}$; Methods Eq. E3). Thus, if the lag between voxels i and j is τ seconds, then the lag between voxels j and i must be exactly $-\tau$ seconds (see Methods).

As TD matrices are anti-symmetric, each diagonal block, which represents intra-RSN lag structure, is anti-symmetric as well. However, the algebra does not impose any relation between lag and RSN membership. Thus, the structure evident in the wake TD matrix (Fig. 5A) is informative, and recapitulates previous findings obtained in a separate, large data set (Mitra et al. 2014). The diagonal blocks show a wide range and well-ordered distribution of lags. This organization reflects propagation within RSNs; the DMN block, highlighted in green in Fig. 5A, is an example of intra-network lag organization. The off-diagonal blocks, which represent lags across RSNs, also contain well-ordered early, middle, and late components, much like the diagonal blocks. This feature is not algebraically imposed. An important implication of the early-to-late organization of the inter-RSN blocks in Fig. 5A is that each RSN is neither early nor late with respect to the others during the wake state, a feature which we have previously reported (Mitra et al. 2014). To illustrate this point, consider the off-diagonal block corresponding to the DMN paired with the dorsal attention network (DAN), outlined in yellow in Fig. 5A. A well-ordered progression from early (blue) to late (red) is evident, indicating that parts of the DMN lead the DAN and *vice versa*; neither the DMN nor the DAN leads or follows the other as a whole.

We next compared the TD matrix in SWS (Fig. 5B) to the TD matrix in wake. Three features emerged from this comparison. First, the range of lag values in SWS is larger than in the wake data, as if the speed of BOLD signal propagation has slowed. We quantitatively represent this effect as the standard deviation (SD), computed over the

upper triangular (hence unique) lag values in wake and SWS. SD during wake was 0.42 $\pm$ 0.05 seconds, whereas SD during SWS was 0.65 $\pm$ 0.07 seconds. This effect was significant ($p < 0.01$, by permutation resampling with 10,000 trials).

Second, inter-RSN lag structure is altered in SWS. This effect appears as a loss of early (blue) to late (red) organization in off-diagonal blocks, e.g., as in the DAN:DMN block (yellow outline in Fig. 5B). To quantitatively assess this change, we computed the rank correlation (Spearman's ρ) between wake and SWS lag values over all voxel pairs in each of the 8·7/2 = 28 unique intra- and inter-RSN blocks (Figs. 5A-B). Blocks exhibiting a significantly low correlation ($p < 0.05$, corrected for 28 multiple comparisons) comparing wake vs. SWS are marked with a white asterisk in Fig. 5C; these effects represent a significant change in lag structure between resting state networks. Importantly, these effects were observed only in off-diagonal (cross-RSN) blocks. In other words, intra-network lag structure was relatively preserved ($\rho > 0.6$) across states, e.g., within the DMN (green outline Fig. 5A-B). In contrast, inter-network lag structure was markedly altered ($\rho < 0.3$) in the majority of off-diagonal blocks. Thus, Fig. 5C demonstrates that, whereas propagation *within* RSNs is relatively preserved during sleep, propagation *across* RSNs is significantly altered. During SWS, most cross-RSN blocks (excluding visual network pairs) develop a "disorganized" structure, in which well-ordered propagation appears to be lost. This effect is not attributable to voxel ordering, as the voxels are ordered identically in the wake and SWS TD matrices (Fig. 5A). The same disorganized appearance persists even if the SWS TD matrix ROIs are ordered according to their own stage-specific lag structure (Fig. 5-figure supplement 1).

A third effect evident in Figs. 5A-B is the appearance of an "all early" organization in the visual network ("VIS", pink box) in SWS. That is, in half the TD matrix, all cross-RSN voxel pairs involving the visual network exhibit negative (early; blue) lag values in SWS, indicating that voxels in the visual network are earlier than nearly all other cortical voxels. Thus, the principle, which applies in wake, that no RSN leads or follows any other (Mitra et al. 2014), does not hold during SWS.

To quantitatively investigate changes in lag structure between the visual network and the rest of the brain, we computed the mean lag value for each off-diagonal (inter-RSN) block in wake and SWS (Figs. 5D and 5E respectively). Anti-symmetry forces a mean lag value of zero within diagonal blocks. Thus, 21 unique blocks are considered in this analysis. If no RSN leads or follows any other in aggregate, the average lag value in each inter-RSN block should be zero. Fig. 5D illustrates that this is the case during wake: The mean lag in each off-diagonal block is very nearly zero, as previously reported in a completely independent dataset (Mitra et al. 2014). Fig. 5E shows that this principle approximately applies also in SWS *except in the visual network* (white asterisks). During SWS, voxels in the visual network become early with respect to other cortical voxels (Fig. 5E). An analogous, but opposite feature also appears in a subset of the cross-RSN sensorimotor (SMN) block, which assumes an "all late" (red) configuration. In other words, this set of voxels becomes late with respect to cortical BOLD signal activity in nearly all other cortical voxels during SWS. The voxels in question correspond to the paracentral lobule (Fig. 2C). That the paracentral lobule

becomes late in SWS is also evident in Fig 4C. This effect is not significant in Fig. 5E because the paracentral lobule is only part of the *a priori* defined SMN.

4.5 Discussion

We investigated apparent propagation of spontaneous infra-slow activity, as measured by rs-fMRI, in wake and slow wave sleep. Our whole-brain comparison identified several cortical and subcortical regions exhibiting significantly different state-dependent lags (Fig. 2). These regions were used for seed-based analyses. Lag maps seeded in the thalamus, brainstem, and putamen demonstrated that subcortical structures are early in relation to cortex during wake, but late during SWS (Fig. 3). In contrast, propagation within the brainstem-thalamic axis was relatively preserved across states (Fig. 3). Cortical seed-based lag maps, computed using visual cortex, medial prefrontal cortex, and paracentral lobule, exhibited complex, regionally specific effects (Fig. 4). Finally, comparison of TD matrices in wake vs. SWS revealed that inter-RSN propagation was significantly altered in SWS whereas intra-RSN propagation was relatively preserved (Fig. 5C).

These findings demonstrate dramatic rearrangements in propagated infra-slow intrinsic activity during SWS as compared to wake. By comparison, the effect of SWS on zero-lag correlation structure (functional connectivity) is much more modest (Fig. 6). State differences in functional connectivity manifest as quantitative changes in the magnitude of correlations, for example, reduced correlations between anterior and posterior brain regions during SWS (Picchioni et al. 2013). However, the overall topography of resting

state networks (RSNs) generally is preserved (Horovitz et al. 2009; Larson-Prior et al. 2009; Picchioni et al. 2013; Samann et al. 2011; Tagliazucchi et al. 2013b) (Fig. 6). Interestingly, some of the present lag findings topographically correspond to effects observed with conventional functional connectivity. Specifically, SWS induces focal functional connectivity changes in visual cortex, paracentral lobule, and thalamus; this topography substantially overlaps some of the presently observed lag effects (compare sagittal views in Figs. 2C and 6D-E). In a similar vein, PET studies show that SWS, as well as pathological disorders of consciousness, both are associated with prominent reductions in thalamic metabolism (Laureys 2005). This finding hypothetically corresponds, in the present results, to the prominent thalamic shift in lag status from early in wake to late in SWS. However, much more work is needed to determine whether these intriguing correspondences are in any way general.

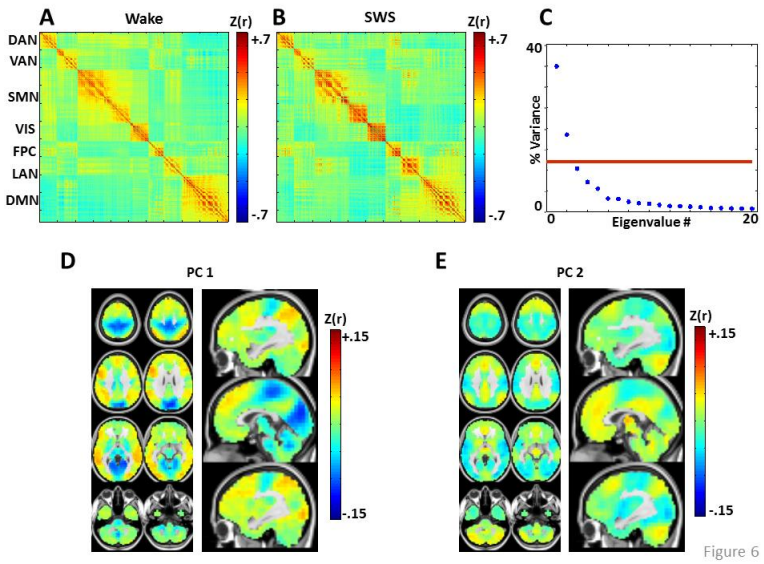

Figure 4-6: Zero-lag correlation (conventional functional connectivity; FC) matrices. (A): wake. (B): slow wave sleep. Voxels shown in the correlation matrices correspond to Figs. 5A-B (see also Fig. 5-figure supplement 2), and matrix values are Fisher-z transformed Pearson correlations averaged over subjects. Note relatively preserved RSN organization across states, in line with previous analyses of these data (Tagliazucchi et al. 2013a). To assess the topography of pair-wise correlation changes, we computed the difference between the SWS and wake correlation matrices (wake minus SWS), and applied spatial principal components analysis (PCA) to the difference matrix. The resulting eigenspectrum (panel C) shows that there are 2 statistically significant ($p < 0.05$; red line) PCs (threshold computed by permutation re-sampling). The topographies of these PC's are shown in panels D and E. These topographies reflect modest FC reductions in visual/somatosensory networks in wake vs. SWS, and modest FC increases in the DMN and thalamus in wake vs. SWS. These results are in accordance with previous findings comparing wake vs. NREM sleep (Horovitz et al. 2008; Picchioni et al. 2013). Importantly, zero-lag correlation structure (panels A-B) is much more preserved across wake and SWS than is lag structure (Figure 5). Axial slices: Z = +69, +57, +45, +33, +9, -3, -27, -39. Sagittal slices: X = +3, +12, -12.

Relation of BOLD signal apparent propagation to electrophysiology

The implications of our findings critically depend on how spontaneous BOLD fMRI signal fluctuations relate to electrophysiology. This question currently remains a topic of active investigation (Florin et al. 2014). Several studies using invasive recordings have found that slow (0.5-4 Hz) and infra-slow (<0.1 Hz) local field potentials correspond most closely to BOLD signal fluctuations and correlation structure. This correspondence has been demonstrated in wake (He et al. 2008; Hiltunen et al. 2014; Nir et al. 2008), sleep (He et al. 2008), and anesthesia (Pan et al. 2013). Thus, a natural hypothesis is that temporal lags in the BOLD signal reflect propagation of slow and infra-slow electrophysiological activity. However, as far as we are aware, temporal lags in infra-slow electrophysiology have not been investigated at the systems level. On the other hand, propagation of slow activity has been widely reported. The spectral content of the slow oscillation at the low end, approximately 0.5 Hz, approaches the infra-slow range. Hence, in the following, we consider correspondence between reports of propagated slow electrophysiology and the present results, with the understanding that future investigations specifically of infra-slow propagation are needed.

Slow electrophysiological activity has been most studied in the context of SWS and anesthesia, during which the slow oscillation, or UP/DOWN states (UDSs), (Steriade et al. 1993) is a characteristic feature. UDSs classically are described as periodic at frequencies in the 0.5-1.5 Hz range, and are known to propagate on a time-scale of 100s of milliseconds (Hahn et al. 2006; McCormick et al. 2015; Petersen et al. 2003). More recently, UDSs have also been described in awake, resting rodents (Ferezou et al.

2007). Although UDS periodicity is a characteristic of single neuron membrane potential recordings (Hahn et al. 2006; Petersen et al. 2003), macro-electrode recordings, e.g., electroencephalography (EEG) and electrocorticography (ECoG), show aperiodic, 1/f-like spectral content during SWS (He et al. 2010; Nir et al. 2011; Sirota et al. 2003). More generally, the spectral content of intrinsic electrophysiologic activity and rs-fMRI is 1/f-like in wake as well as SWS (He et al. 2008; Hiltunen et al. 2014). Moreover, macro-electrode recordings of slow activity also show apparent propagation on time-scales as long as 1-2 seconds during sleep and anesthesia (Nir et al. 2011; Sirota et al. 2003), as in the present rs-fMRI data.

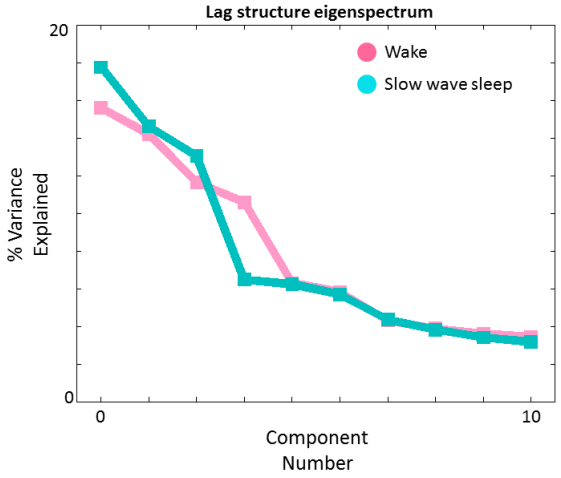

Figure 4-7: Lag structure dimensionality in wake and SWS. We have previously shown that multiple temporal sequences can be extracted from a TD matrix by applying spatial principal components analysis (PCA) to the TD matrix after zero-centering each column (Mitra et al. 2015). Here we show PCA-derived eigenvalues (scree plot) obtained in wake (pink) and SWS (blue). The maximum likelihood dimensionality estimates derived using the method of (Minka 2001) are 4 and 3, respectively, in wake and SWS. N.B.: We previously obtained a maximum likelihood TD dimensionality estimate of 8 in a much larger (N = 688) awake dataset (Mitra et al. 2015). The lower presently obtained figure (4) reflects less statistical power owing to a smaller subject sample (N = 39).

Propagated slow potentials during SWS share additional points of concordance with the present BOLD fMRI results. Electrophysiological studies in both humans and rodents suggest that slow activity tends to originate in medial prefrontal cortex and propagate to more posterior regions (Massimini et al. 2004; Nir et al. 2011; Sheroziya and Timofeev 2014). We also observe a “front-to-back” propagation pattern (see Figs. 4B and 7-supplement 2). However, this pattern should be understood as only one of many. In that

regard, a noteworthy principle that has emerged on the basis of human high-density EEG and ECoG recordings is that slow waves originate in multiple locations and propagate through multiple routes (Massimini et al. 2004; Murphy et al. 2009; Nir et al. 2011). A necessary algebraic consequence of this principle is that the lag structure of propagated slow activity exists in a multi-dimensional space (Mitra et al. 2015). We have recently demonstrated precisely this point by analysis of a very large resting state fMRI dataset acquired in quietly resting awake adults (Mitra et al. 2015). We confirm that the same principle applies in the current fMRI data, both during wake and SWS (Fig. 7). Indeed, the spatial principal components ("lag threads") derived by analysis of the fMRI time-delay matrix provides a compact means of visualizing how the propagation of intrinsic activity becomes rearranged in wake vs. SWS (Fig. 7-figure supplements 1 and 2).

To the best of our knowledge, apparent propagation of either slow or infra-slow electrophysiological activity in the awake state has not been reported in either humans or animals. However, voltage sensitive dye (VSD) studies in quietly resting rodents have demonstrated multiple patterns of propagation of slow intrinsic activity over 100s of milliseconds (Mohajerani et al. 2013; Mohajerani et al. 2010). Moreover, propagation patterns assessed using VSD are bilaterally symmetric (Mohajerani et al. 2010), as are BOLD fMRI patterns of propagation (Mitra et al. 2015; Mitra et al. 2014).

In summary, the available evidence suggests that the BOLD signal and slow/infra-slow electrophysiological activity exhibit similarities in spectral content, correlation structure,

and apparent propagation. The present results motivate future investigations to clarify the physiological links between propagated UDSs, propagated VSD patterns in rodents, and propagated BOLD fMRI signal fluctuations in humans, both during wakefulness and SWS. Direct electrophysiological studies of infra-slow propagation are especially needed. In the following, we discuss hypotheses regarding the possible functions of propagated infra-slow activity, observed using rs-fMRI, in relation to theories originally derived by observations of propagated slow potentials.

Relation of present results to the physiology of slow wave sleep

Cortical re-arrangements in lag structure are complex and regionally dependent, as demonstrated by the seed-based analyses shown in Fig. 4. In the following, we present three hypotheses, informed by prior studies of SWS, suggesting how infra-slow propagation may relate to the physiological functions of sleep. Future work combining rs-fMRI sleep recordings with behavioral data will be required to investigate these hypotheses.

First, slow wave sleep is believed to represent an off-line state during which slow activity enables consolidation of newly acquired memories (Born et al. 2006; Maquet 2001; Marshall et al. 2006; Stickgold 2005). Human imaging studies of word-pair association tasks have shown that the medial prefrontal cortex (mPFC) is implicated in consolidation of declarative memory (Euston et al. 2012; Gais et al. 2007; Takashima et al. 2006). Consolidation is accompanied by increases in mPFC activity during successful later recall (Gais et al. 2007; Takashima et al. 2006). The locus of these

previously reported effects is notably close to the mPFC region illustrated in Fig. 2C (cf. Fig. 3 in (Takashima et al. 2006) and Fig. 4 in (Gais et al. 2007)). Using the same task, Marshall and colleagues found that artificially initiating slow wave activity by applying current via frontal electrodes during SWS boosts subsequent recall (Marshall et al. 2006). Thus, the available data suggest that the mPFC shift towards earliness during SWS may facilitate consolidation of declarative memory. This hypothesis could be tested by relating infra-slow, front-to-back propagation to consolidation of declarative memory.

Second, SWS is also thought to improve procedural memory, e.g., motor sequence learning and motor adaptation (Stickgold 2005). We observed significant wake vs. SWS latency shifts in putamen and paracentral lobule (PCL) (Figs. 2-4), both of which structures are strongly associated with procedural learning (Graybiel 2005; Halsband and Lange 2006; Knowlton et al. 1996). The paracentral lobule is a functional component of the supplementary motor area (SMA) (Lim et al. 1994). Sleep-dependent improvements in procedural tasks have been postulated to involve plasticity in cortico-striatal circuits (Doyon and Benali 2005). Thus, the reversal in the temporal lag between putamen and cortex (Fig. 3B) during SWS could be a correlate of off-line consolidation of procedural memory. Similarly, altered apparent propagation in PCL may relate to offline adjustment of motor programs. Alternatively, PCL lateness during SWS could represent a correlate of the abolition of motor behavior. These possibilities could be investigated by combining rs-fMRI studies of SWS with procedural learning paradigms.

Third, we show that visual cortex is neither wholly late nor early during wake, but that nearly the entire cerebral cortex becomes late with respect to visual cortex during SWS (Fig. 4A, Fig. 5). This visual cortex finding may relate to the now widely recognized fact that dreaming also occurs in NREM sleep (Hobson et al. 2000). Recent work has shown that BOLD fMRI activity in visual cortex predicts NREM dreaming (Horikawa et al. 2013). Hence, there may exist a link between initiation of infra-slow activity in visual cortex and dreaming. The question of whether initiation of infra-slow activity in visual cortices relates to dreaming has not been studied thus far, but could be explicitly examined using the methodology of Horikawa and colleagues (Horikawa et al. 2013).

Relation of present results to thalamic gating of sensory input

Wakefulness is a state during which environmental awareness is possible (Seth et al. 2005). The thalamus plays a critical role in this state by relaying sensory signals to the cerebral cortex (Alkire et al. 2008). Electrophysiological recordings have shown that the awake state is associated with depolarization of thalamocortical cells, which facilitates transmission of ascending input to the cortex (Brown et al. 2012; Franks 2008; McCormick and Bal 1997). Conversely, during SWS, signals from the environment do not reliably reach the cortex owing to hyperpolarization of thalamocortical neurons (Franks 2008; Franks and Lieb 1994; Hirsch et al. 1983; Steriade and Timofeev 2003). Thus, the thalamus “gates" transmission of environmental stimuli to the cortex. Moreover, *in vitro* work suggests that thalamic hyperpolarization in SWS is modulated by propagation of slow (< 1 Hz) activity from cortex to thalamus (Blethyn et al. 2006; Hughes et al. 2002). Our analysis of BOLD signal fluctuations is consistent with this

account: Cerebral cortex leads thalamus during SWS, but thalamus leads cortex during wake (Fig. 3A). Importantly, BOLD signal propagation from brainstem to thalamus is similar in wake and SWS. This result suggests that the thalamus is the site at which ascending signals are impeded during SWS, in accordance with the hypothesized role of the thalamus as a sensory gate.

Relation of present findings to theories of consciousness

Figure 5 shows that cross-network lag structure is extensively altered in SWS as compared to wake. During wake, both diagonal- and off-diagonal blocks of the TD matrix exhibit well-ordered early, middle, and late components. Thus, cross-network and within-network propagation are comparable during wake. During SWS, apparent propagation within and across networks is no longer comparable (Figs. 5B,E). Cross-network (off-diagonal) blocks lose their "early-to-late" structure, whereas within-network (diagonal blocks) lag structure is preserved (Figs. 5A-C). Moreover, most cross-network blocks (excluding visual network pairs) appear disorganized during SWS. Speculatively, the dissociation between preserved within-network propagation and disorganized cross-network propagation suggests that neural communication during SWS, as measured by propagation of BOLD signals, is largely intact within functional networks (RSNs), but is disrupted across functional networks. These observations support theories postulating that reduced subjective awareness ("unconsciousness") during SWS results from loss of integration across networks (Mashour 2005; Tononi 2004). "Conscious" here refers to the awake, or on-line, state. Accordingly, decreased subjective awareness during SWS theoretically results from loss of integration across networks, while within-network

activity is generally preserved (Boly et al. 2012; Mashour 2005; Tagliazucchi et al. 2013a). A corollary is that, during SWS, neural communication is maintained within functional modules, but altered across functional modules, resulting in “network segregation” (Mashour 2013; Tagliazucchi et al. 2013a). Our TD matrix results are consistent with this principle, provided the assumption that BOLD signal propagation reflects neural communication at a broad spatio-temporal scale,

We interpret our findings as follows. During wake, the brain is capable of responding to the environment and functional systems reciprocally communicate to sustain conscious content (Alkire et al. 2008; McCormick et al. 2015). Accordingly, we find ascending BOLD signal propagation from thalamus to cortex (Fig. 3A), as well as well-ordered propagation of activity between resting state networks (Fig. 5A). In SWS, off-line brain activity theoretically serves mechanisms concerned with synaptic homeostasis and memory consolidation (McClelland et al. 1995; McCormick et al. 2015). Features of the off-line state (SWS) include reduced responses to environmental stimuli, altered inter-network communication, but relatively intact intra-network communication (McClelland et al. 1995; McNaughton et al. 2003; Tagliazucchi et al. 2013a). Accordingly, we observe reversal of thalamo-cortical propagation (Fig. 3A), altered cross-RSN propagation (Fig. 5B-C), and intact within-RSN propagation. Future study of BOLD signal propagation and infra-slow activity is necessary to obtain a better understanding of the physiology of spontaneous activity in wake and sleep.

4.6 Materials and Methods

EEG–fMRI Acquisition and Artifact Correction: Acquisition parameters and details for these data have been previously published (Tagliazucchi et al. 2013b). fMRI was acquired using a 3 T scanner (Siemens Trio) with optimized polysomnographic settings (1,505 volumes of T2*-weighted echo planar images, repetition time/echo time = 2,080 ms/30 ms, matrix = 64 × 64, voxel size = 3 × 3 × 2 mm^3, distance factor = 50%; field of view = 192 mm^2). 30 EEG channels were simultaneously recorded using a modified cap (EASYCAP) with FCz as reference (sampling rate = 5 kHz, low pass filter = 250 Hz, high pass filter = 0.016 Hz). MRI and pulse artifact correction were performed based on the average artifact subtraction method (Allen et al. 1998) as implemented in Vision Analyzer2 (Brain Products) followed by ICA-based rejection of residual artifact components (CBC parameters; Vision Analyzer). EEG sleep staging was done by an expert according to the American Academy of Sleep Medicine (AASM) criteria (Iber 2007).

Subjects: 63 non-sleep-deprived subjects were scanned in the evening (starting at ~8:00 PM). Subjects were instructed to keep eyes closed during wakefulness. Hypnograms were inspected to identify epochs of contiguous sleep stages lasting at least 5 min (150 volumes). These criteria yielded 39 subjects contributing to the present analyses. Included are 70 epochs of wakefulness, 47 epochs of N2 sleep, and 38 epochs of N3 sleep (SWS). Detailed sleep architectures of each participant have been previously published (Tagliazucchi et al. 2013b).

fMRI preprocessing: fMRI preprocessing was as described in (Mitra et al. 2014). Briefly, this included compensation for slice-dependent time shifts, elimination of systematic odd-even slice intensity differences due to interleaved acquisition, and rigid body correction of head movement within and across runs. Atlas transformation was achieved by composition of affine transforms connecting the fMRI volumes with the T2-weighted and T1-weighted structural images. Additional preprocessing in preparation for lags analysis included spatial smoothing (6 mm full width at half maximum (FWHM) Gaussian blur in each direction), voxel-wise removal of linear trends over each fMRI run, and temporal low-pass filtering retaining frequencies below 0.1 Hz. Spurious variance was reduced by regression of nuisance waveforms derived from head motion correction and timeseries extracted from regions (of "non-interest") in white matter and CSF as well the BOLD timeseries averaged over the brain (Fox et al. 2009). Frame censoring was computed at a threshold of 0.5% root mean square frame-to-frame intensity change (Power et al. 2012). Epochs containing fewer than 10 contiguous frames were excluded. These criteria removed 5.3 ± 0.9% of frames per individual during wake, 6.1 ± 0.7% during N2 sleep, and 5.8 ± 0.7% during N3 sleep. There were no statistically significant differences in the amount of frame censoring by state.

Computation of lag between BOLD time series

Our method for computing lags between time series has been previously published (Mitra et al. 2014). Conventional seed-based correlation analysis involves computation of the Pearson correlation, r, between the time series, $x_1(t)$, extracted from a seed region, and a second time series, $x_2(t)$, extracted from some other locus (single voxel or region of interest). Thus,

$$r_{x_1x_2} = \frac{1}{\sigma_{x_1}\sigma_{x_2}}\frac{1}{T}\int x_1(t)\cdot x_2(t)dt, \qquad \text{[E1]}$$

where σ_{x_1} and σ_{x_2} are the temporal standard deviations of signals x_1 and x_2, and T is the interval of integration. Here, we generalize the assumption of exact temporal synchrony and compute lagged cross-covariance functions. Thus,

$$C_{x_1x_2}(\tau) = \frac{1}{T}\int x_1(t+\tau)\cdot x_2(t)dt, \qquad \text{[E2]}$$

where τ is the lag (in units of time). The value of τ at which $C_{x_1x_2}(\tau)$ exhibits an extremum defines the temporal lag (equivalently, delay) between signals x_1 and x_2 (Konig 1994). Although cross-covariance functions can exhibit multiple extrema in the analysis of periodic signals, BOLD time series are aperiodic (He et al. 2010; Maxim et al. 2005), and almost always give rise to lagged cross-covariance functions with a single, well defined extremum, typically in the range $\pm$1 sec. We determine the extremum abscissa and ordinate using parabolic interpolation (Mitra et al. 2014).

Given a set of n time series, $\{x_1(t), x_2(t), \cdots, x_n(t)\}$, finding all $\tau_{i,j}$ corresponding to the extrema, $a_{i,j}$, of $C_{x_ix_j}(\tau)$ yields the anti-symmetric, time delay matrix:

$$TD = \begin{bmatrix} \tau_{1,1} & \cdots & \tau_{1,n} \\ \vdots & \ddots & \vdots \\ -\tau_{1,n} & \cdots & \tau_{n,n} \end{bmatrix}. \qquad \text{[E3]}$$

The diagonal entries of TD are necessarily zero, as any time series has zero lag with itself. Moreover, $\tau_{i,j} = -\tau_{j,i}$, since time series $x_i(t)$ preceding $x_j(t)$ implies that $x_j(t)$ follows $x_i(t)$ by the same interval. Here, the timeseries were extracted from $(6mm)^3$ cubic voxels evenly distributed throughout gray matter in the whole brain (Mitra et al. 2015).

We projected the multivariate data represented in the TD matrix onto one-dimensional maps using the technique described by Nikolic and colleagues (Nikolic 2007; Schneider et al. 2006). We refer to these one-dimensional maps as lag projections. Operationally, the projection is done by taking the mean across the columns of TD (*Eq. E3*), that is,

$$T_p = \left[\sum_{j=1}^{n} \tau_{1,j} \ \ldots \ \sum_{j=1}^{n} \tau_{n,j}\right]. \qquad \text{[E4]}$$

Seed-based lag maps were computed according to [E2], except instead of computing lags between all voxels, we computed the lag between a reference timeseries extracted from the seed and timeseries extracted from all $(6mm)^3$ voxels. This procedure produces a one-dimensional seed-based lag map.

Group level TD matrices, lag projections, and seed-based lag maps were obtained in each state (W, N2 sleep, and N3 sleep) by computing each quantity at the individual subject level (averaging across temporally contiguous epochs) and then averaging.

Statistical analysis:

Statistical significance of wake versus SWS differences in lag projection maps was assessed on a cluster-wise basis using threshold-extent criteria computed by extensive permutation resampling (Hacker et al. 2012; Hayasaka and Nichols 2003). Figure 5C reports Spearman ρ correlations over entries in TD matrix blocks in wake and SWS.

Statistical significance was assessed by permutation resampling of the matrix entries within blocks, with correction for multiple comparisons. Figures 5D and E report mean lag values averaged over entries in TD matrix blocks. Statistical significance of the difference in mean lag value across TD matrix blocks was also assessed through permutation resampling, with correction for multiple comparisons.

4.7 Acknowledgements

This work was supported by the National Institute of Health (NS080675 to MER and AZS; P30NS048056 to AZS; F30MH106253 to AM), the Bundesministerium für Bildung und Forschung (grant 01EV0703) and the LOEWE Neuronale Koordination Forschungsschwerpunkt Frankfurt (NeFF).

4.8 References

Abel T, Havekes R, Saletin JM, and Walker MP. Sleep, plasticity and memory from molecules to whole-brain networks. *Current biology : CB* 23: R774-788, 2013.

Achermann P, and Borbely AA. Low-frequency (< 1 Hz) oscillations in the human sleep electroencephalogram. *Neuroscience* 81: 213-222, 1997.

Alkire MT, Hudetz AG, and Tononi G. Consciousness and anesthesia. *Science* 322: 876-880, 2008.

Allen PJ, Polizzi G, Krakow K, Fish DR, and Lemieux L. Identification of EEG events in the MR scanner: the problem of pulse artifact and a method for its subtraction. *Neuroimage* 8: 229-239, 1998.

Beckmann CF, DeLuca M, Devlin JT, and Smith SM. Investigations into resting-state connectivity using independent component analysis. *Philosophical transactions of the Royal Society of London Series B, Biological sciences* 360: 1001-1013, 2005.

Biswal BB, Mennes M, Zuo XN, Gohel S, Kelly C, Smith SM, Beckmann CF, Adelstein JS, Buckner RL, Colcombe S, Dogonowski AM, Ernst M, Fair D, Hampson M, Hoptman MJ, Hyde JS, Kiviniemi VJ, Kotter R, Li SJ, Lin CP, Lowe MJ, Mackay C, Madden DJ, Madsen KH, Margulies DS, Mayberg HS, McMahon K, Monk CS, Mostofsky SH, Nagel BJ, Pekar JJ, Peltier SJ, Petersen SE, Riedl V, Rombouts SA, Rypma B, Schlaggar BL, Schmidt S, Seidler RD, Siegle GJ, Sorg C, Teng GJ, Veijola J, Villringer A, Walter M, Wang L, Weng XC, Whitfield-Gabrieli S, Williamson P, Windischberger C, Zang YF, Zhang HY, Castellanos FX, and Milham MP. Toward discovery science of human brain function. *Proc Natl Acad Sci U S A* 107: 4734-4739, 2010.

Blethyn KL, Hughes SW, Toth TI, Cope DW, and Crunelli V. Neuronal basis of the slow (<1 Hz) oscillation in neurons of the nucleus reticularis thalami in vitro. *J Neurosci* 26: 2474-2486, 2006.

Boly M, Perlbarg V, Marrelec G, Schabus M, Laureys S, Doyon J, Pelegrini-Issac M, Maquet P, and Benali H. Hierarchical clustering of brain activity during human nonrapid eye movement sleep. *Proc Natl Acad Sci U S A* 109: 5856-5861, 2012.

Born J, Rasch B, and Gais S. Sleep to remember. *Neuroscientist* 12: 410-424, 2006.

Boyle PJ, Scott JC, Krentz AJ, Nagy RJ, Comstock E, and Hoffman C. Diminished brain glucose metabolism is a significant determinant for falling rates of systemic glucose utilization during sleep in normal humans. *J Clin Invest* 93: 529-535, 1994.

Braun AR, Balkin TJ, Wesenten NJ, Carson RE, Varga M, Baldwin P, Selbie S, Belenky G, and Herscovitch P. Regional cerebral blood flow throughout the sleep-wake cycle. An H2(15)O PET study. *Brain* 120 (Pt 7): 1173-1197, 1997.

Brown RE, Basheer R, McKenna JT, Strecker RE, and McCarley RW. Control of sleep and wakefulness. *Physiol Rev* 92: 1087-1187, 2012.

Caminiti R, Ghaziri H, Galuske R, Hof PR, and Innocenti GM. Evolution amplified processing with temporally dispersed slow neuronal connectivity in primates. *Proc Natl Acad Sci U S A* 106: 19551-19556, 2009.

Cirelli C, and Tononi G. Gene expression in the brain across the sleep-waking cycle. *Brain Res* 885: 303-321, 2000.

Cirelli C, and Tononi G. Is sleep essential? *PLoS Biol* 6: e216, 2008.

Dang-Vu TT. Neuronal oscillations in sleep: insights from functional neuroimaging. *Neuromolecular medicine* 14: 154-167, 2012.

Doyon J, and Benali H. Reorganization and plasticity in the adult brain during learning of motor skills. *Curr Opin Neurobiol* 15: 161-167, 2005.

Euston DR, Gruber AJ, and McNaughton BL. The role of medial prefrontal cortex in memory and decision making. *Neuron* 76: 1057-1070, 2012.

Everson CA, Bergmann BM, and Rechtschaffen A. Sleep deprivation in the rat: III. Total sleep deprivation. *Sleep* 12: 13-21, 1989.

Ferezou I, Haiss F, Gentet LJ, Aronoff R, Weber B, and Petersen CC. Spatiotemporal dynamics of cortical sensorimotor integration in behaving mice. *Neuron* 56: 907-923, 2007.

Florin E, Watanabe M, and Logothetis NK. The role of sub-second neural events in spontaneous brain activity. *Curr Opin Neurobiol* 32C: 24-30, 2014.

Fox MD, Zhang D, Snyder AZ, and Raichle ME. The global signal and observed anticorrelated resting state brain networks. *J Neurophysiol* 101: 3270-3283, 2009.

Franks NP. General anaesthesia: from molecular targets to neuronal pathways of sleep and arousal. *Nat Rev Neurosci* 9: 370-386, 2008.

Franks NP, and Lieb WR. Molecular and cellular mechanisms of general anaesthesia. *Nature* 367: 607-614, 1994.

Gais S, Albouy G, Boly M, Dang-Vu TT, Darsaud A, Desseilles M, Rauchs G, Schabus M, Sterpenich V, Vandewalle G, Maquet P, and Peigneux P. Sleep transforms the cerebral trace of declarative memories. *Proc Natl Acad Sci U S A* 104: 18778-18783, 2007.

Graybiel AM. The basal ganglia: learning new tricks and loving it. *Curr Opin Neurobiol* 15: 638-644, 2005.

Hacker CD, Laumann TO, Szrama NP, Baldassarre A, Snyder AZ, Leuthardt EC, and Corbetta M. Resting state network estimation in individual subjects. *Neuroimage* 82C: 616-633, 2013.

Hacker CD, Perlmutter JS, Criswell SR, Ances BM, and Snyder AZ. Resting state functional connectivity of the striatum in Parkinson's disease. *Brain : a journal of neurology* 135: 3699-3711, 2012.

Hahn TT, McFarland JM, Berberich S, Sakmann B, and Mehta MR. Spontaneous persistent activity in entorhinal cortex modulates cortico-hippocampal interaction in vivo. *Nat Neurosci* 15: 1531-1538, 2012.

Hahn TT, Sakmann B, and Mehta MR. Phase-locking of hippocampal interneurons' membrane potential to neocortical up-down states. *Nat Neurosci* 9: 1359-1361, 2006.

Halsband U, and Lange RK. Motor learning in man: a review of functional and clinical studies. *Journal of physiology, Paris* 99: 414-424, 2006.

Hayasaka S, and Nichols TE. Validating cluster size inference: random field and permutation methods. *Neuroimage* 20: 2343-2356, 2003.

He BJ, Snyder AZ, Zempel JM, Smyth MD, and Raichle ME. Electrophysiological correlates of the brain's intrinsic large-scale functional architecture. *Proc Natl Acad Sci U S A* 105: 16039-16044, 2008.

He BJ, Zempel JM, Snyder AZ, and Raichle ME. The temporal structures and functional significance of scale-free brain activity. *Neuron* 66: 353-369, 2010.

Hiltunen T, Kantola J, Abou Elseoud A, Lepola P, Suominen K, Starck T, Nikkinen J, Remes J, Tervonen O, Palva S, Kiviniemi V, and Palva JM. Infra-slow EEG fluctuations are correlated with resting-state network dynamics in fMRI. *J Neurosci* 34: 356-362, 2014.

Hirsch JC, Fourment A, and Marc ME. Sleep-related variations of membrane potential in the lateral geniculate body relay neurons of the cat. *Brain Res* 259: 308-312, 1983.

Hobson JA, Pace-Schott EF, and Stickgold R. Dreaming and the brain: toward a cognitive neuroscience of conscious states. *The Behavioral and brain sciences* 23: 793-842; discussion 904-1121, 2000.

Horikawa T, Tamaki M, Miyawaki Y, and Kamitani Y. Neural decoding of visual imagery during sleep. *Science* 340: 639-642, 2013.

Horovitz SG, Braun AR, Carr WS, Picchioni D, Balkin TJ, Fukunaga M, and Duyn JH. Decoupling of the brain's default mode network during deep sleep. *Proc Natl Acad Sci U S A* 106: 11376-11381, 2009.

Horovitz SG, Fukunaga M, de Zwart JA, van Gelderen P, Fulton SC, Balkin TJ, and Duyn JH. Low frequency BOLD fluctuations during resting wakefulness and light sleep: a simultaneous EEG-fMRI study. *Hum Brain Mapp* 29: 671-682, 2008.

Hughes SW, Cope DW, Blethyn KL, and Crunelli V. Cellular mechanisms of the slow (<1 Hz) oscillation in thalamocortical neurons in vitro. *Neuron* 33: 947-958, 2002.

Iber C. *The AASM manual for the scoring of sleep and associated events: rules, terminology and technical specifications*. American Academy of Sleep Medicine, 2007.

Knowlton BJ, Mangels JA, and Squire LR. A neostriatal habit learning system in humans. *Science* 273: 1399-1402, 1996.

Konig P. A method for the quantification of synchrony and oscillatory properties of neuronal activity. *J Neurosci Methods* 54: 31-37, 1994.

Larson-Prior LJ, Zempel JM, Nolan TS, Prior FW, Snyder AZ, and Raichle ME. Cortical network functional connectivity in the descent to sleep. *Proc Natl Acad Sci U S A* 106: 4489-4494, 2009.

Laureys S. The neural correlate of (un)awareness: lessons from the vegetative state. *Trends in cognitive sciences* 9: 556-559, 2005.

Lim SH, Dinner DS, Pillay PK, Luders H, Morris HH, Klem G, Wyllie E, and Awad IA. Functional anatomy of the human supplementary sensorimotor area: results of extraoperative electrical stimulation. *Electroencephalogr Clin Neurophysiol* 91: 179-193, 1994.

Loomis AL, Harvey EN, and Hobart G. Further Observations on the Potential Rhythms of the Cerebral Cortex during Sleep. *Science* 82: 198-200, 1935a.

Loomis AL, Harvey EN, and Hobart G. Potential Rhythms of the Cerebral Cortex during Sleep. *Science* 81: 597-598, 1935b.

Maquet P. The role of sleep in learning and memory. *Science* 294: 1048-1052, 2001.

Marshall L, Helgadottir H, Molle M, and Born J. Boosting slow oscillations during sleep potentiates memory. *Nature* 444: 610-613, 2006.

Mashour GA. Cognitive unbinding in sleep and anesthesia. *Science* 310: 1768-1769; author reply 1768-1769, 2005.

Mashour GA. Cognitive unbinding: a neuroscientific paradigm of general anesthesia and related states of unconsciousness. *Neurosci Biobehav Rev* 37: 2751-2759, 2013.

Massimini M, Huber R, Ferrarelli F, Hill S, and Tononi G. The sleep slow oscillation as a traveling wave. *J Neurosci* 24: 6862-6870, 2004.

Maxim V, Sendur L, Fadili J, Suckling J, Gould R, Howard R, and Bullmore E. Fractional Gaussian noise, functional MRI and Alzheimer's disease. *Neuroimage* 25: 141-158, 2005.

McClelland JL, McNaughton BL, and O'Reilly RC. Why there are complementary learning systems in the hippocampus and neocortex: insights from the successes and failures of connectionist models of learning and memory. *Psychological review* 102: 419-457, 1995.

McCormick DA, and Bal T. Sleep and arousal: thalamocortical mechanisms. *Annu Rev Neurosci* 20: 185-215, 1997.

McCormick DA, McGinley MJ, and Salkoff DB. Brain state dependent activity in the cortex and thalamus. *Curr Opin Neurobiol* 31: 133-140, 2015.

McNaughton BL, Barnes CA, Battaglia FP, Bower MR, Cowen SL, Ekstrom AD, Gerrard JL, Hoffman KL, Houston FP, Karten Y, Lipa P, Pennartz CMA, and Sutherland GR. Off-Line Reprocessing of Recent Memory and its Role in Memory Consolidation: A Progress Report. In: *Sleep and Brain Plasticity*, edited by Maquet P, Smith C, and Stickgold RUniversity Press Scholarship Online, 2003.

Minka TP. Automatic choice of dimensionality for PCA. In: *Advances in Neural Information Processing Systems 13*. Cambridge, MA: MIT Press, 2001, p. 598-604.

Mitra A, Snyder AZ, Blazey T, and Raichle ME. Lag threads organize the brain's intrinsic activity. *Proc Natl Acad Sci U S A* 112: E2235-2244, 2015.

Mitra A, Snyder AZ, Hacker CD, and Raichle ME. Lag structure in resting state fMRI. *J Neurophysiol* 2014.

Mohajerani MH, Chan AW, Mohsenvand M, Ledue J, Liu R, McVea DA, Boyd JD, Wang YT, Reimers M, and Murphy TH. Spontaneous cortical activity alternates between motifs defined by regional axonal projections. *Nat Neurosci* 16: 1426-1435, 2013.

Mohajerani MH, McVea DA, Fingas M, and Murphy TH. Mirrored bilateral slow-wave cortical activity within local circuits revealed by fast bihemispheric voltage-sensitive dye imaging in anesthetized and awake mice. *J Neurosci* 30: 3745-3751, 2010.

Murphy M, Riedner BA, Huber R, Massimini M, Ferrarelli F, and Tononi G. Source modeling sleep slow waves. *Proc Natl Acad Sci U S A* 106: 1608-1613, 2009.

Nikolic D. Non-parametric detection of temporal order across pairwise measurements of time delays. *J Comput Neurosci* 22: 5-19, 2007.

Nir Y, Mukamel R, Dinstein I, Privman E, Harel M, Fisch L, Gelbard-Sagiv H, Kipervasser S, Andelman F, Neufeld MY, Kramer U, Arieli A, Fried I, and Malach R. Interhemispheric correlations of slow spontaneous neuronal fluctuations revealed in human sensory cortex. *Nat Neurosci* 11: 1100-1108, 2008.

Nir Y, Staba RJ, Andrillon T, Vyazovskiy VV, Cirelli C, Fried I, and Tononi G. Regional slow waves and spindles in human sleep. *Neuron* 70: 153-169, 2011.

Pan WJ, Thompson GJ, Magnuson ME, Jaeger D, and Keilholz S. Infraslow LFP correlates to resting-state fMRI BOLD signals. *Neuroimage* 74: 288-297, 2013.

Petersen CC, Hahn TT, Mehta M, Grinvald A, and Sakmann B. Interaction of sensory responses with spontaneous depolarization in layer 2/3 barrel cortex. *Proc Natl Acad Sci U S A* 100: 13638-13643, 2003.

Picchioni D, Duyn JH, and Horovitz SG. Sleep and the functional connectome. *Neuroimage* 80: 387-396, 2013.

Power JD, Barnes KA, Snyder AZ, Schlaggar BL, and Petersen SE. Spurious but systematic correlations in functional connectivity MRI networks arise from subject motion. *Neuroimage* 59: 2142-2154, 2012.

Rechtschaffen A. Current perspectives on the function of sleep. *Perspectives in biology and medicine* 41: 359-390, 1998.

Rechtschaffen A, and Kales A. *A Manual of Standardized Terminology, Techniques and Scoring System for Sleep Stages of Human Subjects.* Brain Research Institute, University of California Los Angeles, 1968.

Riedner BA, Vyazovskiy VV, Huber R, Massimini M, Esser S, Murphy M, and Tononi G. Sleep homeostasis and cortical synchronization: III. A high-density EEG study of sleep slow waves in humans. *Sleep* 30: 1643-1657, 2007.

Samann PG, Wehrle R, Hoehn D, Spoormaker VI, Peters H, Tully C, Holsboer F, and Czisch M. Development of the brain's default mode network from wakefulness to slow wave sleep. *Cereb Cortex* 21: 2082-2093, 2011.

Schneider G, Havenith MN, and Nikolic D. Spatiotemporal structure in large neuronal networks detected from cross-correlation. *Neural Comput* 18: 2387-2413, 2006.

Seth AK, Baars BJ, and Edelman DB. Criteria for consciousness in humans and other mammals. *Consciousness and cognition* 14: 119-139, 2005.

Sheroziya M, and Timofeev I. Global intracellular slow-wave dynamics of the thalamocortical system. *J Neurosci* 34: 8875-8893, 2014.

Sirota A, Csicsvari J, Buhl D, and Buzsaki G. Communication between neocortex and hippocampus during sleep in rodents. *Proc Natl Acad Sci U S A* 100: 2065-2069, 2003.

Steriade M, Nunez A, and Amzica F. A novel slow (< 1 Hz) oscillation of neocortical neurons in vivo: depolarizing and hyperpolarizing components. *J Neurosci* 13: 3252-3265, 1993.

Steriade M, and Timofeev I. Neuronal plasticity in thalamocortical networks during sleep and waking oscillations. *Neuron* 37: 563-576, 2003.

Stickgold R. Sleep-dependent memory consolidation. *Nature* 437: 1272-1278, 2005.

Tagliazucchi E, Behrens M, and Laufs H. Sleep neuroimaging and models of consciousness. *Frontiers in psychology* 4: 256, 2013a.

Tagliazucchi E, von Wegner F, Morzelewski A, Brodbeck V, Jahnke K, and Laufs H. Breakdown of long-range temporal dependence in default mode and attention networks during deep sleep. *Proc Natl Acad Sci U S A* 110: 15419-15424, 2013b.

Takashima A, Petersson KM, Rutters F, Tendolkar I, Jensen O, Zwarts MJ, McNaughton BL, and Fernandez G. Declarative memory consolidation in humans: a prospective functional magnetic resonance imaging study. *Proc Natl Acad Sci U S A* 103: 756-761, 2006.

Tononi G. An information integration theory of consciousness. *BMC neuroscience* 5: 42, 2004.

Yuste R, and Fairhall AL. Temporal dynamics in fMRI resting-state activity. *Proc Natl Acad Sci U S A* 112: 5263-5264, 2015.

Chapter 5: The human cortical-hippocampal dialogue in wake and slow wave sleep

This chapter has been published as a journal article. The citation is:

> **Mitra A**, Snyder AZ, Hacker CD, Pahwa M, Tagliazucchi E, Laufs H, Leuthardt EC, Raichle ME. (2016). Human cortical–hippocampal dialogue in wake and slow-wave sleep. Proceedings of the National Academy of Sciences. doi: 10.1073/pnas.1607289113.

Marc Raichle and I conceived the project and research approach. I designed and implemented the methods and performed the data analysis. Abraham Snyder and I processed the fMRI data, which was provided by Helmut Laufs and Enzo Tagliazucchi. Carl Hacker, Mrinal Pahwa, Eric Leuthardt and I processed and analyzed the electrocorticography data. Abraham Snyder and I wrote the paper; Enzo Tagliazucchi, Helmut Laufs, Eric Leuthardt and Marc Raichle edited it.

5.1 Preface

Chapter 4 demonstrates that the temporal organization of spontaneous resting state fMRI activity is dramatically altered across wake and sleep. On this basis, we theorized that the direction infra-slow signals travel through the brain plays a role in governing broad physiological states, such as wake and sleep. Yet this vague conception does not provide a satisfactory sense of what the computational purpose of directed infra-slow activity may be. Moreover, although we have treated resting state fMRI as a proxy for infra-slow brain activity based on the evidence summarized in the introduction, we have yet to discern whether the temporal structure of resting state fMRI is indeed mirrored in electrophysiological signals.

Chapter 5 addresses these questions in the context of a prominent theory for declarative memory consolidation. The broad idea is that cortex and hippocampus exchange information. During the day, cortex signals to hippocampus to create an index of short-term associations. At night during sleep, it is believed that hippocampus-index associations are activated and conveyed back to cortex for long-term memory consolidation. Importantly, at no time is the signaling between hippocampus and cortex thought to be purely unidirectional. Instead, a slow feedback signal needed for coordinating cortico-hippocampal activity is thought to move in the opposite direction from the “information transfer” direction during wake and sleep. However, evidence of such feedback signaling and directionality reversal had until this point been lacking. Chapter 5 fills this gap by demonstrating infra-slow activity in humans, measured using resting state fMRI and electrocorticography, move in the feedback direction between

cortex and hippocampus, as had been theorized. The correspondence between fMRI and electrophysiology also showed, for the first time, that temporal structure measured in fMRI agrees with electrophysiology. As a final note: the supplemental materials for this paper are well over 40 pages in length. Therefore, the supplementary materials are not included in this thesis. Readers interested in this material can find it online with the published manuscript; the supplemental references in this text correspond exactly the published supplement.

5.2 Abstract

Declarative memory consolidation is hypothesized to require a two-stage, reciprocal cortical-hippocampal dialogue. According to this model, higher frequency signals convey information from cortex to hippocampus during wakefulness, but in the reverse direction during slow wave sleep (SWS). Conversely, lower frequency activity propagates from the information "receiver" to the "sender" to coordinate the timing of information transfer. Reversal of sender/receiver roles across wake and SWS implies that higher and lower frequency signaling should reverse direction between cortex and hippocampus. However, direct evidence of such a reversal has been lacking in humans. Here, we use human resting state fMRI and electrocorticography to demonstrate that delta band activity and infra-slow activity propagate in opposite directions between the hippocampus and cerebral cortex. Moreover, both delta and infra-slow activity reverse propagation directions between hippocampus and the cerebral cortex across wake and SWS. These findings provide direct evidence for state-dependent reversals in human cortical-hippocampal communication.

5.3 Introduction

Declarative memories are initially hippocampus-dependent and gradually become hippocampus-independent over time, that is, consolidated (Scoville and Milner 1957; Squire and Alvarez 1995). It is theorized that a two-stage reciprocal dialogue between the hippocampus and the cerebral cortex underlies memory consolidation (Buzsaki 1996; 1989; Sirota et al. 2008). According to this model, active behavior generates experiential codes in the cortex that are transmitted to the hippocampus, which houses a labile information store. Later, during slow wave sleep (SWS), recently acquired hippocampal information is reactivated and transmitted to the cerebral cortex, where it is integrated into a more permanent memory store (Buzsaki 1996; McNaughton et al. 2003). Thus, the hippocampus and cerebral cortex are proposed to exchange roles in sending and receiving information across wake and SWS (Buzsaki 1996; McNaughton et al. 2003). Importantly, this model does not imply that all signals travel from the "sender" to the "receiver". Instead, the theory proposes that high frequency activity carries information from "sender" to "receiver", that is, from cortex to hippocampus or hippocampus to cortex, depending on the stage of memory consolidation (wake or SWS, respectively) (Sirota et al. 2008). Conversely, low frequency activity propagates from the "receiver" back to the "sender" to coordinate the transfer of high-frequency information through modulation of the "sender's" excitability (Hahn et al. 2012; Isomura et al. 2006; Sirota et al. 2008; Wilson and McNaughton 1994). Hence, the two-stage reciprocal dialogue model predicts that lower and higher frequency activity between hippocampus and cortex should propagate in opposite directions across wake and SWS, as illustrated

in the schematic in Figure 1. However, such reversal has not been directly observed in humans.

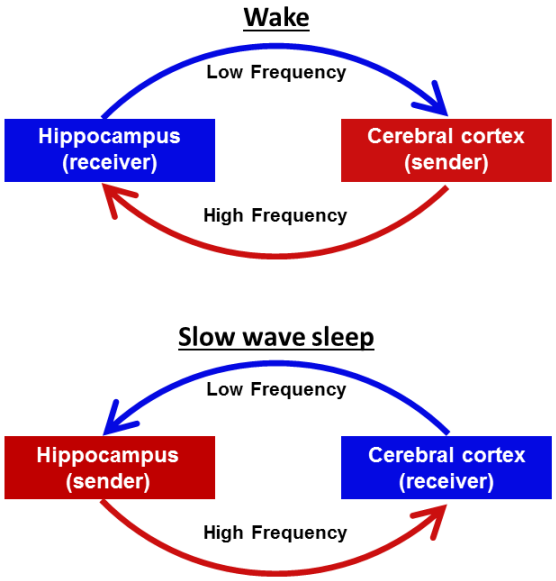

Figure 5-1: Schematic representation of the two-stage reciprocal cortical-hippocampal dialogue. Information is carried by high frequency signals. During wake and SWS, the information "receiver" coordinates the timing of transmissions from the "sender" via propagated low frequency signals.

We have recently analyzed temporal lags (delays) in neural signals to study the net propagation of spontaneous activity. In particular, we investigated resting state fMRI (rs-fMRI) blood oxygen level dependent (BOLD) signals and demonstrated directed propagation of infra-slow activity (<0.1 Hz) in normal young adults (Mitra et al. 2015a; Mitra et al. 2014). Although rs-fMRI data is generally analyzed on the basis of zero-lag correlation topographies (e.g., functional connectivity) (Biswal et al. 1995; Fox and Raichle 2007), our prior work has established that the resting state BOLD signal also exhibits a highly reproducible propagation structure in awake adults (Mitra et al. 2015a; Mitra et al. 2014). Moreover, in a data-driven analysis, we found that BOLD signal propagation is markedly altered in wake versus SWS, including state-dependent reversal of propagation between subcortical structures (thalamus and striatum) and the

cerebral cortex (Mitra et al. 2015b). On this basis, we hypothesized that the reciprocal cortico-hippocampal dialogue (Fig. 1) may manifest a lower frequency component in infra-slow signals, whereas a higher frequency component may be found in oscillations more traditionally associated with hippocampal function (Buzsaki et al. 2013; Jacobs 2014; Sirota et al. 2008).

To investigate this hypothesis, we here analyze two data sets: (1) combined non-invasive electroencephalography (EEG) and rs-fMRI acquired in 38 normal, young adults during wake and SWS, and (2) invasive electrocorticography (ECoG) data collected during wake and SWS in 5 patients undergoing evaluation for surgical management of epilepsy. We study infra-slow propagation by examining temporal lags in cortico-hippocampal rs-fMRI signals as well as electrophysiological infra-slow signals extracted from ECoG. Higher frequencies are examined by studying temporal lags in local field potentials (LFPs) measured using ECoG. On this basis, we investigate cortical-hippocampal propagation of both slow and fast signals in humans during wakefulness and SWS.

5.4 Results

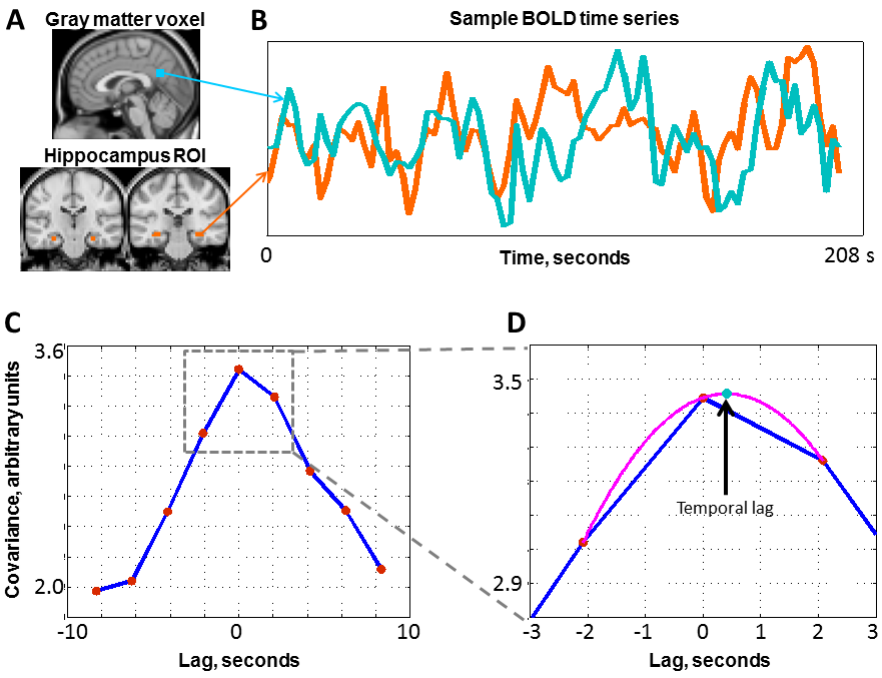

Figure 5-2: Calculation of rs-fMRI temporal lags using parabolic interpolation. Lags are derived by pairwise analysis of time series derived from the hippocampus region of interest (ROI) and every cortical voxel. (A): Hippocampal ROI and a sample gray matter voxel. (B): Time series extracted from the regions in (A). (C): The corresponding lagged cross-covariance function. The range of the plotted values is restricted to ±8.32 s, which is equivalent to ±4 frames (red markers) as the repetition time was 2.08 s. The lag between the time series is the value at which the absolute value of the cross-covariance function is maximal. (D):This extremum (arrow, teal marker) can be determined at a resolution finer than the temporal sampling density by parabolic interpolation (magenta line) through the computed values (red markers). In this example, the cortical time series is on balance ~0.5 seconds later than the hippocampal time series. See Methods and (Mitra et al. 2014) for further detail.

Resting state fMRI

We first examined infra-slow signaling using rs-fMRI in 38 normal adults, on the basis of prior work demonstrating state-dependent reversal of BOLD signal propagation between cortex and subcortical structures (Mitra et al. 2015b). As illustrated in Figure 2, we compute temporal lags in rs-fMRI data by applying parabolic interpolation to lagged covariance curves derived over pairs of time series (this methodology has been previously described in detail (Mitra et al. 2014)). Parabolic interpolation allows the detection of temporal lags finer than the temporal sampling density of fMRI. The temporal lag between the hippocampus region of interest (ROI) and each gray matter voxel represents, on average, whether the BOLD signal in the hippocampus leads or

follows the cortical voxel.

The set of all temporal lags with respect to the hippocampus, during wake and SWS, is shown in Figure 3 in the form of a lag map. Negative lag values (cool hues) in Fig. 3 indicate voxels where activity on average leads the hippocampus; positive lag values (warm hues) indicate voxels where activity on average follows the hippocampus. The range of lags in Fig. 3, ~±1 second, agrees with previous findings (Mitra et al. 2015a).

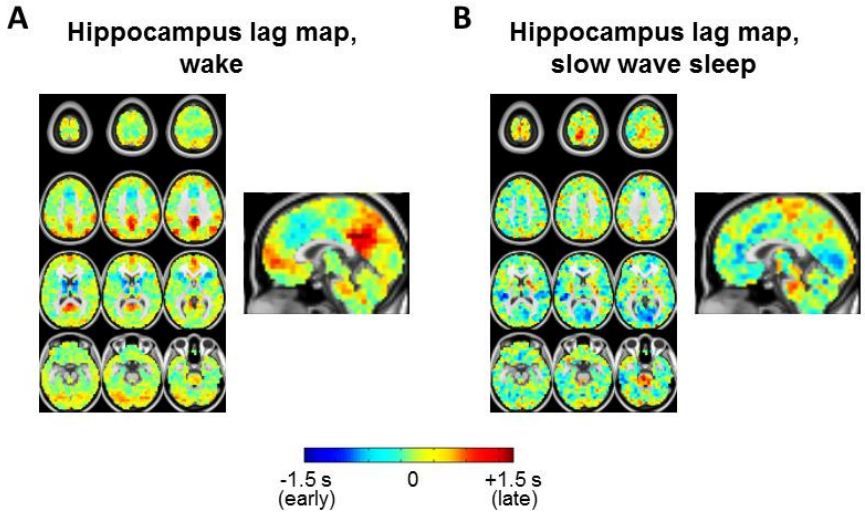

Figure 5-3: Hippocampus seed-based lag maps (using the ROI in Figure 2A) of infra-slow rs-fMRI BOLD activity in wake (A) and SWS (B). Maps depict the mean delay between each voxel and the hippocampus seed-region. Negative lag values indicate regions where activity leads the hippocampus; positive lag values indicate regions where activity follows the hippocampus. The range of lags is ~±1 second as shown in the color scale.

Contrasting Figs. 3A-B, it is evident that the hippocampal lag maps are substantially altered across wake and SWS. To assess the distribution of these effects over functional systems, we computed the mean lag between the hippocampus and an array of neocortical RSNs

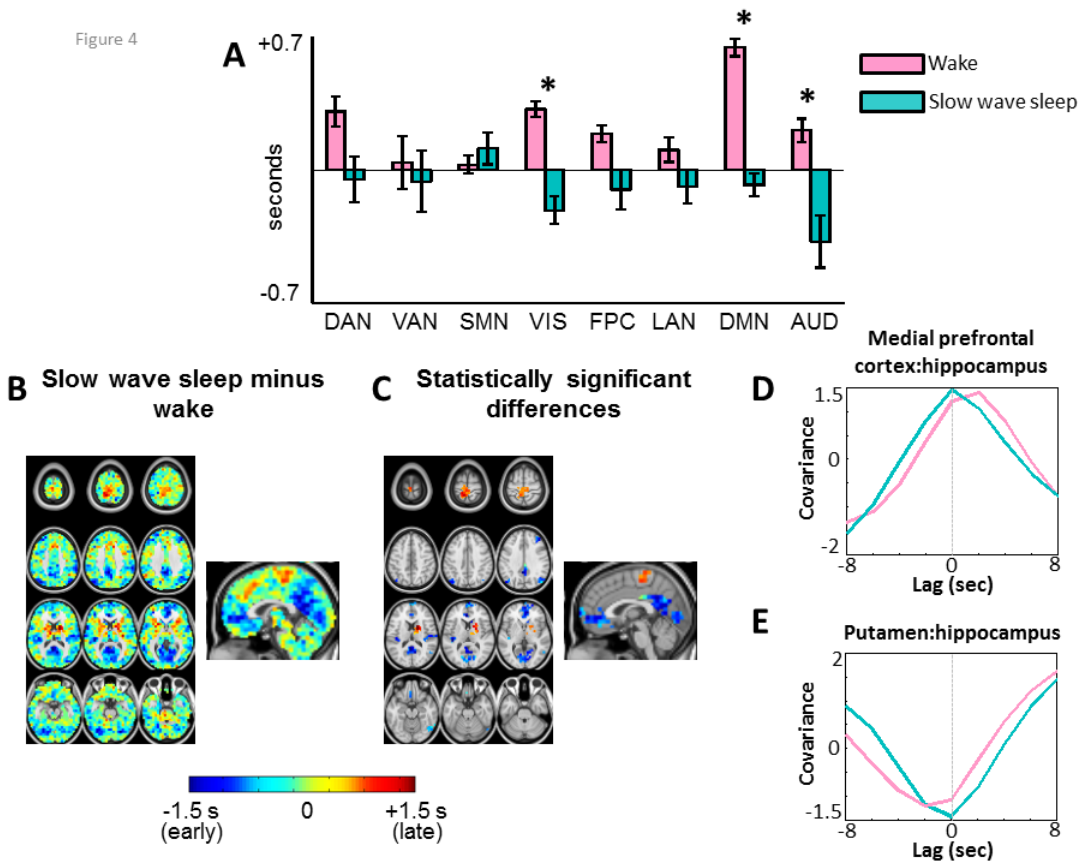

Figure 5-4: Topography of wake vs. SWS rs-fMRI hippocampal lag differences. (A): Mean lag between the hippocampus and each of cortical 8 networks during wake and SWS (see Fig. S1 for network topographies). Error bars represent 95% confidence intervals over subjects. (B): SWS minus wake hippocampus lag difference map, e.g., Fig. 3B minus Fig. 3A. (C): Difference map in (B), masked for statistical significance at the spatial cluster level (|Z| > 4.5, p < 0.05 corrected). (D)-(E): Group-level lagged covariance curves, in wake and SWS, between medial prefrontal cortex (mPFC) and hippocampus as well as between putamen and hippocampus. mPFC and putamen ROIs were derived from spatial clusters in (C). It is evident that mPFC shifts from "late" to "early", across wake and SWS, with respect to the hippocampus. In contrast, the putamen shifts from "early" to "late" across wake and SWS. Abbreviations: dorsal attention network (DAN), ventral attention network (VAN), sensory motor network (SMN), visual network (VIS), frontoparietal control network (FPC), language network (LAN), default mode network (DMN), and auditory network (AUD). * designates statistically significant reversal in propagation direction (p < 0.05, Bonferroni corrected; see Methods).

in wake and SWS (see supplemental Figure S1A for topographic network definitions). The results, shown in Figure 4A, demonstrate that every neocortical RSN is late with respect to the hippocampus during wake. In contrast, during SWS, every RSN is early

with respect to the hippocampus, with the exception of the sensory motor network (SMN). Thus, infra-slow rs-fMRI activity generally propagates from hippocampus to cerebral cortex during wake, but in the opposite direction, from cerebral cortex to hippocampus, during SWS. This reversal in propagation is statistically significant in three networks: the visual network, the auditory network, and the default mode network (DMN).

To examine lags at a finer spatial scale, we next analyzed voxel-wise lag differences (Fig. 4B). Statistically significant spatial clusters are shown in Fig. 4C. Clusters with negative lag values (blue) in Fig. 2C are earlier with respect to hippocampus during SWS as compared to wake. These clusters include the posterior cingulate precuneus, parietal cortex, and medial prefrontal cortex, a constellation of regions corresponding to the default mode network (Raichle et al. 2001). Additional significant spatial clusters of increased earliness were found in the calcarine sulcus (visual network) and auditory cortex (auditory network).

Positive lag values, indicating voxels that are later with respect to hippocampus during SWS as compared to wake, are also found in Fig. 4B. This effect was statistically significant in two spatial clusters (Fig. 4C): the paracentral lobule and parts of the right dorsal striatum (caudate nucleus and putamen). The paracentral lobule is a functional component of the supplementary motor area (SMA) (Lim et al. 1994), which belongs to the SMN. Thus, increased lateness in paracentral lobule accounts for the exceptional status of the SMN in Fig. 4A. The SMA and dorsal striatum both play a major role in

procedural motor learning (Halsband and Lange 2006). Hence, our results raise the possibility that regions integral to motor learning exhibit increased lateness with respect to the hippocampus during SWS. Indeed, a trend toward increased lateness was also observed at the voxel-level in rostral cingulate cortex (Fig. 4B), another area implicated in procedural motor learning (Halsband and Lange 2006).

In control analyses, we verified that BOLD signal amplitude in the hippocampal ROI is unchanged in wake vs. SWS (Supplemental Fig. S1B), as is zero-lag correlation (e.g., conventional functional connectivity) between the hippocampus and the major cortical networks (Supplemental Figure S1C). Therefore, the observed shifts in BOLD signal lag cannot be attributed to loss of hippocampal signal or loss of cortical-hippocampal functional connectivity. Moreover, entorhinal cortex lag analyses yielded results nearly identical to those obtained using the hippocampus (Supplemental Figure S2). Therefore, the findings in Figs. 3-4 should be understood as applying to the hippocampal system, including entorhinal cortex.

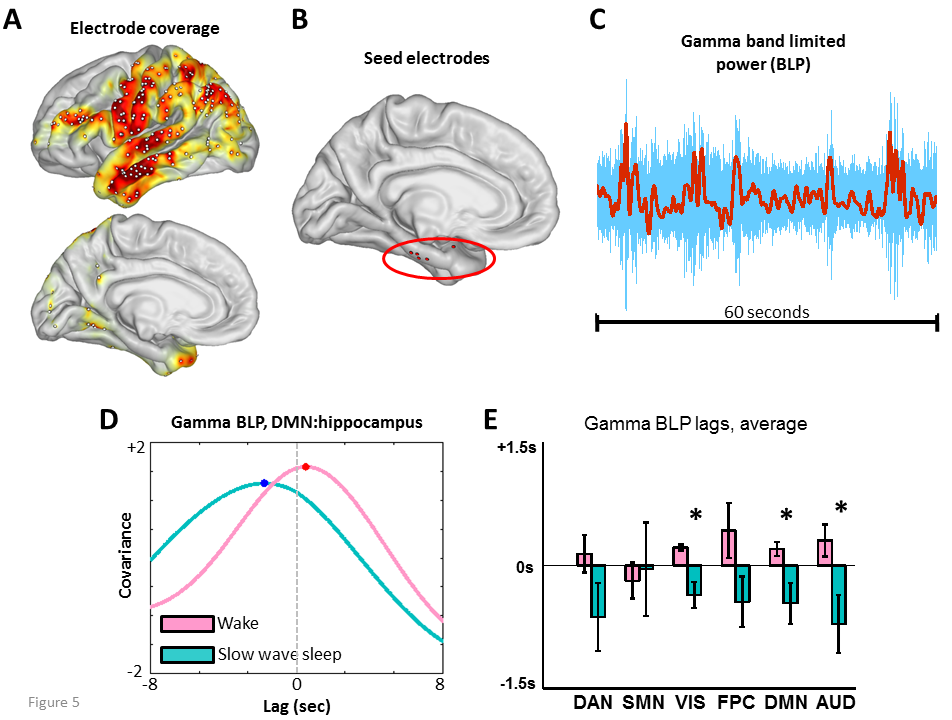

Figure 5-5: Cortical-hippocampal lags in infra-slow gamma BLP fluctuations. (A): Group-level electrode coverage; heat-map indicates cross-subject coverage density. (B): Hippocampal system seed-electrode locations for each of the 5 subjects. One seed electrode is more anterior than the rest; however, the results obtained in this subject are comparable to the others (see "PT 5" in Figs. S3-S5). (C): Sample 60 sec gamma band LFP timeseries (blue), along with the corresponding infra-slow BLP timeseries (red). (D): Sample lagged covariance curves between two gamma BLP time series (a hippocampal time series and a DMN time series) in one subject, in wake and SWS. Note that in this example, the DMN electrode is late with respect to the hippocampus during wake, and early during SWS. (E): Group level cortical-hippocampal lags for infra-slow gamma BLP. To accommodate variable cortical electrode coverage across subjects, lag results were computed at the RSN level (as in Fig. 4A). Note shift from positive (late) to negative (early) temporal lags across most networks, with significant effects in VIS, DMN, and AUD. * designates statistically significant reversal in propagation direction. Lag results for delta, theta, and alpha BLP are shown in Fig. S3.

Infra-slow electrophysiology

We have thus far examined temporal lags in rs-fMRI data. We next examined lags in infra-slow activity using ECoG data collected during wake and SWS in 5 patients undergoing evaluation for surgical management of epilepsy (see Supplemental Table S1 for patient details and Supplemental Methods for sleep staging). These patients had no medial temporal lobe pathology and were grossly cognitively normal including intact memory function. Cortical electrode coverage across subjects is illustrated in Figure 5A; the locations of electrodes in the hippocampal system in each of the 5 patients are

shown in Figure 5B.

Infra-slow activity in ECoG has previously been assessed two ways, either through infra-slow local field potentials (LFPs) (He et al. 2008) or infra-slow fluctuations in band limited power (BLP) (Foster et al. 2015; Leopold et al. 2003; Nir et al. 2008). Both infra-slow potentials and infra-slow fluctuations in BLP exhibit temporal correlation patterns that have been shown to correspond to RSNs derived using rs-fMRI (Foster et al. 2015; He et al. 2008). Owing to clinical amplifier limitations, infra-slow potentials were not available in the present data; hence, we examined cortical-hippocampal lags in infra-slow BLP fluctuations, parametric in carrier frequency: delta (0.5-4 Hz), theta (4-8 Hz), alpha (8-12 Hz) and gamma (40-100 Hz). Use of infra-slow BLP to assess infra-slow fluctuations in electrophysiology is well established (Foster et al. 2015; Leopold et al. 2003; Liu et al. 2014; Nir et al. 2008).

Accordingly, we computed lags in each subject between the hippocampal electrode and all cortical electrodes using infra-slow BLP time series parametric in carrier frequency. An example of lagged covariance curves in wake and SWS, illustrated using gamma BLP timeseries, is shown in Figure 5D. To accommodate variable cortical electrode coverage across subjects, group-average lag results were computed at the network level (as in Fig. 4A). The most robust evidence of statistically significant reversal of lags in infra-slow BLP between cortex and hippocampus was found in the gamma BLP, as shown in Figure 5E. Notably, infra-slow fluctuations in gamma BLP exhibited cortical-hippocampal lags closely matched to our rs-fMRI results (compare Figs. 5E, 4A). The

range of gamma BLP lags is similar to that reported in Fig. 4A (~±1 second). Moreover, with one exception, each cortical RSN was late with respect to hippocampus during wake, whereas the reverse was true during SWS. This reversal was statistically significant in the visual, default mode and auditory networks ($p < 0.05$, corrected). The lone exception to the finding of increased earliness in SWS was the SMN, which exhibited increased lateness with respect to hippocampus in SWS as compared to wake (Fig. 5E). Notably, the same SMN effect was observed in the rs-fMRI results (Fig. 4A).

We found no statistically significant wake vs. SWS reversal of infra-slow BLP lags in the alpha or theta bands (Supplemental Figure S3A-B). Interestingly, one significant lag reversal was found in the visual network in delta BLP, but the direction of this lag reversal is opposite to what was observed for gamma BLP (see Supplemental Figure S3A-B for further discussion). We also computed zero-lag correlations for BLP signals between the hippocampal electrode and each cortical network, and found that none of the lag changes can be attributed to statistically significant changes in correlation between wake and SWS (Supplemental Figure S3C). Stable infra-slow BLP correlations across wake and SWS agree with previously reported work (Foster et al. 2015; Nir et al. 2008). Finally, we verified that the cortical and hippocampal electrodes in each patient had power at all analyzed frequencies during both wake and SWS (Supplemental Figure 4). Although there is more delta band power during SWS than wake (by definition), power in delta frequencies is present during wakefulness. Moreover, as has been previously reported, gamma oscillations are present during wake and SWS (Le Van Quyen et al. 2010).

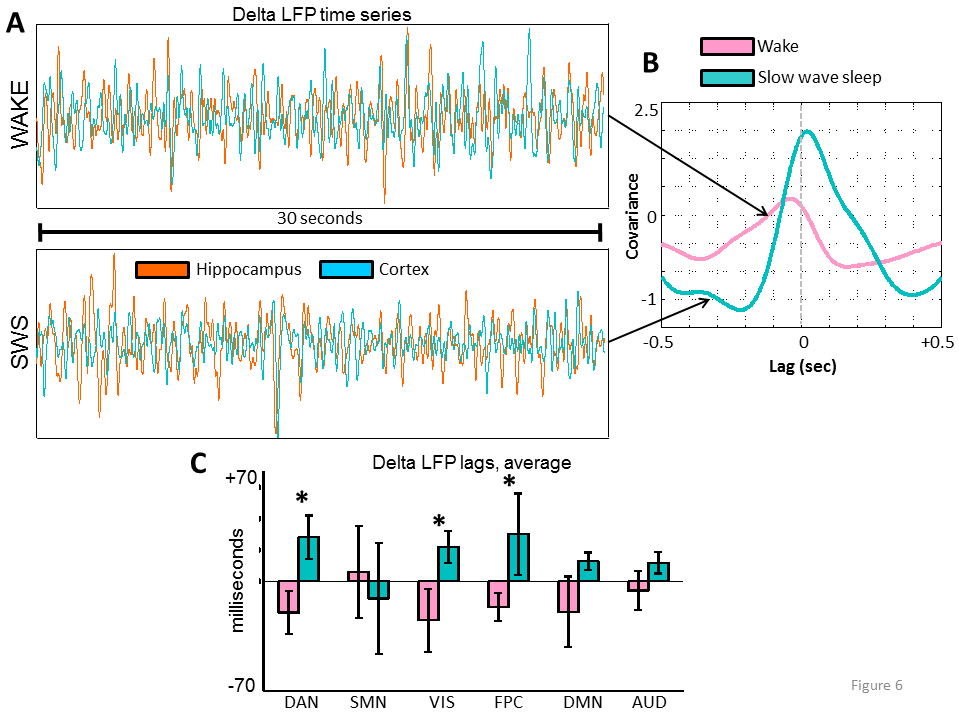

Figure 5-6: Cortical-hippocampal lags in delta LFPs. (A): Sample 30 seconds of time series from the hippocampus (orange) and cortex (blue) in one subject during wake and SWS. (B): Lagged covariance curves corresponding to the time series in (A). Note that in this example, the cortex is early with respect to the hippocampus during wake, and late during SWS. (C) Group level cortical-hippocampal lags for delta LFPs. Note shift from negative (early) to positive (late) temporal lags across most networks, with significant effects in DAN, VIS, and FPC. * designates statistically significant reversal in propagation direction. Lag results for theta, alpha, and gamma LFPs are shown in Fig. S5.

Local field potentials

The reciprocal two-stage model predicts the existence of high-frequency signals that propagate from cerebral cortex to hippocampus during wake, and from hippocampus to cerebral cortex during SWS (Figure 1). To test this feature of the model, we analyzed temporal lags in local field potentials. Although low frequency LFPs, such as delta, are generally considered “slow”, in the present context they are treated as “fast” as these frequencies are at least one order of magnitude higher than the infra-slow range. As before, we analyzed lags computed between the hippocampal electrode and every cortical electrode, parametric in frequency. An example is illustrated in Figure 6A: the top trace shows delta band activity in the hippocampus and a cortical electrode during wakefulness. The bottom trace shows delta band activity in the same electrodes in the

same patient during SWS. Lagged covariance curves computed from the time series during wake and SWS are illustrated in Figure 6B; in the illustrated example, it is evident that the cortex leads the hippocampus during wake (negative lag value), whereas the reverse is true during SWS (positive lag value). Group-average lag results for delta band activity, computed at the network level, are shown in Figure 6C. The range of the temporal lags in Fig. 6C, approximately $\pm$ 50 milliseconds, are much faster than the ~1 second infra-slow lags reported in Fig. 5E. In general, cortex leads hippocampus during wake, and hippocampus leads cortex during SWS. This reversal in propagation direction was statistically significant in the dorsal attention network, the visual network, and the frontoparietal control network. It is notable that the SMN exhibited the opposite effect although this contrast was not statistically significant. That is, the net balance of propagation during wakefulness is from hippocampus to cortex in the SMN, and vice versa during SWS. Thus, the SMN appears as an exception in both infra-slow and delta band lag analyses.

We found no statistically significant wake vs. SWS reversal of LFP lags in the theta, alpha, or gamma bands (Supplemental Figure S5A-B). We also found that, at the network level, correlations in LFP activity between the hippocampus and cerebral cortex were stable across wake and SWS in all analyzed bands (Supplemental Figure S5C). Thus, the changes in the direction of temporal lag found in delta activity are not attributable to changes in correlation structure.

5.5 Discussion

Summary of present findings

We analyzed human cortical-hippocampal signaling, as a function of wake and SWS, at multiple timescales using both rs-fMRI and electrocorticography. In general, we find that infra-slow activity, as measured using spontaneous BOLD signals and fluctuations in gamma BLP, propagates from the hippocampus to the cerebral cortex during wake, but in the opposite direction during SWS. In contrast, spontaneous delta band LFPs measured using ECoG generally propagate from cerebral cortex to hippocampus during wake, and from hippocampus to cerebral cortex during SWS. Taken together, these results demonstrate reversal of cortical-hippocampal signaling in humans, across wake and slow wave sleep, in two distinct frequency ranges. Our findings are consistent with the two-stage reciprocal theory of cortico-hippocampal communication (Fig. 1), if infra-slow signals are taken to represent the low frequency component of the model, and delta band activity is viewed as the higher frequency component. These results represent a departure from rodent hippocampus studies which associate delta/theta activity with low frequency signaling, and gamma/sharp-wave activity with higher frequency signals (Buzsaki 2002; Roumis and Frank 2015; Sirota and Buzsaki 2005; Sirota et al. 2003). We speculate that the differences may be attributable to cross-species effects (Jacobs 2014) as well as different signaling processes captured by macro- as opposed to micro-electrode recordings (discussed further in “Hippocampal Delta”) (Buffalo et al. 2011).

Our data also reveal significant exceptions to the general infra-slow/delta scheme in the

SMN and putamen. In these regions, the directions of the temporal lags we observed are precisely reversed from findings in the rest of the cortex, for both infra-slow and delta band activity. Thus, not only is the direction of cortical-hippocampal signaling a function of wake vs. sleep and frequency, the direction of signaling also depends on the part of cortex in question (Figure 7).

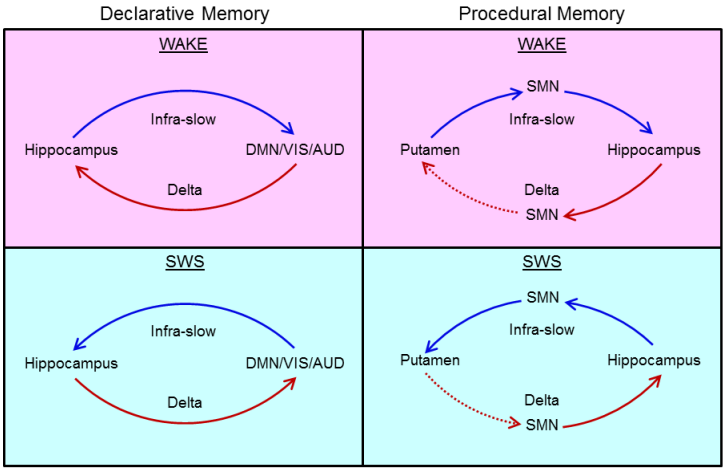

Figure 5-7: Schematic of present findings. The left column depicts infra-slow and delta LFP lags between the hippocampus and most of cortex, highlighting the DMN, VIS, and AUD. The temporal delays found between the hippocampus and these cortical systems agrees with the directions predicted by the two-stage reciprocal dialogue model (Fig. 1), if infra-slow activity is taken to represent the low frequency component of the model, and delta LFPs represent the higher frequency component. However, the right column demonstrates that precisely the opposite lags are found when considering the putamen and the SMN with respect to the hippocampus. Dotted red lines designate temporal lags implied, but not directly observed, by mirrored dissociation between systems. We hypothesize that the temporal lags depicted in the left and right columns may represent the parallel functions of the declarative and procedural memory systems, respectively. As depicted in the right column, our results suggest that the hippocampus is in an ongoing dialogue with the procedural memory system.

Infra-slow signaling

Our results highlight the role of infra-slow activity, measured by both rs-fMRI and fluctuations in gamma BLP, in the cortico-hippocampal dialogue. The findings suggest that the direction of infra-slow propagation between cortex and hippocampus is related the cortical-hippocampal state (encoding vs. consolidating). The procedural memory system may be subject to a similar principle, as we have previously found reversal in propagated infra-slow activity between putamen in cortex across wake and SWS (Mitra et al. 2015b).

Infra-slow activity has been widely implicated in organizing brain function. First, prior work has demonstrated infra-slow modulation of high frequency cortico-hippocampal interactions during SWS (Sirota et al. 2003). Second, it is now well-known that infra-slow fluctuations (assessed by rs-fMRI and electrophysiological techniques) are temporally correlated within functional systems (or resting state networks) spanning the entire brain (He et al. 2008; Nir et al. 2008). Indeed, zero-lag correlation topographies in rs-fMRI activity have been previously shown to correspond most closely to correlation topographies derived using gamma BLP, as opposed to BLP fluctuations at other frequencies (Foster et al. 2015; Leopold et al. 2003; Nir et al. 2008). Our findings extend the correspondence between rs-fMRI and infra-slow fluctuations in gamma BLP by demonstrating agreement in their temporal lag structure, with respect to cortical-hippocampal delays. The agreement between rs-fMRI and gamma BLP suggests that large-scale coordinated infra-slow fluctuations in activity, assessed by these techniques, likely correspond to spatially broad changes in cortical excitability (He et al. 2008; Leopold et al. 2003; Monto et al. 2008).

In accordance with the two-stage reciprocal dialogue model, we suggest that slow, coordinated changes in excitability play a role in coordinating higher frequency information exchange between the cortex and hippocampus. It has been previously demonstrated that spontaneous infra-slow activity modulates broad-band electrophysiological activity through cross-frequency, phase-amplitude coupling (Monto et al. 2008). Thus, given its broad influence over multiple temporal scales and large

distances, temporal lags in infra-slow activity are well suited for the coordination of systems level activity necessary for cortical-hippocampal communication. Importantly, the long temporal lags (~1 second) observed in infra-slow activity indicate that these very slow frequencies do not propagate via direct axonal transmission; instead, we hypothesize that infra-slow signals travel at the population level to act as a slow feedback signal to regulate higher frequency activity.

Our study does not address the mechanisms that cause the direction of propagated infra-slow activity between hippocampus and cortex to reverse. However, prior evidence suggests that the differences in neuromodulator tone between wake and SWS (Stickgold 2005), especially cholinergic input (Hahn et al. 2012; Hasselmo 1999), play a role in altering patterns of intrinsic activity. Specifically, the reduction of cholinergic tone during SWS (Hasselmo 1999) may differentially alter the excitatory:inhibitory balance in different parts of the brain (Buzsaki et al. 2007). Regionally variable differences in excitatory tone could underlie reversals in the net propagation of activity. The physiology underlying infra-slow propagation over 100's-1000's of milliseconds is also presently unknown. This mechanistic uncertainty extends to propagation of ~1 Hz activity over 100's of milliseconds, where prior work has implicated factors ranging from purinergic signaling to the balance in excitatory and inhibitory activity (Hahn et al. 2012; Poskanzer and Yuste 2011). Future work is required to resolve these questions.

Hippocampal delta

We find that, on balance, spontaneous delta LFPs propagate from the cerebral cortex to

the hippocampus during wakefulness, and from hippocampus to cerebral cortex during SWS. These results, in the context of the two-stage reciprocal dialogue model, suggest that delta band activity plays a role in human cortical-hippocampal information exchange in both wake and sleep. Although hippocampal function has been traditionally associated with theta (4-8 Hz) band activity on the basis of rodent studies (Battaglia et al. 2011; Buzsaki 2002), recent work has shown that memory related activity in the primate (including human) hippocampus manifests also in the delta (0.5-4 Hz) range (Arnolds et al. 1980; Jacobs 2014; Lega et al. 2012; Moroni et al. 2012; Moroni et al. 2014; Watrous et al. 2011). Human ECoG studies have shown that delta LFP activity propagates from cortex to hippocampus with a delay of ~30 milliseconds during recall tasks (Lega et al. 2012), in agreement with the delay time and direction observed in our awake data (Fig. 6B). Furthermore, delta power in the human hippocampus increases during SWS following a memory task, and the degree of this increase is correlated with post-sleep memory recall (Moroni et al. 2014), suggesting a role for hippocampal delta in memory consolidation during SWS. To the best of our knowledge, phase delays in delta LFPs between hippocampus and cortex have not been previously studied in human SWS. However, our finding of signaling from hippocampus to cerebral cortex in SWS is consistent with delta activity facilitating consolidation by transfer of information from hippocampus to cortex.

The propagation of delta LFPs from hippocampus to much of cortex during SWS may appear, at first blush, to contradict prior work, which has demonstrated propagation of slow waves from cortex to hippocampus (Isomura et al. 2006; Nir et al. 2011). However,

much of the prior work examining slow wave (or Up/Down state) propagation has used motor cortex recordings to examine the cortico-hippocampal relationship (Isomura et al. 2006; Nir et al. 2011). In agreement with these studies, we find that delta LFPs in the motor cortex propagate to the hippocampus during SWS (Fig. 5E). Thus, in evaluating cortical-hippocampal propagation of activity, cortical location is a critical factor, as further discussed below in Network Specificity. In this regard, a present limitation is the lack of medial electrode coverage (Fig. 5A); it is quite possible that these medial structures have a different lag relation to the hippocampus, in delta LFPs, than the lateral regions we measured. Finally, it is important to note that delta LFPs represent a broader set of neural processes than slow waves (Amzica and Steriade 1998). Our focus on contrasting wake vs. SWS informed the present focus on delta LFPs rather than slow wave events, but differences between these phenomena may drive some differences in cortico-hippocampal relations (see Supplemental Appendix A for further discussion).

We did not observe consistent cortical-hippocampal temporal lags in theta, alpha, or gamma LFPs. However, this negative finding does not mean that activity in these frequencies does not play an essential role in cortical-hippocampal communication. Our temporal lags analysis detects biases in the direction of signaling; thus, strongly reciprocal signaling, which may be equally important for cortical-hippocampal communication, may not produce a clear lag direction. Moreover, our LFP data is acquired on the basis of ECoG electrodes on the surface of the brain. These electrodes do not provide the cortical laminar specificity which has been essential for detecting

directed alpha and gamma band activity in other parts of the brain (Buffalo et al. 2011; van Kerkoerle et al. 2014). Finally, it is important to note the caveat that the present electrophysiological recordings are obtained in epilepsy patients. Hence, it is possible that the findings reported here may not generalize to normal human physiology. The agreement between the results obtained using rs-fMRI in normal subjects and gamma BLP in epilepsy patients is a good control with respect to infra-slow signaling, but ethical considerations prevent any similar comparison with normal participants with respect to LFP data.

Network specificity

In general, infra-slow activity (rs-fMRI and gamma BLP) propagates from the hippocampus to the cerebral cortex during wakefulness, and in the reverse direction during SWS. Delta LFP activity between the hippocampus and cortex generally travels in the opposite direction as infra-slow activity during wake and SWS. These reversals are especially prominent in the DMN, the visual network, and the auditory network. A prominent DMN effect is significant given the emerging work associating the ongoing function of this network with declarative memory processes both during waking recall (Foster et al. 2015; Stevens et al. 2010) and during offline consolidation (Kaplan et al. 2016). Functional signaling between the hippocampus and the DMN is also consistent with the robust anatomical connections between these systems (Lavenex and Amaral 2000). Therefore, our findings add to growing evidence that the ongoing activity in the DMN is intimately related to declarative memory function.

Prominent lag reversals in the visual and auditory networks suggest the key role of sensory systems in both encoding and consolidating declarative memories. Previous work has shown that sensory information is conveyed to the hippocampus during wakefulness (Battaglia et al. 2011; Buzsaki 1996; 1989) and that neurons in both the auditory and visual cortices engage in coordinated high frequency replay with the hippocampus during SWS (Bendor and Wilson 2012; Haggerty and Ji 2015; Ji and Wilson 2007). Temporal lag reversals between hippocampus and visual/auditory cortices may reflect systems level manifestations of these processes.

Propagation between the sensory motor network (SMN), including the putamen (as measured in rs-fMRI), and the hippocampus occurs in the opposite direction with respect to the rest of the cortex, at infra-slow and delta frequencies, during wake and SWS. These results are consistent with prior work which has demonstrated a fundamental dissociation between the declarative memory system, which is hippocampus-dependent, and the procedural memory system, which depends on the striatum and supports motor learning and habitual behavior ((DeCoteau et al. 2007; Eichenbaum et al. 1992; Knowlton et al. 1996; Logothetis et al. 2012; Stickgold 2005); Figure 7). However, although the direction of propagation dissociates the procedural memory system from other parts of the brain, we also find evidence of signaling between the elements of the procedural system (SMN and putamen) and the hippocampus. Thus, our data suggest that in addition to functional dissociation, there is ongoing communication between the declarative and the procedural memory systems, in which the hippocampus appears to play an important role. This view is consistent with

prior work demonstrating coordination between the declarative and procedural memory systems (DeCoteau et al. 2007).

Conclusion:

Analysis of human spontaneous brain activity reveals direct evidence for reciprocal cortical-hippocampal communication across lower (infra-slow rs-fMRI and gamma BLP) and higher (delta LFP) frequency signals. As predicted by the two-stage model of declarative memory consolidation, the direction of propagation in both the slower (infra-slow) and faster (delta) signals reverses direction in SWS vs. wake. However, the direction of hippocampal signaling with sensory motor areas differs as compared to the rest of the brain. Future work is required to determine the behavioral role of this propagated activity, as well as to investigate how these frequencies relate to other cortical and hippocampal rhythms.

5.6 Methods

EEG–fMRI Acquisition and Artifact Correction:

Acquisition parameters and details for these data have been previously published (Tagliazucchi et al. 2013). fMRI was acquired using a 3 T scanner (Siemens Trio) with optimized polysomnographic settings (1,505 volumes of T2*-weighted echo planar images, repetition time/echo time = 2,080 ms/30 ms, matrix = 64 × 64, voxel size = 3 × 3 × 2 mm^3, distance factor = 50%; field of view = 192 mm^2). 30 EEG channels were simultaneously recorded using a modified cap (EASYCAP) with FCz as reference (sampling rate = 5 kHz, low pass filter = 250 Hz, high pass filter = 0.016 Hz). MRI and

pulse artifact correction were performed based on the average artifact subtraction method (Allen et al. 1998) as implemented in Vision Analyzer2 (Brain Products) followed by ICA-based rejection of residual artifact components (CBC parameters; Vision Analyzer). EEG sleep staging was done by an expert according to the American Academy of Sleep Medicine (AASM) criteria (Iber 2007).

fMRI Subjects:

63 non-sleep-deprived subjects were scanned in the evening (starting at approximately 8:00PM). Written informed consent was obtained from all subjects whose data was analyzed in this study, and data collection for this study was approved by the Goethe University ethics committee. Hypnograms were inspected to identify epochs of contiguous sleep stages lasting at least 5 min (150 volumes). These criteria yielded 38 subjects contributing to the present analyses. Included are 70 epochs of wakefulness and 38 epochs of N3 sleep (SWS). Detailed sleep architectures of each participant have been previously published (Tagliazucchi et al. 2013).

Electrocorticography Subjects:

All participants were patients at Barnes Jewish Hospital or St. Louis Children's Hospital with drug-resistant epilepsy undergoing electrocorticographic (ECoG) monitoring to localize seizure foci. All participants provided informed consent with oversight by the local Institutional Review Board in accordance with the National Institutes of Health guidelines and the ethical standards of the Declaration of Helsinki. Participants were selected from a large ECoG database in which least 4 days of clinical ECoG recordings

as well as pre-operative structural and functional MRI and post-implant X-ray computed tomography (CT) images were acquired (n=25). Five subjects passed stringent electrophysiologic and spatial coverage criteria (see Supplemental Experimental Procedures) for inclusion in the study. We only analyzed data from patients who did not show any sign of medial temporal lobe pathology, were grossly cognitively normal by clinical neurological assessment, showed no signs of memory impairment, and had a combined IQ > 80 as assessed by Wechsler Adult Intelligence Scale—Fourth Edition (WAIS–IV). Furthermore, 4 of the 5 subjects in the present analysis were not on any medications during the ECoG recording period. See Supplemental Table S1 for individual subject profiles.

Epochs of wakefulness and sleep in the patients were identified behaviorally with video records. Periods of SWS during sleep were identified electrophysiologically on the basis of delta power in ECoG electrodes. Delta power was assessed using ECoG electrodes as opposed to traditional scalp EEG because, as noted by prior studies, the post-surgical condition of the skull precludes collection of usable EEG/polysomnography data (Hangya et al. 2011). Thus, following previously established practice (Hangya et al. 2011; He et al. 2008), we classified sustained periods (≥5 minutes) of delta power (> 20% power in the 0.5-2 Hz range) in ECoG electrodes during behaviorally identified sleep as SWS (He et al. 2008; Iber 2007). We only analyzed SWS epochs lasting a minimum of 5-minutes to match the fMRI analysis.

Statistical analysis:

Statistical significance of wake versus SWS differences in lag maps (Fig. 4) was assessed on a cluster-wise basis using threshold-extent criteria computed by extensive permutation resampling (Hacker et al. 2012; Hayasaka and Nichols 2003). Statistical significance in group-level lag reversals (Figs. 4-6) is computed using a one-sample t-test, where statistically significant reversals are inferred only when mean lag values are significantly different from zero, and in opposite directions, across wake and SWS. p-values in Fig. 4 were Bonferroni corrected for 8 comparisons; p-values in Figs. 5-6 were Bonferroni corrected for 24 comparisons (6 networks $\times$ 4 frequency bands).

Details regarding preprocessing of fMRI and ECoG data, as well as further explanation of lags computations, are found in the Supplemental Experimental Procedures, found online.

5.7 Acknowledgments

This work was supported by the National Institute of Health (NS080675 to MER and AZS; P30NS048056 to AZS; R01MH096482-01 to ECL; F30MH099877-02 to CDH; F30 MH106253-02 to AM), the Bundesministerium für Bildung und Forschung (grant 01EV0703) and the LOEWE Neuronale Koordination Forschungsschwerpunkt Frankfurt (NeFF). We thank Gyorgy Buzsaki, Manu Goyal, and Tyler Blazey for helpful discussion.

5.8 References

Allen PJ, Polizzi G, Krakow K, Fish DR, and Lemieux L. Identification of EEG events in the MR scanner: the problem of pulse artifact and a method for its subtraction. *Neuroimage* 8: 229-239, 1998.

Amzica F, and Steriade M. Electrophysiological correlates of sleep delta waves. *Electroencephalogr Clin Neurophysiol* 107: 69-83, 1998.

Arnolds DE, Lopes da Silva FH, Aitink JW, Kamp A, and Boeijinga P. The spectral properties of hippocampal EEG related to behaviour in man. *Electroencephalogr Clin Neurophysiol* 50: 324-328, 1980.

Battaglia FP, Benchenane K, Sirota A, Pennartz CM, and Wiener SI. The hippocampus: hub of brain network communication for memory. *Trends Cogn Sci* 15: 310-318, 2011.

Bendor D, and Wilson MA. Biasing the content of hippocampal replay during sleep. *Nat Neurosci* 15: 1439-1444, 2012.

Biswal B, Yetkin FZ, Haughton VM, and Hyde JS. Functional connectivity in the motor cortex of resting human brain using echo-planar MRI. *Magn Reson Med* 34: 537-541, 1995.

Buffalo EA, Fries P, Landman R, Buschman TJ, and Desimone R. Laminar differences in gamma and alpha coherence in the ventral stream. *Proc Natl Acad Sci U S A* 108: 11262-11267, 2011.

Buzsaki G. The hippocampo-neocortical dialogue. *Cerebral cortex* 6: 81-92, 1996.

Buzsaki G. Theta oscillations in the hippocampus. *Neuron* 33: 325-340, 2002.

Buzsaki G. Two-stage model of memory trace formation: a role for "noisy" brain states. *Neuroscience* 31: 551-570, 1989.

Buzsaki G, Kaila K, and Raichle M. Inhibition and brain work. *Neuron* 56: 771-783, 2007.

Buzsaki G, Logothetis N, and Singer W. Scaling brain size, keeping timing: evolutionary preservation of brain rhythms. *Neuron* 80: 751-764, 2013.

DeCoteau WE, Thorn C, Gibson DJ, Courtemanche R, Mitra P, Kubota Y, and Graybiel AM. Learning-related coordination of striatal and hippocampal theta rhythms during acquisition of a procedural maze task. *Proc Natl Acad Sci U S A* 104: 5644-5649, 2007.

Eichenbaum H, Otto T, and Cohen NJ. The hippocampus--what does it do? *Behavioral and neural biology* 57: 2-36, 1992.

Foster BL, Rangarajan V, Shirer WR, and Parvizi J. Intrinsic and task-dependent coupling of neuronal population activity in human parietal cortex. *Neuron* 86: 578-590, 2015.

Fox MD, and Raichle ME. Spontaneous fluctuations in brain activity observed with functional magnetic resonance imaging. *Nat Rev Neurosci* 8: 700-711, 2007.

Hacker CD, Perlmutter JS, Criswell SR, Ances BM, and Snyder AZ. Resting state functional connectivity of the striatum in Parkinson's disease. *Brain : a journal of neurology* 135: 3699-3711, 2012.

Haggerty DC, and Ji D. Activities of visual cortical and hippocampal neurons co-fluctuate in freely moving rats during spatial navigation. *eLife* 4: 2015.

Hahn TT, McFarland JM, Berberich S, Sakmann B, and Mehta MR. Spontaneous persistent activity in entorhinal cortex modulates cortico-hippocampal interaction in vivo. *Nat Neurosci* 15: 1531-1538, 2012.

Halsband U, and Lange RK. Motor learning in man: a review of functional and clinical studies. *Journal of physiology, Paris* 99: 414-424, 2006.

Hangya B, Tihanyi BT, Entz L, Fabo D, Eross L, Wittner L, Jakus R, Varga V, Freund TF, and Ulbert I. Complex propagation patterns characterize human cortical activity during slow-wave sleep. *J Neurosci* 31: 8770-8779, 2011.

Hasselmo ME. Neuromodulation: acetylcholine and memory consolidation. *Trends Cogn Sci* 3: 351-359, 1999.

Hayasaka S, and Nichols TE. Validating cluster size inference: random field and permutation methods. *Neuroimage* 20: 2343-2356, 2003.

He BJ, Snyder AZ, Zempel JM, Smyth MD, and Raichle ME. Electrophysiological correlates of the brain's intrinsic large-scale functional architecture. *Proc Natl Acad Sci U S A* 105: 16039-16044, 2008.

Iber C. *The AASM manual for the scoring of sleep and associated events: rules, terminology and technical specifications*. American Academy of Sleep Medicine, 2007.

Isomura Y, Sirota A, Ozen S, Montgomery S, Mizuseki K, Henze DA, and Buzsaki G. Integration and segregation of activity in entorhinal-hippocampal subregions by neocortical slow oscillations. *Neuron* 52: 871-882, 2006.

Jacobs J. Hippocampal theta oscillations are slower in humans than in rodents: implications for models of spatial navigation and memory. *Philos Trans R Soc Lond B Biol Sci* 369: 20130304, 2014.

Ji D, and Wilson MA. Coordinated memory replay in the visual cortex and hippocampus during sleep. *Nat Neurosci* 10: 100-107, 2007.

Kaplan R, Adhikari MH, Hindriks R, Mantini D, Murayama Y, Logothetis NK, and Deco G. Hippocampal Sharp-Wave Ripples Influence Selective Activation of the Default Mode Network. *Curr Biol* 2016.

Knowlton BJ, Mangels JA, and Squire LR. A neostriatal habit learning system in humans. *Science* 273: 1399-1402, 1996.

Lavenex P, and Amaral DG. Hippocampal-neocortical interaction: a hierarchy of associativity. *Hippocampus* 10: 420-430, 2000.

Le Van Quyen M, Staba R, Bragin A, Dickson C, Valderrama M, Fried I, and Engel J. Large-scale microelectrode recordings of high-frequency gamma oscillations in human cortex during sleep. *J Neurosci* 30: 7770-7782, 2010.

Lega BC, Jacobs J, and Kahana M. Human hippocampal theta oscillations and the formation of episodic memories. *Hippocampus* 22: 748-761, 2012.

Leopold DA, Murayama Y, and Logothetis NK. Very slow activity fluctuations in monkey visual cortex: implications for functional brain imaging. *Cereb Cortex* 13: 422-433, 2003.

Lim SH, Dinner DS, Pillay PK, Luders H, Morris HH, Klem G, Wyllie E, and Awad IA. Functional anatomy of the human supplementary sensorimotor area: results of extraoperative electrical stimulation. *Electroencephalogr Clin Neurophysiol* 91: 179-193, 1994.

Liu X, Yanagawa T, Leopold DA, Fujii N, and Duyn JH. Robust Long-Range Coordination of Spontaneous Neural Activity in Waking, Sleep and Anesthesia. *Cereb Cortex* 2014.

Logothetis NK, Eschenko O, Murayama Y, Augath M, Steudel T, Evrard HC, Besserve M, and Oeltermann A. Hippocampal-cortical interaction during periods of subcortical silence. *Nature* 491: 547-553, 2012.

McNaughton BL, Barnes CA, Battaglia FP, Bower MR, Cowen SL, Ekstrom AD, Gerrard JL, Hoffman KL, Houston FP, Karten Y, Lipa P, Pennartz CMA, and Sutherland GR. Off-Line Reprocessing of Recent Memory and its Role in Memory Consolidation: A Progress Report. In: *Sleep and Brain Plasticity*, edited by Maquet P, Smith C, and Stickgold RUniversity Press Scholarship Online, 2003.

Mitra A, Snyder AZ, Blazey T, and Raichle ME. Lag threads organize the brain's intrinsic activity. *Proc Natl Acad Sci U S A* 112: E2235-2244, 2015a.

Mitra A, Snyder AZ, Hacker CD, and Raichle ME. Lag structure in resting-state fMRI. *J Neurophysiol* 111: 2374-2391, 2014.

Mitra A, Snyder AZ, Tagliazucchi E, Laufs H, and Raichle ME. Propagated infra-slow intrinsic brain activity reorganizes across wake and slow wave sleep. *eLife* 4: 2015b.

Monto S, Palva S, Voipio J, and Palva JM. Very slow EEG fluctuations predict the dynamics of stimulus detection and oscillation amplitudes in humans. *J Neurosci* 28: 8268-8272, 2008.

Moroni F, Nobili L, De Carli F, Massimini M, Francione S, Marzano C, Proserpio P, Cipolli C, De Gennaro L, and Ferrara M. Slow EEG rhythms and inter-hemispheric

synchronization across sleep and wakefulness in the human hippocampus. *Neuroimage* 60: 497-504, 2012.

Moroni F, Nobili L, Ianria G, Sartori I, Marzano C, Tempesta D, Proserpio P, Lo Russo G, Gozzo F, Cipolli C, De Gennaro L, and Ferrara M. Hippocampal slow EEG frequencies during NREM sleep are involved in spatial memory consolidation in humans. *Hippocampus* 24: 1157-1168, 2014.

Nir Y, Mukamel R, Dinstein I, Privman E, Harel M, Fisch L, Gelbard-Sagiv H, Kipervasser S, Andelman F, Neufeld MY, Kramer U, Arieli A, Fried I, and Malach R. Interhemispheric correlations of slow spontaneous neuronal fluctuations revealed in human sensory cortex. *Nat Neurosci* 11: 1100-1108, 2008.

Nir Y, Staba RJ, Andrillon T, Vyazovskiy VV, Cirelli C, Fried I, and Tononi G. Regional slow waves and spindles in human sleep. *Neuron* 70: 153-169, 2011.

Poskanzer KE, and Yuste R. Astrocytic regulation of cortical UP states. *Proc Natl Acad Sci U S A* 108: 18453-18458, 2011.

Raichle ME, MacLeod AM, Snyder AZ, Powers WJ, Gusnard DA, and Shulman GL. A default mode of brain function. *Proc Natl Acad Sci U S A* 98: 676-682, 2001.

Roumis DK, and Frank LM. Hippocampal sharp-wave ripples in waking and sleeping states. *Curr Opin Neurobiol* 35: 6-12, 2015.

Scoville WB, and Milner B. Loss of recent memory after bilateral hippocampal lesions. *J Neurol Neurosurg Psychiatry* 20: 11-21, 1957.

Sirota A, and Buzsaki G. Interaction between neocortical and hippocampal networks via slow oscillations. *Thalamus Relat Syst* 3: 245-259, 2005.

Sirota A, Csicsvari J, Buhl D, and Buzsaki G. Communication between neocortex and hippocampus during sleep in rodents. *Proc Natl Acad Sci U S A* 100: 2065-2069, 2003.

Sirota A, Montgomery S, Fujisawa S, Isomura Y, Zugaro M, and Buzsaki G. Entrainment of neocortical neurons and gamma oscillations by the hippocampal theta rhythm. *Neuron* 60: 683-697, 2008.

Squire LR, and Alvarez P. Retrograde amnesia and memory consolidation: a neurobiological perspective. *Curr Opin Neurobiol* 5: 169-177, 1995.

Stevens WD, Buckner RL, and Schacter DL. Correlated low-frequency BOLD fluctuations in the resting human brain are modulated by recent experience in category-preferential visual regions. *Cereb Cortex* 20: 1997-2006, 2010.

Stickgold R. Sleep-dependent memory consolidation. *Nature* 437: 1272-1278, 2005.

Tagliazucchi E, von Wegner F, Morzelewski A, Brodbeck V, Jahnke K, and Laufs H. Breakdown of long-range temporal dependence in default mode and attention networks during deep sleep. *Proc Natl Acad Sci U S A* 110: 15419-15424, 2013.

van Kerkoerle T, Self MW, Dagnino B, Gariel-Mathis MA, Poort J, van der Togt C, and Roelfsema PR. Alpha and gamma oscillations characterize feedback and feedforward processing in monkey visual cortex. *Proc Natl Acad Sci U S A* 111: 14332-14341, 2014.

Watrous AJ, Fried I, and Ekstrom AD. Behavioral correlates of human hippocampal delta and theta oscillations during navigation. *J Neurophysiol* 105: 1747-1755, 2011.

Wilson MA, and McNaughton BL. Reactivation of hippocampal ensemble memories during sleep. *Science* 265: 676-679, 1994.

Chapter 6: Distinct Temporal Dynamics and Laminar Relationships in Infra-slow Brain activity

6.1 Preface

In Chapter 5 we examined the temporal structure of infra-slow activity between human cortex and hippocampus to find that there is correspondence between fMRI and electrophysiology, and that moreover, delta frequency (1-4 Hz) activity moves in a different direction than even lower frequency infra-slow activity. Taken together, these findings raise a host of questions. For one, is the temporal structure correspondence between infra-slow fMRI and electrophysiology a property that extends to the rest of cortex? Furthermore, does the difference in directionality between infra-slow and delta activity manifest more broadly? And what about higher frequencies? If infra-slow activity is moving in a different direction than other canonical high frequency activity bands, is it possible that infra-slow brain physiology is a distinct process that moves through distinct layers of the cortex as compared to higher frequency activity? We consider these questions in Chapter 6 by moving to a mouse model and applying optical imaging as well as laminar electrophysiology.

6.2 Abstract

Long-distance systems-level functional connectivity in spontaneous infra-slow (<0.1Hz) blood oxygen level dependent (BOLD) signals has become a major theme in the study of brain function using resting state fMRI and optical imaging in both humans and animal models. Yet the neurophysiology of how spontaneous BOLD signals become

organized over long distances remains largely unknown. Here, using whole-cortex calcium/hemoglobin imaging and laminar electrophysiology in mice, we show that infra-slow activity (ISA) in each of these modalities travels through the cortex along stereotypical trajectories that are distinct from trajectories in delta (1-4Hz) activity. Moreover, both infra-slow and delta activity trajectories reverse directions across wakefulness and anesthesia. Finally, we find that ISA travels through distinct cortical layers as compared to both delta activity and higher frequencies. These findings expand our understanding of resting state BOLD signal relationships and illustrate the unique physiology of long-distance organization in spontaneous infra-slow brain activity.

6.3 Introduction

Imaging of spontaneous brain activity, from human resting state functional magnetic resonance imaging (rs-fMRI) to murine optical imaging, reveals long-distance relationships even in the absence of explicit input or output (Biswal et al. 1995; Fox and Raichle 2007; Kenet et al. 2003; Ma et al. 2016; Vanni et al. 2017; White et al. 2011). Initially dismissed as noise or artifact, the long-distance organization of spontaneous low frequency activity is now a widely studied property of brain function (Fox and Raichle 2007). Infra-slow (<0.1Hz) fluctuations in the blood oxygen level dependent (BOLD) signal are of particular interest as they are spontaneously correlated (functionally connected) within large task-associated systems (Fox and Raichle 2007) and because BOLD signal functional connectivity has been related to a wide array of cognitive traits and neuropsychiatric conditions (Greicius 2008; Mitra et al. 2015b; Smith et al. 2015).

Yet, despite the popularity of resting state fMRI (rs-fMRI) as a method for studying brain function, the neurophysiology of how spontaneous patterns arise in BOLD signals is not well understood. One prominent viewpoint posits that synchronization of action potentials is an inherent property of connected neural networks; therefore, high frequency neural activity naturally tends toward synchrony within highly structurally connected large-scale networks (Honey et al. 2009). In this model, infra-slow correlations in the BOLD signal simply reflect a vascular low-pass filtering of much higher frequency neural activity (de Zwart et al. 2005; Honey et al. 2009). However, simulations modeling spontaneous BOLD signal organization as low-pass filtered action potentials synchronized through known white-matter connections yield only modest agreement with measured BOLD signal correlations (Honey et al. 2009). Furthermore, a simple anatomical connectivity model cannot explain the dramatic changes in functional organization across wake versus sleep states (Mitra et al. 2015b).

As an alternative, previous work has linked spontaneous BOLD signals to infra-slow activity (ISA) in local field potentials (He et al. 2008; Leopold et al. 2003; Pan et al. 2013). Historically, infra-slow local field potential activity has been shown to be structured in space and time (Aladjalova 1962), and recent studies in humans (Mitra et al. 2015a; Mitra et al. 2014) and mice (Matsui et al. 2016) have reported that BOLD signals propagate through the cerebral cortex along stereotypical spatio-temporal sequences to give rise to long-distance organization. Taken together, these findings suggest that there is a bona fide infra-slow brain process that propagates over long

distances to establish systems-level BOLD signal organization. However, key questions raised by this hypothesis remain unanswered.

First, do spontaneous temporal sequences in BOLD signals correspond specifically to infra-slow neural activity, or do they somehow reflect higher frequency spatio-temporal trajectories, such as in delta (1-4Hz) activity? Second, does the temporal organization of infra-slow activity correspond to the functional state of the brain? Third, distinct high frequency spectral bands such as gamma (>40 Hz) and alpha (8-12 Hz) are known to travel through specific layers of the cortex (Bastos et al. 2015; Buffalo et al. 2011; van Kerkoerle et al. 2014): if there is a distinct infra-slow temporal structure, does it travel through specific cortical layers as well? This third question is especially important as it raises the possibility that the extant literature on rs-fMRI functional connectivity reflects heretofore unsuspected laminar specificity.

To explore these questions, we explicitly focus on the spatio-temporal structure of infra-slow BOLD signals and their relation to both infra-slow and higher frequency neural activity. We first use simultaneous hemoglobin/calcium optical imaging of mouse cortex to demonstrate that spontaneous infra-slow blood oxygen signals travel through the cortex in a stereotyped trajectory closely matching that of infra-slow calcium activity, yet distinct from delta (1-4Hz) calcium trajectories. Furthermore, in studying spontaneous activity in awake and anesthetized mice, we find that ISA trajectories are highly state-dependent, such that their directions are nearly reversed across states of consciousness. Finally, we record infra-slow laminar electrophysiology in the mouse

cortex and find that specific cortical layers are indeed responsible for directed long-distance relationships in ISA.

6.4 Results

Stability of functional connectivity over frequencies and state

We first acquired simultaneous, wide-field calcium/hemoglobin imaging in 7 transgenic mice expressing GCaMP6f under control of a *Thy1* promoter (Figure 1A; Figure S1A-B). Imaging was acquired in a "resting state": mice were stationary and not subjected to any imposed experimental condition (see Methods). Spontaneous activity was imaged both during wakefulness and under ketamine/xylazine anesthesia; each mouse was imaged twice on two separate days.

We focused our analysis of the imaging data on spontaneous infra-slow (0.02-0.1 Hz) and delta (1-4 Hz) activity, using functional connectivity (FC) and temporal delays (TD) (Figures 1B-C). Both measures are derived from lagged-correlations between pairs of time series (Methods; (Mitra et al. 2014)). FC is zero-lag correlation and TD is the temporal offset corresponding to the peak correlation. Temporal offsets measure lead-lag relationships between regions, allowing us to detect temporal sequences in spontaneous activity. The matrices in Figs. 1D-E (dimensions pixels x pixels) illustrate FC and TD between all pairs of cortical calcium time series. FC matrices in Fig. 1D show that, as previously reported (Chan et al. 2015; Ma et al. 2016; Silasi et al. 2016),

the correlation structure of spontaneous activity is stable over a range of frequencies (ISA vs. delta) and across states of consciousness (wake vs. anesthesia).

Distinct spatio-temporal sequences in ISA and delta in anesthesia and wake

The TD matrices in Fig. 1E demonstrate that temporal structure differs significantly ($p < 0.001$; see Methods) over frequency and state. The patterns of blue and red hues in each TD matrix, indicating temporally early and late pixels respectively, are different across the four conditions (ISA and delta, anesthesia and wake). The timescales vary as well, ranging from +/- 0.5 sec in ISA to +/- 10 msec in delta activity. TD matrices were highly reproducible across the two days of imaging (Figure S1C). Thus, TD structure is far more frequency and state-dependent than FC.

We visualized the cortical topography of spontaneous temporal sequences with *lag projections* (images 1-4; Figure 2A), which are row-wise means of TD matrices (images 1-4; Figure 1E). Lag projections depict the degree to which, on average, each pixel is early (blue) or late (red) compared to the rest of the cortex. Hence, image 1 of Fig. 2A illustrates that that on average, under anesthesia, anterior delta leads posterior delta by ~100 msec, consistent with prior reports of anterior-posterior propagation of delta activity in anesthesia and sleep (Massimini et al. 2004; Stroh et al. 2013). In contrast, posterior ISA leads anterior ISA by ~0.5 sec (image 2; Fig. 2A). Posterior (visual) earliness under anesthesia is consistent with ISA findings in human sleep (Mitra et al. 2015b). During wake, delta and ISA exhibit back-to-front and front-to-back temporal

patterns, respectively, again at very different timescales (images 3-4 in Fig. 2A). In sum, Fig. 2A illustrates that spontaneous delta and ISA, measured using GCaMP6 fluorescence, travel in distinct trajectories at different speeds. Moreover, both delta and ISA generally reverse direction in wake vs. anesthesia.

To investigate how blood oxygen level dependent signals relate to infra-slow and delta activity, we repeated the analyses in Fig. 2A with hemoglobin signals (Fig. 2B). ISA lag projections for total hemoglobin and calcium are highly similar (images 2 and 4, in Figs. 2A-B), consistent with prior reports of correspondence between infra-slow neural activity and hemodynamic signals (Huang et al. 2014; Leopold et al. 2003; Li et al. 2015; Pan et al. 2013). However, delta frequency total hemoglobin lag projections do not match delta-band calcium signals (images 1 and 3, in Figs. 2A-B) and are not reproducible (Figure S1D). Analysis of oxyhemoglobin and deoxyhemoglobin yields concordant findings (Figure S2A-C). Thus, the correspondence of hemoglobin and calcium temporal structure is limited to infra-slow frequencies.

To verify our calcium temporal delay findings, we further analyze directionality using Granger Causality (GC). Figure 2C shows GC for two calcium time series, extracted from visual and motor regions, filtered into delta and ISA. GC reveals statistically significant causation in the same direction as the temporal sequences shown in Fig. 2A, with the exception of wake delta (GC direction matches TD but is not statistically significant).

We also computed phase-frequency curves using the visual and motor regions defined in Fig. 2C. The result (Fig. 2D) illustrates that phase offsets are stable over 0.02-0.32Hz and over 1-5Hz with a sharp directionality transition at ~0.64 Hz, in both wakefulness and anesthesia. Figure 2D suggests that there are only two, as opposed to many, spontaneous temporal patterns over 0.02-5Hz. We explored this hypothesis over the whole-cortex by computing TD matrices (as in Fig. 1E) for calcium signals filtered into double octave frequency bins (0.02-5.12 Hz; Fig. 2D). We then computed the similarity between all pairs of TD matrices using rank-order correlations (Figure 2E). In both anesthesia and wake, two blocks of high correlation are apparent, in the 0.02-0.32 Hz range, and in the 0.64-5 Hz range. Thus, there are only two spectral regimes of temporal sequences over 0.02-5.12Hz. Additionally, infra-slow and delta TD matrices are anti-correlated, indicating that activity moves in roughly the opposite direction across infra-slow vs. delta frequency ranges. The same approach also quantifies reversal of directionality across wake and anesthesia (figure S2D-F).

Frequency and state-dependent laminar relationships

Having found distinct temporal structures in infra-slow and delta activity, we next consider whether distinct cortical layers coordinate long-distance spontaneous relationships in these two frequency bands. We explored this hypothesis by inserting two 16-channel depth electrodes in the visual and motor cortices of mice (Figure 3A) to record wide-spectrum (0.02-100Hz) local field potentials (LFPs). Visual and motor cortices were chosen to match the analyses in Figure 2.

Figures 3B-C illustrate 16 x 12 FC and TD matrices between motor and visual cortices. These matrices show relationships between 16 recording sites from superficial-to-deep in motor cortex to 12 sites along the depth of visual cortex (visual cortex is thinner than motor cortex). It is evident that the cross-laminar FC and TD structure of ISA and delta are distinct ($p < 0.001$; see Methods) both from each other and across wake and anesthesia. Indeed, ISA cross-laminar relationships are also distinct compared to higher frequencies up to 100 Hz (Figure S3A). Note Figure 3C only reports statistically significant temporal delays ($p<0.05$ Bonferroni-corrected; see Methods); non-significant results are gray.

The cross-laminar TD matrices (Fig. 3C) further show bi-directional temporal offsets, between motor and visual cortex, within a frequency band. For example, in ISA under anesthesia (image 2; Fig. 3C), layers II-V in motor cortex lead layers II-IV in visual cortex (light blue). However, ISA in deeper visual layers leads superficial/middle layers in motor cortex (red). The relative strength of signaling in each direction can be inferred from the correlation matrices. Comparing image 2 across Figs. 3B-C, note that the correlations corresponding to the red (visual-to-motor) temporal offsets are stronger than correlations corresponding to the blue (motor-to-visual) temporal offsets. Hence, for ISA under anesthesia, the visual-to-motor direction predominates, in accordance with calcium imaging in Figure 2A. In contrast, we find the reverse during wake: the motor-to-visual direction predominates in ISA (image 4; Figs. 3B-C). The same principle is seen in spontaneous delta activity; deep motor leads visual under anesthesia, and

visual leads superficial layers of motor while in wake state (images 1 and 3; Figs. 3B-C). Schematics summarizing cross-laminar relationships in delta and ISA are shown in Figure 3D.

Finally, although we find that ISA and delta are functionally distinct, prior task-based work has shown cross-frequency interaction between ISA phase and delta amplitude (Monto et al. 2008). To explore whether this occurs spontaneously, we computed phase-amplitude coupling (PAC) between ISA phase and delta amplitude (Fig. 3E). PAC was computed both over all electrodes in our electrophysiological recordings, as well as separately over all pixels in GCaMP6 imaging. In both cases, there is a robust, statistically significant ($p<0.001$; see Methods) relationship between ISA phase and delta amplitude, and the phase of this relationship shifts between wake and anesthesia.

6.5 Discussion

In summary, we find that spontaneous infra-slow brain activity exhibits a lawful temporal structure as it moves through specific layers of the mouse cerebral cortex. Furthermore, the direction of ISA travel depends on the state (awake versus anesthetized) of the brain. In each state, the direction and topography of ISA temporal sequences are concordant across hemoglobin imaging, calcium imaging, and electrophysiology. Moreover, the spatio-temporal and cross-laminar organization of spontaneous ISA differs from both delta activity and higher frequencies up to 100 Hz. Taken together, these results demonstrate that there is a distinct infra-slow neurophysiological process in the brain whose temporal structure is state-dependent, and that blood oxygen signals

specifically correspond to the temporal and laminar organization of infra-slow brain activity.

Implications for BOLD imaging

The question of whether directed signal flow through specific cortical layers is responsible for the long distance organization of blood oxygen signals and ISA has not been previously explored. Yet, understanding the specific basis for the systems-scale organization of BOLD signals is essential for interpreting the large and growing field of rs-fMRI. In line with prior work, we find that the correlation structure of ISA and delta are quite similar (Chan et al. 2015; Ma et al. 2016). However, the present imaging results clearly differentiate directed trajectories in spontaneous ISA, as measured using blood oxygen and calcium signals, from spontaneous delta band activity (Figure 2A-B). We find that, whereas ISA temporal structure is quite similar across blood oxygen and calcium signals, the temporal structure of delta activity in the calcium signal is not mirrored in blood oxygen signals (Fig. 2). In fact, the delta band temporal structure of blood oxygen signals was not statistically reliable (Fig. S1D), demonstrating that the temporal structure of blood oxygen signals corresponds specifically to ISA.

Laminar electrophysiology further shows that, not only do delta and ISA travel in different directions, they also travel through different layers of the cortex. Anterior-to-posterior delta waves under anesthesia (Massimini et al. 2004) originating in deep cortical layers (Stroh et al. 2013), and visual-to-superficial motor travel of wake delta

activity (Shimaoka et al. 2017) have been reported separately before. Directed laminar travel of ISA has not been previously reported. On the basis of temporal delays (Figures 2-3), we infer that ISA in anesthesia tends to travel from deep visual layers (V-VI) to most of motor cortex (I-V). During wake, ISA tends to travel from layers I-V in motor cortex to layers I-IV in visual cortex (Fig. 3C image 4); however, the shortest motor-visual lags are between layer V of motor cortex and layers I-IV of visual cortex (Figure 3C-D, image 4). Assuming the shortest temporal delays reflect the most direct relationships, we conclude that ISA tends to be sent from deep layers (V-VI) and received in more superficial layers (I-IV).

In addition to providing laminar information, the directionality of ISA in our electrophysiological recordings is in agreement with results derived from both calcium and blood oxygen imaging. Hence, we can infer that the temporal organization found in ISA imaging data, in both calcium and blood oxygen signals, is attributable to the deep-to-superficial laminar relationships uncovered through electrophysiology. These findings, linking infra-slow electrophysiology, calcium, and hemoglobin signals, establish a new basis for interpreting the neurophysiology of long-distance relationships in rs-fMRI, but many questions remain. Spread of low-frequency spontaneous activity from deep layers is consistent with prior work (Sakata and Harris 2009), but further details of traveling ISA remain to be understood, with possible roles for polysynaptic connectivity (Van Dijk et al. 2010), subcortical connections (Xiao et al. 2017), subthreshold spread of activity (Berger et al. 2007), and even glial cells and metabolic signaling (Poskanzer and Yuste 2011).

Relationship between ISA and delta activity

Although ISA and delta activity travel across the cortex in different directions and through different cortical layers, two of the present findings suggest that spontaneous activity in these two spectral regimes may nonetheless be functionally linked. First, ISA and delta travel in approximately opposite directions along the anterior-posterior axis of the dorsal mouse cortex, during both wakefulness and anesthesia (Fig. 2E). We have previously observed delta and ISA traveling in reciprocal directions between the human hippocampus and cerebral cortex (Mitra et al. 2016), and hypothesized that this was a unique feature of cortico-hippocampal communication. Our present results in the mouse suggest, instead, that reciprocal travel of delta and ISA occurs more broadly. A possible function of this reciprocal travel is the conveyance of slow (delta) feedforward and slower (ISA) feedback influences, as has been observed for gamma and alpha activity in visual cortex during visual tasks (Bastos et al. 2015; Buffalo et al. 2011; van Kerkoerle et al. 2014), although the concepts of feedforward and feedback must be expanded to address spontaneous activity.

Second, the phase of ISA is coupled with the amplitude of delta band activity, in both calcium and electrophysiological recordings, and during both wakefulness and sleep (the phase relationship shifts slightly across states of consciousness; Fig. 3E). The computational purpose of this phase amplitude coupling is presently unclear, but in the context of prior work (Bastos et al. 2015; Monto et al. 2008), we speculate that

spontaneous activity may be hierarchically organized by frequency, such that the function of ISA is found in its interactions with higher frequencies, especially the delta band.

State-dependence

Finally, we find a reversal in the prevailing direction of temporal sequences in both delta and ISA across wake and anesthesia. This reversal of directionality is not observed in higher frequencies (Figure S3A). We therefore hypothesize that the temporal structure of low frequency activity, especially its direction of cortical travel, plays a special role in governing functional brain states. Future studies are required to explore precisely how spontaneous spatio-temporal sequences relate to conscious awareness.

Our present laminar electrophysiology findings also suggest that, mechanistically, the reversal in the predominant direction of travel in ISA and delta activity is accomplished by changing the relative weighting of bi-directional signaling in distinct cross-laminar relationships, as illustrated in Figure 3D. The basis of this re-weighting requires further investigation, but it is natural to suggest that neuromodulation may play a role in directionality shifts across wake vs. anesthesia (Lydic and Baghdoyan 2005; Marder 2012).

6.6 Figures

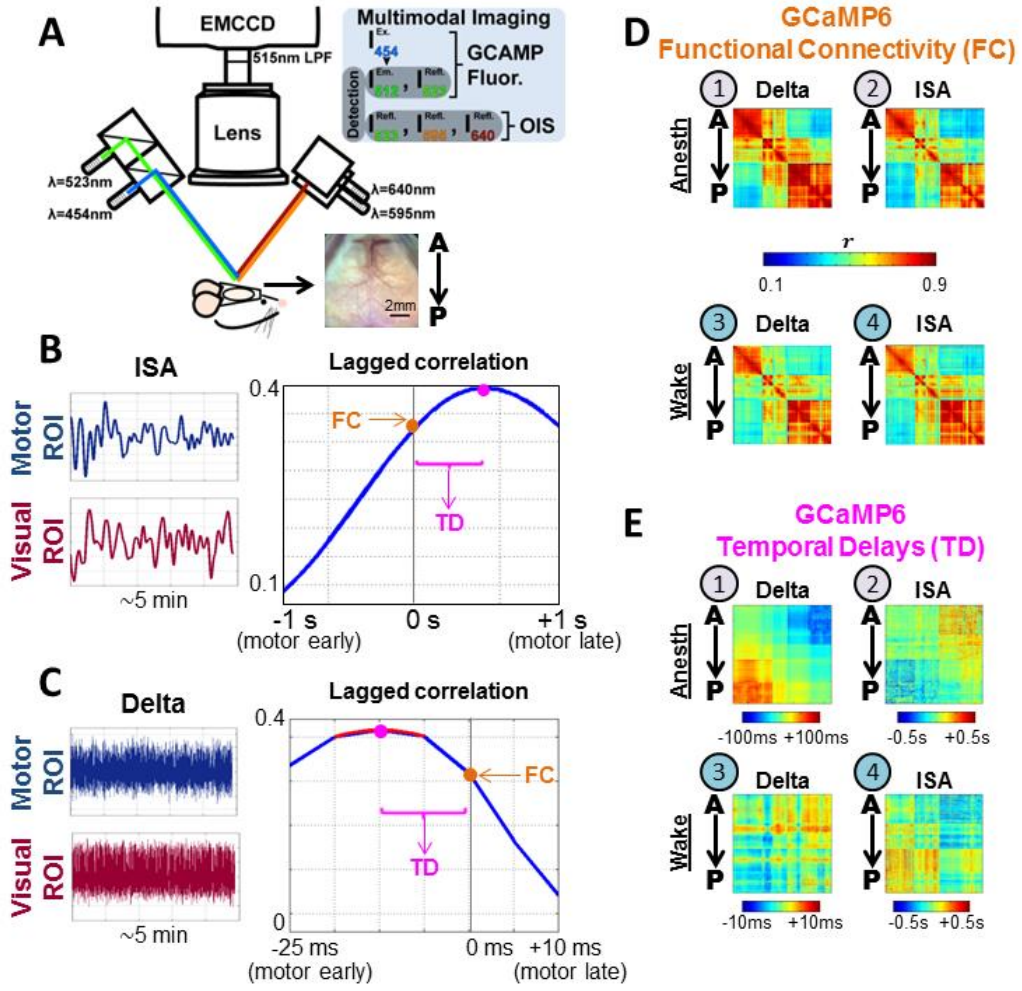

Fig. 6-1 Correlations and temporal sequences in wide-field imaging of spontaneous calcium activity in mouse cortex. ***(A)*** **Calcium fluorescence and hemoglobin absorbance were concurrently imaged in the dorsal cortical surface of transgenic Thy1/GCaMP6 mice using sequential illumination by four high-power LEDs (see Methods).** ***(B)*** **An example lagged correlation curve computed using two infra-slow activity (ISA) timeseries extracted from motor and visual regions of interest (ROIs). The zero-lag correlation value defines functional connectivity (FC); abscissa corresponding to the extremum value of the correlation defines the temporal delay (TD) for the pair of ROIs.** ***(C)*** **Same as (B), but for delta band activity.** ***(D)*** **FC matrices, illustrating correlations between all pixels, shown for delta and ISA, in wake and anesthesia. FC matrices are by definition symmetric ($r_{i,j} = r_{j,i}$). The rows and columns of the matrix are individual pixels from the dorsal surface of the mouse cortex arranged from anterior to posterior.** ***(E)*** **TD matrices representing the temporal delay between every pair of pixels, where the matrices are organized as in (D). TD matrices are by definition anti-symmetric ($\tau_{i,j} = -\tau_{j,i}$). See also Figure S1.**

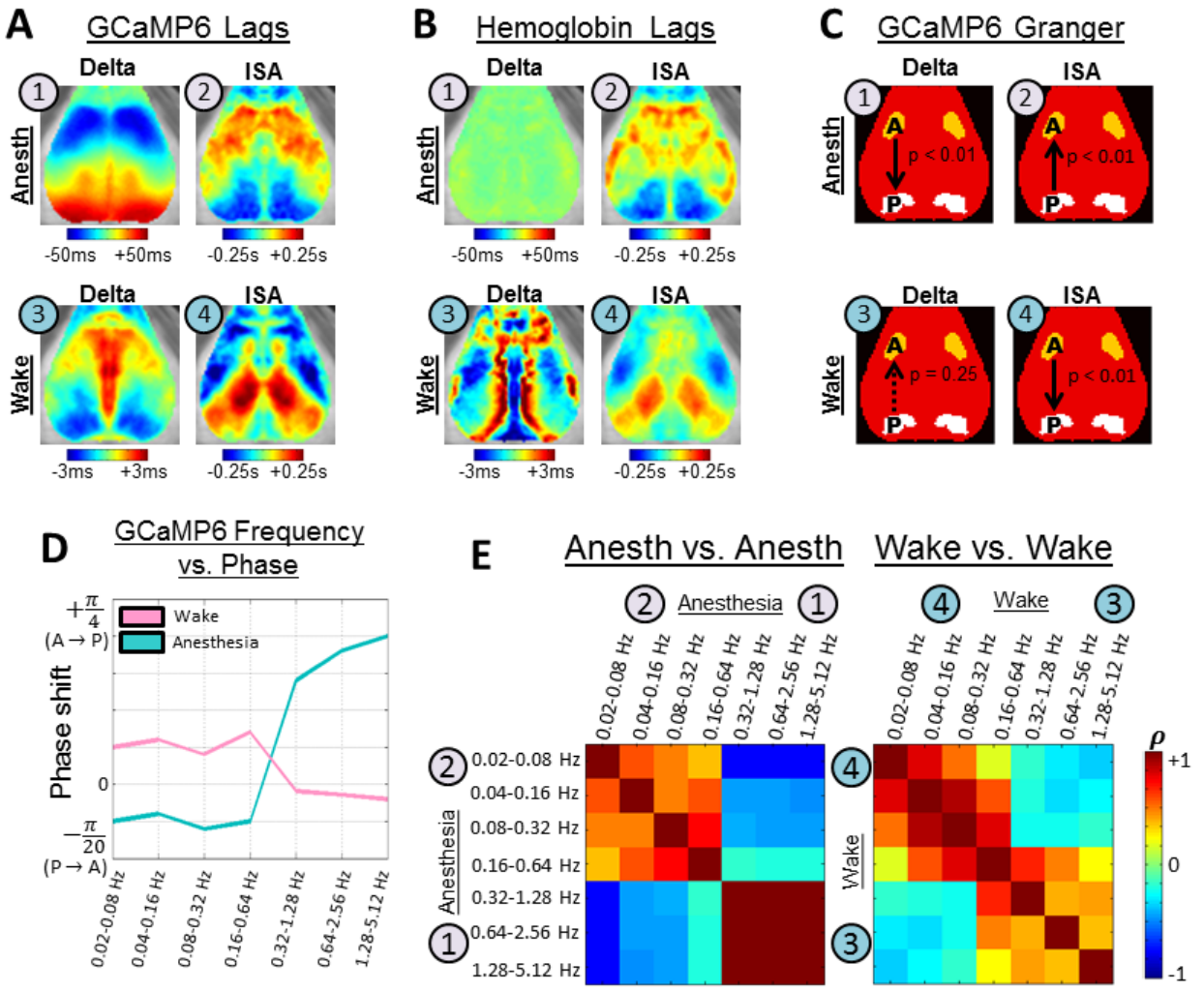

Fig. 6-2 Spontaneous temporal sequences systematically differ across frequencies and states of consciousness. ***(A)*** **GCaMP6 lag projections illustrating the mean delay between each pixel and the rest of cortex. Infra-slow and delta activity move in distinct trajectories, at different speeds, during both wake and anesthesia.** ***(B)*** **Total hemoglobin lag maps, derived as in (A), with matching timescales.** ***(C)*** **Granger causality analysis of GCaMP6 activity. Two ROIs in visual and motor cortices were defined by identifying regions of maximal lag in panel (A1-4); see Methods for coordinates. Statistically significant ($p < 0.01$; see Methods) Granger causality was found in agreement with (A), except in wake delta.** ***(D)*** **Frequency vs. phase analysis between the two ROIs in (C) in wake (pink) and anesthesia (blue).** ***(E)*** **Whole-cortex GCaMP6 TD matrix comparisons parametric in frequency under anesthesia (left panel) and wake (right panel). Each matrix entry reports the similarity (rank-order correlation) between a pair of TD matrices. See also Figure S2.**

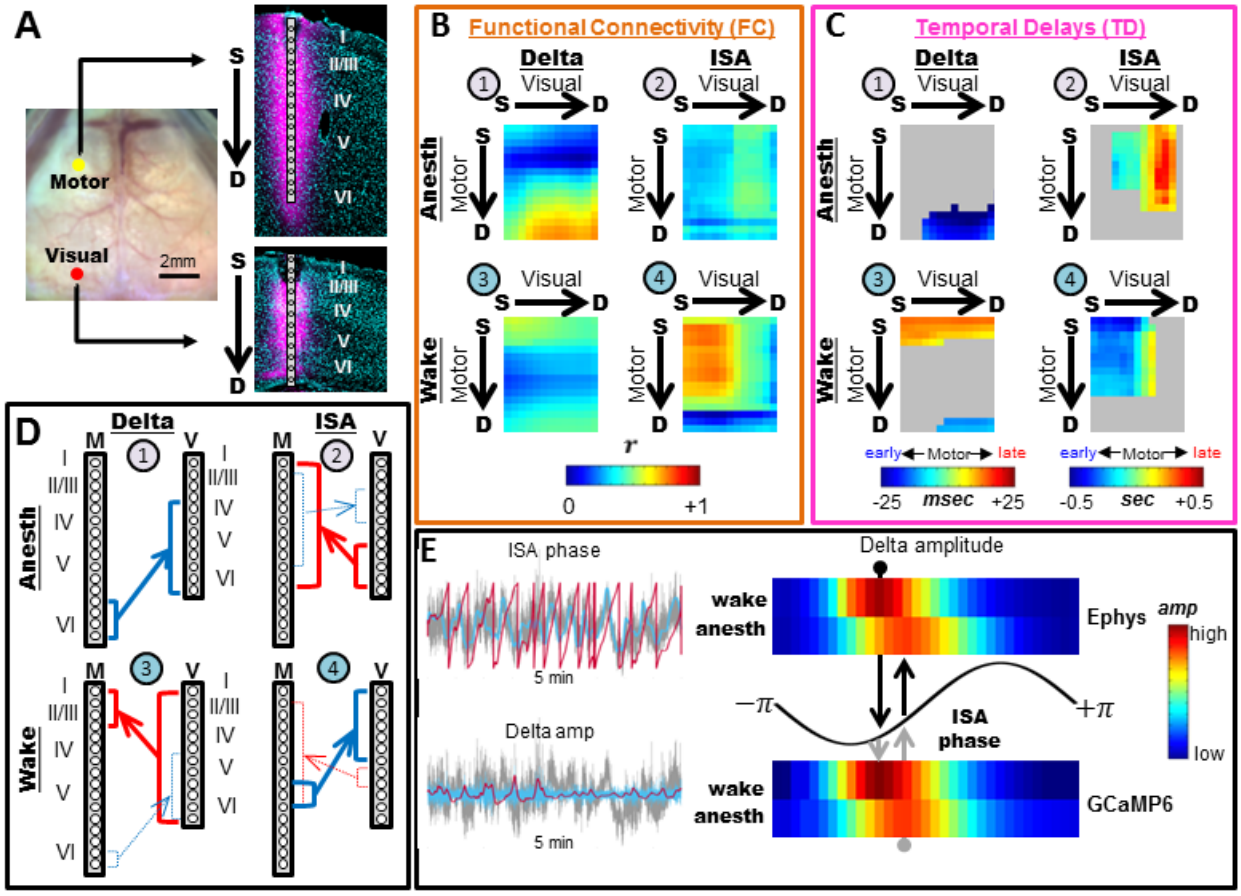

Fig. 6-3 Cross-laminar relationships in spontaneous visual-motor activity vary systematically across frequency and state. *(A)* 16-channel 1.5mm depth probes were inserted into motor and visual cortices. The thinner visual cortex is fully spanned by 12-channels. Probes were painted with DiI; position was confirmed in histologic sections counterstained with DAPI. *(B)* Cross-laminar FC. The four 16 x 12 matrices illustrate correlations between the 16 electrodes in motor cortex (rows) and the 12 electrodes in visual cortex (columns); electrodes are arranged from superficial (S) to deep (D). *(C)* Cross-laminar temporal delay matrices, arranged as in panel (B). Blue designates motor leading visual cortex; red indicates motor following visual cortex. Non-significant temporal delays are grey. *(D)* Schematic representation of the results in (B)-(C), highlighting the shortest delays between regions. Thick lines designate the predominant direction of signaling. Layer labels are approximate. *(E)* Phase-amplitude coupling (PAC) between ISA phase and delta amplitude. Sample 5 minute time series (gray) demonstrates ISA phase and delta amplitude are computed by first filtering (blue) and then applying a Hilbert transform (red). Delta amplitude is binned by infra-slow phase for each time series (electrode or pixel), and averaged to produce PAC histograms for electrophysiology and GCaMP6 imaging, in wake and anesthesia. See also Figure S3.

6.7 References

Aladjalova NA. *Slow electrical processes in the brain*. New York, New York: Elsevier, 1962.

Bastos AM, Vezoli J, Bosman CA, Schoffelen JM, Oostenveld R, Dowdall JR, De Weerd P, Kennedy H, and Fries P. Visual areas exert feedforward and feedback influences through distinct frequency channels. *Neuron* 85: 390-401, 2015.

Berger T, Borgdorff A, Crochet S, Neubauer FB, Lefort S, Fauvet B, Ferezou I, Carleton A, Luscher HR, and Petersen CC. Combined voltage and calcium epifluorescence imaging in vitro and in vivo reveals subthreshold and suprathreshold dynamics of mouse barrel cortex. *J Neurophysiol* 97: 3751-3762, 2007.

Biswal B, Yetkin FZ, Haughton VM, and Hyde JS. Functional connectivity in the motor cortex of resting human brain using echo-planar MRI. *Magn Reson Med* 34: 537-541, 1995.

Buffalo EA, Fries P, Landman R, Buschman TJ, and Desimone R. Laminar differences in gamma and alpha coherence in the ventral stream. *Proc Natl Acad Sci U S A* 108: 11262-11267, 2011.

Chan AW, Mohajerani MH, LeDue JM, Wang YT, and Murphy TH. Mesoscale infraslow spontaneous membrane potential fluctuations recapitulate high-frequency activity cortical motifs. *Nature communications* 6: 7738, 2015.

de Zwart JA, Silva AC, van Gelderen P, Kellman P, Fukunaga M, Chu R, Koretsky AP, Frank JA, and Duyn JH. Temporal dynamics of the BOLD fMRI impulse response. *Neuroimage* 24: 667-677, 2005.

Fox MD, and Raichle ME. Spontaneous fluctuations in brain activity observed with functional magnetic resonance imaging. *Nat Rev Neurosci* 8: 700-711, 2007.

Greicius M. Resting-state functional connectivity in neuropsychiatric disorders. *Curr Opin Neurol* 21: 424-430, 2008.

He BJ, Snyder AZ, Zempel JM, Smyth MD, and Raichle ME. Electrophysiological correlates of the brain's intrinsic large-scale functional architecture. *Proc Natl Acad Sci U S A* 105: 16039-16044, 2008.

Honey CJ, Sporns O, Cammoun L, Gigandet X, Thiran JP, Meuli R, and Hagmann P. Predicting human resting-state functional connectivity from structural connectivity. *Proc Natl Acad Sci U S A* 106: 2035-2040, 2009.

Huang L, Liu Y, Li M, and Hu D. Hemodynamic and electrophysiological spontaneous low-frequency oscillations in the cortex: directional influences revealed by Granger causality. *Neuroimage* 85 Pt 2: 810-822, 2014.

Kenet T, Bibitchkov D, Tsodyks M, Grinvald A, and Arieli A. Spontaneously emerging cortical representations of visual attributes. *Nature* 425: 954-956, 2003.

Leopold DA, Murayama Y, and Logothetis NK. Very slow activity fluctuations in monkey visual cortex: implications for functional brain imaging. *Cereb Cortex* 13: 422-433, 2003.

Li JM, Bentley WJ, and Snyder LH. Functional connectivity arises from a slow rhythmic mechanism. *Proc Natl Acad Sci U S A* 112: E2527-2535, 2015.

Lydic R, and Baghdoyan HA. Sleep, anesthesiology, and the neurobiology of arousal state control. *Anesthesiology* 103: 1268-1295, 2005.

Ma Y, Shaik MA, Kozberg MG, Kim SH, Portes JP, Timerman D, and Hillman EM. Resting-state hemodynamics are spatiotemporally coupled to synchronized and symmetric neural activity in excitatory neurons. *Proc Natl Acad Sci U S A* 113: E8463-E8471, 2016.

Marder E. Neuromodulation of neuronal circuits: back to the future. *Neuron* 76: 1-11, 2012.

Massimini M, Huber R, Ferrarelli F, Hill S, and Tononi G. The sleep slow oscillation as a traveling wave. *J Neurosci* 24: 6862-6870, 2004.

Matsui T, Murakami T, and Ohki K. Transient neuronal coactivations embedded in globally propagating waves underlie resting-state functional connectivity. *Proc Natl Acad Sci U S A* 113: 6556-6561, 2016.

Mitra A, Snyder AZ, Blazey T, and Raichle ME. Lag threads organize the brain's intrinsic activity. *Proc Natl Acad Sci U S A* 112: E2235-2244, 2015a.

Mitra A, Snyder AZ, Hacker CD, Pahwa M, Tagliazucchi E, Laufs H, Leuthardt EC, and Raichle ME. Human cortical-hippocampal dialogue in wake and slow-wave sleep. *Proc Natl Acad Sci U S A* 113: E6868-E6876, 2016.

Mitra A, Snyder AZ, Hacker CD, and Raichle ME. Lag structure in resting-state fMRI. *J Neurophysiol* 111: 2374-2391, 2014.

Mitra A, Snyder AZ, Tagliazucchi E, Laufs H, and Raichle ME. Propagated infra-slow intrinsic brain activity reorganizes across wake and slow wave sleep. *eLife* 4: 2015b.

Monto S, Palva S, Voipio J, and Palva JM. Very slow EEG fluctuations predict the dynamics of stimulus detection and oscillation amplitudes in humans. *J Neurosci* 28: 8268-8272, 2008.

Pan WJ, Thompson GJ, Magnuson ME, Jaeger D, and Keilholz S. Infraslow LFP correlates to resting-state fMRI BOLD signals. *Neuroimage* 74: 288-297, 2013.

Poskanzer KE, and Yuste R. Astrocytic regulation of cortical UP states. *Proc Natl Acad Sci U S A* 108: 18453-18458, 2011.

Sakata S, and Harris KD. Laminar structure of spontaneous and sensory-evoked population activity in auditory cortex. *Neuron* 64: 404-418, 2009.

Shimaoka D, Song C, and Knopfel T. State-Dependent Modulation of Slow Wave Motifs towards Awakening. *Frontiers in cellular neuroscience* 11: 108, 2017.

Silasi G, Xiao D, Vanni MP, Chen AC, and Murphy TH. Intact skull chronic windows for mesoscopic wide-field imaging in awake mice. *J Neurosci Methods* 267: 141-149, 2016.

Smith SM, Nichols TE, Vidaurre D, Winkler AM, Behrens TE, Glasser MF, Ugurbil K, Barch DM, Van Essen DC, and Miller KL. A positive-negative mode of population covariation links brain connectivity, demographics and behavior. *Nat Neurosci* 18: 1565-1567, 2015.

Stroh A, Adelsberger H, Groh A, Ruhlmann C, Fischer S, Schierloh A, Deisseroth K, and Konnerth A. Making waves: initiation and propagation of corticothalamic Ca2+ waves in vivo. *Neuron* 77: 1136-1150, 2013.

Van Dijk KR, Hedden T, Venkataraman A, Evans KC, Lazar SW, and Buckner RL. Intrinsic functional connectivity as a tool for human connectomics: theory, properties, and optimization. *J Neurophysiol* 103: 297-321, 2010.

van Kerkoerle T, Self MW, Dagnino B, Gariel-Mathis MA, Poort J, van der Togt C, and Roelfsema PR. Alpha and gamma oscillations characterize feedback and

feedforward processing in monkey visual cortex. *Proc Natl Acad Sci U S A* 111: 14332-14341, 2014.

Vanni MP, Chan AW, Balbi M, Silasi G, and Murphy TH. Mesoscale mapping of mouse cortex reveals frequency-dependent cycling between distinct macroscale functional modules. *J Neurosci* 2017.

White BR, Bauer AQ, Snyder AZ, Schlaggar BL, Lee JM, and Culver JP. Imaging of functional connectivity in the mouse brain. *PLoS One* 6: e16322, 2011.

Xiao D, Vanni MP, Mitelut CC, Chan AW, LeDue JM, Xie Y, Chen AC, Swindale NV, and Murphy TH. Mapping cortical mesoscopic networks of single spiking cortical or sub-cortical neurons. *eLife* 6: 2017.

6.8 Methods and Supplementary Materials

Methods

Mice

All procedures described below were approved by the Washington University Animal Studies Committee in compliance with AAALAC guidelines. Imaging studies were performed on transgenic mice expressing GCaMP6f under control of a mouse *Thy1* promoter acquired from Jackson Laboratories (JAX Strain: C57BL/6J-*Tg(Thy1-GCaMP6f)GP5.5Dkim*; stock: 024276) (Chen et al. 2013; Dana et al. 2014). GCaMP6/Thy1 transgenic genotypes were confirmed by PCR using the forward primer 5'-CATCAGTGCAGCAGAGCTTC-3' and reverse primer 5'-CAGCGTATCCACATAGCGTA-3'. Histology of GCaMP6 fluorescence is shown in supplemental Figure S1. Electrophysiology studies were performed on C57Bl6/J mice

(Jackson Laboratories; stock: 664). All mice were raised in standard cages in a dedicated mouse facility with a 12hr-12hr light/dark cycle.

Animal Preparation for Optical Imaging

Seven GCaMP6 mice (12-16weeks of age, 28-36g) were used for imaging in this study. Mice were sedated with isoflurane (3% induction, 1% maintenance, 0.5 L/min) and placed in a stereotactic holder. The head was then shaved, and a midline incision made to expose the skull. Body temperature was maintained at 37°C using a temperature controlled heating pad. Chronic cranial windows made of Plexiglas and with pre-tapped holes were fixed to the skull using dental cement (C&B-Metabond, Parkell Inc., Edgewood, NY, USA).

Animal Preparation for Electrophysiology

Ten C57Bl6/J mice were used to obtain electrophysiological recordings. Mice were given dexamethasone (20μL 4mg/mL, S.C.) 4 hours prior to surgery, and mannitol (150 μL, 20% manitol, I.P.) immediately prior to surgery. Mice were anesthetized using isoflurane anesthesia (3% induction, 1.5% maintenance). Once anesthetized, lidocaine anesthetic was given locally, scalp hair was removed, a midline incision was made in the scalp, and the scalp was retracted. The periosteal membranes were removed. Two craniectomies (1mm in diameter) were performed over the motor and visual locations determined by stereotactic coordinates derived from the Granger Causality analysis shown in main text Figure 2C (Motor cortex = 1.5 mm Left of bregma, 1.6 mm anterior to bregma; visual cortex = 2.6 mm Left of bregma, 3.0 mm posterior to bregma). A third

craniotomy was made on the right hemisphere (2.3 mm Right of bregma, 0.9 mm anterior to bregma), and a permanent ground wire was placed and secured with C&B Metabond dental cement (Parkell Inc., Edgewood, NY, USA). A custom-made fixation block with screw threading was attached to the skull with dental cement (to enable head fixation during recording). The left hemisphere craniectomies were covered with a self-healing silicone polymer that allowed silicone electrodes to pass through undamaged. Mice were given S.C. buprenorphine at the end of the procedure for pain control, and mice were given 5 days of recovery time before any recording was performed.

Optical Imaging System

Sequential illumination was provided by four LEDs: 470nm (measured peak λ=454nm (referred to as 454nm LED in this study), LCS-0470-15-22, Mightex Systems, Pleasanton, CA, USA), 530nm (measured peak λ=523nm, LCS-0530-15-22), 590nm (measured peak λ=595nm, LCS-0590-10-22), and 625nm (measured peak λ=640nm, LCS-0625-03-22). The 454nm LED is used for GCaMP excitation, and the 523nm, 595nm, and 640nm LEDs are used for multispectral oximetric imaging. The 523nm LED was also used as an emission reference for GCaMP6 fluorescence in order to remove any confound of hemodynamics in the fluorescence signal (described below). Both the 454nm and 523nm LED light paths were made collinear by using a multi-wavelength beam combiner dichroic mirror (LCS-BC25-0505, Mightex Systems, Pleasanton, CA, USA). For image detection, we used a cooled, frame-transfer EMCCD camera (iXon 897, Andor Technologies, Belfast, Northern Ireland, United Kingdom) in combination

with an 85mm f/1.4 camera lens (Rokinon, New York, NY, USA). The acquisition framerate was 16.8Hz per channel, with the overall framerate of the camera as ~67HZ. This framerate is well above the temporal resolution necessary to adequately characterize hypothesized GCaMP6 activity. To increase frame rate as well as increase SNR, the CCD was binned at 4 x 4 pixels; this reduced the resolution of the output images from full-frame 512 x 512 pixels to 128 x 128 pixels. Both the LEDs and the exposure of the CCD were synchronized and triggered via a DAQ (PCI-6733, National Instruments, Austin, TX, USA) using MATLAB (MathWorks, Natick, MA, USA). The field-of-view was adjusted to be approximately 1 cm^2 resulting in an area that covered the majority of the convexity of the cerebral cortex with anterior-posterior coverage from the olfactory bulb to the superior colliculus. The resulting pixels were approximately 78µm x 78µm. To minimize specular reflection from the skull, we used a series of linear polarizers in front of the LED sources and the CCD lens. The secured mouse was placed at the focal plane of the camera. The combined, collimated LED unit was placed approximately 8 cm from the mouse skull, with a working distance of approximately 14cm as determined by the acquisition lens. A 515nm longpass filter (Semrock, Rochester, NY, USA) was placed in front of the CCD to filter out 470nm fluorescence excitation light and a 460/60nm bandpass filter (Semrock, Rochester, NY, USA) was used in front of the excitation source to further minimize leakage of fluorescence excitation light through the 515nm longpass filter. The pulse durations for the LEDs are 20ms, 5ms, 3ms, 1ms for 454nm, 523nm, 595nm, and 640nm, respectively.

Electrophysiology system

For electrophysiology recordings, mice were placed on a felt hammock and the skull was fixed to a secure bar via the fixation block. Two 1.5mm 16-channel linear array electrodes (NeuroNexus model number A1x16-5mm-100-703-A16, Ann Arbor, MI, USA) were attached to separate micromanipulators (David Kopf Instruments, Los Angeles, California, USA). Electrodes were painted with DiI (1,1'-Dioctadecyl-3,3,3',3'-Tetramethylindocarbocyanine Perchlorate; Sigma-Aldrich, St. Louis, MO, USA), and placed into the brain (through the transparent silicone sealant which enabled direct visualization of the cortex) under direct visualization using a surgical stereoscope (Olympus, Tokyo, Japan). Electrode placement was confirmed in three ways: 1) the most superficial contact was visually guided to just under the cortical surface; 2) the electrophysiological signal in the most superficial contact during the transition from noise/air to brain was monitored 3) electrodes were painted with DiI and placement was confirmed with histologic sections of the mouse brain (main text Fig. 3A). Local field potentials were recorded using an amplifier with high-pass filter cutoff of .02Hz (Intan RDH2132) connected to the recording computer through an acquisition board (OpenEphys), with a reference wire positioned on the right hemisphere contralateral to the electrodes (2.3 mm Right of bregma, 0.9 mm anterior to bregma). All recordings were made in a completely dark room. For each mouse, awake recordings were done first, followed by ketamine/xylazine administration via I.P. injection in the same session (i.e., without removing the electrodes from the brain).

Awake recordings

As described in the electrophysiology system description, awake mouse recordings (imaging and electrophysiology) were performed by mice on a felt hammock with head-fixation, either to the optical window in the case of imaging or to the skull in the case of electrophysiology. The hammock provided a dark, comfortable environment while preventing the awake mouse from applying torque on their restrained head. After recovery from surgery, the mouse was acclimated to the hammock apparatus by a training period consisting of two 20min sessions. Acclimation is indexed by a return to normal behavior (e.g., whisking, grooming, and walking with head restrained). Though no accelerometers or other behavioral measures were used to track motion within the pouch during recordings, mice were qualitatively observed to be relaxed with infrequent limb motion after completion of the acclimation protocol. Awake imaging was performed for 60 minutes on two separate days, separated by two weeks, in each of the 7 mice analyzed in this study. The 60 minute imaging sessions were acquired over 12 5-minute runs. Awake electrophysiology was acquired continuously for 60 minutes in 10 mice.

Anesthetized recordings

For anesthetized imaging and electrophysiology, mice were anesthetized with I.P. injection of a ketamine/xylazine cocktail (86.9 mg/kg Ketamine, 13.4 mg/kg Xylazine). Anesthetic effect was verified by confirming that the animal was not responsive to a hind paw pinch. The animal was placed and kept on a solid state water circulating heating pad (T/Pump Classic, Stryker Co., Kalamazoo, MI, USA), maintained at 42°C. Anesthetized imaging was performed for 45 minutes (the duration of anesthetic effect) on two separate days, separated by two weeks, in each of the 7 mice analyzed in this

study. The 45 minute imaging sessions were acquired over 9 5-minute runs. Anesthetized electrophysiology was acquired continuously for 45 minutes in 10 mice.

Epifluorescence and Confocal Imaging

Mice were deeply anesthetized with FatalPlus™ (Vortech Pharmaceuticals, Dearborn, MI, USA) and transcardially perfused with 0.01 M PBS. The brains were removed and fixed in 4% paraformaldehyde for 24 h and transferred to 30% sucrose in 0.2 M PBS. After brains were saturated, they were snap-frozen on dry ice and coronal sections, 50 µm thick, were made with a sliding microtome. Sections were stored in 0.2 M PBS, 30% sucrose, and 30% ethylene glycol at −20°C. For viewing, cut sections were washed in PBS, mounted, and intrinsic GCaMP6 fluorescence was examined with epifluorescence microscopy (Nikon Eclipse 80i, Nikon Instruments Inc., Melville, NY, USA). For viewing using confocal microscopy, additional cut sections were washed in PBS, mounted, and coverslipped in DAPI containing mounting media (Vector Laboratories, Burlingame, CA, USA). Fluorescent images were acquired with a Nikon A1-Rsi inverted confocal microscope using a 10x objective. DAPI labeled cells and electrode marker DiI were excited with 405nm and 560nm laser lines, respectively (Nikon A1-Rsi, Nikon Instruments Inc., Melville, NY, USA).

Image Processing

A representative frame of baseline light levels in a dark environment, calculated from a mean of dark images collected over 1 minute, was subtracted from the raw data. All pixel time traces were individually detrended to remove any variations in light levels due

to photobleaching, LED current drift, and nonuniformity across the skull (Kubota et al. 2008). Reflectance changes in the 523nm, 595nm, and 640nm LED channels were used in combination to provide oximetric data using the Modified Beer-Lambert Law, described previously (White et al. 2011). Images in each contrast were smoothed with a Gaussian filter (5x5 pixel box with a 1.3 pixel standard deviation). The GCaMP6 fluorescent signal must be corrected for any contribution from vascular activity and varying concentrations of absorptive hemoglobin. Though the effects of hemodynamics will likely not mask the emission signals entirely, they will influence them. Common correction methods to calculate relative fluorescence changes include using a reference wavelength for applying subtraction and ratiometric techniques. We implemented a ratiometric correction algorithm (Equation 1) to correct fluorescent emission for any absorption by hemoglobin and deoxyhemoglobin using the reflectance channels at the GCaMP6 emission wavelengths (523nm LED) as a reference.

$$y(t) = \frac{I^{em}(t)}{I^{ref}(t)} \cdot \frac{I_0^{ref}}{I_0^{em}} \qquad \text{[E1]}$$

I^{em} refers to the detected fluorescent emission intensity. I^{ref} describes the measured reflectance changes at the emission wavelength. A single frame from the 628nm reflectance channel was loaded into Adobe Photoshop CC 2014 (Adobe Systems, San Jose, CA, USA) and all regions not corresponding to brain were manually painted white. The image was loaded back into MATLAB and used to create a binary brain mask. All subsequent analysis was performed on those pixels labeled as brain. Image sequences from each mouse (as well as the brain mask for each mouse) were affine-transformed to a common atlas space (based on the Paxinos mouse atlas) using the positions of bregma and lambda (Franklin & Paxinos, 2008).

Electrophysiology Signal Processing

16-channel recordings were referenced to a ground wire positioned on the right hemisphere contralateral to the electrodes (2.3 mm Right of bregma, 0.9 mm anterior to bregma). To further verify that 16 channels spanned the depth of motor cortex and 12 channels spanned the depth of visual cortex (main text Figure 2A), we analyzed the spectral content of all channels. We found very similar spectral content in all 16 channels of motor cortex in all recordings, indicating that all channels were likely in cortex. In contrast, channels 13-16 in visual cortex exhibited far lower power than channels 1-12, indicating that 12 channels span the depth of visual cortex, and that channels 13-16 were in underlying white matter (and hence excluded from analysis). 60Hz notch filtering was applied to remove electronic noise from the data (Supplemental Figure S6).

Computation of correlation and temporal lags:

As described in main text Figure 1B-C, conventional correlation analysis involves computation of the Pearson correlation, r, between the time series, $x_1(t)$, extracted from a seed region, and a second time series, $x_2(t)$, extracted from some other locus (single pixel or region of interest). Thus,

$$r_{x_1x_2} = \frac{1}{\sigma_{x_1}\sigma_{x_2}}\frac{1}{T}\int x_1(t)\cdot x_2(t)dt, \qquad \text{[E2]}$$

where σ_{x_1} and σ_{x_2} are the temporal standard deviations of signals x_1 and x_2, and T is the interval of integration. Here, we generalize the assumption of exact temporal synchrony and compute lagged cross-correlation functions. Thus,

$$r_{x_1x_2}(\tau) = \frac{1}{\sigma_{x_1}\sigma_{x_2}}\frac{1}{T}\int x_1(t+\tau)\cdot x_2(t)dt, \qquad \text{[E3]}$$

where τ is the lag (in units of time). In both optical and electrophysiological recordings, lagged correlation curves were computed between pairs of recordings (pixels and electrodes, respectively). The value of τ at which $r_{x_1x_2}(\tau)$ exhibits an extremum defines the temporal lag (equivalently, delay) between signals x_1 and x_2 (Konig 1994). The value of $r_{x_1x_2}(0)$ is the traditional zero-lag Pearson correlation. All pairs of temporal lags and zero-lag correlations define time-delay (TD) and functional connectivity (FC) matrices, respectively. In the imaging data, 16.8Hz temporal sampling density limits detection of empirical temporal delays to ~60ms; however, we apply parabolic interpolation to imaging-derived lagged cross-correlation curves to detect temporal delays shorter than the temporal sampling rate, as previously described (Mitra et al. 2016; Mitra et al. 2014). There is strong agreement between empirical temporal delay matrices and temporal delay matrices computed using parabolic interpolation (Pearson r = 0.99 between measurements) in delta activity under anesthesia, as well as infra-slow activity measured in wake and anesthesia. The exception is delta activity during wake, where parabolic interpolation uncovers short temporal lags (+/-10 ms in main text Figure 1E) that cannot be measured empirically. Critically, wake delta activity temporal delays computed using parabolic interpolation are stable over two days of measurement (Supplemental Figure 1), agree with previous findings in the literature acquired with higher temporal sampling rates (Shimaoka et al. 2017), and agree with the present electrophysiological findings sampled at 300Hz (main text Figure 3C). Parabolic interpolation was only applied to the imaging data; electrophysiological temporal delays were computed empirically as the data was acquired at a much higher temporal sampling density.

Computation of group-level FC and TD matrices

In the imaging data, lagged-correlations were computed between every pair of pixels in the brain for each 5 minute run. FC and TD matrices computed over 5 minute runs were then averaged for each mouse across wake and anesthesia sessions. Separate averages computed for each mouse for each day of imaging allowed us to verify cross-day stability (Supplemental Figure 1). Occasionally, the spectral content of an awake imaging run contained delta signatures of sleep (see Figure S3B-D); these runs were omitted from the awake analysis, leading to a loss of 5.2% of the total wake imaging data collection. Group level FC and TD matrices are computed from the average of individual mouse FC and TD matrices over both days of imaging. A similar strategy was applied to compute FC and TD matrices in the electrophysiology data. Although the electrophysiological data was acquired continuously, to match the imaging analyses, we split the recordings into 5 minute epochs and computed FC and TD matrices in each epoch. Epochs were then averaged first within a mouse (wake and anesthesia), and then across mice, to produce main text Figure 3 and Supplemental Figure 2. As in the imaging data, we also used delta power to exclude likely periods of sleep from the wake electrophysiology (see Figure S3). As a result, one of the ten mice from which we recorded electrophysiology yielded no usable wake data, leading to nine mouse data sets in the electrophysiology analyses. In the remaining 9 mice, 8.3% of total wake data was omitted due to putative sleep.

Computation of group-level phase-frequency plot

Time series were extracted, in the imaging data, from visual and motor regions of interest (ROIs), shown in main text Figure 2. Then, in each 5 minute epoch of usable data, ROI time series were filtered into a double-octave frequency bin (0.02-0.08Hz ranging to 1.28-5.12Hz). For each 5 minute epoch and each double-octave frequency bin, the phase relationship between motor and visual time series was computed. These phase relationships were then averaged first within, then across, sessions as described for the computation of FC and TD matrices.

Computation of group-level Granger Causality (GC)

GC analysis was performed in the time domain using Anil Seth's GC toolbox (Barnett and Seth 2014). Time series were extracted, in the imaging data, from visual and motor ROIs shown in main text Figure 2. These time series were then filtered into delta (1-4Hz) and ISA (0.02-0.1) frequency ranges, in anesthesia and wake. As GC does not lend itself to averaging over epochs, we concatenated 5 minute epochs of time series, in each frequency band, over sessions and mice. We then applied time domain GC analysis to these concatenated time series in each frequency band, where the auto-regressive model order was set to 150% of the lowest frequency in the frequency bin (e.g., 75 seconds for ISA, 1.5 seconds for delta), as recommended (Barnett and Seth 2014). Statistically significant GC was found in every case ($p < 0.01$) except wake delta, where GC was detected but with a p-value of 0.25.

Computation of statistical significance

The high dimensionality of the presently analyzed data required the use of various non-parametric means for assessing statistical significance, described below:

(1) Statistical differences in TD matrices in Figure 1E: As described in the computation of group-level FC and TD matrices, group-level TD matrices are computed by averaging TD matrices computed over 5 minute epochs first within then across mice. Therefore, to test for statistical significance between group-level TD matrices, we computed group-level TD matrices in which the underlying 5 minute epoch TD matrices were randomly permuted (either over ISA vs. delta, or wake vs. anesthesia). We then computed a null-distribution of magnitude difference (Euclidian distance) between surrogate group-level TD matrices. On the basis of this null-distribution, we conclude that differences in the TD matrices in Figure 1E are statistically significant ($p < 0.001$), both across ISA vs. delta, as well as across wake vs. anesthesia.

(2) Statistical differences in lag projections in Figure 2A: Same strategy as (1) above, except surrogate group-level TD matrices were transformed into lag projections (through column-wise means) to produce surrogate group-level lag projections. The null-distribution was then computed as a vector Euclidian distance between lag projections, treating the images as 1-dimensional vectors (e.g., one number per brain pixel). On the basis of this null-distribution, we conclude that differences in the lag projections in Figure 2A are statistically significant ($p < 0.001$), both across ISA vs. delta, as well as across wake vs. anesthesia.

(3) Statistical differences in FC and TD matrices in Figures 3B-C: Precisely the same approach outlined in (1) above, applied to electrophysiology FC and TD matrices.

(4) Statistical thresholding of temporal delays in Figure 3C: Surrogate temporal delays were computed for each pair of recordings by randomly phase-permuting filtered time series prior computation of lagged correlations, resulting in a null-distribution of temporal delays. The empirical distribution of temporal delays between each pair of channels (recall TD was computed for each mouse over 5-minute epochs) was then compared to the null-distribution with the Kolmogorov-Smirnov test. The correlation matrices in Supplemental Figure S3G-I makes plain that channels within a cortical layer are not independent; thus, we apply a Bonferroni-correction on layers (6*6 = 36) such that only temporal delays with $p < 0.001$ are shown as significant.

(5) Statistical significance of phase-amplitude coupling (PAC) in Figure 3E: The null-hypothesis for the phase-amplitude histograms shown in Figure 3E is a uniform distribution. Therefore, we tested for significant PAC by using the Kolmogorov-Smirnov test to compare the empirical PAC histograms to a uniform distribution, resulting in a p-value < 0.001. We also applied a second permutation-based test of PAC using modulation index as described in (Canolty et al. 2006). In essence, PAC can be thought of as a vector on a circle depicting a preferred phase relationship between a pair of signals; the length of this vector is the modulation index. By randomly permuting the underlying signals, a surrogate PAC vector is computed, along with its length (e.g., a surrogate modulation index). The null-distribution of surrogate modulation indices provides a test of statistical significance. By this measure as well, the presently observed PAC (imaging and electrophysiology) is highly significant ($p < 0.001$).

Supplemental Figures

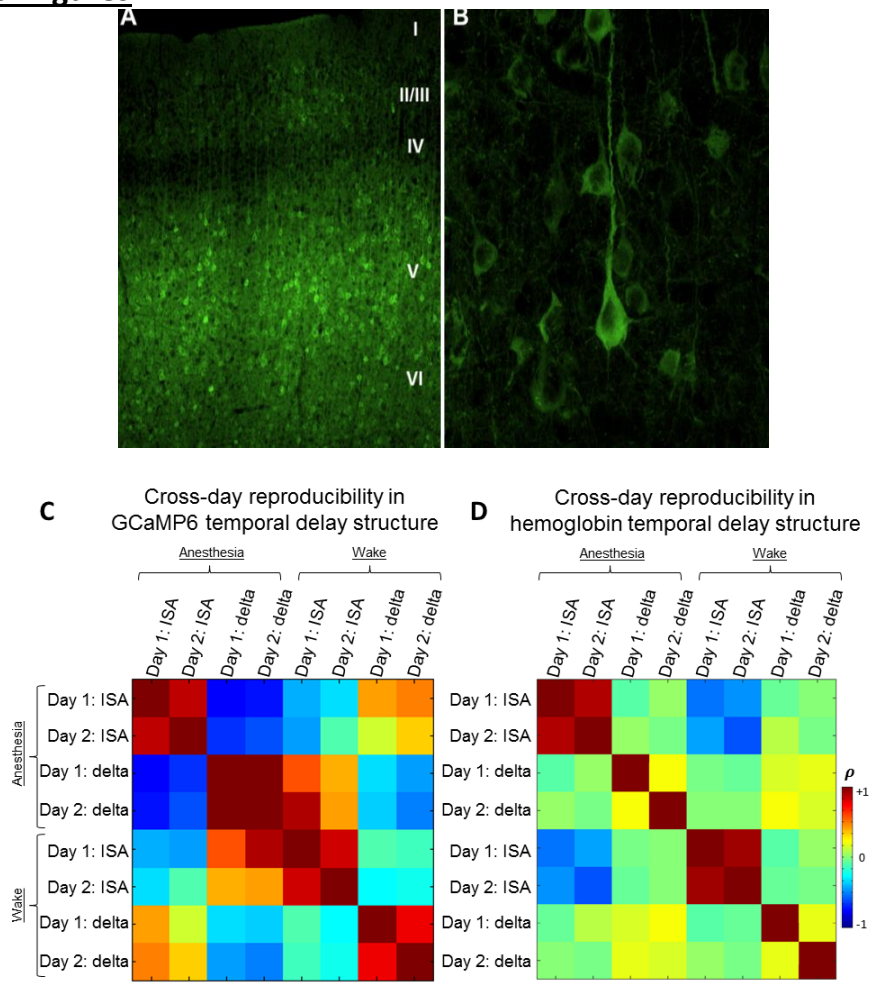

Figure S1: Confocal fluorescence images of a 50 µm section from a representative *Thy1*-GCaMP6f mouse. *(A)* GCaMP is expressed in all cortical layers, while strongest expression is deeper in cortical layers V/VI (100 µm scale bar). *(B)* GCaMP expression is cytoplasmic, and its fluorescence reflects calcium dynamics in both the cell body and distal processes (20 µm scale bar). GCaMP6 temporal delay structure is highly reproducible across two days of imaging. Each of the seven mice analyzed in this study was imaged in two separate sessions (wake and anesthesia) separated by two weeks. We therefore compared group-average day 1 vs. day 2 TD matrices using Spearman rho correlations, in ISA vs. delta, over anesthesia and wake. *(C)* TD comparisons in the GCaMP6 signal. The 2x2 blocks along the diagonal establish that day 1 and day 2 TD matrices are highly similar. Moreover, the anti-correlations between delta and ISA within state (e.g., within anesthesia and within wake) demonstrate that the reciprocal travel of ISA and delta is also highly reproducible. *(D)* TD comparisons in the total hemoglobin signal. Note that only ISA temporal delay structure is strongly reproducible across day 1 and day 2; delta TD structure is not nearly as reproducible. Moreover, anti-correlations are only observed between ISA in anesthesia vs. wake.

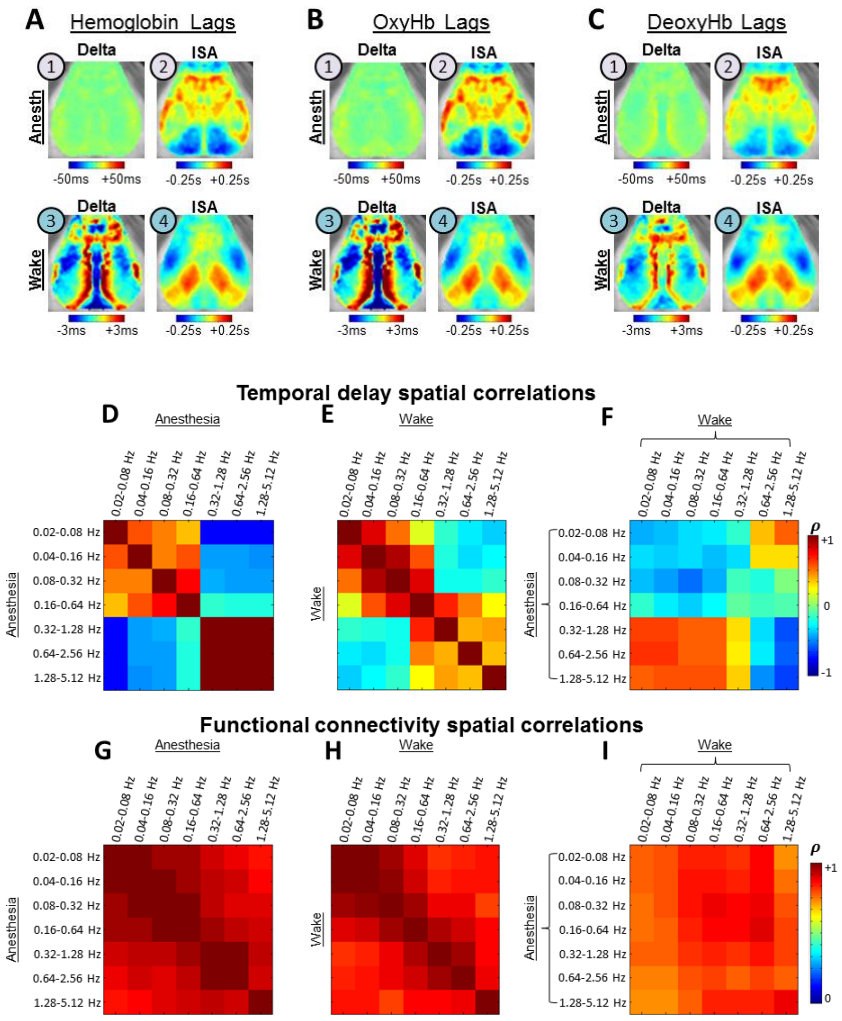

Figure S2: **Lag projections are concordant across total hemoglobin, oxyhemoglobin (OxyHb), and deoxyhemoglobin (DeoxyHb) signals. *(A)* Re-capitulation of total hemoglobin lag projection images from main text Figure 2B, computed in anesthesia and wake, in delta and infra-slow frequencies. *(B)* Lag projections computed using oxyhemoglobin signals. *(C)* Lag projections computed using deoxyhemoglobin signals. Whole-cortex GCaMP6 TD and FC matrix comparisons parametric in frequency under anesthesia and during wakefulness. *(D-F)* Each matrix entry reports the similarity (rank-order correlation) between a pair of TD matrices. (D-C) repeat the analyses in Figure 2E. (F) Similarities between anesthesia TD matrices and wake TD matrices. Note that higher frequency (>0.64Hz) anesthesia TD matrices resemble lower frequency (<0.32Hz) wake TD matrices. Similarly, higher frequency (>0.64Hz) wake TD matrices resemble lower frequency (<0.16Hz) anesthesia TD matrices. Moreover, lower frequency anesthesia vs. wake TD matrices are anti-correlated, as are higher frequency anesthesia vs. wake TD matrices. These results establish that temporal sequences reverse directions between wake and anesthesia. *(G-I)* The same analyses as in (D-F), but now applied to FC matrices. Note that FC matrices over double-octaves are much more similar than are the corresponding TD matrices. FC matrices are also more similar across state (wake vs. anesthesia in panel (I)) than are TD matrices.**

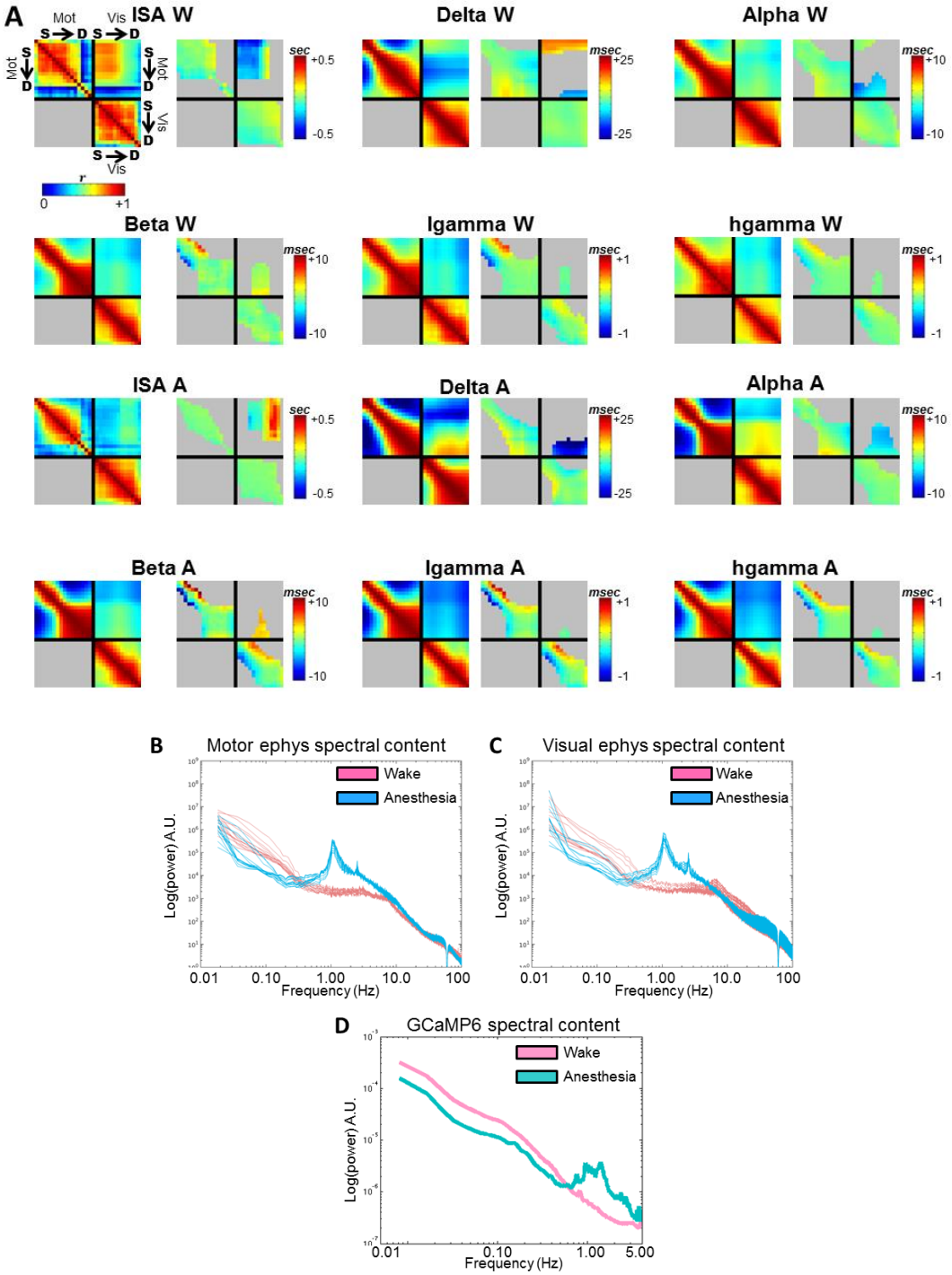

<u>Figure S3:</u> Laminar correlation and time delay matrices, as in Figure 3B-C, over 0.02-100Hz. *(A)* Each analyzed frequency band, for example ISA, appears twice in this figure: once for the wake analysis (W) and once for the anesthetized analysis (A). Frequency bands are defined as follows: ISA = 0.02-0.1Hz, delta = 1-4Hz, alpha = 8-12Hz, beta = 12-30Hz, lgamma = 30-60Hz, hgamma = 60-100Hz. We omitted theta (4-6Hz) from this figure as the results look nearly identical to the delta band analyses. Looking at the ISA wake (ISA W) in detail, the two matrices correspond to correlations (FC; on the left) and time delays (TD; on the right). Furthermore, each matrix displays intra- and inter-laminar relationships. Thus, the upper left (16x16) block of the FC matrix in ISA

wake shows intra-laminar relationships within the motor cortex, where row and columns are sorted from superficial to deep. The lower right (12x12) block of the FC matrix in ISA wake shows intra-laminar relationships within the visual cortex, where row and columns are sorted from superficial to deep. Finally, the upper right block (16x12) shows inter-laminar relationships between motor and visual cortex. Hence, the upper right block of the ISA W FC matrix is a repeat of image 4 in main text Figure 3B. These images demonstrate frequency specificity of spontaneous cross-laminar relationships between visual and motor cortex. Moreover, note that the apparent reversal of visual-motor signal direction in ISA and delta activity, between wake and anesthesia, is not observed in higher frequencies. Spectral content of spontaneous activity in wake vs. anesthesia. *(B)* Spectral content of spontaneous activity of 16-channels in motor cortex, during wake (pink) and anesthesia (teal). Note that a prominent delta power peak is present during anesthesia. Delta power peaks are also seen during sleep, and this spectral feature was used to exclude putative sleep periods from the wake data. Spectral drop-out and 60Hz reflects notch-filtering to reduce electronic noise. *(C)* Spectral content of spontaneous activity of 12-channels in visual cortex, during wake (pink) and anesthesia (teal). *(D)* Spectral content of spontaneous GCaMP6 activity, averaged over all pixels, during wake (pink) and anesthesia (teal).

Supplemental References

Barnett L, and Seth AK. The MVGC multivariate Granger causality toolbox: a new approach to Granger-causal inference. *J Neurosci Methods* 223: 50-68, 2014.

Canolty RT, Edwards E, Dalal SS, Soltani M, Nagarajan SS, Kirsch HE, Berger MS, Barbaro NM, and Knight RT. High gamma power is phase-locked to theta oscillations in human neocortex. *Science* 313: 1626-1628, 2006.

Chen TW, Wardill TJ, Sun Y, Pulver SR, Renninger SL, Baohan A, Schreiter ER, Kerr RA, Orger MB, Jayaraman V, Looger LL, Svoboda K, and Kim DS. Ultrasensitive fluorescent proteins for imaging neuronal activity. *Nature* 499: 295-300, 2013.

Dana H, Chen TW, Hu A, Shields BC, Guo C, Looger LL, Kim DS, and Svoboda K. Thy1-GCaMP6 transgenic mice for neuronal population imaging in vivo. *PloS one* 9: e108697, 2014.

Konig P. A method for the quantification of synchrony and oscillatory properties of neuronal activity. *J Neurosci Methods* 54: 31-37, 1994.

Kubota Y, Kamatani D, Tsukano H, Ohshima S, Takahashi K, Hishida R, Kudoh M, Takahashi S, and Shibuki K. Transcranial photo-inactivation of neural activities in the mouse auditory cortex. *Neuroscience research* 60: 422-430, 2008.

Mitra A, Snyder AZ, Hacker CD, Pahwa M, Tagliazucchi E, Laufs H, Leuthardt EC, and Raichle ME. Human cortical-hippocampal dialogue in wake and slow-wave sleep. *Proc Natl Acad Sci U S A* 113: E6868-E6876, 2016.

Mitra A, Snyder AZ, Hacker CD, and Raichle ME. Lag structure in resting-state fMRI. *J Neurophysiol* 111: 2374-2391, 2014.

Shimaoka D, Song C, and Knopfel T. State-Dependent Modulation of Slow Wave Motifs towards Awakening. *Frontiers in cellular neuroscience* 11: 108, 2017.

White BR, Bauer AQ, Snyder AZ, Schlaggar BL, Lee JM, and Culver JP. Imaging of functional connectivity in the mouse brain. *PLoS One* 6: e16322, 2011.

Chapter 7: Conclusions

7.1 Summary of Results

Spontaneous activity has played a prominent role in our growing understanding of brain function over the past decades. Thanks in large part to advances in neuroimaging, we now understand that spontaneous activity accounts for a majority of the brain's metabolic cost (Raichle 2011; Raichle and Mintun 2006), that spontaneous fluctuations in brain activity are dominated by very low frequencies (He et al. 2008; Leopold et al. 2003; Ma et al. 2016; Pan et al. 2013), and that these low frequency fluctuations in brain activity are correlated (functionally connected) within large systems spanning the entire brain (Fox and Raichle 2007; Fox et al. 2005; Power et al. 2011; Yeo et al. 2011). The aim of this thesis was to ask, can we go further? In particular, is there any meaningful temporal organization in infra-slow brain activity, and might this reveal to us anything about the fundamental neurophysiology underlying the remarkable systems organization of very low frequencies?

The answer, as detailed in the previous chapters, is an emphatic "yes". In Chapter 2, we laid out an analytic technique for measuring brain-wide temporal structure in infra-slow fMRI data, demonstrating that parabolic interpolation can be applied to cross-correlation functions to measure temporal delays below the resolution of the fMRI temporal sampling rate. We also found that the temporal structure of resting state fMRI is highly stable at the group level, is not attributable to simple blood flow metrics, and exhibits a relationship to canonical resting state networks. In Chapter 3, we explored this relationship between temporal and correlation structure to find that correlations within

networks arise as a consequence of structured temporal relations in resting state fMRI data which we call “lag threads”.

Chapters 4-6 aimed to better understand the function and neurophysiology of directed temporal structure of resting state fMRI signals. Chapter 4 showed that the temporal organization of resting state fMRI is drastically altered across human wakefulness and slow wave sleep, suggesting that the direction very low frequency signals move through the brain might shape the broad state of brain function. Chapter 5 built on this hypothesis by exploring directed infra-slow signaling between human hippocampus and cortex in wakefulness and slow wave sleep in the context of the two-stage theory for memory consolidation. We demonstrate that the direction of infra-slow signals between hippocampus and cortex is consistent with the direction of feedback “coordination” signals (Buzsaki 1996; 1989; Sirota and Buzsaki 2005) during both wake and sleep. Furthermore, in Chapter 5, we showed for the first time correspondence between temporal structures across infra-slow fMRI and electrophysiology, at least between the hippocampus and cortex. Agreement between electrophysiology and fMRI bolstered our assumptions that fMRI measures an infra-slow brain process, and validated our use of parabolic interpolation in fMRI cross-correlation functions, as temporal offsets derived from electrophysiology with fast temporal sampling were empirical. Finally, in Chapter 5 we found that delta band (1-4 Hz) activity travels in the reciprocal direction, between hippocampus and cortex, from that of infra-slow activity. This finding suggested that the temporal structure of spontaneous activity might be frequency-specific.

In Chapter 6, we moved to the mouse model and used optical imaging and laminar electrophysiology to explicitly explore the idea that temporal structure varies across frequencies of neural activity. Through a combined analysis of calcium activity, blood oxygen level dependent signals, and electrophysiology, we found that infra-slow activity travels through spatio-temporal trajectories across the mouse cortex that are distinct from trajectories found in higher frequencies, including the relatively slow delta band. Moreover, we found that the temporal structure of infra-slow blood oxygen signals corresponds specifically to infra-slow electrophysiology and calcium activity, demonstrating that a specific neurophysiology is responsible for the temporal organization of blood oxygen signals. We also found that infra-slow brain activity travels across mouse cortex through specific cortical layers which are again differentiable from delta and higher frequency activity. Finally, the directions of travel in spontaneous infra-slow and delta activity are reciprocal, and are to a first approximation reversed across states of conscious awareness.

These investigations represent merely a beginning of our understanding of the way infra-slow signals move through the brain, and what the significance of directed infra-slow signaling in spontaneous activity may be. However, we can summarize the previous chapters into a set of rules and principles, which I outline below

7.2 Principle 0: Never fear to compute, but never compute out of fear

This dictum is more philosophical than scientific, but nonetheless bears mentioning. We have faced surprising resistance to the idea that interpolation can be used to compute super resolution temporal delays in fMRI, even though the concept of smoothing

auto/cross-correlation functions (whether in space or time) to achieve super resolution is quite old, and in fact forms the basis of super resolution light microscopy (Betzig et al. 2006). Of course, it is important to verify that the results of an interpolation-based computation are stable and robust. Yet, even having done so (Mitra et al. 2014), the fMRI community has proven somewhat wary, with many arguing that higher resolution technologies are necessary to achieve further insight. The present work argues against the absolute need for better technology to achieve better scientific understanding. By overcoming our pre-conceived fears of data limitations and doing some simple computations, it is surprising how much can be learned from extant technologies.

On the other hand, the general skepticism of new analytic methodologies in the fMRI community may stem from the proliferation of measures, ranging from a menagerie of graph theoretic measures (modularity, efficiency, connectedness, spring embedding, etc.) to measures like entropy, dynamic functional connectivity, dynamic connectivity modeling, and so on. The jury is still out, but in hindsight many of these approaches may prove to be “computation out of fear”, that is, applications of advanced computational machinery without a clear basis or purpose. One of the nice features of computing temporal delays is that they are theoretically simple, easily interpreted, and they imply a clear falsifiable hypothesis: that there is directed signaling with a system. I suspect that computational methods meeting these criteria will, over time, add more value than those that do not.

7.3 Principle 1: Infra-slow activity generally moves unidirectionally within networks

Lagged correlation curves indicate the average directionality between a pair of time series. Thus, finding a directed temporal lag in a cross-correlation does not preclude occasional signaling in the reverse direction, but it does imply that signaling in one direction is more prominent than the other. With this caveat in mind, when we computed the temporal structure of resting state fMRI signals in Chapter 2, we found that there is a clear directionality to signal travel within resting state networks. Each of the commonly studied resting state networks (Hacker et al. 2013) has early and late nodes. For example, as shown in Figure 1A-B, within the dorsal attention network (DAN), the frontal eye fields (FEF) are early with respect to the intra-parietal sulci (IPS). Another example, illustrated in Figure 1C-D, is the default mode network (DMN), where retrosplenial cortex (RSC) leads posterior parietal, precuneus, and medial frontal cortices (PPC, PCC, mPFC). Thus, common statements of the type “functional connectivity between the RSC and mPFC means that these cortices talk to each other” are incorrect. Instead, the RSC very specifically sends infra-slow signals to the mPFC (bearing in mind the caveat regarding the interpretation of lagged correlations we mentioned already).

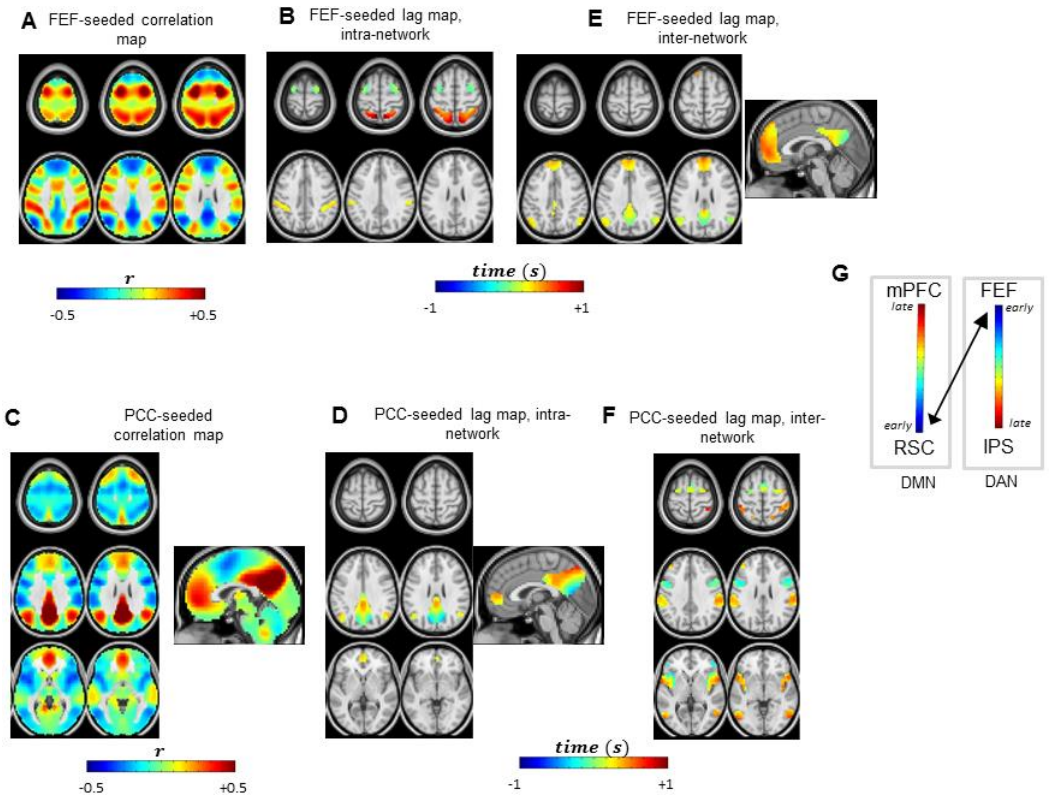

Figure 7-1: Intra- and inter-network signaling in the dorsal attention and default mode networks. (A) A frontal eye field (FEF)-seeded correlation map, as in conventional functional connectivity studies. The red areas reveal the dorsal attention network (DAN) topography; blue areas highlight regions outside the DAN, especially the default mode network (DMN). (B) A FEF-seeded lag map within areas of eye correlation with the FEF, defined using (A). The idea is to examine temporal lags within the DAN. (B) shows that FEF regions are blue whereas areas in the intra-parietal sulcus (IPS) are red, indicating that BOLD signals tend to move from FEF to IPS within the DAN. (E) A FEF-seeded lag map with areas anti-correlated with the FEF, defined using (A). The idea is to examine temporal lags between activity in the FEF and activity in nodes of another network, the DMN. Note that the PCC is blue/green, whereas the posterior parietal cortex (PPC) is yellow, and the medial prefrontal cortex is orange/red. Hence, the PCC is the least delayed with respect to the FEF, followed by the PPC, and finally the mPFC. (C) A posterior precuneus cingulate (PCC)-seeded correlation map, as in conventional functional connectivity studies. The red areas reveal the DMN topography; blue areas highlight regions outside the DMN, especially the DAN. (D) A PCC-seeded lag map within areas of eye correlation with the FEF, defined using (C). The idea is to examine temporal lags within the DMN. (D) shows that PCC regions are blue whereas areas in the PPC are yellow, and the mPFC region is orange. This result demonstrates the back-to-front temporal sequence for activity within the DMN. (F) A PCC-seeded lag map with areas anti-correlated with the PCC, defined using (D). The idea is to examine temporal lags between activity in the PCC and activity in nodes of another network, the DAN. Note that the FEF is green/yellow, whereas the IPS is orange/red. Hence, in the DAN, the FEF is the least delayed with respect to the IPS. (G) A schematic summary of the spatial and temporal relationships between the DMN and the DAN depicted in the images (A) through (F).

In Chapter 3 we further found that the strong correlations within resting state networks are in fact a consequence of unidirectional signal travel, and in Chapter 4, we showed that this one-way within-network signal travel is preserved across wake and sleep. The idea that infra-slow signals move unidirectionally within networks, and that this unidirectional travel is preserved across very different states of brain function, adds a new dimension to the interpretation of resting state networks. As opposed to reflecting noisy cross-talk within the elements of the network, it would appear that infra-slow signals may have a computational role in coordinating activity within networks; otherwise, it is difficult to imagine why the brain would take the trouble to maintain such order in intra-network infra-slow signaling. Yet, for now, what this computational role might be, and how it is physiologically enacted in the brain, is not known.

Probing the computational purpose of unidirectional infra-slow activity within networks may prove tricky, as disrupting this property may entail significantly altering brain function, with all its attendant difficulties in interpretation. Finding the physiological basis of early versus late nodes within a network may be simpler. Examining commonalities in receptor make-up and gene expression within “early” nodes in the cortex, for example, might be a promising start

7.4 Principle 2: Cross-network infra-slow activity is bi-directional and initiated by early intra-network nodes

We have focused a great deal on the unidirectional travel of infra-slow fMRI activity within networks, but what about inter-network signaling? In Chapter 2, we showed that one property of cross-network temporal organization is that, in awake adults, no network leads or follows any other network. That is, on average, we cannot say, for example, that spontaneous BOLD signals originate in the visual network and move to the motor network. Instead, we find that across time, some elements of the visual network lead the motor network, but there are also elements of the motor network that lead the visual network.

Thus, there is bi-directional infra-slow signaling between resting state networks. Can we say anything else? It turns out we can. Consider infra-slow signaling between the DMN and the DAN, illustrated in Figure 1E-F. Starting with the DAN, we first examine temporal lags between the FEF and all nodes of the DMN. We find that the FEF is approximately equi-latent (zero-lag) with the RSC, but that the FEF is early compared to all the other nodes of the DMN (PCC, PPC, mPFC). Thus, let us suppose DAN → DMN signals originate in the FEF (we will prove this shortly): then we know that FEF signals travel the RSC/PCC, before moving to the rest of the DMN. In other words, the earliest part of the dorsal attention network sends cross-network signals to the earliest node in the DMN, the RSC/PCC. Therefore, it appears that cross-network signals move between early nodes.

Do we find the same principle when examining DMN → DAN signals? In fact we do (Figure 1F). The earliest node of the DMN, the RSC, has approximately zero-lag with the FEF, but leads all the other nodes of the DAN. The fact that the PCC leads all nodes in the DAN except the FEF implies that DAN → DMN signals must originate in the FEF, as claimed. Thus we find reciprocal signaling between early nodes of the DAN and DMN, with near zero-lag between the FEF and PCC rising from bi-directional signaling between these nodes, as summarized in Figure 1G.

What about the rest of the brain? We could attempt to verify bi-directional cross-network signaling between early nodes one network pair at a time, but there is an easier way. The principle we articulated implies that intra-network signals travel in the same direction as inter-network signals. If this does not seem obvious, consider an intra-network signal arising in the DMN: it will start in the RSC and move toward the mPFC (Fig. 1). Now consider a cross-network signal moving from the DAN to the DMN: it will start in the FEF, then move to the RSC and continue along to the mPFC. Thus it's clear that intra- and cross-network signals in these examples have the same direction within the DMN. But what of the FEF leading the RSC? This relationship would appear to differentiate cross-network signal travel from intra-network signal travel, except for the fact that we know signals travel from the DMN to DAN as well, going from the RSC to the FEF, nullifying any net directionality between these two early nodes of the DMN and the DAN, respectively.

Therefore, whether we study intra- or inter-network signaling, the areas that tend to be "early" or "late" are the same, at least in our analysis of the DMN and DAN thus far. We can examine whether this idea is true in general by computing *lag projections*, which are simply images of the average temporal delay between a particular voxel and the rest of the brain. We have previously computed lag projections by averaging over all delays between all pairs of voxels, whether those delays corresponded to inter- or intra-network relations, to produce an average picture of where infra-slow activity tends to start and terminate in the brain.

However, we can modify this technique to produce two lag projections (Figure 2B): First, we produce a projection over only positive correlations in the brain representing, to a first approximation, intra-network relationships (Fig. 2B, left). Thus, the positive correlation lag projection captures the temporal structure of within-network signaling. The reader will notice that there are some positive correlations outside of the defined RSNs; parcellation schemes for RSNs require arbitrary decisions that affect boundaries. This, and the hierarchical architecture of resting state networks (RSNs), largely accounts for the positive correlations outside of our specified RSNs (Yeo et al. 2011).

Next, we can compute a lag projection over only negative correlations in the brain (Figure 2B, right). As RSNs are defined by positive correlations, it follows that all negative correlations are between networks, and hence the resulting lag projection captures the temporal structure of inter-network signaling.

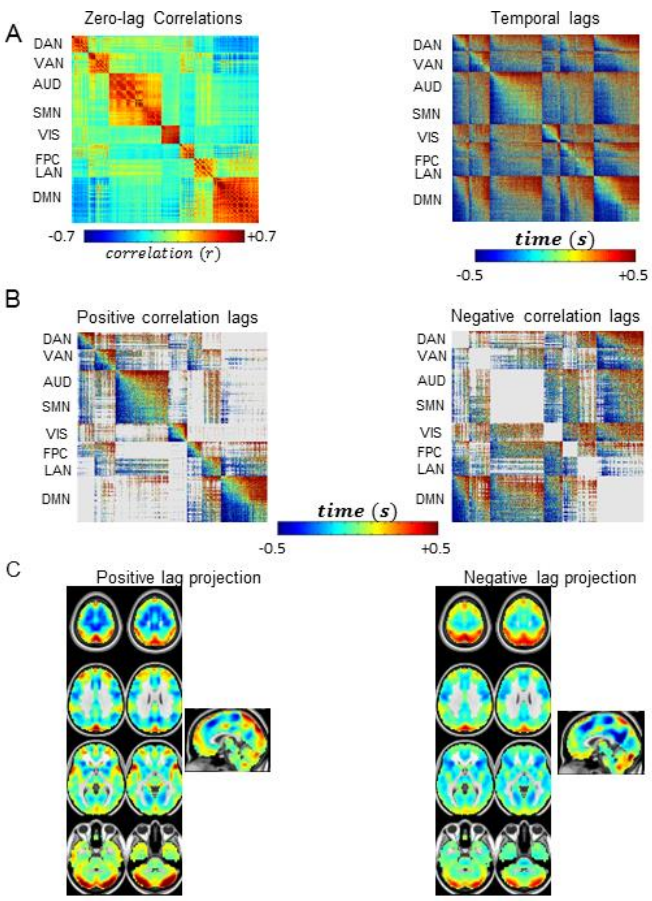

Figure 7-2: A general analysis of intra- vs. inter-network signaling in resting state fMRI. (A) For every pair of voxels in the brain, we can define a zero-lag correlation matrix, shown on the left, and a temporal lags matrix, shown on the right. Together these matrices contain all functional connectivity and temporal delay information in the system. (B) Since resting state networks are defined as areas with high positive correlations (Mitra and Raichle, 2016; Mitra et al., 2015a), we can approximate intra-network signaling by only considering temporal delays which correspond to positive correlations, and ignore the rest. This as shown on the left where the masked temporal lags matrix is computed only over positive correlations. In contrast, shown on the right, we can approximate inter-network signaling by only considering temporal delays which correspond to negative correlations as these are by definition inter-network relationships in resting state data. This reveals areas that tend to be early or late in inter-network communication. Critically (C), positive (left) and negative (right) lag projection maps are highly similar (spatial correlation r = 0.92), indicating that the temporal structure of within-network signaling mimics the temporal structure of cross-network signaling.

If it is true that cross-network signals originate in early parts of the sending network, and then travel through the same route and intra-network signals in the receiving network, then the overall temporal structure of lag projections computed over positive vs. negative correlations should be highly similar. Indeed, as illustrated in Figure 2C, the two lag projection topographies are nearly identical (spatial correlation r = 0.92).

Principles 1 and 2 can be summarized by way of a traffic analogy: RSNs represent one-way streets, in which signals travel unidirectionally. Cross-network interactions are bi-directional, but the two-way streets are found only between early nodes in networks. So

if we want to drive from the DMN to the DAN, we must start in the RSC, visit the FEF, then continue through the DAN along its one-way street. Similarly, to drive from the DAN to the DMN, we start in the FEF, travel the other direction to the RSC, and continue along the DMN one-way street.

As articulated in Principle 1, the functional meaning of this structure is presently unclear. However, we can say one more thing: cross-network temporal structure is malleable, as shown in Chapter 4. During slow wave sleep, there is no organized cross-network lag structure in general, with the exception of the visual network, which precedes all other networks in terms of spontaneous infra-slow activity. On this basis, it is tempting to suggest that the specific cross-network organization observed in awake adults is a correlate of conscious awareness, but this hypothesis requires further study.

The study of temporal structure during state contrasts in Chapter 6 also reveals a mechanism for the malleability of cross-network flow of infra-slow activity, at least between mouse visual and motor cortices. Using laminar electrophysiology, we find that infra-slow activity moves bi-directionally (visual to motor and motor to visual) through different cortical layers during wake and anesthesia; however, the relative strength of signaling in each direction, as measured by correlation magnitudes, is modulated across states to arrive at a predominant direction of travel. Critically, the predominant directionality of the infra-slow laminar electrophysiology agrees with that found using infra-slow blood oxygen signals, establishing a mechanistic bridge to our human fMRI findings.

7.5 Principle 3: Blood oxygen signals reflect a distinct, infra-slow brain process

As the organization of resting state fMRI activity becomes linked to ever more complex phenomena, such as individual variability in brain function (Smith et al. 2015) and diagnosis of neuropsychiatric conditions (Emerson et al. 2017), it is imperative to have some understanding of the underlying physiology of blood oxygen signals, especially the physiology underlying their spatio-temporal organization.

Chapter 6 adds to mounting evidence, reviewed in the Introduction, that blood oxygen signals correspond specifically to an infra-slow brain process that is distinct from higher frequencies, even the relatively slow delta band, as evidenced by clear differences in spontaneous spatio-temporal trajectories across frequencies. Indeed, Chapter 6 further demonstrates that cortical spatio-temporal relationships measured using resting state fMRI are likely attributable to a heretofore unsuspected level of specificity in cross-laminar relationships. The finding that infra-slow brain processes have distinct spatio-temporal and laminar structure not only informs our understanding of blood oxygen signals and fMRI, it also raises a critical question: how should infra-slow phenomena be interpreted?

There is no clear answer at present, but given its aforementioned differences from higher frequencies, one implication is that we should not assume that infra-slow physiology is just a slow version of higher frequency physiology. For example, we know that a visual stimulus leads to the firing of action potentials in primary visual cortex.

Thus, when we observe an infra-slow visual-evoked fMRI response in primary cortex, it is generally assumed that the infra-slow fMRI response is a low frequency correlate of action potentials firing in response to visual stimulus (Bianciardi et al. 2009). If this were the case, it should follow that we should not observe an infra-slow fMRI response in the absence of a visual stimulus. Yet, Heeger and colleagues have shown that the mere expectation of a visual stimulus, with no actual visual stimulus present, evokes an infra-slow fMRI response in early visual areas that is nearly identical to when a visual stimulus is in fact present (Ress et al. 2000). In a follow up experiment, Sirotin and Das showed that the infra-slow visual fMRI response driven by the expectation of a stimulus, in the absence of actual visual stimulus, could not be predicted from either multi-unit activity or local field potentials (LFPs) in the 10-150 Hz range (Sirotin and Das 2009). The natural conclusion, in light of the work shown in this thesis, is that there is a distinct infra-slow brain process responsible for the blood oxygen response, and that this infra-slow brain process somehow codes predictions/expectations in primary visual cortex. Strangely, Sirotin and Das never analyzed their low frequency LFP data (at least in print), instead arriving at the bizarre conclusion that the cerebral vasculature is able to predict future stimuli. In fact, to this day, the obvious prediction that infra-slow electrophysiology underlies expectation-based responses in early visual cortex has gone untested.

I hope that the present work along with Heeger's observations (among many others: see for example (Maier et al. 2008)) will reignite a serious consideration of the meaning of infra-slow brain processes, and how they differ from higher frequencies. Indeed, the

findings in Chapter 6 that infra-slow activity travels in a reciprocal direction compared to delta band activity, and that there is a ~90 degree relationship between infra-slow phase and delta amplitude, suggest a functional hierarchy across frequencies, but there is much that must yet be understood regarding both the “function” and the “hierarchy”.

7.6 Principle 4: The direction of spontaneous infra-slow activity is state-dependent

In Chapters 4-6, we have emphasized differences in the temporal structure of infra-slow activity between wakeful versus sleep/anesthetized states. Differences in the direction infra-slow activity travels through the brain across states of arousal/awareness have informed the hypothesis that the patterns of traveling low frequency activity (infra-slow and delta) govern broad states of brain function. How this works precisely is not known, but one could imagine a structured state-space landscape established by the spontaneous spatio-temporal organization of very low frequencies. If we view this state-space landscape in terms of organization of broad-scale neural excitability, it follows that this state-space landscape might constrain and guide the movement of higher frequency activity. Thus, the striking differences we have observed between wake and sleep/anesthesia might be interpreted as shifts in the landscape underlying broad changes in brain state.

Does the spatio-temporal organization of infra-slow activity change across other kinds of brain states, not associated with differences in arousal or awareness? Preliminary evidence suggests yes. For one, as shown in Chapter 2, there are differences in the

temporal structure of fMRI activity before versus after task performance. Moreover, in work not presented in this thesis, we have shown that the putamen is “abnormally early” in high-functioning adults with autism spectrum disorders (ASD), and that the degree of putamen earliness in individual subjects correlates with the severity of their repetitive motor behaviors, a core trait of ASD (Mitra et al. 2015).

There is even emerging evidence that the temporal structure of infra-slow fMRI activity may be a correlate of an early language sensitive period (Figure 3). Pioneering work over the past decades has demonstrated that early-life language acquisition proceeds through a predictable trajectory. Infants begin life with the capacity to perceive phonetic differences across all languages, but by 12 months of age infant phoneme perception narrows such that native-language phonemes are perceived more accurately while non-native phoneme discrimination declines (Kuhl et al. 2006; Kuhl et al. 1992; Werker et al. 1981; Werker and Tees 1983). These findings have led to the hypothesis that the first year of life represents a “sensitive-period” for acquiring language comprehension, such that the brain is initially optimized to detect and learn statistical regularities in spoken language, and develops during the first year and beyond toward a configuration that allows efficient extraction of meaning from spoken language(Kuhl 2004; Werker and Hensch 2015). However, functional correlates of the sensitive-period for human language network remain elusive.

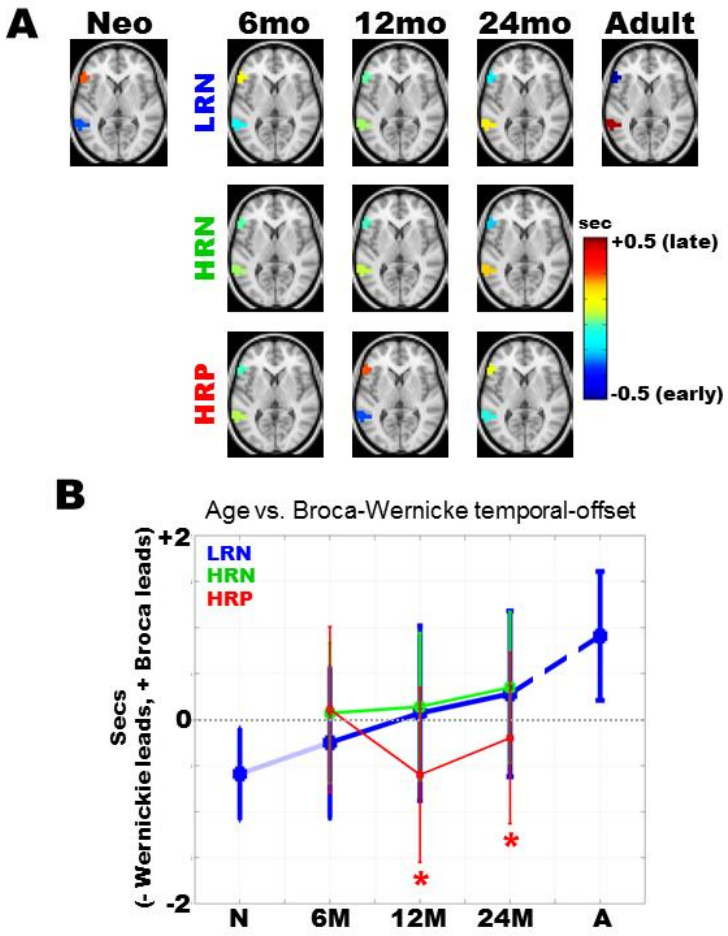

Figure 7-3: Reversal of the spontaneous temporal relationship between Broca's and Wernicke's area over development. *(A)* Temporal offsets between Broca's and Wernicke's area over development. Blue indicates early; red indicates late. LRN, HRN, and HRP stand for low genetic risk ASD-negative, high genetic risk ASD-positive, and high-genetic risk ASD-positive, respectively. *(B)* Mean and standard error of Broca-Wernicke temporal offsets over development . Red asterisks denote statistically significant differences ($p<0.05$, Bonferonni corrected) between HRP and LRN groups. Neonates are connected using a dotted line as they are presumed ASD-negative; adults are connected using a dashed line as their genetic risk status is unknown.

Figure 3 shows preliminary evidence (unpublished) that the direction of infra-slow fMRI activity within the language system changes over time. In adults, Broca's area is early compared to Wernicke's area, in line with the unidirectional travel of infra-slow activity through networks posited in Principle 1. In neonates, on the other hand, infra-slow activity still moves unidirectionally, but in the opposite direction as compared to adults, from Wernicke's area to Broca's area. The shift from this neonatal directionality to the adult directionality occurs over the 6-12 month age: just as the early sensitive period for phoneme recognition is drawing to a close. Moreover, the orderly shift from a typical neonatal to adult language temporal structure is altered in children with ASD, which is significant as language delays/disorders are common in ASD. Therefore, it seems

possible that the direction of infra-slow activity in the language network marks the brain's passage through an early sensitive period. Future work will have to investigate this connection, but these results add evidence to the perspective that travel patterns in infra-slow activity relate to and possibly govern govern important changes in the state of the brain.

7.7 Final Comments:

These four principles offer a summary of what we have learned over the course of this thesis, some ideas for future investigations, and more importantly, a set of falsifiable rules. Future work must continue to test these principles. If the rules are contradicted by future work, they will be abandoned. However, if these principles prove useful, not by being completely correct, but by offering a stepping stone to a greater understanding of brain function, then we will have achieved what we set out to accomplish.

7.8 References

Betzig E, Patterson GH, Sougrat R, Lindwasser OW, Olenych S, Bonifacino JS, Davidson MW, Lippincott-Schwartz J, and Hess HF. Imaging intracellular fluorescent proteins at nanometer resolution. *Science* 313: 1642-1645, 2006.

Bianciardi M, Fukunaga M, van Gelderen P, Horovitz SG, de Zwart JA, and Duyn JH. Modulation of spontaneous fMRI activity in human visual cortex by behavioral state. *Neuroimage* 45: 160-168, 2009.

Buzsaki G. The hippocampo-neocortical dialogue. *Cerebral cortex* 6: 81-92, 1996.

Buzsaki G. Two-stage model of memory trace formation: a role for "noisy" brain states. *Neuroscience* 31: 551-570, 1989.

Emerson RW, Adams C, Nishino T, Hazlett HC, Wolff JJ, Zwaigenbaum L, Constantino JN, Shen MD, Swanson MR, Elison JT, Kandala S, Estes AM, Botteron KN, Collins L, Dager SR, Evans AC, Gerig G, Gu H, McKinstry RC, Paterson S, Schultz RT, Styner M, Network I, Schlaggar BL, Pruett JR, Jr., and Piven J. Functional neuroimaging of high-risk 6-month-old infants predicts a diagnosis of autism at 24 months of age. *Science translational medicine* 9: 2017.

Fox MD, and Raichle ME. Spontaneous fluctuations in brain activity observed with functional magnetic resonance imaging. *Nat Rev Neurosci* 8: 700-711, 2007.

Fox MD, Snyder AZ, Vincent JL, Corbetta M, Van Essen DC, and Raichle ME. The human brain is intrinsically organized into dynamic, anticorrelated functional networks. *Proc Natl Acad Sci U S A* 102: 9673-9678, 2005.

Hacker CD, Laumann TO, Szrama NP, Baldassarre A, Snyder AZ, Leuthardt EC, and Corbetta M. Resting state network estimation in individual subjects. *Neuroimage* 82C: 616-633, 2013.

He BJ, Snyder AZ, Zempel JM, Smyth MD, and Raichle ME. Electrophysiological correlates of the brain's intrinsic large-scale functional architecture. *Proc Natl Acad Sci U S A* 105: 16039-16044, 2008.

Kuhl PK. Early language acquisition: cracking the speech code. *Nat Rev Neurosci* 5: 831-843, 2004.

Kuhl PK, Stevens E, Hayashi A, Deguchi T, Kiritani S, and Iverson P. Infants show a facilitation effect for native language phonetic perception between 6 and 12 months. *Developmental science* 9: F13-F21, 2006.

Kuhl PK, Williams KA, Lacerda F, Stevens KN, and Lindblom B. Linguistic experience alters phonetic perception in infants by 6 months of age. *Science* 255: 606-608, 1992.

Leopold DA, Murayama Y, and Logothetis NK. Very slow activity fluctuations in monkey visual cortex: implications for functional brain imaging. *Cereb Cortex* 13: 422-433, 2003.

Ma Y, Shaik MA, Kozberg MG, Kim SH, Portes JP, Timerman D, and Hillman EM. Resting-state hemodynamics are spatiotemporally coupled to synchronized and symmetric neural activity in excitatory neurons. *Proc Natl Acad Sci U S A* 113: E8463-E8471, 2016.

Maier A, Wilke M, Aura C, Zhu C, Ye FQ, and Leopold DA. Divergence of fMRI and neural signals in V1 during perceptual suppression in the awake monkey. *Nat Neurosci* 11: 1193-1200, 2008.

Mitra A, Snyder AZ, Constantino JN, and Raichle ME. The Lag Structure of Intrinsic Activity is Focally Altered in High Functioning Adults with Autism. *Cereb Cortex* 2015.

Mitra A, Snyder AZ, Hacker CD, and Raichle ME. Lag structure in resting-state fMRI. *J Neurophysiol* 111: 2374-2391, 2014.

Pan WJ, Thompson GJ, Magnuson ME, Jaeger D, and Keilholz S. Infraslow LFP correlates to resting-state fMRI BOLD signals. *Neuroimage* 74: 288-297, 2013.

Power JD, Cohen AL, Nelson SM, Wig GS, Barnes KA, Church JA, Vogel AC, Laumann TO, Miezin FM, Schlaggar BL, and Petersen SE. Functional network organization of the human brain. *Neuron* 72: 665-678, 2011.

Raichle ME. The restless brain. *Brain Connect* 1: 3-12, 2011.

Raichle ME, and Mintun MA. Brain work and brain imaging. *Annu Rev Neurosci* 29: 449-476, 2006.

Ress D, Backus BT, and Heeger DJ. Activity in primary visual cortex predicts performance in a visual detection task. *Nat Neurosci* 3: 940-945, 2000.

Sirota A, and Buzsaki G. Interaction between neocortical and hippocampal networks via slow oscillations. *Thalamus Relat Syst* 3: 245-259, 2005.

Sirotin YB, and Das A. Anticipatory haemodynamic signals in sensory cortex not predicted by local neuronal activity. *Nature* 457: 475-479, 2009.

Smith SM, Nichols TE, Vidaurre D, Winkler AM, Behrens TE, Glasser MF, Ugurbil K, Barch DM, Van Essen DC, and Miller KL. A positive-negative mode of population

covariation links brain connectivity, demographics and behavior. *Nat Neurosci* 18: 1565-1567, 2015.

Werker JF, Gilbert JH, Humphrey K, and Tees RC. Developmental aspects of cross-language speech perception. *Child development* 52: 349-355, 1981.

Werker JF, and Hensch TK. Critical periods in speech perception: new directions. *Annual review of psychology* 66: 173-196, 2015.

Werker JF, and Tees RC. Developmental changes across childhood in the perception of non-native speech sounds. *Canadian journal of psychology* 37: 278-286, 1983.

Yeo BT, Krienen FM, Sepulcre J, Sabuncu MR, Lashkari D, Hollinshead M, Roffman JL, Smoller JW, Zollei L, Polimeni JR, Fischl B, Liu H, and Buckner RL. The organization of the human cerebral cortex estimated by intrinsic functional connectivity. *J Neurophysiol* 106: 1125-1165, 2011.